

The influence of fissures on landslide hydrology



Dominika KRZEMINSKA

**THE INFLUENCE OF FISSURES
ON
LANDSLIDE HYDROLOGY**

Dominika KRZEMINSKA

THE INFLUENCE OF FISSURES ON LANDSLIDE HYDROLOGY

Proefschrift

ter verkrijging van de graad van doctor
aan de Technische Universiteit Delft,
op gezag van de Rector Magnificus prof. ir. K.C.A.M. Luyben,
voorzitter van het College voor Promoties,
in het openbaar te verdedigen

op 11 december 2012 om 12:30 uur

door

Dominika Malgorzata KRZEMINSKA

Master of Science
Warsaw University of Technology
geboren te Warsaw, Poland

Dit proefschrift is goedgekeurd door de promotor:

Prof. dr. ir. **H.H.G. Savenije**

Copromotor: Dr. **T.A. Bogaard**

Samenstelling promotiecommissie:

Rector Magnificus	<i>voorzitter</i>
Prof.dr.ir. H.H.G. Savenije	<i>Technische Universiteit Delft, promotor</i>
Dr. T.A. Bogaard	<i>Technische Universiteit Delft, copromotor</i>
Prof.dr. S. Uhlenbrook	<i>Technische Universiteit Delft en UNESCO-IHE</i>
Prof.dr. V.G. Jetten	<i>ITC en Universiteit Twente</i>
Prof.dr.ir. M.F.P. Bierkens	<i>Universiteit Utrecht en TNO</i>
Dr. Th.W.J. van Asch	<i>Universiteit Utrecht</i>
Dr. R. Greco	<i>Seconda Università di Napoli, Italy</i>
Prof.dr.ir. T.N. Olsthoorn	<i>Technische Universiteit Delft, reservelid</i>

The research described in this dissertation was performed at the Water Resources Section, Faculty of Civil Engineering and Geosciences, Delft University of Technology. The research was financed from the budget of ‘Mountain Risks’ project funded under the Marie Curie Research Training Network programme within the 6th Framework Programme of the European Commission, the ANR-ECCO ‘Ecou-PRef’ Programme financially supported by the French Ministry of Research and the French Research Agency, and ‘Safe Land’ project.

Copyright by D.M. Krzeminska, 2012

All rights reserved. No part of this publication may be reproduced or utilized in any form or by any means, electronic or mechanical, including photocopying, recording or by any information storage and retrieval system, without the prior written permission of the author.

ISBN: 978-90-6562-309-6

Keywords: DTS, small-scale sprinkling, fissure flow, spatially distributed hydrological model.

SUMMARY

Preferential flow occurs in many soils and it is recognized to influence soil moisture distribution and hydrological fluxes at different scales. Preferential flow paths are formed for example by soil fauna, by plant roots or soil erosion. Water plays an important role in mass movement processes: rainwater or snow melt infiltrates into the soil and recharges the groundwater system. The unsaturated zone controls groundwater recharge allowing for the loss of soil moisture by evaporation and attenuation of percolation towards the groundwater system. An increase in pore water pressure results in a decrease in an effective stress and internal strength of slopes. The preferential fluxes may change the spatial and temporal hydrological response of a landslide and influence intensity, duration and differentiation of mass movement.

The quantification of groundwater recharge, especially by means of preferential flow, is a research challenge for an advanced understanding of hydrological systems in hillslopes and landslides. The main difficulties stem from heterogeneity of landslide lithology and spatial and temporal variations of hydraulic properties. The complexity of preferential fissure flow processes, and their high spatial and temporal variability, makes it very difficult to measure the processes in the field and to include them in hydrological modeling.

This thesis focuses on preferential fissure flow, where fissure is defined as geo-mechanically induced cracks commonly present in slow-moving landslides, and their influence on landslide hydrological behaviour. Research work included both extended field measurements and hydrological modelling. All experiments described in this thesis were done at the Super-Sauze landslide: a persistently active clay shale landslide that covers 0.17 km² of surface with the average slope of 25°. The landslide kinematics of the Super-Sauze is controlled by hydrology. The mass movement occurs as a consequence of the rise of groundwater table and hence the development of positive pore pressure.

In order to monitor and quantify preferential flow processes *on site* two methodologies were proposed: Distributed Temperature Sensing (DTS) and combined hydrological and hydrochemical analysis of small-scale sprinkling tests. Both methodologies allowed for qualitative analysis of preferential flow patterns and showed the potential for quantification of dominant hydrological processes observed across the landslide:

- qualitative analysis of measured soil temperature variation allowed observing spatial differences in soil moisture state and estimating the location of surface and subsurface water flow paths;
- quantitative analysis of measured soil temperature made it possible to detect the spatial and temporal variations in apparent soil thermal conductivity and correlated them with measured soil moisture content; promising empirical relationships were obtained when accounting for local heterogeneities in soil characteristics;
- analyses of small scale sprinkling experiments, combining the hydrological and hydrochemical analysis of two consecutive days of sprinkling, were able to capture the dominant hydrological process occurring in the area and show the potential for their quantification; based on the analysis of all available field data, conceptual models of the hydrological responses were proposed.

The literature review and the analyses of the extensive field data sets consisting of day-to-day monitoring as well as sprinkling experiments, resulted in the formulation of a conceptual model of the hydrological influence of fissures on landslide activity. Special attention was given to spatial and temporal variation in fissures connectivity, which makes fissures act both as preferential flow paths for deep vertical infiltration and as lateral groundwater drains. These dynamics were included in a spatially distributed hydrological and slope stability model and applied to a 'simple' landslide. The results highlight that fissure connectivity and fissure permeability play an important role in distributing water within a landslide. Making the fissures connectivity a function of soil moisture content resulted in a strong seasonality of the hydrological response on infiltrating rainwater or snowmelt: increased soil moisture content leads to more lateral water drainage through the fissures towards the lower part of the landslide, while decreased soil moisture content increases the water storage in the fissures.

Furthermore, an analysis was made of all available field monitoring data of the Super-Sauze landslide. Hereafter, the distributed hydrological and slope stability model was applied to the Super-Sauze case study. The main objective was to model the influence of fissures on the

hydrological behaviour of slow moving landslide and the dynamic feedbacks between fissures, hydrology and slope stability. In addition to hydrological feedback (fissure connectivity being the function of soil moisture content), the mechanical feedback was implemented as a relationship between fissure volume and level of landslide activity.

Overall, from this research it can be concluded that preferential fissure flow may significantly influence the timing and duration of the periods of elevated pore pressure conditions in landslides depending on fissure network characteristics, especially fissure volume and connectivity between them. The field measurements outline the spatial heterogeneity of soil hydraulic properties and dominant hydrological processes existing in slow-moving clay shale landslides. The analyses of field data together with presented modelling results confirms the importance of distributed approaches when modelling differential hydrological response of complex heterogeneous landslides and stresses the need for including spatio-temporal changes in soil hydraulic properties of both fast (i.e. fissures) and slow (i.e. matrix) responding domain.

SAMENVATTING

In een bodem stroomt het water voornamelijk via een beperkt aantal voorkeurstroombanen. Dit heeft grote invloed op de vochtverdeling en op de hydrologische fluxen in een bodem. Voorkeurstroombanen worden gevormd door o.a. bodemfauna, plantenwortels en bodemerosie. Water speelt een belangrijke rol bij aardverschuivingen: regenwater of sneeuwsmelt infiltreert in een (onverzadigde) bodem. Bodemverdamping vermindert deze hoeveelheid water en het overtollige water stroomt naar het grondwater. Water in de grond leidt tot een toename van de poriedruk, wat zorgt voor een afname van effectieve spanning in de grond en daarmee voor een afname van de interne sterkte. Dit kan leiden tot het instabiel worden van een helling. Het belang van waterstroming in voorkeurstroombanen bij aardverschuivingen is dat het een regulerende rol speelt bij de intensiteit en de duur van de massabeweging.

Het kwantificeren van grondwateraanvulling, vooral door voorkeurstroombanen, is een wetenschappelijke uitdaging. Hierbij gaat het vooral om het beter begrip krijgen van het functioneren van hydrologische systemen in hellingen en aardverschuivingen. Het grootste probleem ligt in de heterogeniteit van aardverschuivingen en de ruimtelijke en temporele variatie van de hydraulische eigenschappen van de bodem. De complexiteit van waterstroming in voorkeurstroombanen en de ruimtelijke en temporele variabiliteit, zorgen ervoor dat deze processen moeilijk te meten zijn in het veld en daarmee ook lastig zijn op te nemen in hydrologische modellen.

Dit proefschrift richt zich op waterstroming in spleten (scheuren in de grond) die ontstaan zijn door differentiële beweging van de grond, zoals we dat tegenkomen in langzaam bewegende aardverschuivingen, en naar de invloed hiervan op de hydrologie van een aardverschuiving. Het onderzoek beslaat zowel uitgebreid veldonderzoek als het hydrologisch modelleren. Alle

veldexperimenten zijn uitgevoerd op de Super-Sauze aardverschuiving: een actieve aardverschuiving in tot silt-klei verweerde mergelafzettingen. De aardverschuiving beslaat 0,17 km² en heeft een gemiddelde hellingshoek van 25°. De bewegingsdynamiek van Super-Sauze is direct gerelateerd aan de hydrologie: bij stijgend grondwater, en dus toename van de poriedruk, zal de aardverschuiving in beweging komen of versnellen.

Voor het monitoren en kwantificeren van voorkeurstroming stelt dit proefschrift twee *in-situ* methodes voor: ‘Distributed Temperature Sensing’ (DTS) en kleinschalige beregeningsproeven waarbij hydrologische en hydrochemische metingen gecombineerd worden. Beide methodes leveren een kwalitatief inzicht in de patronen van voorkeurstroombanen en een kwantitatief inzicht in de dominante hydrologische processen die in een aardverschuiving optreden. De belangrijkste resultaten van de *in-situ* methodes zijn:

- Kwalitatieve analyse van bodemtemperatuur fluctuaties levert inzicht op in ruimtelijke verschillen van bodemvochtigheid en geeft een indicatie van de locatie van oppervlakkige en ondergrondse stroombanen.
- Kwantitatieve analyse van gemeten bodemtemperaturen maakt het mogelijk om ruimtelijke en temporele verschillen in de thermische geleiding van de bodem te detecteren, die zijn gecorreleerd met bodemvocht gehalten. Er werden interessante empirische relaties gevonden tussen thermische geleiding en gemeten bodemvocht mits rekening wordt gehouden met de locale heterogeniteit van bodemkarakteristieken.
- De analyses van de kleinschalige beregeningsproeven waarbij hydrologische en hydrochemische analyses gecombineerd werden, toonden aan dat op deze manier de dominante hydrologisch processen op verschillende locaties op de aardverschuiving kunnen worden gevonden en kwantificeerbaar zijn.

Naar aanleiding van een literatuurstudie en uitgebreide veldexperimenten waaronder beregeningsproeven, is een conceptueel model van de invloed van scheuren op de hydrologie en dus aardverschuivingactiviteit gemaakt. Met name is gekeken naar de dynamische hydrologische verbindingen tussen de individuele spleten. Het is deze hydrologische verbinding tussen spleten die ervoor zorgt dat voorkeurstroombanen ofwel diepe infiltratie bevorderen ofwel de laterale drainage van het water faciliteren. Deze dynamiek is wiskundig beschreven in een ruimtelijk gedistribueerd hydrologisch en hellingstabiliteit model dat is

toegepast op een synthetische aardverschuiving. De resultaten tonen aan dat de hydrologische verbinding tussen spleten onderling en de doorlatendheid van de spleten zelf een heel belangrijke rol spelen in de waterverdeling in een aardverschuiving. Als de verbinding tussen de spleten een functie wordt gemaakt van het bodemvochtgehalte ontstaat een sterk seizoenseffect in de hydrologische reactie van de aardverschuiving op regen en sneeuw infiltratie: bij toenemende vernatting wordt meer water gedraineerd door de spleten naar het onderste deel van de aardverschuiving. Dit kan ofwel leiden tot hogere grondwaterstanden onderin de aardverschuiving ofwel tot een grondwaterstand afname als het water de aardverschuiving verlaat via het oppervlakte water systeem.

Vervolgens is een analyse gemaakt van de lange reeks gegevens die verzameld zijn door middel van het continue monitoringsysteem van de Super-Sauze aardverschuiving. Hierna is het gedistribueerde hydrologische en hellingstabiliteitsmodel toegepast op de Super-Sauze aardverschuiving. Het doel van deze case study was om de invloed van spleten op de hydrologische dynamiek van een langzaam bewegende aardverschuiving te modelleren en om de dynamische interactie tussen spleten, hydrologie en hellingstabiliteit te bestuderen. Behalve hydrologische koppeling tussen de hydrologische verbindingen tussen spleten en bodemvochtgehalte is een mechanische interactie voorgesteld: een relatie tussen het volume aan spleten in de bodem en het stabiliteitsniveau van de aardverschuiving.

Uit dit onderzoek kan worden geconcludeerd dat voorkeurstroombanen een significante invloed kunnen hebben op het moment en duur van poriedruk toename en dus op het initiëren van massabewegingen. Hierbij zijn vooral het volume aan spleten en de hydrologische verbindingen tussen de spleten van groot belang. De veldmetingen tonen de enorme ruimtelijke heterogeniteit van de hydraulische eigenschappen van de bodem en de dominante hydrologische processen die plaatsvinden in langzaam bewegende aardverschuivingen. Het hier gepresenteerde onderzoek bevestigt het belang van ruimtelijke modellering van hydrologische processen in complexe, heterogene aardverschuivingen en benadrukt het belang van het meenemen van ruimtelijk en temporele veranderingen van bodemeigenschappen voor het modelleren van waterstroming.

List of abbreviations

DTS	Distributed Temperature Sensing
EMMA	End-Member Mixing Analysis
FOM	Field Operated Meter
GPS	Global Positioning System
HG	Hydro-geomorphological unit
MaxStor	Storage Capacity
LBC	Lower Boundary Condition
RMSE	Root Mean Square Error
SB	Sprinkling Block
SSF	Sub-surface flow
TCS	Thermal Conductivity Scanner
TDR	Time-Domain Reflectometry
WCR	Water Content Reflectometer

List of symbols

A	Surface area [L^2]
A_T	Amplitude of the surface temperature [$^{\circ}$]
a_{fis}	Mean fissure aperture [L]
C	Concentrations [$M L^{-3}$]
C_{fis}	Fissure connectivity [-]
C_v	Volumetric heat capacity [$L^{-1} M T^{-2} K^{-1}$]
c	Cohesion [$M L^{-1} T^{-2}$]
c'	Effective cohesion [$M L^{-1} T^{-2}$],
c'_r	Residual cohesion [$M L^{-1} T^{-2}$],
D	Thermal diffusivity of the soil [$L^2 T^{-1}$]
E_M	Pressiometric modulus [$M L^{-1} T^{-2}$]
F_{fis}	Fraction of the surface area covered by fissure [$L^2 L^{-2}$]
f_s	Factor of safety [-]
h	Groundwater height [L]
h_A	Air entry valuve [L]
$ h $	Absolute matrix suction [L]
I_p	Plasticity index [-],
K	Depletion factor in Ch.4 [T]
k	Hydraulic conductivity [$L T^{-1}$]
L	Length [L]
N_{fis}	Number of fissures [-]

n	Porosity [-]
P	Precipitation [$L T^{-1}$]
P_e	Percolation [$L^3 T^{-1}$]
Q_d	Resistance [$M L^{-1} T^{-2}$]
Q_{sat}	Saturated flow [$L^3 T^{-1}$]
q	Quartz content [-]
R^2	Correlation coefficient [-]
S_C	Snow cover [L]
t	Time [T]
T_{air}	Air temperature [$^{\circ}K$]
T_{soil}	Soil temperature [$^{\circ}K$]
u	Pore water pressure [$M L^{-1} T^{-2}$]
V	Volume [L^3]
v	Water flow rate [$L T^{-1}$]
W	Total fraction weight [$M L^{-1} T^{-2}$]
W_L	Liquid limit [-]
W_P	Plastic limit [-]
W_R	Shrinkage limit [-]
x	Percent of the area in Ch.4 [-]
z	Depth [L]
α	Shape factor in Ch.5 [-]
α, β	Mixing proportions in Ch.4 [-]
γ_d	Dry unit weight [$M L^{-2} T^{-2}$]
γ_{sat}	Saturated unit weight [$M L^{-2} T^{-2}$]
γ_w	Specific weight of water [$M L^{-2} T^{-2}$]
ΔS	Change in storage [L^3]
Δx	Cell length in Ch. 5 [L]
θ	Soil moisture content [-]
θ_E	Effective saturation [-]
λ	Thermal conductivity [$M L T^{-3} K^{-1}$]
σ	Total normal stress [$M L^{-1} T^{-2}$]
σ'	Effective normal stress [$M L^{-1} T^{-2}$]
τ	Shear strength [$M L^{-1} T^{-2}$]
τ	Tortuosity parameter in Ch. 5
ϕ	Angle of internal friction [$^{\circ}$]
ϕ'	Effective angle of friction [$^{\circ}$]
ϕ'_r	Residual angle of friction [$^{\circ}$]
ω	Angular frequency
Γ	Lateral exchange [$L^3 T^{-1}$]

List of Subscripts

av	average
E	evaporation
EW	event water
fc	field capacity
fis	fissure fraction
FM	fissure to matrix
GWin	groundwater inflow
GWout	groundwater outflow
INF	infiltrated water
mat	matrix fraction
max	maximum
MF	matrix to fissure
min	minimum
obs	observed
OF	overland flow
P	precipitation
PE	pre-event water
r	relative
sat	saturated
sim	simulates
SSF	subsurface flow
unsat	unsaturated

CONTENTS

Summary.....	v
Sumenvatting	ix
List of Symbols	xii
1. INTRODUCTION	1
1.1 Problem definition	2
1.2 The role of hydrology in mass movement processes	3
1.2.1 General principles of slope instability	3
1.2.2 Landslide causes and triggering	4
1.2.3 Precipitation induced landslides	5
1.3 Preferential fissure flow.....	6
1.3.1 Definition of preferential flow.....	6
1.3.2 Macropore flow	7
1.3.3 Fissure formations	8
1.3.4 Influence of fissure flow on landslide hydrology	10
1.3.5 Monitoring of preferential flow processes	12
1.4 Hydrological modeling of precipitation induced landslide	12
1.5 Objective of the thesis	15
1.6 Outline of the thesis.....	16
1.7 Mountain Risks project.....	16
2. THE SUPER - SAUZE LANDSLIDE.....	19
2.1 Location and climate	20
2.2 Geological setting of Barcelonnette basin.....	21
2.3 Development and geometry of the Super-Sauze landslide.....	22
2.3.1 Evolution of the Super-Sauze landslide	22
2.3.2 Geotechnical structure of the Super-Sauze landslide.....	26
2.4 Kinematics and hydrology of Super-Sauze landslide	29
2.4.1 Landslide kinematics	29
2.4.2 Landslide hydrology	31
2.4.3 Relationship between kinematics and hydrology	35
2.5 Identification of the fissure patterns within the Super-Sauze landslide	37

3. HIGH RESOLUTION TEMPERATURE OBSERVATION TO MONITOR SOIL THERMAL PROPERTIES AS A PROXY FOR SOIL MOISTURE CONDITIONS	39
3.1 Introduction.....	40
3.2 Estimation of soil thermal properties from soil temperature observations	41
3.2.1 Soil thermal properties	41
3.2.2 Amplitude method	43
3.2.3 Inversion method	44
3.3 Description of experimental set-ups	44
3.3.1 Temperature profiles.....	44
3.3.2 Distributed Temperature Sensing	45
3.3.3 Thermal Conductivity Scanner.....	45
3.3.4 Field Experimental set-ups.....	46
3.3.5 Laboratory experiment.....	50
3.4 Analysis and interpretation of the temperature time series	50
3.4.1 Temperature data	50
3.4.2 Qualitative and quantitative analysis of temperature data.....	52
3.4.3 The influence of the lower boundary condition and the soil moisture distribution on the apparent thermal diffusivity.....	59
3.5 Discussion.....	61
3.6 Summary and conclusions	63
4. FIELD INVESTIGATION OF FISSURE FLOW WITH SMALL-SCALE SPRINKLING EXPERIMENTS ON A HYDROLOGICALLY TRIGGERED LANDSLIDE.....	65
4.1 Introduction.....	66
4.2 Methodology	67
4.2.1 Experimental design	67
4.2.2 Analysis methodology	68
4.2.3 Characteristics of experimental plots.....	71
4.3 Results of sprinkling experiments - hydrological and hydrochemical responses	73
4.3.1 Plot A	73
4.3.2 Plot B	75
4.3.3 Plot C	77
4.4 Discussion of experimental results and model conceptualisation	78
4.4.1 Water balance and tracer mass balance analysis	78
4.4.2 Hydrological and hydrochemical observation.....	80
4.5 Discussion of conceptual models for Super-Sauze landslide.....	87
4.6 Conclusions.....	89

5. A CONCEPTUAL MODEL OF A HYDROLOGICAL INFLUENCE OF FISSURES ON LANDSLIDE ACTIVITY	91
5.1 Introduction.....	92
5.2 Adaptation of STARWARS	92
5.2.1 General model description	92
5.2.2 Representation of fissures	94
5.2.3 Adaptation of fluxes calculations	96
5.3 Methodology	99
5.3.1 ‘Simple’ landslide representation	99
5.3.2 Modelling strategy	100
5.4 Simulation results	102
5.4.1 General water balance components of a landslide.....	102
5.4.2 patial and temporal differences in groundwater level	104
5.5 Sensitivity analysis	109
5.6 Discussion and Conclusions.....	113
6. A MODEL OF HYDROLOGICAL AND MECHANICAL FEEDBACKS OF PREFERENTIAL FISSURE FLOW IN A SLOW-MOVING LANDSLIDE.....	115
6.1 Introduction.....	116
6.2 Conceptualisation of hydrological and mechanical feedbaks of fissure flow	117
6.2.1 Hydrological feedback	117
6.2.2 Mechanical feedback	117
6.3 Modelling of the Super-Sauze landslide	119
6.3.1 Model representation of the Super-Sauze landslide.....	119
6.3.2 Meteorological data	121
6.3.3 Model calibration and validation	122
6.4 Simulation results and discussion.....	125
6.5 Conclusions	132
7. SYNTHESIS.....	133
7.1 Monitoring of soil moisture patterns and dominant procceses within a landslide.....	134
7.1.1 Potential of DTS for long term monitoring of soil moisture patterns	134
7.1.2 Potential of Small Scale Sprinkling Experiments for identification and quantification of dominant hydrological processe	137
7.2 Modelling the influence of fissure flow on landslide hydrology.....	138
REFERENCES	143
ACKNOWLEDGEMENTS.....	157
CURRICULUM VITAE	159

Chapter 1

INTRODUCTION

1.1 Problem definition

The growth of society results in expansion of infrastructure building activities into environmentally privileged but often hazardous places as river beds and slopes. At the same time, society all over the world demands for improvement of living standard and an increasing level of protection against natural risks.

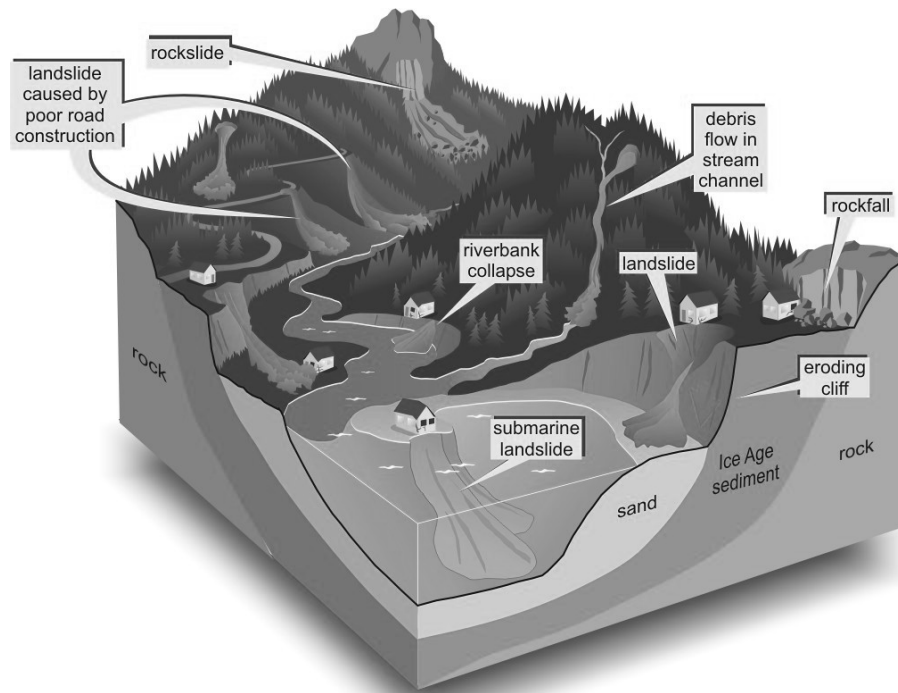


Figure 1-1. Landslide hazard in the mountainous regions (Geoscape Nanaimo website, 2012)

In mountain regions the communities are exposed to several hydro-geomorphological hazardous processes, such as snow avalanches, floods, landslides, rockfalls and debris flows (Figure 1-1). Among these, “landslides represent a major threat to human life, property, infrastructure and natural environment in most mountainous and hilly regions of the world” (Lacasse & Farrokhi, 2008) being the most destructive natural hazard on earth (Brabb, 1991). During the last two decades 321 catastrophic landslides were registered worldwide and more than half of those landslides occurred in Asia. While landslides cause the highest rate of deaths and injuries in Asia and America those in Europe are the most expensive – average damage of around \$44 million per landslide (EM-DAT, 2012). However, it is important to note that EM-DAT database covers only the disastrous events when they fulfil one of the following criteria: 10 or more people reported killed, 100 or more people reported affected, there was a call for international assistance or there was a declaration of state of emergency.

The hazard events in mountain regions often show disastrous dimensions. It indicates that there is a need for improvement of preventive measures and early warning systems. Advanced development and improvement of risk management, especially increased knowledge of processes inducing hazards and improved risk prediction, is required (Glade & Crozier, 2005; Van Asch et al., 2007). Although various methods to carry out quantitative landslide risk analysis are available (Bell & Glade, 2004), in most cases they are based on empirical cause-effect analysis of the events which occurred in the past (historical data). This approach does not give sufficient information to predict and identify changes in hazards caused by changes in hydro-geomorphological characteristics of the area (Van Beek & Van Asch, 1999; Van Beek, 2002).

Water plays an important role in mass movement processes and hydrological triggers are a common mechanism of initiation and reactivation of landslides. Variations in groundwater level result from fast (e.g., rainfall, infiltration) and slow (e.g. deep bedrock flows) hydrological processes (Iverson, 2000). However, despite improved monitoring techniques and notion of landslide dynamics (McDonnell, 1990; Haneberg, 1991; Uchida, 2001; Kirchner, 2003; Bogaard et al., 2004; Malet et al., 2005; Tromp-van Meerveld & McDonnell, 2006; deMontety et al, 2007; Wienhöfer et al, 2011) our understanding of the hydrological processes in landslides is still incomplete, especially when dealing with infiltration and percolation processes, subsurface flowpaths and residence time of landslide groundwater (Bogaard et al., 2004; Van Asch et al., 2007).

1.2 The role of hydrology in mass movement processes

1.2.1 General principles of slope instability

Gravity, mobilised friction, buoyancy and seepage are the forces that work on a soil body. The potential soil movement is resisted by the shear strength of the soil that can be mobilised along the slip surface. The mobilised shear strength (τ) of a soil is commonly approximated using the Mohr-Coulomb equation:

$$\tau = c + \sigma' \cdot \tan(\varphi) \quad (1.1)$$

c = cohesion [kPa]

φ = angle of internal friction [°]

$$\begin{aligned}
 \sigma' &= \text{effective normal stress [kNm}^{-2}\text{]} \\
 \sigma' &= \sigma - u \\
 \sigma &= \text{total normal stress [kNm}^{-2}\text{]} \\
 u &= \text{pore water pressure [kNm}^{-2}\text{]}
 \end{aligned}
 \tag{1.2}$$

The shear strength describes the magnitude of the shear stress (i.e. gravitational forces) that a soil can sustain as the result of friction and cohesion forces. Cohesion and angle of internal friction are material properties and can be measured in laboratory experiments.

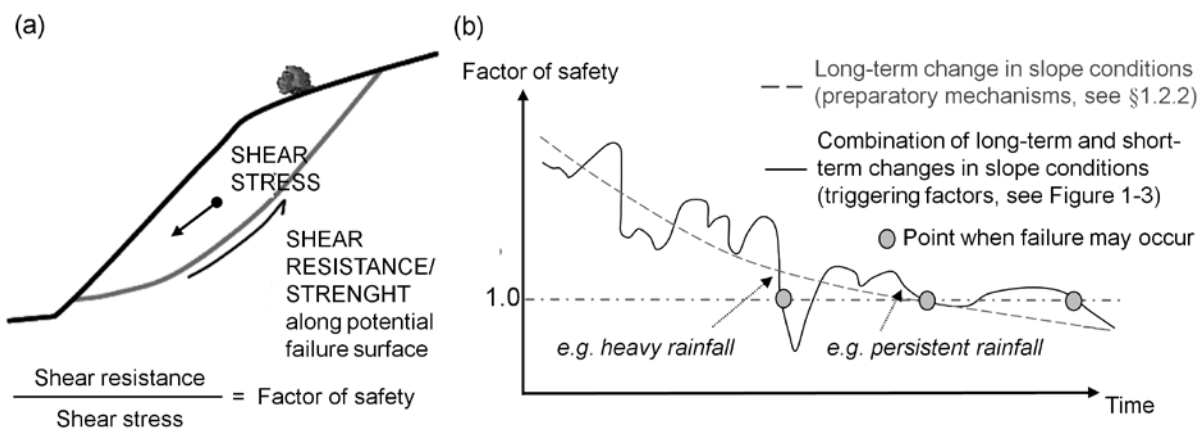


Figure 1-2. (a) Forces working on the slope; (b) Triggering condition of the precipitation induced landslides (Nettleton et al., 2005).

The ration between maximum shear strength calculated with Mohr-Coulomb model and gravity - induced shear stress (factor of safety, f_s) is a conventional measure for slope stability (Figure 1-2a). When the shear stress mobilises the maximum shear strength ($f_s=1$) failure is imminent.

1.2.2 Landslide causes and triggering

A lot of research has been dedicated to the causes of landsliding also called as preparatory mechanisms (e.g. Varnes, 1978; Crozier, 1986; Hutchinson, 1988; Wieczorek, 1996). These are the cumulative events which make a slope unstable or marginally stable (Figure 1-2b). In general, the causes of slope movement can be grouped into two subdivisions (e.g. Chandler, 1986; Gostelow, 1996; Bogaard, 2001):

- *internal causes* – reduction of frictional force caused by changes in water regime (e.g. pore pressure increase) or decrease of material strength properties (e.g. weathering, internal erosion);
- *external causes* – increase of gravitational shear stresses by changing the slope geometry (e.g.: slope erosion, undercutting the slope), vibration (e.g.: tectonic activities, earthquakes) and changes in surcharges (e.g.: vegetations, buildings, increase weight because of wetting).

As summarised by Bogaard (2001), “the difference between triggering and slope instability causes is the time domain”. Causes are long-term, often simultaneously existing, processes while the trigger is a short- time event that results in a nearly–immediate response of mass movement (Figure 1-2b and Figure 1-3). In other words, triggers are those events, or conditions, that actually initiate movement of the slope.

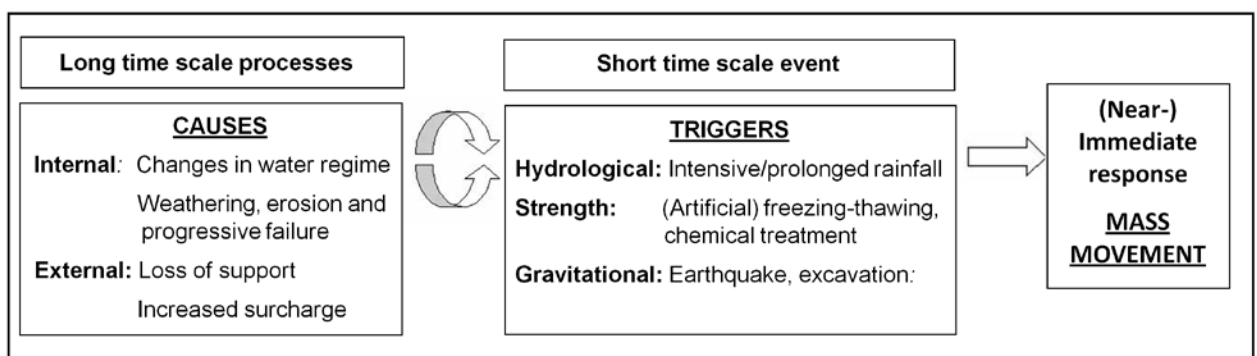


Figure 1-3. Examples of mechanisms (causes and triggers) initiating landslides.

1.2.3 Precipitation induced landslides

Precipitation induced landslides refer to landslides triggered by infiltration and the resultant transient changes in the hydrological systems. The most common and known hydrological triggering mechanism occurring in both shallow and deep–seated landslides is related to an increase in pore water pressure resulting in a decrease in an effective stress and internal strength of slopes (Van Asch et al., 2007). The increase of pore water pressure necessary to initiate slope movement is proportional to the depth of the slip surface (Bishop, 1954).

With the exception of a moist unsaturated zone in a shallow landslide, precipitation has limited predictive value for groundwater level fluctuations in hillslopes and thus for landslide activity (Bogaard, 2001; Bogaard & Van Asch, 2002; Hencher, 2010). The unsaturated zone controls groundwater recharge allowing for the loss of soil moisture by evaporation and

attenuation of percolation. It also provides preferential flow paths (formed by soil fauna, by plant roots, soil erosion, etc; Beven & German, 1982) for infiltrating water (Bogaard & Van Asch, 2002; Hencher, 2010). The quantification of groundwater recharge, especially by means of preferential flow, is a research challenge for an advanced understanding of hydrological systems in hillslopes and landslides (Savage et al., 2003; Coe et al., 2004; Van Asch et al., 2007; Weiler & McDonnell, 2007). The main difficulties stem from heterogeneity of landslide lithology and spatial and temporal variations of hydraulic properties. Additionally, in slow-moving landslide, (constant) movement of the sliding material results in fissure formation due to compression and extension, providing preferential flow paths for infiltrating water. This creates a dual-permeability network with dynamically changing hydraulic properties.

1.3 Preferential fissure flow

1.3.1 Definition of preferential flow

The term preferential flow refers to “mechanisms where transport of water (...) is primarily associated with a smaller fraction of the total pore network, at any scale much larger than the microscopic scale” (Alaire et al., 2009). In other words it describes “all phenomena where water and solutes move along certain pathways, while bypassing a fraction of the porous matrix” (Hendrickx & Flury, 2001). Three types of preferential flow can be distinguished (Figure 1-4):

- rapid macropore flow (e.g. Beven & German, 1982) that may result from bio-pores (formed by the soil fauna or by plant roots), cracks in clayey soil or soil aggregates, as well as from natural soil pipes;
- unstable finger flow (e.g. Ritsema & Dekker, 1994; deRooij, 2000), occurring in finger-shaped regions, that is the result of wetting front instability mainly caused by water repellency, soil layering or air entrapment;
- funnel flow (e.g. Roth, 1995; Ju & Kung, 1997) which is the redirection of the main flow over sloping layers, lenses or stones.

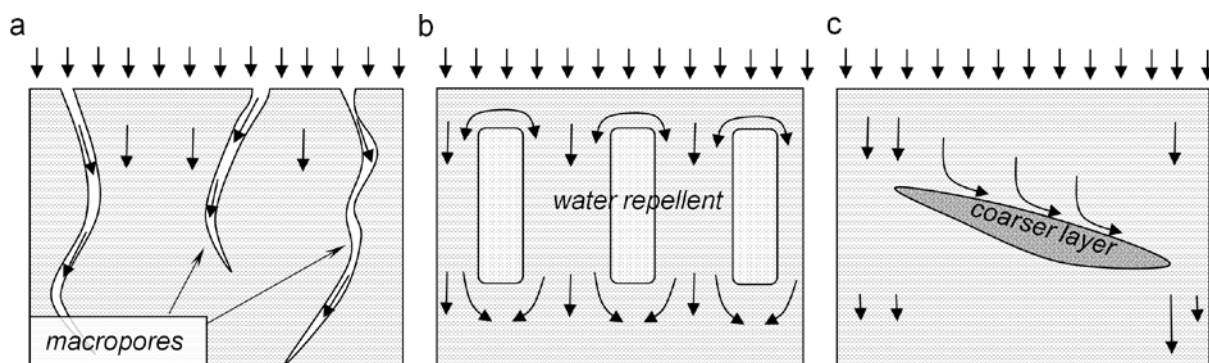


Figure 1-4. Schematic representation of different types of preferential flow: (a) macropore flow – flow through the highly permeable macropores, (b) finger flow due to repellency difference - lateral water flow to the fingers at the soil surface, vertical finger flow down to the subsoil, spread of the fingers in the lower subsoil, (c) funnel flow – redirecting of water flow by sloping layers of coarser or lower permeability material, flow accumulation at a lower region.

Many field studies show that preferential flow is widespread phenomena being more the rule than the exception (Flury et al., 1994; Steenhuis et al, 1996; Ritsema & Dekker, 2000; Roulier & Schulin, 2008). Preferential flow may strongly affect temporal and spatial behaviour of local hydrological regimes. It influences soil water availability, groundwater level fluctuation and water distribution within the catchment. For a review of finger flow and funnel flow the reader is referred to Van Schaik (2010).

The focus of this research is on preferential macropore flow related to geo-mechanically induced cracks in slow-moving mudslide – fissure flow.

1.3.2 Macropore flow

There is not a standard definition that characterizes a given soil pore as a macropore (Beven & German, 1982; Allaire et al, 2009). However, it can be generalised that macropores refer to structural pores which are much larger than the average soil matrix pores (Greco, 2002) and drain mainly by gravitational forces (not influenced by capillarity). Initiation of macropore flow depends mainly on antecedent soil moisture content, rainfall amount and intensity, hydraulic conductivity of the soil matrix, density and distribution of macropores and soil texture (Bouma, 1990; Trojan & Linden, 1992; Weiler & Naef, 2003). Macropore flow can be initiated either at the soil surface or from (partially-) saturated soil layer, when the rainfall or percolation intensity exceeds the infiltration rate of the lower soil layer. The interaction between macropores and the surrounding soil-matrix depends on soil matrix properties, soil

water content and the properties of macropores and matrix-macropore interface (Weiler & Naef, 2003).

The effectiveness of macropores for transmitting water downslope depends upon their size, spatial distribution, and connectivity (Beven & Germann, 1982; McDonnell, 1990; Cameira et al., 2000; Nobles et al., 2004). The larger the macropores are, the more water they can potentially conduct or store, depending on the connectivity between macropores. The macropores themselves are not considered to be continuous throughout the soil profile or the hillslope. It is more likely that they are separated by matrix blocks located at the endpoints of the individual macropores (e.g.: Noguchi et al., 1999; Sidle et al., 2001; Figure 1-5). In this way, the macropore connectivity and transmissivity depends on the water content in the separating matrix stretches, and the degree of macropore effectiveness increases with wetness (Tsuboyama et al., 1994; Sidle et al., 2000, Van Schaik et al., 2008). However, despite field evidence, laboratory experiments and analytical research, the relationship between soil moisture and macropore connectivity is qualitative only (Nieber & Sidle, 2010) and its quantification remains difficult.

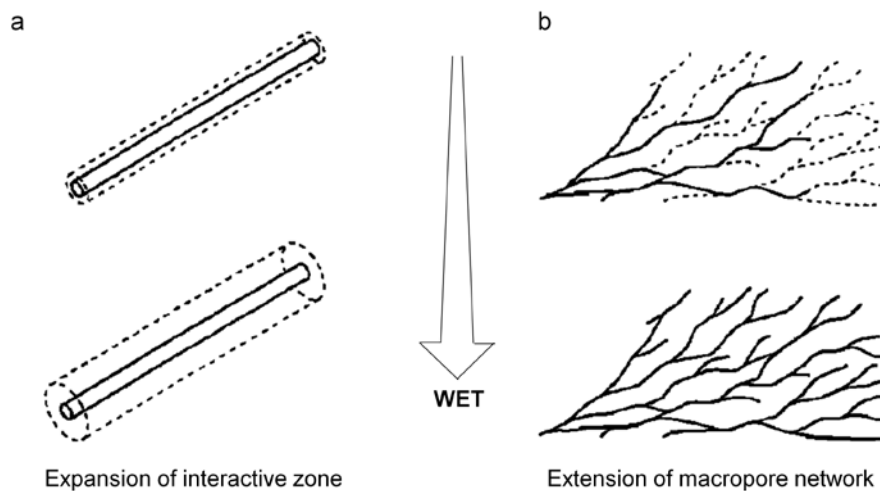


Figure 1-5. Conceptual model of (a) an expansion of surrounding soil that interacts with water in macropores and (b) the extension of macropore network with increasing wetness of the soil (Tsuboyama et al., 1994).

1.3.3 Fissure formations

The terms fissure and crack are often used as synonymous to refer to a variety of surface discontinuities (Fleming & Johnson, 1989; Cruden & Varnes, 1996; Walter et al., 2009). In this thesis the term 'fissures' is used to refer to geo-mechanically induced cracks, creating

surface discontinuities observed on natural slopes. These fissures can be filled or partly filled with reworked material (Figure 1-6).

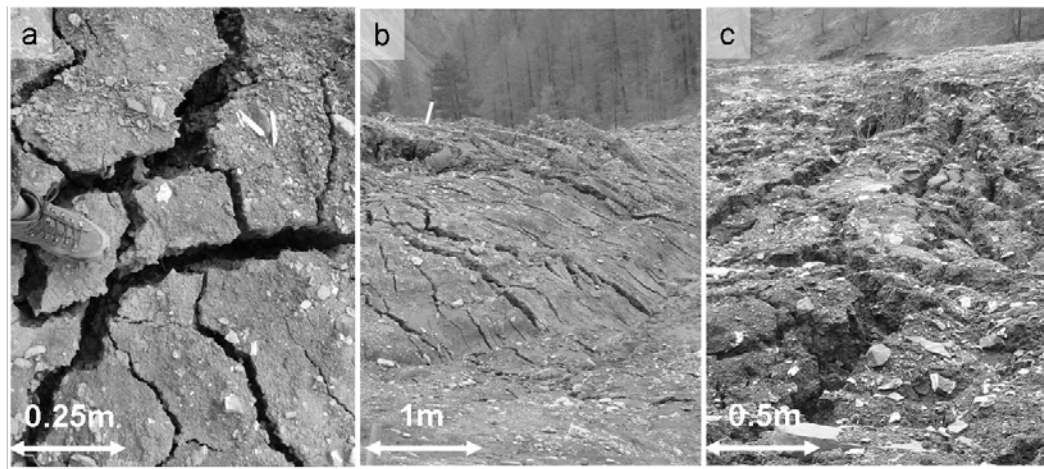


Figure 1-6. (a) Open fissures; dry matrix on the surface but saturated at the bottom of the fissures; (b) Dry fissures; (c) Wet fissures, filled or partly filled with reworked material. Pictures were taken during the field campaigns at Super-Sauze landslide in May and July 2008.

The location and morphology of the fissures within a landslide corresponds to mechanical processes. There are three basic modes of fissure propagation: tensile opening, sliding and tearing (Figure 1-7a; Anderson, 2005; Schulson & Duval, 2009). The occurrence of tension fissures depends on the bedrock topography, lateral bedrock boundary, cavity and slope changes (Wilhelm, 1975). Mudslides often display typical fissures patterns (e.g., Keaton and Graff, 1996; Figure 1-7). These patterns, together with landslide material characteristic and knowledge about landslide geometry allows for mechanical interpretation and classification of the fissures (Stumpf et al., *submitted*):

- Transversal tension fissures and open shears between blocks (also called traction fissures), associated with the tension and shearing in the areas with significant changes in slope angle (e.g. in upper part, close to the scarp);
- Diagonal shear-tension fissures, resulting from shear stresses between the areas characterised with different displacement rate (i.e. boundary site of landslide), on the sides. This type of fissures runs in accordance with the shear strain conditions. They start from the solid rock (or stable area) boundary in the direction of the sliding body with an angle of 30°-45° up the slope which is in accordance to other research observation (Wilhelm, 1975; Hambrey & Alean, 1994).

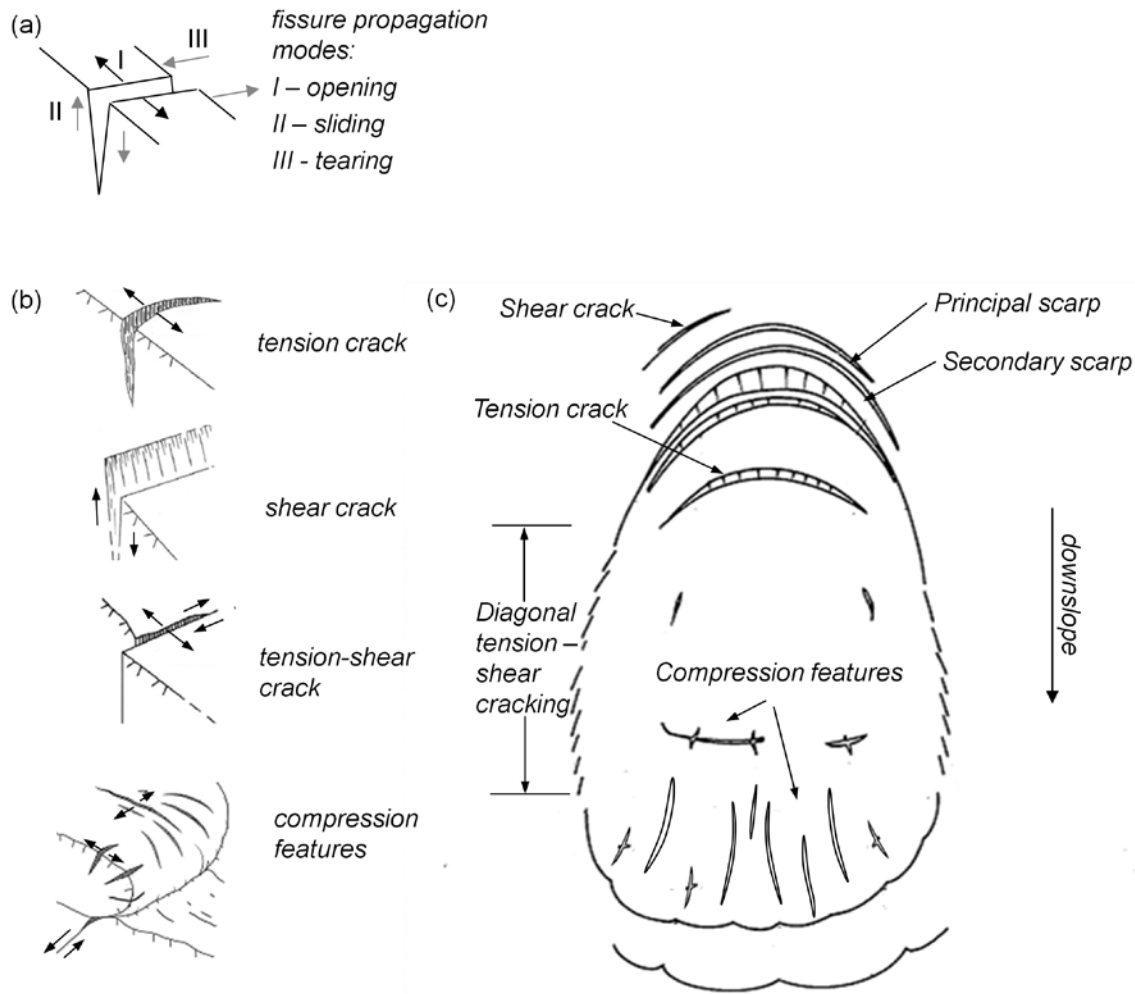


Figure 1-7. (a) Models of fissure propagation (Stumpf et al., *submitted*); (b) Typical surface fissures patterns and (c) their spatial occurrence within mudslide (modified after Keaton and Graff);

- Longitudinal and transversal fissures resulting from compressive stress and lateral extension (e.g. accumulation zone).

In case of landslides with more complex geometry the combination of all the surface fissure types can be observed throughout landslide area.

1.3.4 Influence of fissure flow on landslide hydrology

The term ‘preferential fissure flow’ is used to refer to rapid water flow in fissures bypassing the bulk flow of the less pervious matrix (Beven & German, 1982; Hendrickx & Flury, 2001). Fissures are a special case of macropores with apertures that vary from few millimetres up to tens of centimetres. The importance of macropore flow for slope hydrology (including slope stability) was recognised in the early 1980s (Pierson, 1983; Brand et al., 1986) and has

subsequently been receiving a great deal of research attention (Tsuboyama et al., 1994; Noguchi et al., 1999; Nobles et al., 2004; Nieber & Sidle, 2010).

Various authors reported adverse and beneficial effects of macropore flow (including fissure flow) on landslide activity (McDonnell, 1990; Van Beek & Van Asch, 1999; Fannin et al., 2000; Uchida et al., 2001; Hencher, 2010). The presence of fissures may influence storage capacity of the soil and affect the infiltration processes of rainfall and snow melt by re-routing surface and subsurface water flow paths (Figure 1-8). Fast flow through fissures may increase the rate of vertical infiltration, providing direct access to the lower groundwater and increasing the rate of groundwater recharge. On the other hand, an extended fissure network may increase the rate of natural soil drainage, which limits the build up of water pressure. However, when dead-end fissures are present, once their storage capacity is exceeded, they contribute to maintaining high pore water pressures in the surrounding soils (McDonnell, 1990; Van Asch et al., 1996; Uchida et al., 2001; Hencher 2010). In general, the importance of the influence of fissures on local hydrological regimes depends on fissure system geometry: fissures density and their volume.

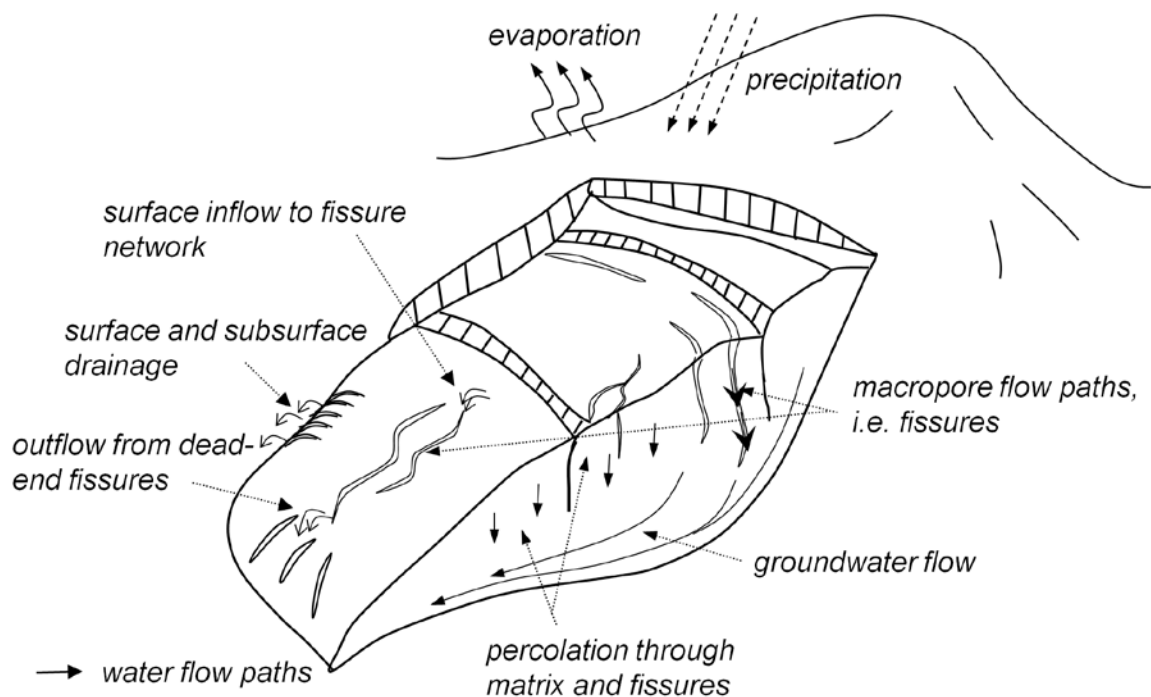


Figure 1-8. Macropore preferential flow path (i.e. fissure flow) in landslide, schematisation of simplified landslide profile.

1.3.5 Monitoring of preferential flow processes

Preferential flow processes can be studied at different spatial scales: from micro-scale studies of pore structure, throughout core and profile scale analysis of specific conditions and processes initiating and controlling preferential flow, up to field scale monitoring (Alaire et al., 2009). As summarised by Alaire et al. (2009) “at the core and profile scales, most of the emphasis is on identifying vertical preferential flow, probably because it is easier to measure and more obvious to observe. At large scale, however, lateral preferential flow is at least as important as vertical preferential flow and the interaction between vertical and lateral preferential flow is undoubtedly a crucial aspect of preferential flow”.

The complexity of preferential fissure flow processes, and their high spatial and temporal variability, makes it very difficult to measure the processes in the field and to upscale the information to the catchment scale (Van Asch et al., 2007; Van Schaik, 2009). There are few experimental techniques that are used to gain insight into processes controlling preferential flow in the field, e.g. dye tracing (Flury et al., 1994), tension infiltrometers (Angulo-Jaramillo et al., 1996) and continuous sampling of water drainage (e.g. multi sampler Wicky lysimeter; Boll et al., 1992). The environmental tracing (Kabeya et al., 2007) and artificial tracing (Mali et al., 2007) in combination with hydrological surveying are the most convenient investigation methods in field conditions. A combination of hydrodynamic and hydrochemical responses observed during sprinkling tests can give valuable information about natural preferential water pathways (Debieche et al., 2011). However, a consistent measurement method is not yet achieved.

1.4 Hydrological modelling of precipitation induced landslide

To analyse precipitation induced landslides, governed by either unsaturated or saturated conditions, several models were proposed (Wu & Sidle, 1995; Van Beek & Van Asch, 1999; Iverson, 2000; Brooks et al., 2002; Cappa et al., 2003). Numerical codes vary from simple 1-D empirical models to complex physically based 3-D models and can involve either lumped or distributed approaches (Van Asch et al., 2007). Distributed approaches are the most suitable to account for spatial and temporal heterogeneity of the hydrological systems (e.g.: Miller & Sias, 1998) and thus, they improve forecasting of spatio-temporal probabilities of landslide occurrence (Van Westen et al, 2005; Malet et al, 2005).

Incorporating preferential flow modelling into a hillslope scale hydrological model is difficult due to the complexity of the phenomena. The main component to be defined while modelling preferential macropore flow is the nature of the flow in both matrix and macropore domain and the interaction between the two domains (Beven & German, 1982; Šimůnek et al., 2003; Van Genuchten, 2011).

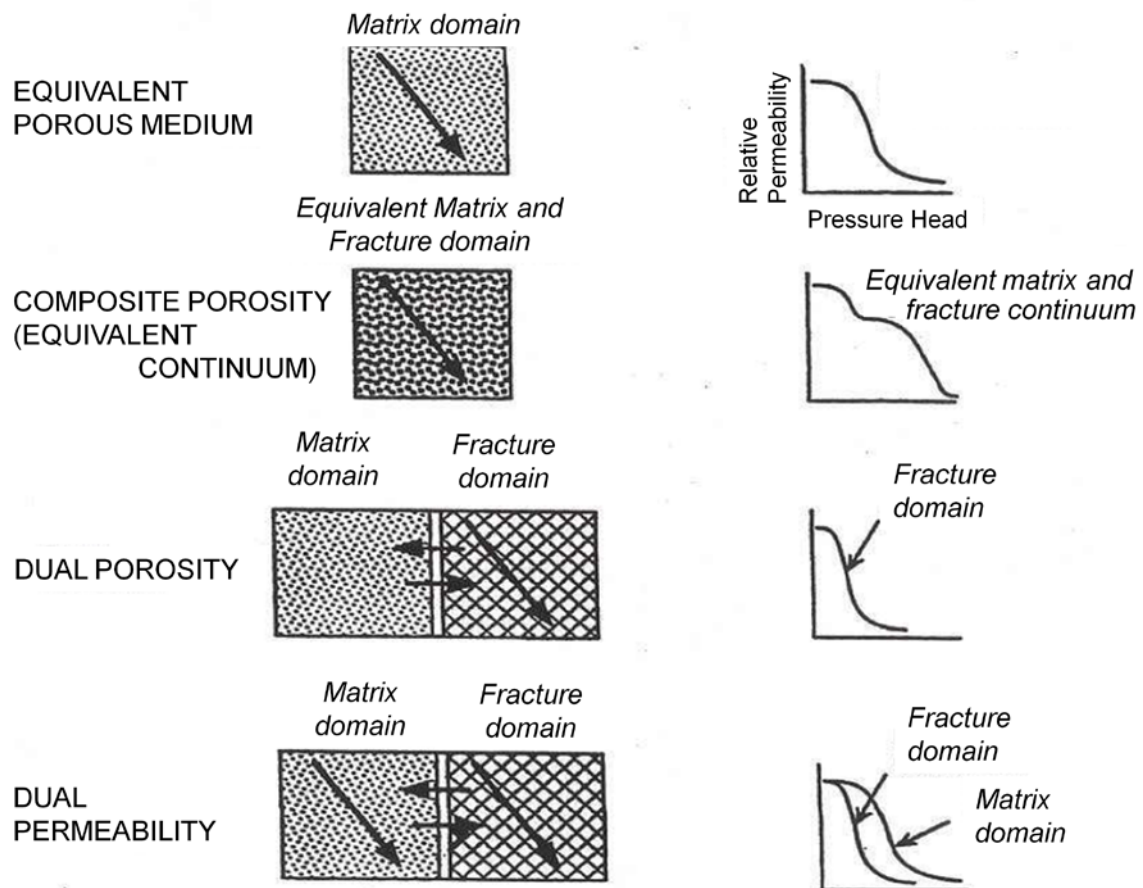


Figure 1-9. Model concepts for physically based model dealing with preferential macropore flow (Altman et al., 1996).

Most of the physically based models dealing with preferential flow can be classified in the following model concepts (Figure 1-9; Altman et al., 1996; Van Genuchten et al., 1999):

- *equivalent continuum approach* – where the Richards equation is used with composite hydraulic conductivity (permeability) curves ($k(\theta)$);
- *dual - porosity or multi - porosity approach* – which is based on Richards equation, extended with the concept of mobile (macropore) and immobile (matrix) fractions of soil water. Exchange is possible between the two fractions but no vertical flow in the

matrix domain occurs. The interaction between the two domains is usually treated as first-order linear function of pressure gradients, but infiltration models and other approaches are also used. Examples of models based on dual-porosity are presented by Zurmühl & Durner (1996) and Šimůnek et al. (1999);

- *dual - permeability approach* – where the flow occurs in both macropore and matrix domain, or more domains (multiple flow domain models) with different pore size and distinct velocities. The water flow can be treated differently for the different domains, using Richards equation, kinematic wave equation, unit hydraulic gradient assumption or tube flow assumption. Examples of models that implement dual – permeability approach are: 1D model of Gerke & Van Genuchten (1993), MACRO model (Larsbo & Jarvis, 2003) or the model proposed by Greco (2002).

Preferential flow models typically consist of two model approaches: stochastic and deterministic. Stochastic models are based on probability density functions (Kung et al., 2005), multi-component end-member mixing analysis (Christophersen & Hooper, 1992), fractal analysis (Liu et al., 2005) or time series analysis. Deterministic models are based on the Richards flow equation and the assumption of uniform flow within the particular flow domains. At the field scale, the majority of macropore flow models use deterministic methods to study water and solute transport.

At the hillslope or catchment scale preferential flow is often modelled indirectly as a simplified system with preferential vertical fluxes (e.g.: Bogaard, 2002) or rapid slope-parallel flow on the bedrock surface without taking into account the distributed nature of the soil macropores system (e.g. Beckers & Alila, 2004, Kosugi et al, 2004). Moreover, in many large scale models, preferential flow is included as a modification of hydraulic conductivity function (e.g. Mulungu et al., 2005; Zhang et al., 2006). Zehe and Blöschl (2004) proposed a threshold function to switch on macropores flow and established a linear increase of the hydraulic conductivity with increasing relative saturation of the soil for both plot and catchment scale hydrological modelling.

For the majority of the above mentioned models accounting for preferential flow results in improvement of model performance. Nevertheless, these models are largely simplified and they do not account for differences in spatio-temporal characteristics of macropore flow domain. Weiler and McDonnell (2007) stressed that incorporation of the spatially dynamic

nature of preferential flow systems for conceptualisation and parameterisation of the effect of lateral preferential flow on hillslope hydrology is one of the greatest challenge.

In 1999, Van Beek and Van Asch proposed a spatially distributed physically based model coupling hydrological and stability dynamics, developed in the PCRaster environmental modelling software package. The use of meta-language of PCRaster GIS package provides an expedient way to include and change spatially distributed hydrological and geotechnical parameters. In the subsequent development of the STARWARS model (Van Beek, 2002), fissure flow was introduced in a simple manner, allowing a fraction of the surface detention, equal the volume of free pore space (i.e. fissures), to bypass the unsaturated matrix and directly recharge the groundwater.

Since its development, the STARWARS model has been used by many researchers to study different hydrological and ecological issues for both synthetic and real case studies (Van Beek, 2002; Malet et al, 2005; Kuriakose et al., 2009; Brotsma et al., 2010). In 2005, Malet and co-authors applied the STARWARS model to the Super-Sauze landslide using the simple bypass flow scheme representing only shallow bypassing flow without fissure – matrix interaction. They concluded that accounting for fissure flow was an important improvement in modelling the hydrology of the landslide, and stressed a need for further specific research on this topic.

1.5 Objective of the thesis

The main objective of this thesis is to identify, monitor and quantify the heterogeneity of dominant hydrological processes, especially preferential flow, within landslides and to analyse the influence of fissure flow on landslide hydrology and slope stability.

The specific questions to be answered are:

1. How to monitor and quantify spatial differences in hydrological condition over the landslide?
2. How to measure and quantify preferential flow processes and their spatial variability?
3. What is the influence of fissure preferential flow on landslide hydrology and landslide activity?

1.6 Outline of the thesis

Following this introduction, Chapter 2 is the detailed description of Super-Sauze landslide. It includes the general description of geology and morphology of the Barcelonnette region and a more in-depth description of the geomorphology of the Super-Sauze landslide and its surroundings. The current knowledge about Super-Sauze landslide geometry, kinematics and hydro-geomorphology is presented and summarised.

Chapter 3 and Chapter 4 investigate the potential of distributed temperature sensing (DTS) and small-scale sprinkling tests to monitor, study and quantify the spatial and temporal differences in soil moisture patterns (Chapter 3) and dominant hydrological processes (Chapter 4) related to the presence of preferential flow (i.e. fissure flow) at field scale.

The first step into modelling of preferential fissure flow and its influence on landslide hydrological responses is made in Chapter 5, where a conceptual model of fissure flow is presented and tested on a simplified landslide. The model accounts for feedback between hydrology and the dynamic nature of fissure connectivity.

In Chapter 6, the conceptual model of fissure flow is applied to model the hydrology of the Super-Sauze landslide. In addition to the hydrological feedback tested in Chapter 5, the model includes mechanical feedback: the relationship between the volume of fissures and the level of landslide activity expressed as factor of safety.

Finally, Chapter 7 synthesizes all findings and gives some recommendations for future work.

1.7 Mountain Risks project

The research outlined in this thesis originates from the Mountain Risk project which is a Marie Curie Research Training Network “Mountain Risks: From prediction to management and governance” in the 6th Framework Program of the European Commission (Contract MCRTN-035798; <http://www.unicaen.fr/mountainrisks>). The main goal of the Mountain Risks project was to promote research and training in all aspects of mountain hazards and risks assessment, as well as management. This European network intended to develop an advanced understanding of how mountain hydro-geomorphological processes behave and to apply this knowledge for long term cohabitation with these hazards.

The Mountain Risk Project involved 14 partners' institutes throughout Europe each hosting Post-Doc and Ph.D position. Mountain Risk was coordinated by the Department of Physical Geography and the Environment, University of Caen-Basse-Normandie, Caen, France and the CNRS.

Chapter 2

THE SUPER-SAUZE LANDSLIDE – STATE OF THE ART

The monitoring, quantification and modelling of dominating hydrological processes and their distributions within landslides require a large amount of field data and knowledge of landslide geometry, geomorphology and its kinematics. Therefore all field experiments and data collections have been carried out at the Super-Sauze mudslide located in the Barcelonnette basin, in Southern French Alps, that has been extensively surveyed by the School and Observatory of Earth Science (Strasbourg, France) and University of Caen Basse-Normandie (Caen, France). On-site measurements of meteorological characteristics, hydrological responses and hydrological parameters began in 1991. The displacements of the landslide are observed also since 1991 by combining topometrical and GPS survey of a network of ca. 40 benchmarks, extensometer observations at one location (since 1999), aerial-photographs analysis and since 2007 by terrestrial photographs and terrestrial laser scan acquisitions. In 1996 geophysical and geotechnical investigation (dynamic penetration tests, percussion drillings, pressuremeter tests, inclinometer survey) combined with a photogrammetric analyses was initiated in order to determine the structure of the accumulated mass.

2.1 Location and climate

The Barcelonnette basin is located about 100 km north of Nice, in the department 'Alpes-de-Haute-Provence', in the middle reach of the Ubaye River. The basin extends over an area of 200 km²: 22km length (W-E) and maximal 10 km width (N-S). The region has an elevation between 1100 m a.s.l. and 3100 m a.s.l (Figure 2-1b). The valley is drained by several torrents on the North- and South-facing slopes which confluence with the Ubaye River.

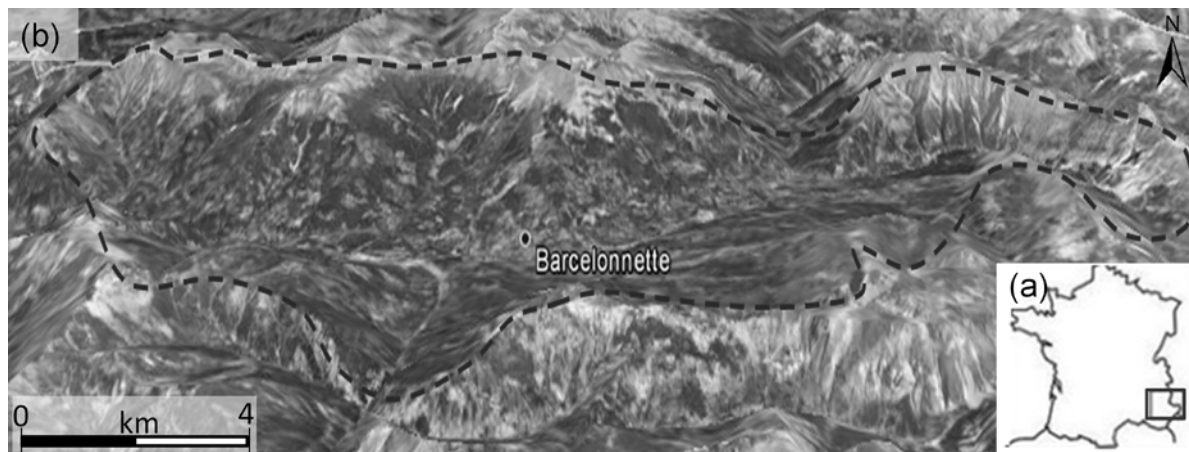


Figure 2-1. (a) Location of Barcelonnette basin in France; (b) the area of French Alps with indication of the borders of Barcelonnette basin.

The landscape of the Barcelonnette Basin is characterised by badland-type morphology with successions of crest and gullies (Figure 2-2). In addition to the erosion activity of glaciers (Figure 2-3a), intense torrential erosion by the Ubaye River has progressively carved out the landscape. Additionally, the intense agricultural activities (nearly complete deforestation during the 18th and 19th century) increased torrential activity.

The Barcelonnette Basin belongs to the dry intra-Alpine zone. The area is characterised by (1) a mountainous climate with a high mountain irradiance ($> 2700 \text{ h. year}^{-1}$), summer drought, strong inter annual rainfall variability ($400\text{--}1300 \text{ mm. year}^{-1}$ over the period 1928–2010) and approximately 130 days of freezing per year (Maquaire et al., 2003), (2) a Mediterranean influence with high storm intensities ($\text{over } 50 \text{ mm.h}^{-1}$) during summer and autumn, and (3) a continental influence with significant daily thermal amplitudes ($>20^\circ$) and numerous freeze – thaw cycles. The annual average temperature at 1140 m a.s.l (Barcelonnette) is 9.6°C (over the period 1928–2002; Malet, 2003). These climatological settings give rise to weathering and mechanical degradation of soil surface lithology.

2.2 Geological setting of Barcelonnette basin

The geological environment of the Barcelonnette Basin is very complex. It constitutes a geological window, bearing the autochthonous bedrock of Callovo-Oxfordian black marls (so-called ‘Terres Noires’) under the allochthonous Eocene sheet thrusts (Autapie and Parpaillon flysch), made of strong limestone or sandstone formations (Figure 2-3b; Maquaire et al., 2003). The thickness of the black marls reaches 250-300 m and it comprises four subsets (Maquaire et al., 2003; Remaître, 2006): some rare outcrops of Argovian black marl (20 - 30 m thick), the Upper Oxfordian black marl (80-150m thick), the Middle and Lower Oxfordian black marl (150 - 250 m thick) and the Callovian black marl with detrital plates (80 - 100 m thick).

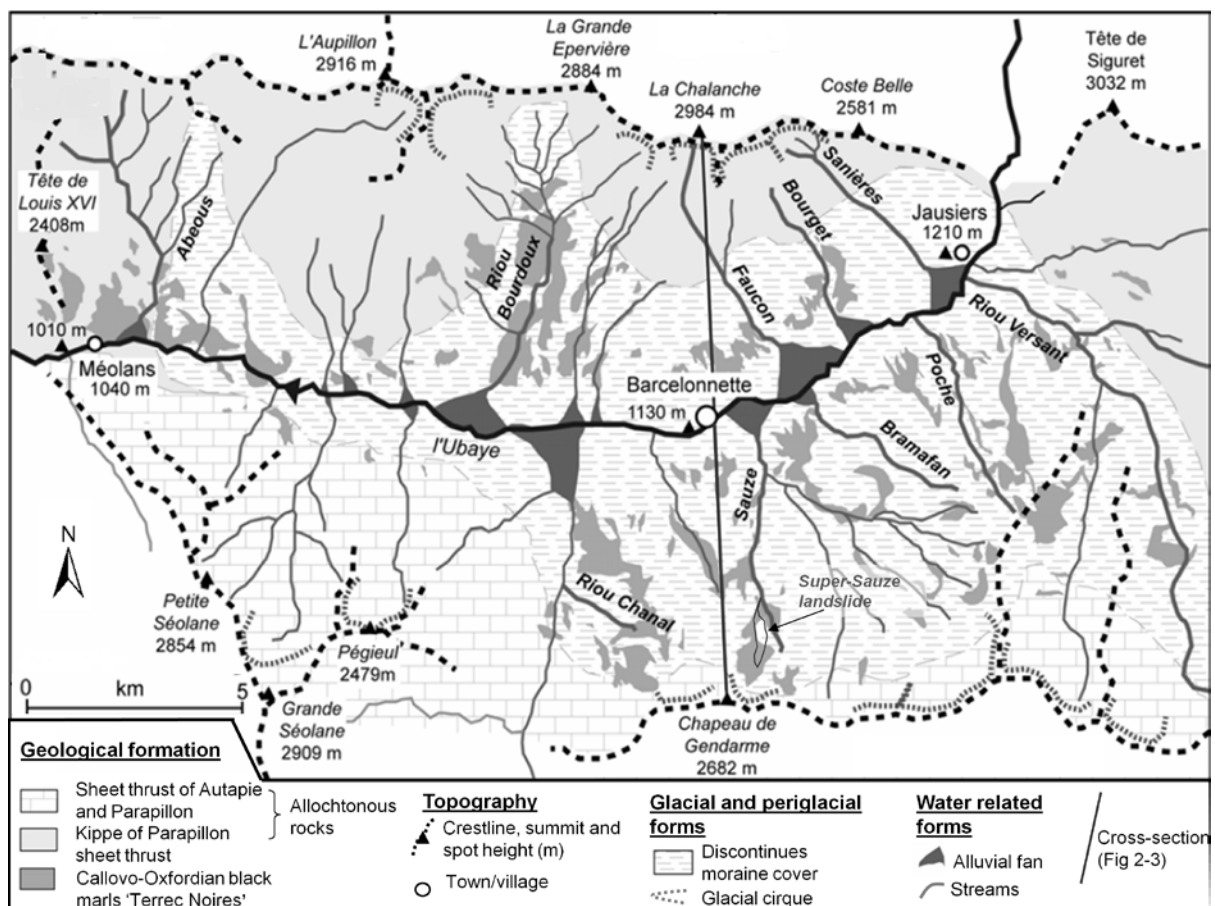


Figure 2-2. Simplified geological map of the Barcelonnette basin (Maquaire et al., 2003)

The Barcelonnette basin was heavily affected by a glacial cover during the Würm glaciations (Figure 2-3). Many glacial landforms and deposits are common in the Ubaye valley: terraces, rock glaciers, bows and cords, moraine ‘roche moutonnées’. Glacial and periglacial deposits, very rich in fine matrix, overlaid the impermeable marly substrate especially on the shady side

(Flageollet et al., 1999). The thickness of the morainic deposits is approximately 10-20 m. The glacial erosion deepened valleys and subsequent fluvial erosion incised the valleys even more, making it prone to landslide and erosion. Consequently, large slope failures and extended badlands are integrated part of the Barcelonnette Basin landscape and slope instabilities are one of the most common geomorphological hazards in the Barcelonnette basin (Weber, 1994; Flageollet et al., 1996).

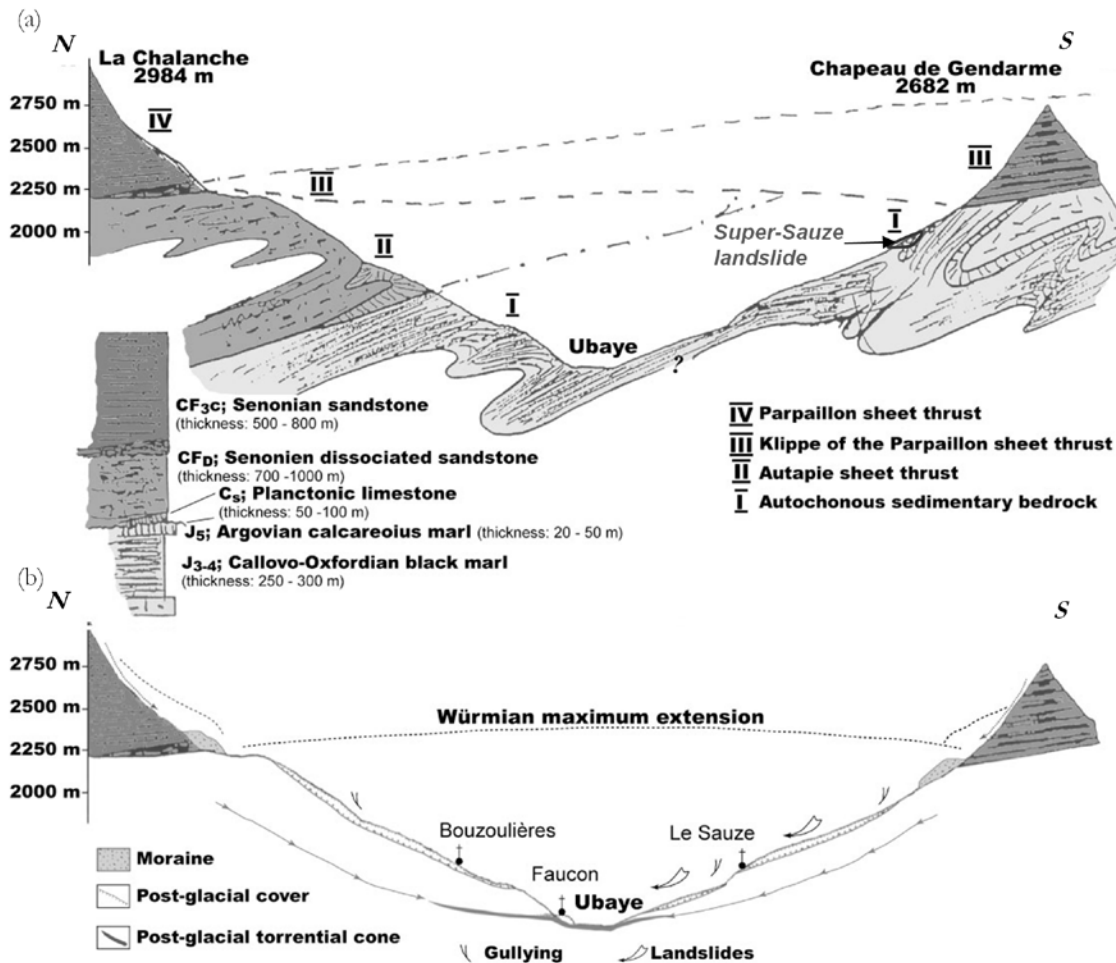


Figure 2-3. Geological cross- sections of the Barcelonnette basin (Maquaire et al., 2003).

2.3 Development and geometry of the Super-Sauze landslide

2.3.1 Evolution of the Super-Sauze landslide

The Super-Sauze mudslide has developed on the south slope of the Barcelonnette Basin (Figure 2-2). Before initial failure, the scarp was affected by a deep seated slope deformation

controlled by regional faults. The initiation of the slope movement started in the 1960s with a succession of shallow plane and wedge failures as well as falls of blocks and structural slides at the interface between moraine and autochthonous black marls. The accumulation of material started in late 1970s and it progressively filled the Sauze torrent thalweg (Malet et al., 2000). There were two main morphological processes noticeable in the landslide development: uphill regression of the main scarp by mass movements (rockfalls and landslides), and the downslope development of the mudslide. Figures 2-4 and 2-5 show the main stages of geomorphological evolution of the mudslide.

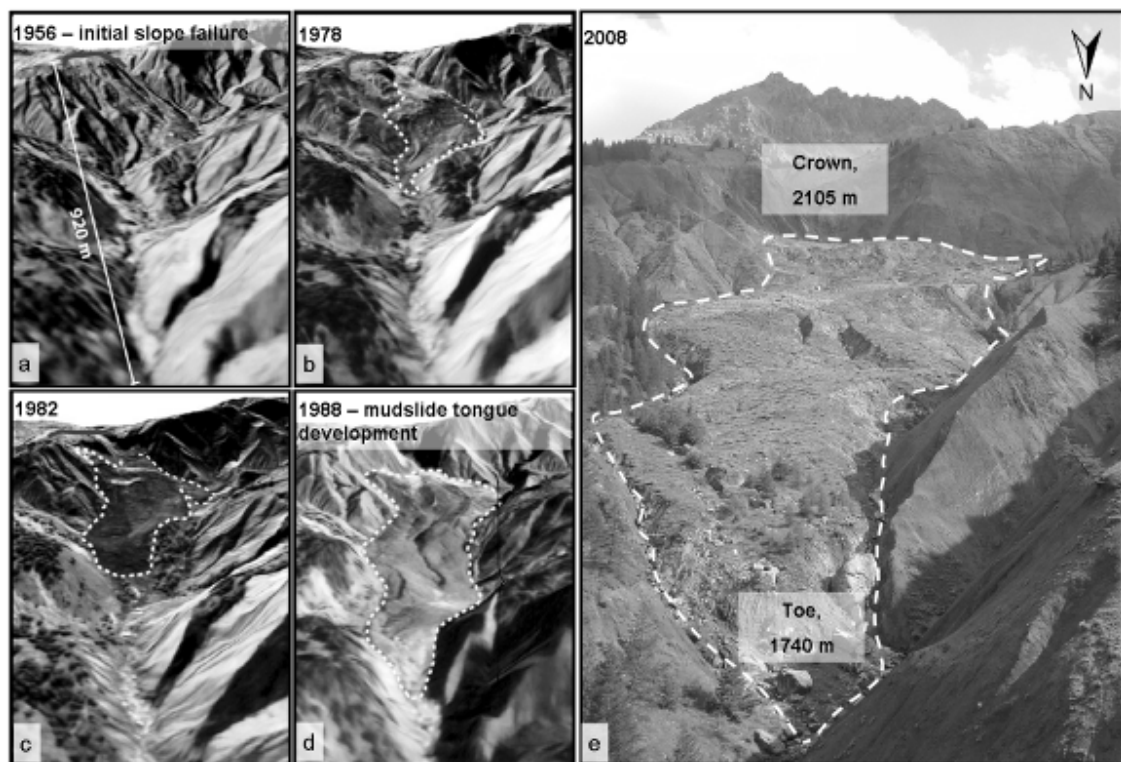


Figure 2-4. Geomorphological evolution of the Super-Sauze landslide: (a) start of slope failure in 1956, (b) the extension of the accumulated material from 1978 onward, (c) and (d) the movement of the toe (adapted from Travelletti & Malet, 2012); (e) the Super-Sauze mudslide in 2008, All pictures taken from the downslope, North of the landslide.

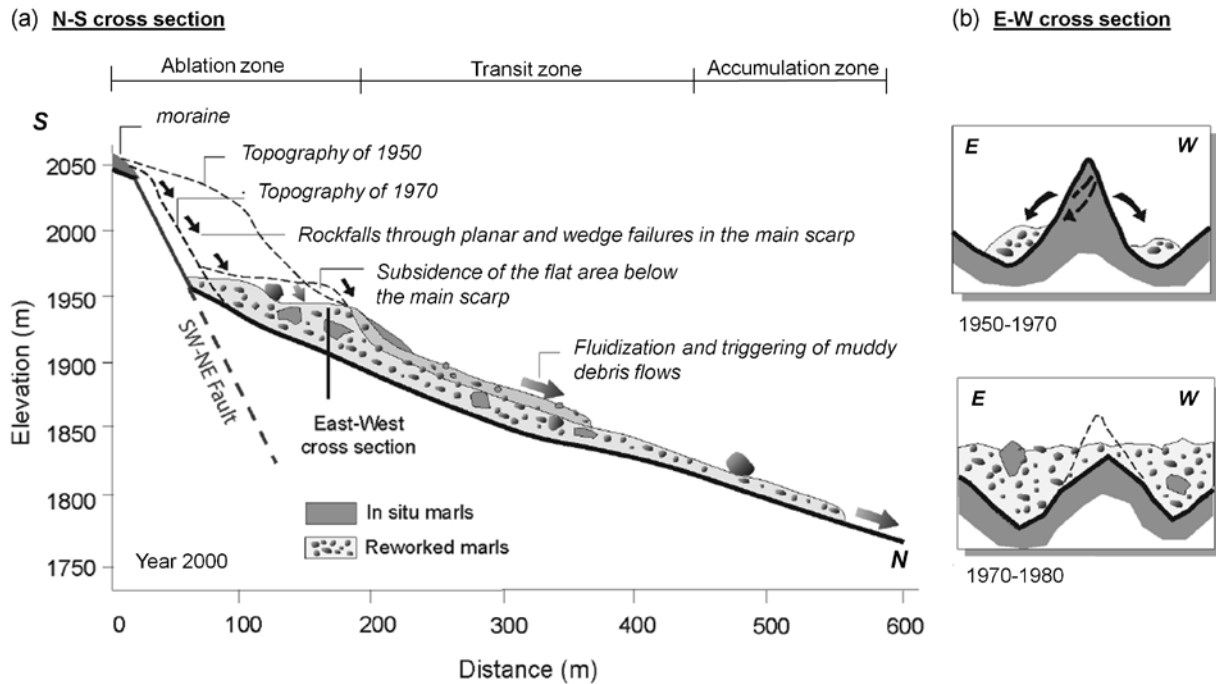


Figure 2-5. Development of the Super-Sauze landslide: North-South (a) and East-West (b) cross sections (Malet et al., 2000)

In 2008 (Figure 2-4e) the Super-Sauze landslide extended over a distance of 920 m from its highest point at an elevation of 2105 m a.s.l. (the crown), to its base at an elevation of approximately 1740 m a.s.l. (toe of the flow) with the average width of 135 m. It covers 0.17 km² of surface with average slope of 25°. The total volume of the landslide is estimated at approximately 560 000 m³ (Travelletti & Malet, 2012) and the maximal depth of the sliding surface is approximately 20 m. The topography covered by the mudslide is composed of sub-parallel crests and gullies (Figure 2-4, Figure 2-5b and Figure 2-6). Some of them emerge from the mudslide, whereas others are located a few meters below the ground surface.

The upper part of the landslide – ablation zone – consists of the crown, the main scarp, and so-called ‘upper shelf’. The crown is covered with moraine deposit (several meters thick) and on top of that a rock and scree deposit has developed (Figure 2-6). The main scarp of the landslide consists of *in-situ* black marls of about 80-100 m high and is inclined at approximately 70° (Figure 2-5a). The rockfalls commonly occurring in this area cumulate in the upper shelf and feed the main landslide mass. The upper shelf (between 1930 and 1970 m) appears as a field of marly blocks at different stages of weathering, with black marls panels buried in a very heterogeneous matrix formation. The upper shelf ends in a secondary scarp in reworked material (Figure 2-6).

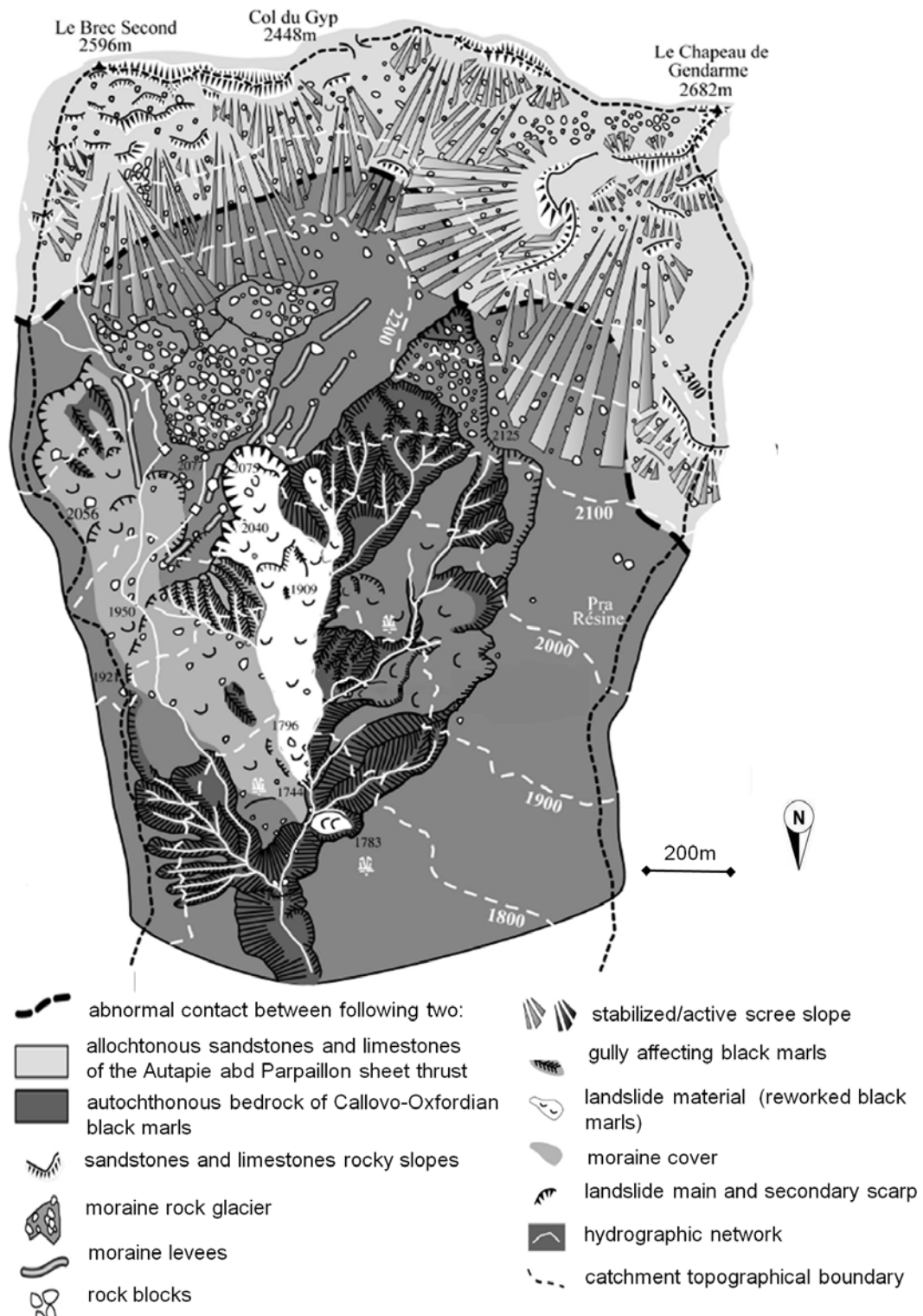


Figure 2-6. Geomorphological map of the Super-Sauze landslide area (Malet, 2003)

The middle part of the landslide – transit zone – is characterised by an average slope of 23° . It consists of strongly heterogeneous clayey material, reworked blocks and panels of marls at various stages of weathering, clasts of all sizes and silty-clay matrix with calcite and moraine blocks (Figure 2-10; Malet et al., 2003). The grain size of the material decreases while progressing downstream, corresponding to more advanced stages of disaggregation (Malet et al., 2003). The transit zone is the most active area of the landslide with average annual surface velocities reaching 0.05 m.d^{-1} . The occurrence of fractures, e.g. tension cracks, traction fissures, is very common in this area.

The lowest part of the landslide - accumulation zone - ends in the valley. The accumulated material is compressed and affected by shear cracks. It is partly eroded by the Sauze torrent, however, the erosion processes do not stop the downstream progression of the toe of the landslide which is approximately $0.004 - 0.009 \text{ m.d}^{-1}$.

2.3.2 Geotechnical structure of the Super-Sauze landslide

The geotechnical surveys of the Super-Sauze landslide consisted of: borehole analysis, dynamic penetration tests, in-situ pressiometric and water injections tests, soil sampling for laboratory testing, inclinometer measurements and aerial photography analysis (Genet & Malet, 1997; Flageollet et al., 2000; Weber & Herman, 2000; Schmutz et al., 2001; Malet et al., 2003). Based on these investigations, a first interpretation of the Super-Sauze landslide geometry was proposed by Fageollet et al. (2000) and Malet (2003).

Based on the mechanical properties, three layers can be distinguished in the internal structure of the Super-Sauze landslide (Figure 2-7 and Figure 2-8). The surficial layer (C1) with thickness ranging between 5 to 9 m, is a very wet viscous formation, very active from a hydrological and mechanical point of view (see also section 2.4, and Figure 2-11). For hydrogeological analysis this layer can be divided in two sub-layers, C1a and C1b, depending on the seasonal position of the groundwater table and the shape of paleotopography. The deeper layer (C2) with the maximum thickness of 10 m, is a compact, plastic and stable formation, associated to a 'dead body' (see also Figure 2-11). These layers overlay the bedrock composed of autochthonous black marls (S - substratum).

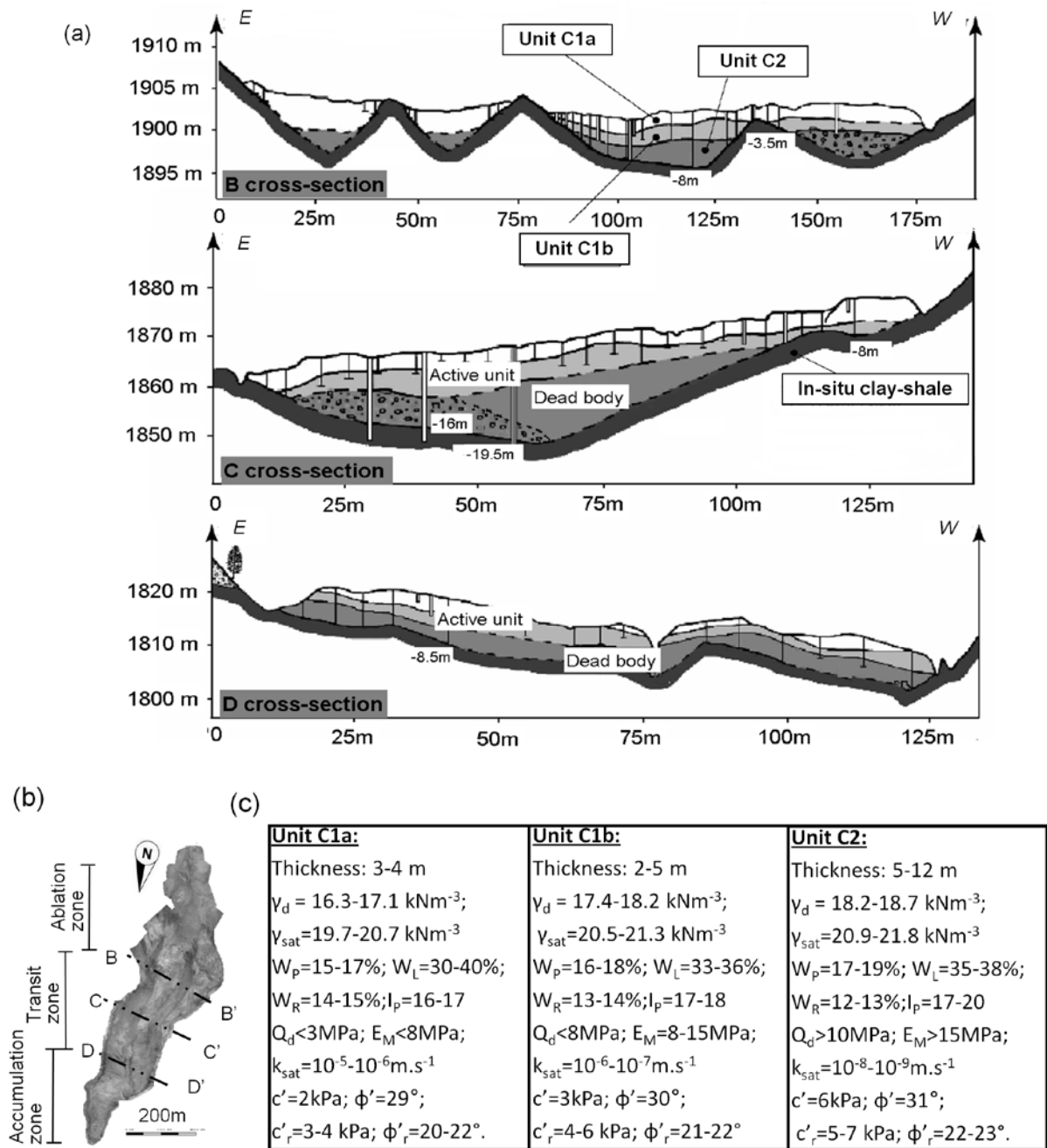


Figure 2-7. (a) The internal structure and geometry of the Super-Sauze landslide (after Malet, 2003); (b) location of cross-sections; (c) The mechanical properties of the three layers. The meaning of the symbols is as follow: γ_d – dry unit weight, γ_{sat} – saturated unit weight, W_p – plastic limit, W_L – liquid limit, W_R – shrinkage limit, I_p – plasticity index, Q_d – cone tip resistance, E_M – pressiometric modulus, k_{sat} – saturated conductivity, c' – effective cohesion, ϕ' – effective angle of friction, c'_r – the residual cohesion, ϕ'_r – the residual angle of friction.

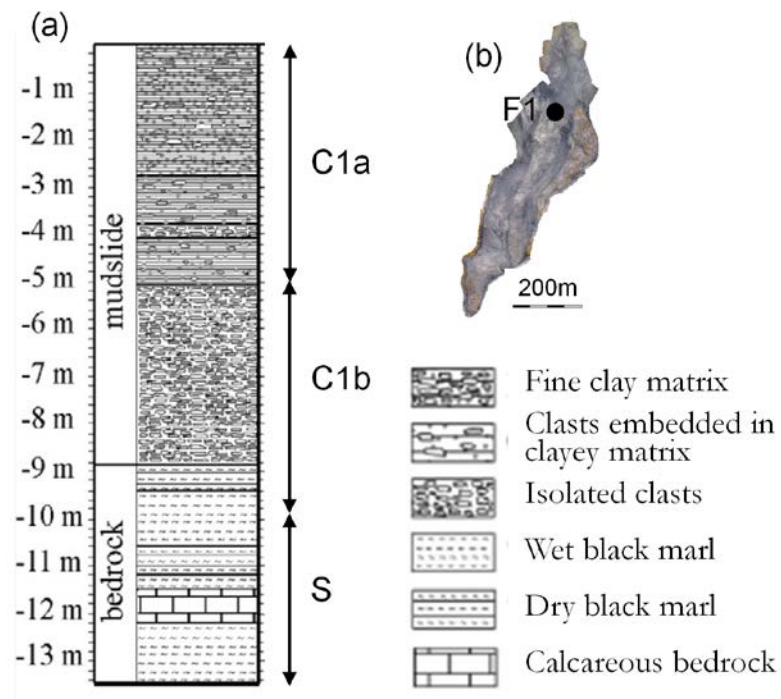


Figure 2-8. (a) An example of internal vertical structure derived from inclinometer measurements at the borehole F1 (Malet, 2003); (b) localisation of the F1 borehole; note that at this position the layer C2 is not observed (see also Figure 2-9).

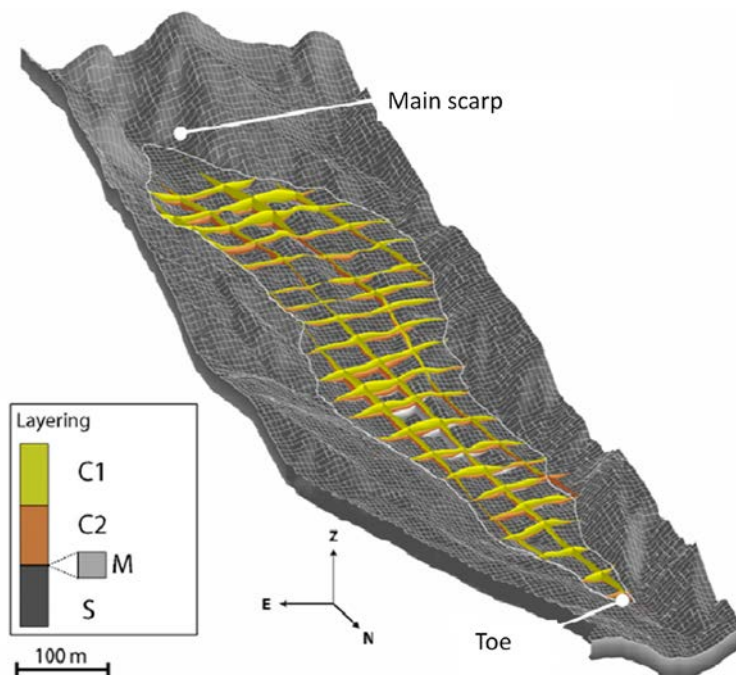


Figure 2-9. 3D geometrical model of the Super-Sauze landslide illustrated through stratigraphic cross-sections (from Travelletti & Malet, 2012). Layer M is the moraine deposits in the main channel at the pre-failure stage.

The soil surface is highly irregular and affected by cracking due to mechanical tension (fissures from around 0.5 m to more than 1.0 m deep) (Figure 1-6 and Figure 2-13).

Between 2004 and 2009 26 2D electrical resistivity tomography profiles were done in order to improve the knowledge about the spatial distribution of geotechnical and geological characteristics (Schmutz et al., 2001; Grandjean et al., 2007; Méric et al., 2007). This spatial information was integrated with all other available data and consequently, a 3D characterization of the geometry of the Super-Sauze landslide was proposed (Travaletti & Malet, 2012; Figure 2-9).

2.4 Kinematics and hydrology of the Super-Sauze landslide

2.4.1 Landslide kinematics

The surficial displacement of the Super-Sauze landslide is monitored since 1991 with monitoring network consisting of topometric, permanent differential Global Positioning System (dGPS) and extensometer (Weber, 2001; Malet et al., 2002). Moreover, the long-term kinematics of the landslide was studied with aerial photographs (1956-2000) allowing to produce digital topography models with horizontal accuracy of 2 to 7 m and vertical accuracy of 1 m (Figure 2-4 and Figure 2-5; Weber & Herrmann, 2000; Malet, 2003).

The activity of the ablation zone is the effect of regularly occurring rock falls and landslides involving volumes of a few cubic decimeters to several thousand cubic meters (Weber & Herrmann, 2000; Malet, 2003). Additionally, isolated rock falls occur regularly throughout the year. These rockfalls continuously provide material for the ablation zone. The pathways of the moving material, in the middle part of the landslide, are vertically delimited by buried parallel crests and gullies. The surface displacement rates vary significantly over the landslide area. The highest average surface displacement rates, around 0.05 m.d^{-1} , are observed in the middle of the upper part of the landslide and they decrease when moving downslope and to the edges of the landslide (Figure 2-10). The Western part of the landslide is the most stable part with surface displacement rate smaller than 0.002 m.d^{-1} . The long-term behavior is characterized by continuous movements with a seasonal trend of two acceleration periods (with velocities up to 3 m.d^{-1}) in spring and autumn, and two deceleration periods in summer and in winter (Malet, 2003; Travaletti et al., 2012).

Based on the inclinometer measurements (geotechnical survey, section 2.3.2) velocity profiles were computed (Figure 2-11; Malet, 2003). The mudslide exhibits a complex style of movement, associating strong displacements along an internal slip surface, located within the reworked landslide body, superimposed by a plastic-state body (with a shear rate estimated at $10^{-10} \text{ m.s}^{-1}$ assuming a 5-m thick unit) and a solid-state body on top.

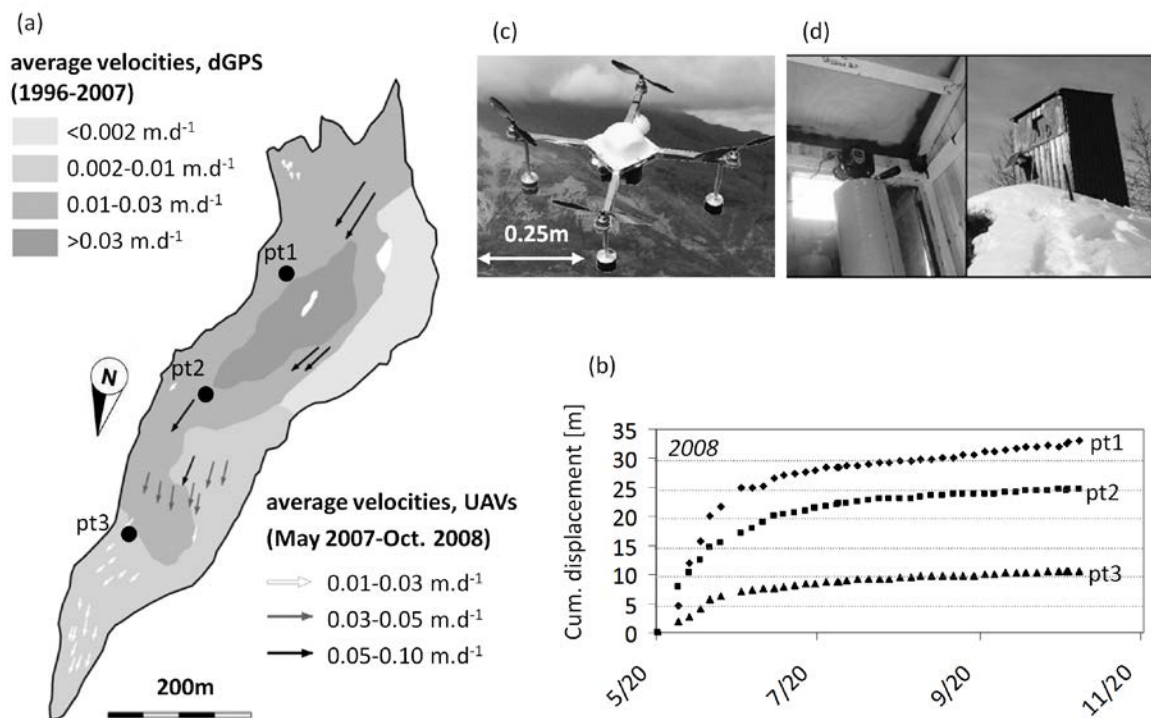


Figure 2-10. (a) The Super-Sauze landslide with average surface velocities monitored by dGPS (1996-2007) and the horizontal surface displacement vectors based on UAVs photography (modified after Malet, 2003 and Niethamer et al., 2011); (b) Cumulated displacements at three locations in the upper (pt1), middle (pt2) and lower (pt3) parts of the landslide based on correlated images (Travelletti et al., 2012a); (c) the UAV and (d) terrestrial optical photography monitoring system.

Currently, landslide kinematics is continuously monitored by differential Global Positioning System (dGPS) and, from 2007, by a remote camera monitoring system based on optical images analyses with a normalized Image Correlation technique (Travelletti et al., 2012a). Moreover, the landslide is a test site for implementation of radio controlled unmanned aerial vehicles (UAVs) for making high-temporal and spatial resolution aerial photography for monitoring of displacement dynamics and occurrence of small landslide features, such as fissures (Niethammer et al., 2012). The results coming from different techniques mentioned above are comparable and are summarized in Figure 2-10.

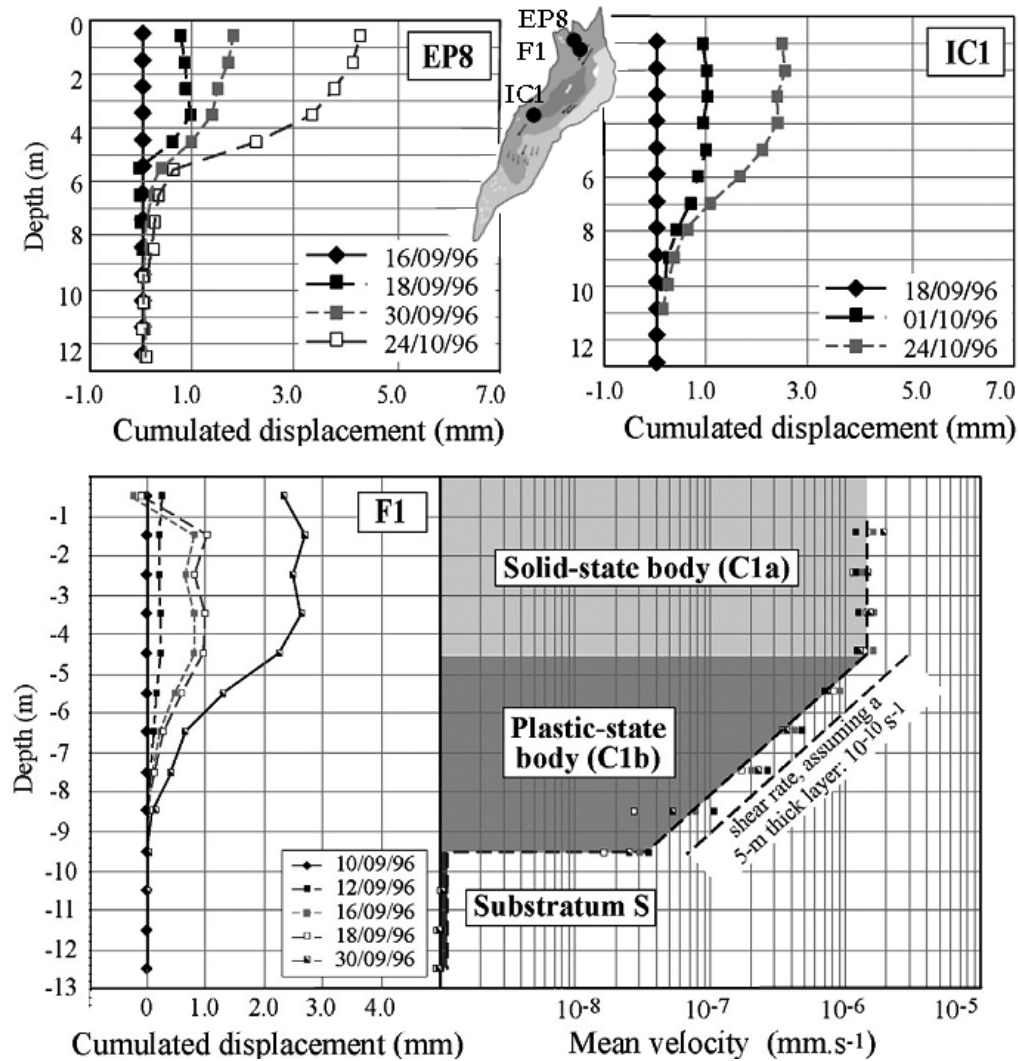


Figure 2-11. The vertical profiles of displacement and velocities at three boreholes locations (Malet, 2003); note that at the position of F1 borehole layer C2 is not observed.

2.4.2. Landslide hydrology

The monitoring of hydroclimatic conditions and hydrology of the Super-Sauze landslide began in 1991 (Fageollet et al., 2004). The monitoring equipment installed in the landslide changed over the years but generally it consists of: 1) monitoring groundwater with pressure cells and open standpipes with different filter depths, several of which equipped with automated recorders, 2) monitoring of soil moisture content by use of several time domain reflectrometry (TDR) sensors placed at different depths and 3) a full meteorological station located 800m from the landslide.

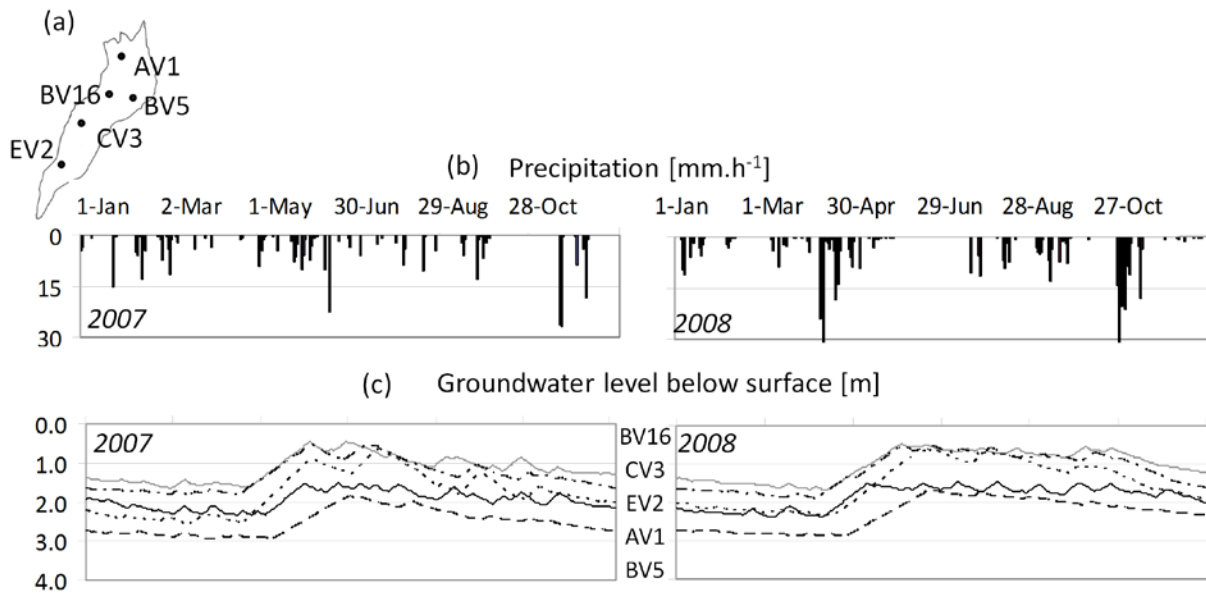


Figure 2-12. Example of groundwater level fluctuation observed in 2007 and 2008: (a) localisation of the piezometers within the Super-Sauze landslide; (b) observed precipitation; (c) observed groundwater level.

The main water bearing layers are C1a and C1b units (see Figure 2-7a), and the eastward and westward streams may be considered as lateral boundaries of the landslide system (Figure 2-13a). The average groundwater table is between -0.5 and -1.5m in the upper parts of the landslide and it slowly decreases while moving downslope. In the western part of the landslide the groundwater table is between -2.5 m and -3.5 m (Malet et al., 2005).

The heterogeneity of the material and local surface mass movement processes (e.g. small surface mudflow accumulation lobes, local runoff wash deposits) explain important variation of porosity (from 0.33 to 0.49) and vertical hydraulic conductivity (from 10^{-8} to 10^{-4} m.s⁻¹) over the area (Malet, 2003; Malet et al., 2005). The observed range of hydraulic conductivity values classifies the material as semi-permeable.

On the basis of geomorphological observations (grain size and soil surface characteristics) and soil hydraulic properties and long-term groundwater level observation, Malet et al. (2005) divide the Super-Sauze mudslide into three hydro-geomorphological units (Figure 2-13). The upper unit (HG1) is characterised by very rapid piezometric response and large groundwater level variations at the event scale (up to 0.5 m) and relatively medium variation at the yearly time scale (0.5 to 1 m). The soil texture of the HG1 unit consists of silty sand with gravel and pebbles. The percentage of coarse fragments varies from 10 to 30 % and the size of these coarse fragments is 2-5 cm. The extended network of surface fissures filled or partly filled

with loosely packed material is present in this area providing the paths for fast preferential infiltration. The lower unit (HG2) has modest short-term (i.e. event time scale) groundwater level fluctuations (0.05 to 0.30 m) but relatively high seasonal variation (0.1- 2.5 m). Infiltration processes occurs mainly through the matrix porosity since fissure systems have limited horizontal and vertical extent. This area is covered with a finer fragmented structural crust of sandy silty texture, including some clasts or calcite fragments. Finally, the HG3 unit, on the western side of the upper (HG1) unit, is the most stable part of the landslide with very limited groundwater level fluctuations (centimetres) on both long-term and short-term time scale. Within this unit reworked material and debris flow deposits are covered with dense and compacted clayey - silty texture depositional crusts. There is negligible vegetation cover throughout the area, with exception of the stable western part (HG3) of the mudslide where some shrubs grow.

Groundwater originates mostly from rainfall and snow melt infiltration both in the soil matrix and in large fractures. There is also water recharge from the moraine aquifer, fed by rock glacier located upstream (Figure 2-5) and torrents bordering the landslide, but they do not influence the groundwater level variation (Malet et al., 2005). Therefore, inputs (rainfall, snowfall) and outputs (surface water, evaporation) of the saturated zone represent the annual mass balance of the hydrological system (Malet et al., 2005; deMontety et al., 2007).

The hydrochemical analyses and geochemical modelling performed by de Montety et al. (2007) give insights about the water circulations in the Super-Sauze landslide (Figure 2-13). This survey reveals the existence of deep water sources along the major faults providing very highly mineralized water. However, besides the hydrochemical consequence, this deep source water has limited contribution in building up the pore water pressure. Furthermore, the spatial distribution of major cations and anions (Mg^{2+} , SO_4^{2-} , Ca^{2+} and Na^+) in the groundwater system along the landslide profile (i.e. flow line) combined with long-and short-term variation of local pore pressure and water quality gave indications for the dominated hydrological processes along the landslide: preferential flow dominating in the upper part of the landslide (the upper part of the transit zone) and matrix flow dominating in the lower part (accumulation zone) while the ablation zone could be seen as a 'transition' zone (Figure 2-14).

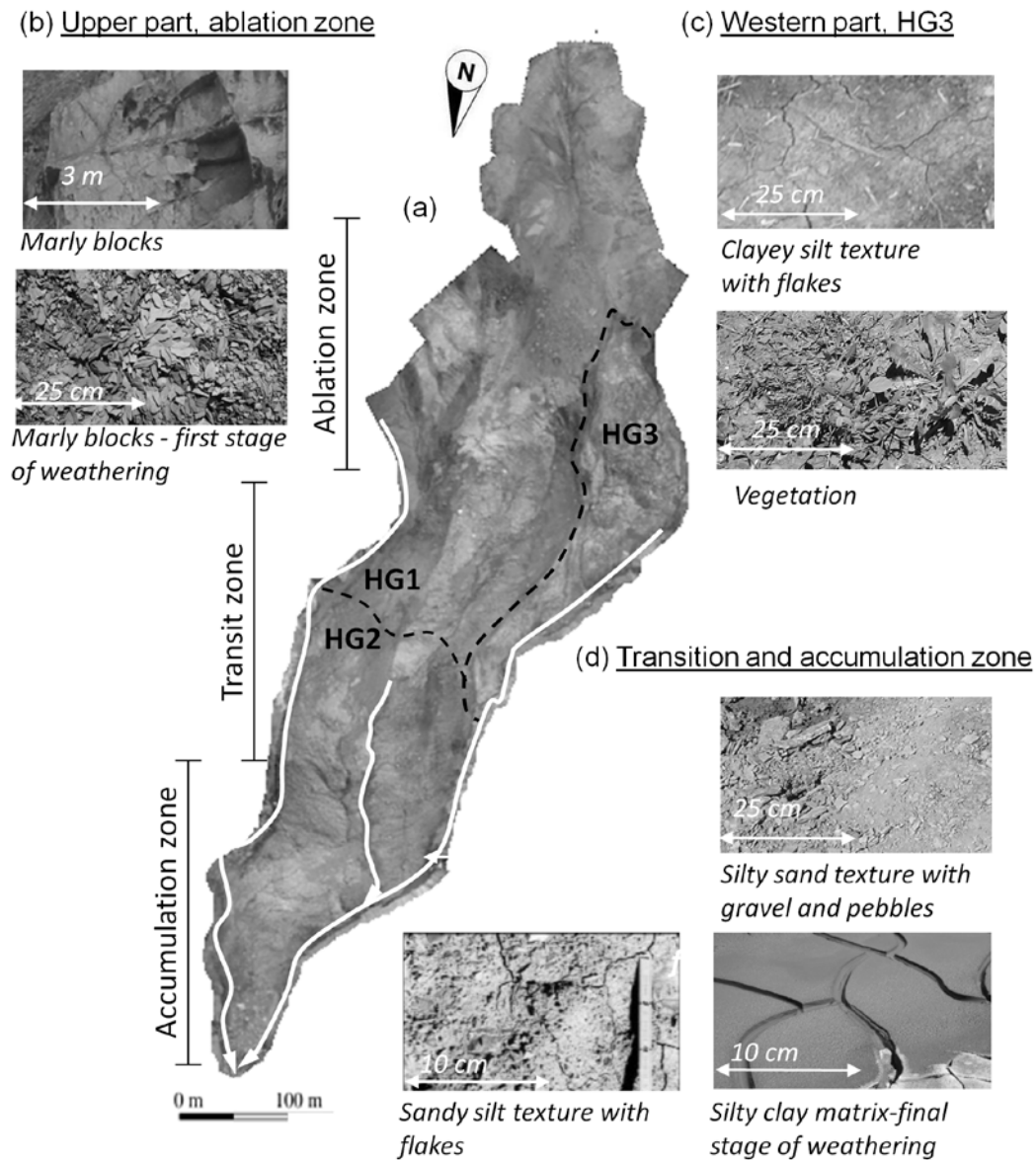


Figure 2-13. (a) Boundaries of the hydro-geomorphological units of the Super-Sauze landslides and (b,c,d) examples of soil surface characteristics observed across the Super-Sauze landslide (Malet, 2003); the white lines indicate the main streams.

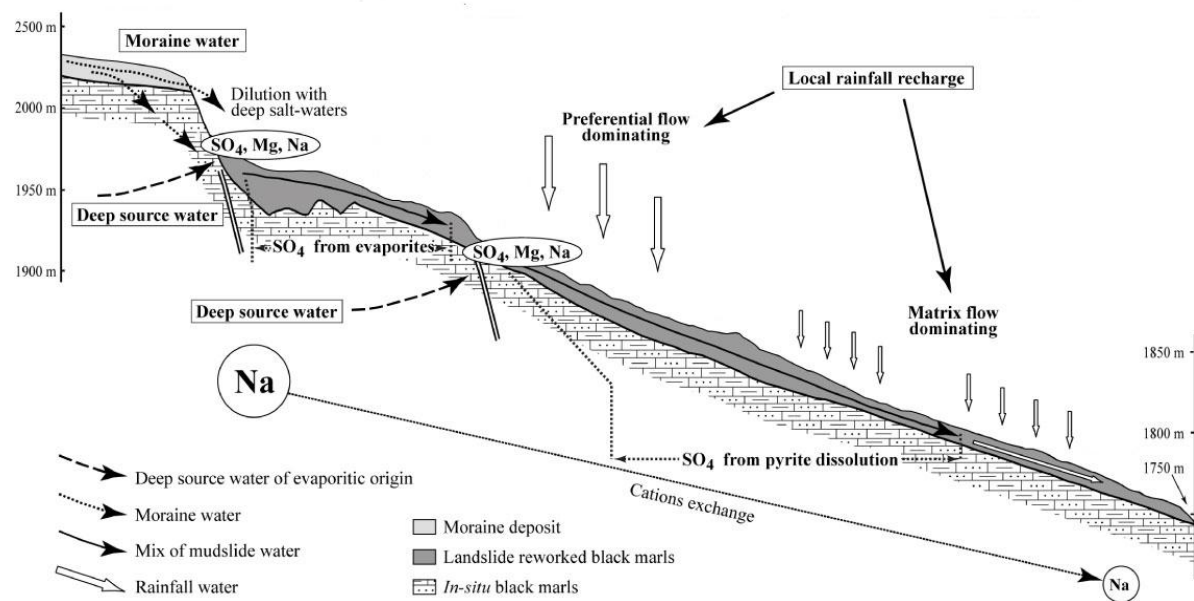


Figure 2-14. Hydrological concept of the Super-Sauze mudslide as interpreted from hydrochemical analysis (deMontety et al., 2007).

2.4.3 Relationship between kinematics and hydrology

Hydrology is the main controlling factor of the mudslide activity. The mass movement occurs as a consequence of groundwater table rise and hence the development of positive pore pressure (Figure 2-15; Malet, 2003).

As stated in section 2.4.1 the landslide kinematics show seasonal trends with two acceleration periods (spring and autumn) and two deceleration periods in summer and winter (Figure 2-15). This variation in landslide surficial displacement rates correlate with the hydrological behaviour at both the annual (Figure 2-15a) and event scales (Figure 2-15b). During a pore pressure decrease the landslide velocity decreases, however cessation of the movement is not observed.

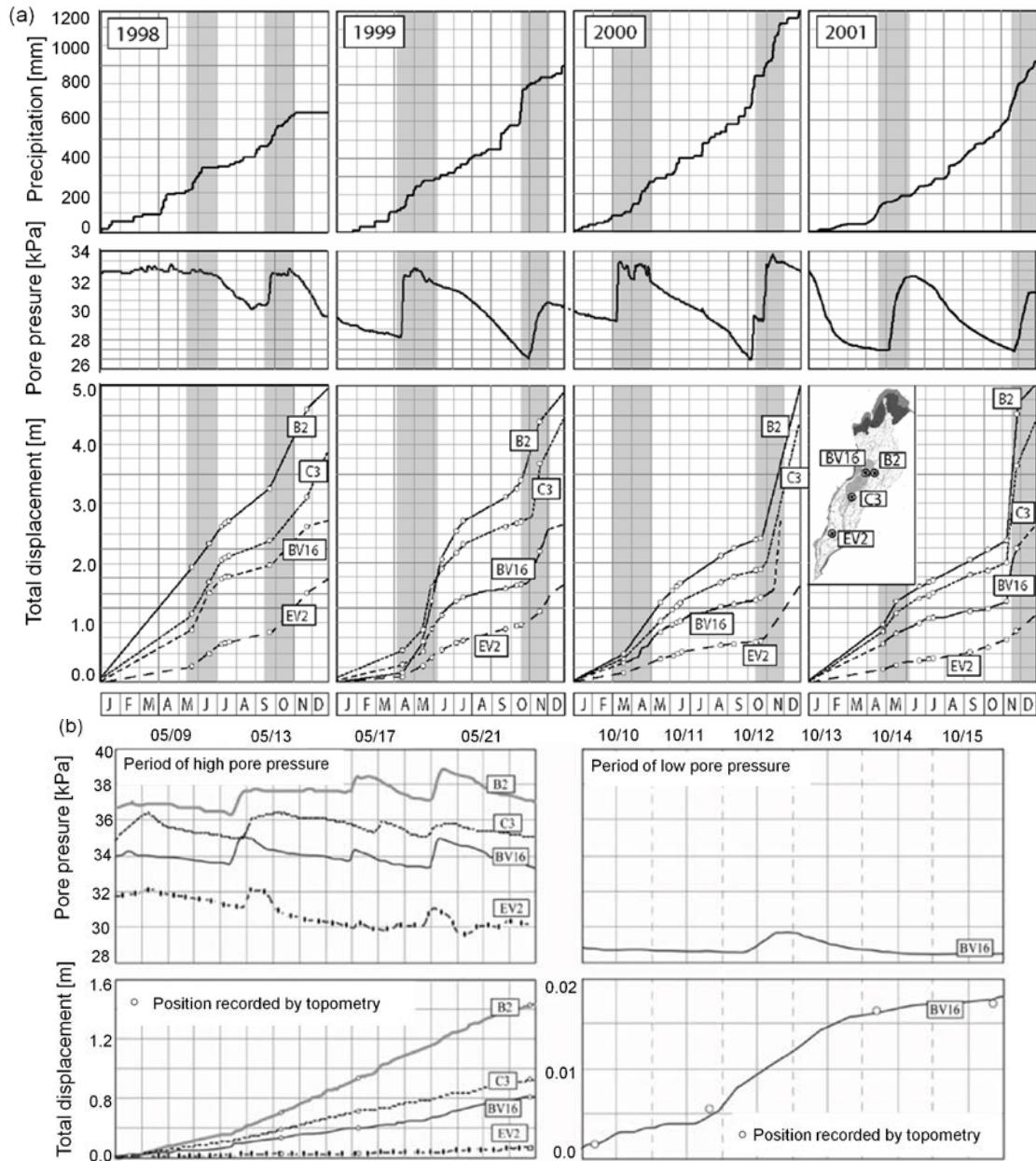


Figure 2-15. Relationship between surface displacement, pore water pressure and precipitation monitored at four boreholes within the Super-Sauze landslide at both the (a) annual scale (1998-2001) and (b) event scale (1998) (Malet, 2003). Gray areas indicate spring's and autumn's acceleration periods.

Groundwater fluctuations exhibit the same trend throughout the landslide. However, the relative position of the groundwater level is dependent on local conditions: the highest pore water pressure is observed in the upper part of the landslide (cross-section B; see Figure 2-7) and it decreases downslope. Consequently, displacement rates are also variable and decrease from the upper to the lower part of the mudslide (see Figure 2-10).

Generally, the long-term dynamics of the Super-Sauze landslide is characterized by continuous movements with a seasonal trend. The mass moves significant distances each rainy season, however, the timing, duration and the speed of the movement vary over the landslide area and do not correlate directly with the timing and amount of rainfall (Malet et al., 2002; Malet, 2003; Figure 2-15). The unsaturated zone strongly attenuates and delays the precipitation. Moreover, preferential fissure flow has a considerable influence on recharge of the groundwater table (Malet et al., 2005).

2.5 Identification of the fissure patterns within the Super-Sauze landslide

As mentioned before, the surface of the Super-Sauze landslide is strongly affected by cracking due to mechanical tension. The long-term field monitoring and airborne ortho-photo or UAV-based ortho-mosaic analysis (Malet et al., 2002; Malet, 2003; Niethammer et al., 2012) allows for monitoring of surface fissure patterns and their distribution across the landslide. All types of surface fissures (see Ch.1§1.3.3) can be found through the Super-Sauze landslide. However, it is mainly tensile fracturing that dominates the fissure formation at the free surface of the Super-Sauze landslide (Travelletti & Malet, 2012; Stumpf et al., *submitted*). Due to heterogeneous landslide geometry of the Super-Sauze landslide, the observed surface fissure structures can be somewhat different in shape and orientation than the idealised ones presented in Ch.1§1.3.3. Moreover, more complex patterns can be observed (e.g. cross-shaped fissures) which results from the combination of the shearing, tension and tearing forces. Examples of fissures patterns observed within the Super-Sauze landslide are presented at Figure 2-16.

It is interesting to note that the spatial distribution of fissure patterns is not changing significantly in time despite continuous landslide activity. This indicates that in case of the Super-Sauze landslide the fissure patterns are strongly linked to the geometry of the stable bedrock (Figure 2-9; Niethammer et al., 2012; Walter et al., 2012; Stumpf et al., *submitted*). Consequently, observed surface fissures are good indicators of local deformation level, that could be extended over the whole soil profile with relatively brittle top soil behaviour (0-1 m) and more ductile behaviour in deeper layers (Stumpf et al., *submitted*)

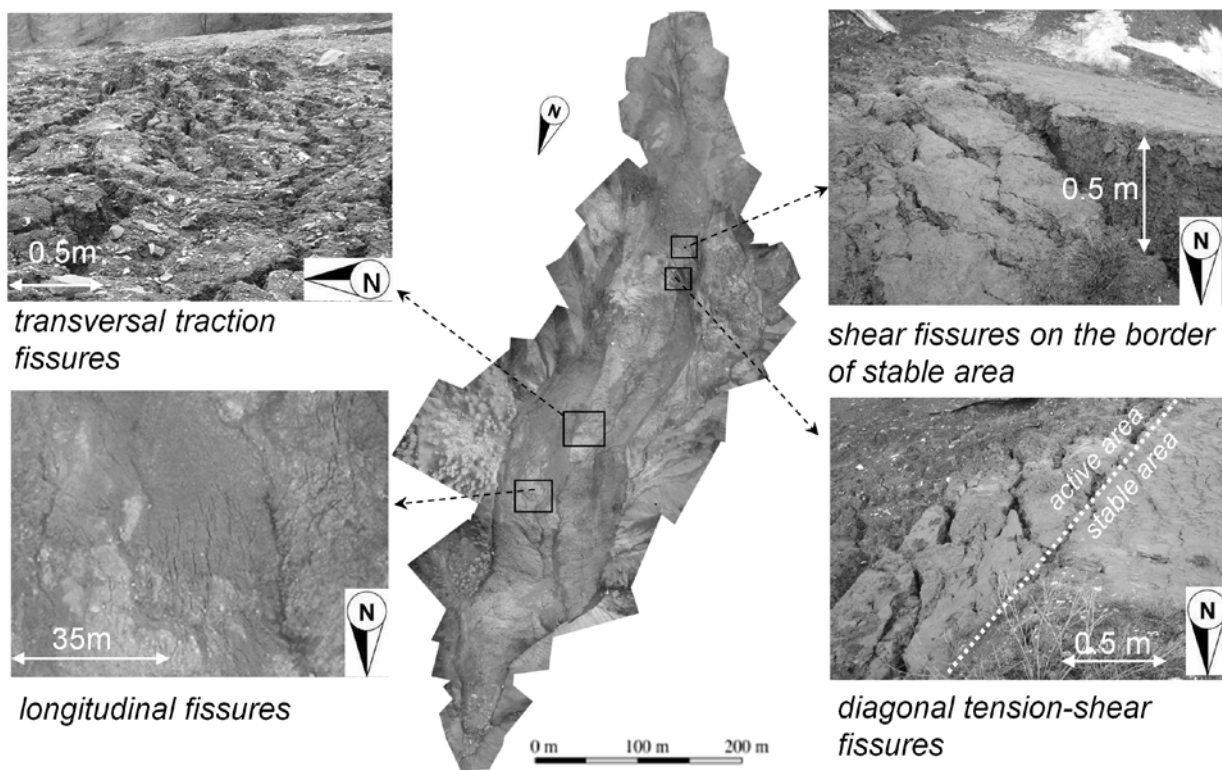


Figure 2-16. Ortho-mosaic of the Super-Sauze landslide from October 2008 (Niethamer et al., 2009) and the examples of observed fissure patterns.

Chapter 3

HIGH RESOLUTION TEMPERATURE OBSERVATION TO MONITOR SOIL THERMAL PROPERTIES AS A PROXY FOR SOIL MOISTURE CONDITIONS

The heterogeneity of hillslope material and variations in its hydrological characteristics affect the spatial and temporal fluctuation of soil moisture patterns within a landslide. Moisture conditions of the unsaturated zone influence the distribution, intensity and time delay of groundwater recharge from precipitation. High resolution monitoring of hydrological features of the near surface soil layer is necessary to advance understanding of the temporal behaviour of complex landslides and their displacement dynamics.

This chapter shows the potential of high temporal and spatial resolution temperature sensing for hydrological analysis of unstable slopes. The main idea is to detect the spatial and temporal variation in soil moisture conditions through the monitoring of soil thermal properties. The soil temperature data were collected during three field campaigns in the black marls mudslide of Super-Sauze (France). In addition, soil thermal properties were determined in the laboratory. The temperature data were used to determine soil thermal parameters which are affected by bulk density and soil moisture content. Based on spatial and temporal variation of the soil thermal parameters the information about soil moisture content fluctuations could be obtained. Promising empirical relationships between apparent thermal diffusivity and soil moisture content have been obtained when accounting for local heterogeneities in soil characteristics. Furthermore, the requirements and limitation of the proposed methodology for clay shale material is elaborated.

Based on: Krzeminska D.M., Steele-Dunne S.C., Rutten M.M., Bogaard T.A., Sailhac P., 2012c. High resolution temperature observations to monitor soil thermal properties as a proxy for soil moisture condition in clay-shale landslide. *Hydrological Processes*, 26:2143-2156, DOI: 10.1002/hyp.7980

3.1 Introduction

The soil moisture condition in the unsaturated zone controls the distribution, intensity and time delay of groundwater recharge. After dry periods, significant amounts of water can be stored in the unsaturated zone, while after prolonged wet periods the storage capacity is limited. Moreover, especially in more saturated soil conditions, preferential, fast, downward water transport can take place.

The heterogeneity of hillslope materials and their hydraulic characteristics affect the spatial and temporal soil moisture patterns. This is particularly true when dealing with clay shale slopes such as black marls. Malet et al. (2005) showed that in the black marls mudslide of Super-Sauze the groundwater level fluctuates seasonally and depends strongly on the state of unsaturated zone. Moreover, in active landslides, local hydrological regimes are complicated by the continuous opening and closing of fissures and cracks. These dynamics have a large influence on the distribution of soil moisture along the slope (Bogaard, 2001; Van Asch et al., 2001). Therefore, monitoring of hydrological conditions of the near surface soil layer is beneficial for advanced understanding of the spatial and temporal behaviour of landslides and their displacement dynamics.

Temperature measurements are often used in soil science to recover soil properties (Jackson & Taylor, 1986). In-situ soil moisture probes that are based on the dual-probe heat-pulse method (Campbell et al., 1991; Mori et al., 2003) provide high accuracy measurements in both laboratory tests (e.g. Tarara & Ham, 1997; Basinger et al., 2003) and field experiments (e.g. Campbell et al., 2002; Heitman et al., 2003). These methods involve applying a heat pulse into the soil and measuring its volumetric heat capacity. The soil water content is determined from the linear relationship between soil volumetric heat capacity and soil saturation. These probes provide local, single point soil moisture measurement.

Recently, a lot of research has been focused on using temperature measurements as a surveying technique in studies of environmental processes. Subsurface temperature measurements are very useful in climatology (e.g. Pollac & Huang, 2000; Harris et al., 2001) and agronomy (e.g. Groffman et al., 1999). They are also widely used in hydrogeology for the analysis of concurrent heat and water flow along vertical profiles to estimate groundwater recharge and discharge rates (e.g. Tabbagh et al., 1999; Cheviron et al., 2005) and percolation rates in the vadose zone (e.g. Constantz et al., 2003). Behaegel et al. (2007) interpreted similar

temperature measurements in a modelling approach to estimate the soil moisture content. This method involves inverting the heat equation using soil and surface temperature fluctuation (resulting directly from net radiation) to estimate soil thermal parameters and thus soil water content.

Fibre optics for distributed temperature measurements has been in use since 1980s (e.g. Dakin et al., 1985). Distributed Temperature Sensing (DTS) is a flexible and powerful tool to monitor the hydrological systems (e.g. Johansson & Farhadiroushan, 1999; Selker et al., 2006). DTS using a fibre optic cable provides continuous temperature measurements with high spatial and temporal resolution (up to 1 m spatial resolution and a 60 s integration time depending on the laser configuration). Steele-Dunne et al. (2010) presented a feasibility study to obtain soil moisture information from passive soil DTS in a sand dune in the Netherlands.

The research presented in this chapter investigates the use of high resolution temperature measurements to monitor the spatial and temporal distribution of soil moisture conditions. Soil thermal properties depend strongly on soil water content and are therefore a good indicator of changes in soil moisture conditions in time and space. Soil temperatures were collected during three field campaigns carried out on the Super-Sauze mudslide (South French Alps). They consist of data from day-to-day monitoring as well as from sprinkling experiments. In addition, soil thermal properties were determined in the laboratory. These data sets are complementary and are used to study the feasibility of passive DTS to assess soil moisture conditions in unstable clay-shale slopes.

3.2 Estimation of soil thermal properties from soil temperature observations

3.2.1 Soil thermal properties

Thermal properties describing heat transfer in the soil column depend among others on water content and can therefore be used as indirect estimate of soil moisture variation. The relation between soil thermal diffusivity and water content can be described with the model of Johansen (1975). The thermal diffusivity (D) of the soil is the ratio between its thermal conductivity (λ) and volumetric heat capacity (C_v). The volumetric heat capacity of the soil is a linear function of the air-water composition of the soil and is straightforward to calculate (e.g. Hillel, 2004), while the calculation of soil thermal conductivity is more complex. In the

Johansen (1975) model, the thermal conductivity of a soil is defined as a combination of dry and saturated thermal conductivities (calculated based on bulk density, porosity and quartz content of the soil) using a so-called Kersten coefficient (Kersten, 1949). For the Super-Sauze landslide, the soil properties reported by Maquaire et al. (2003) were applied: quartz content = 10 % \pm 5 %, porosity = 23-33 % and mass of solids = 2710 kg.m⁻³. Figure 3-1 shows the relationship between thermal properties and relative saturation for the Super-Sauze soils.

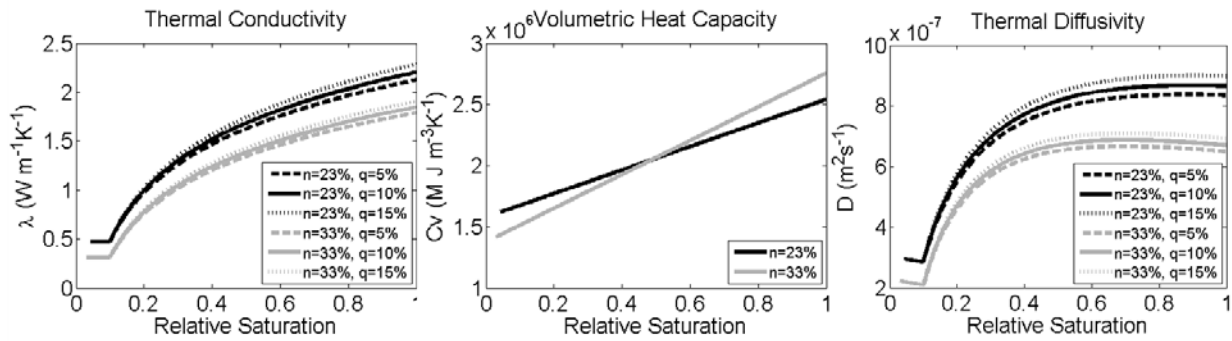


Figure 3-1. Relationships between soil thermal parameters and relative saturation (Johansen, 1975) for Super-Sauze soil quartz content ($q = 5 - 15$ %), porosity ($n = 23 - 33$ %) and solids unit weight of 2710 kg.m⁻³.

To determine the relative importance of heat advection and conduction processes the Péclet number (Pe) is used (see also Behaegel et al., 2007): $Pe = L \cdot v / D$, with L the characteristic length (in our case $L \approx 10^{-1}$ m), v being the water flow rate (from 10^{-8} to $1 \cdot 10^{-7}$ m.s⁻¹; Malet et al., 2005) and D the thermal diffusivity (order of magnitude 10^{-7} m².s⁻¹; Figure 3-1). For the Super-Sauze case study, the Péclet number is in the range from 10^{-2} to 10^{-1} which implies that the advection processes are of less importance. Furthermore, only vertical heat transfer within each separate soil profile is considered.

Consequently, assuming that temperature is governed by conduction within a homogeneous half-space, the heat transfer in the soil column can be described by the diffusion equation:

$$\frac{\partial T_{soil}}{\partial t} = D(\theta) \cdot \frac{\partial^2 T_{soil}}{\partial z^2} = \frac{\lambda(\theta)}{C_v(\theta)} \cdot \frac{\partial^2 T_{soil}}{\partial z^2} \quad (3.1)$$

where T_{soil} is soil temperature [K], t is time [s] and z is depth of soil column [m], and thermal parameters are functions of soil moisture content (θ). The thermal diffusivity referred to here is a so-called ‘apparent’ thermal diffusivity (Horton, 2002) because the convection of heat by

means of sensible and latent heat fluxes is neglected. This has to be taken into account when interpreting the results, especially in moist soil conditions and during high intensity rainfall periods.

3.2.2 Amplitude analysis

The amplitude method was applied to provide a first estimate for soil thermal properties (Horton et al., 1983). This method is based on the simplest mathematical representation of temperature fluctuation in the soil, assuming that at all depths in the soil the temperature oscillates as a sinusoidal function of time. The period of the thermal wave in the soil remains unchanged while its amplitude decreases exponentially with depth. The amplitude method is derived from the diffusion equation (Eq.3.1) with the following boundary conditions:

- the temperature at the surface is specified as a sinusoidal function of time:

$$T_{soil}(0, t) = \overline{T_{soil}} + A_{T,0} \cdot \sin(\omega \cdot t) \quad (3.2)$$

- the temperature at infinite depth ($z = \infty$) is given by:

$$T_{soil}(\infty, t) = \overline{T_{soil}} \quad (3.3)$$

where $\overline{T_{soil}}$ is the average soil temperature [K], $A_{T,0}$ is the amplitude of the surface temperature and ω is the angular frequency ($=2\pi/\text{period}$). Therefore, the apparent thermal diffusivity can be calculated from:

$$D = \frac{\omega}{2} \cdot \left[\frac{z_2 - z_1}{\ln(A_{T,1} / A_{T,2})} \right]^2 \quad (3.4)$$

where D is the apparent thermal diffusivity [$\text{m}^2 \cdot \text{s}^{-1}$], z_1, z_2 are the soil depths (m), and $A_{T,1}, A_{T,2}$ are the amplitudes at depths z_1 and z_2 respectively. The estimated apparent thermal diffusivity is assumed to be constant over the considered period and depth.

3.2.3 Inversion method

The inversion method, used to estimate apparent thermal diffusivity, is similar to the approach presented by Steele-Dunne et al. (2010) and Behaegel et al. (2007). This method is based on

solving the heat equation for a homogenous half-space (Eq. 3.1) with the use of an implicit finite difference scheme at a resolution of 10 mm and 60 s. It optimises the apparent thermal diffusivity value to obtain the best fit between simulated and observed soil temperature within the 24-hour window. The inversion method requires temperature information at three points within the soil profile: the main temperature observation point and the upper and lower boundary conditions. The effect of the lower boundary condition and the vertical soil moisture content distribution on the inferred thermal properties is discussed in § 3.4.3.

When no external energy is applied to the soil the soil temperature changes that are observed, are responses to the diurnal radiation cycle only. Therefore, the minimum period (window) to analyse temperature data is limited to 24 hours. For detailed description of the optimization algorithm the reader is referred to Steele-Dunne et al. (2010).

3.3 Description of experimental set-ups

This section gives technical specification of the field and laboratory equipment followed by the detailed description of different experimental set-ups.

3.3.1 Temperature profiles

Three nests of temperature sensors (TMC50-HD HOB0[®], Onset Computer Corporation) were used to monitor soil temperature changes within vertical soil profiles. For each temperature profile four temperature sensors were installed in the soil, at 0.1, 0.2, 0.3 and 0.4 m depth respectively. The groups of sensors were combined with U12-006 HOB0[®] 4-Channel External Data Loggers. This set of equipment can provide soil temperature measurements from -40° C to 50°C with an accuracy of $\pm 0.25^\circ \text{C}$ at 20°C.

The aim of the temperature sensor profiles is to provide continuous long term soil temperature monitoring over depth. For this reason, taking data storage capacity and battery life into account, temperature measurements were collected in a 30 minutes time resolution.

3.3.2 Distributed Temperature Sensing

DTS is based on the observation of backscattering and light travel time in a fibre optic cable. The equipment sends a laser pulse into the fibre optic cable, and backscattered light shows a

frequency shift referred to as Stokes and anti-Stokes Raman backscatter. The ratio of anti-Stokes to Stokes scattered intensity is used to determine the fibre temperature. A detailed description of the method is given by Selker et al. (2006).

The temperature measurements were performed using two commercially available DTS systems: the Sentinel DTS-LR® (from Sensornet, UK), which allows 1 m spatial resolution, and the Sensa DTS 800® (from Sensa, UK) with a spatial resolution of down to 0.25 m. Both systems ensure high accuracy, e.g. $\sim 0.1^{\circ}\text{C}$ for an integration time of 1 minute or more, however this accuracy strongly depends on calibration precision.

The two DTS equipments were calibrated using reference coils. To do this, several metres of fibre optic cable were coiled up at the point of interest and placed in open air or in a water reservoir. The temperature at those locations was also measured independently using temperature sensors (i.e. 830-T2 Infrared Thermometer from Testo Inc and Tidbit Data Loggers from Onset Computer Corporation) and used for slope calibration and verification of the DTS equipment. Additionally, several T107 temperature probes (from Campbell Scientific) and Tidbits were installed in the soil, close to the fibre optic cables. The temperature values from the DTS and from the individual temperature sensors were in close agreement, especially for the range of daily temperature fluctuations. The exact locations of the fibre optic cable, soil moisture sensors and independent temperature sensors were determined using a differential Global Positioning System.

3.3.3 Thermal Conductivity Scanner

The Thermal Conductivity Scanner (TCS) was used in the laboratory experiment to determine the thermal conductivity of soil samples. It was developed by Popov (Moscow State Geological Prospecting Academy) and produced by Lippmann and Rauen GbR. The TCS scans the sample with a focused, mobile and continuously operated heat source in combination with infrared temperature sensors. The thermal conductivity of the sample is determined based on the comparison of excess temperatures of standard samples (with known thermal conductivity) with excess temperatures of the sample being heated by the movable concentrated heat source (Popov et al., 1999; Popov, 2005). The measurement range of TCS is between 0.2 and $25.0 \text{ W}\cdot\text{m}^{-1}\cdot\text{K}^{-1}$, and the manufacturer quotes the error of 3%. During the measurement phase, the temperature increase is less than 5°C . A set of measurements is

collected along the core axis with a precision of 1 mm. The arithmetic mean of these values gives the thermal conductivity of the sample.

3.3.4 Field Experimental set-ups

Figure 3-2 shows the locations of the experiments within the Super-Sauze landslide. The details of the set-ups are described below and summarised in Table 3-1 and Figure 3-3.

Temperature profile set-up – 1st experiment

The first experimental set-up is based on temperature profile measurements. All the sensors were installed within the HG3 unit, the most stable part of the landslide (Figure 2-13 and Figure 3-2). Sensor locations were chosen carefully to ensure representative measurements for each of the defined sub-areas. Profile T1 was placed in a dry area with a dense and compacted soil texture. Profile T2 was positioned in the wettest area of the HG3 unit where, after rain, ponding water is usually observed. The third temperature profile (T3) was located in a dry area where the soil texture is less dense than at T1, and consists of unweathered marl aggregates. We focus on analysing the temperature profiles measurements from 1/07/2008 to 1/09/2008, during which four rain events of intensity greater than 0.6 mm.h^{-1} occurred (20/07/2008, 25-26/07/2008, 11-12/08/2008 and 15/08/2008).

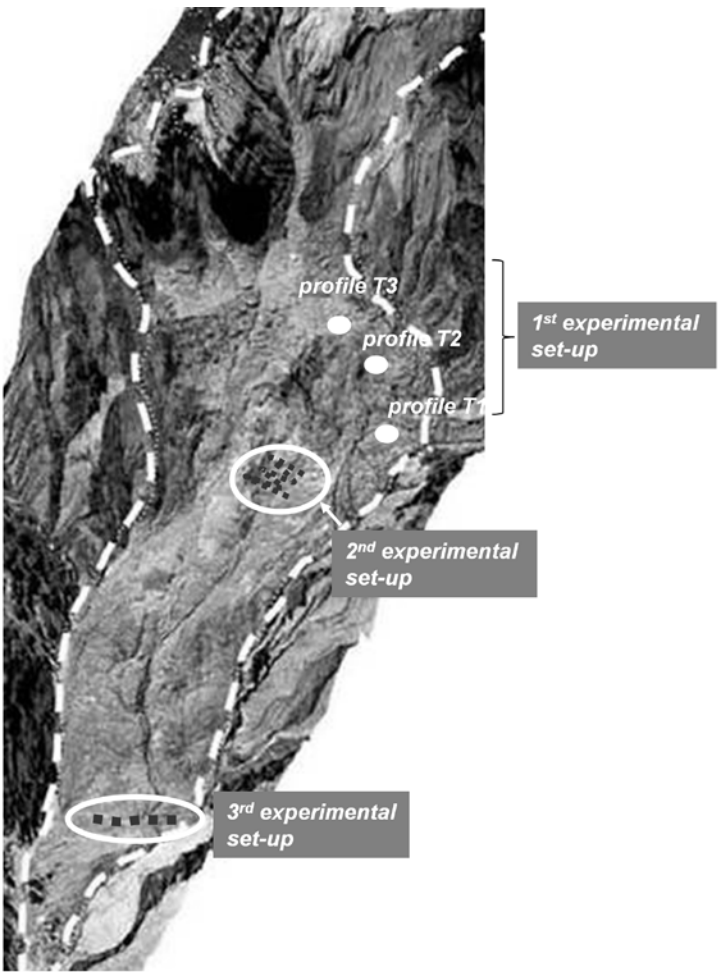


Figure 3-2. Location of the field experimental set-ups: three temperature profiles (1st experimental set-up) and two fibre optic cables (2nd and 3rd experimental set-up).

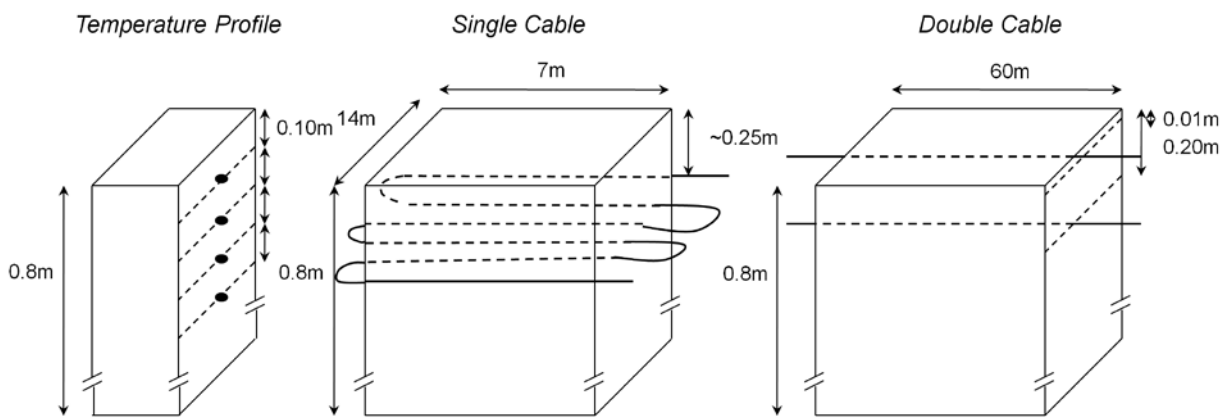


Figure 3-3. Schematisation of three field experimental set-ups

Single cable set-up – 2nd experiment

The first cable (130 m) was installed within the HG1 unit of the Super-Sauze landslide (Figure 2-13 and Figure 3-2). This was also the site of the sprinkling experiment of 2007 (described in detail by Debieche et al., 2012), which consisted of two three-day periods of continuous sprinkling with an average intensity of approximately 10 mm.h^{-1} . The fibre optic cable was put in the soil at an average depth of 0.25 m. This particular depth was a trade-off between analysing a representative soil volume, avoiding the influence of direct solar radiation on the fibre optic cable, and ensuring that the daily atmospheric temperature signal within the soil was not fully attenuated. Continuous DTS measurements were performed during a 14-day field campaign (10-23/07/2007) with a spatial resolution of 1 m and a temporal resolution of 1 min. Additionally, soil moisture content was monitored with CS615 and CS616 Water Content Reflectometers (WCR; Campbell Scientific, Logan, UT) with a reported accuracy of $0.03 \text{ m}^3.\text{m}^{-3}$. Five WCRs were installed in two nests within the sprinkling experiment area at depths between 0.35 and 0.80 m. However, only the WCR sensor at 0.35 m depth was used for comparison with the DTS measurements as it is the most representative for shallow subsurface conditions.

Table 3-1. Description of the experimental set-ups

Experimental Set-up	Temperature sensor	Location/period of monitoring	Installation depth	Upper Boundary Condition	Lower Boundary Condition
Temperature profile	HOBO [®] sensors	HG3 / July - August 2008	0.1, 0.2, 0.3, 0.4 m	Dynamic - T_{soil} at 0.1m	Dynamic - T_{soil} at 0.4 m depth
Single cable	DTS, fibre optic cable	HG1 / July 2007	~0.25 m	Constant in space - T_{air} surfacing cable	Constant - T_{soil} at 0.8 m depth
Double cable	DTS, fibre optic cable	HG2 / July 2009	0.01 and 0.20 m	Spatially distributed - T_{soil} at 0.01 m	Constant - T_{soil} at 0.8 m depth

Double cable set-up – 3rd experiment

In July 2009, a second DTS experiment was conducted with a new fibre optic cable set-up. Two 60 m long cables were installed at 0.20 m and 0.01 m depth within the lower unit (HG2) of the landslide (Figure 2-13 and Figure 3-2). The cable was dug into a secondary wash-out fan originating from a local erosion gully. The washed debris fills a local depression within the accumulation lobes of the mudslide (Figure 3-4). The western part of the wash deposits consists of well sorted, compacted, fine grained sediments (sub-area 1) and it represents

relatively young debris. Then the cable continues into eastern direction through less compacted, heterogeneous sediments ranging from clay to gravel size (sub-area 2) – dried debris deposit. The cable ends in a dry and partly vegetated accumulation lobe of the mudslide, consisting of an unsorted mixture of weathered marls and rock gravel and clasts (sub-area 3). Special attention was given to control the depths of cable installation and to ensure the upper cable was full covered by 1 cm of soil to avoid direct solar radiation on the fibre optic cable. The temperature was measured with a spatial resolution of 0.25 m and a temporal resolution of 2 minutes. The soil moisture content along the cable was monitored with a manual field operated meter (FOM) in combination with a Time-Domain Reflectometry probe (TDR), produced by the Institute of Agrophysics of the Polish Academy of Science. The reported accuracy of the FOM TDR is $0.02 \text{ m}^3 \cdot \text{m}^{-3}$ (IA PAS, 2006). During this experiment one rain event of 10.5 mm with an average intensity of $2 \text{ mm} \cdot \text{h}^{-1}$ was recorded (on 17/07/2009).

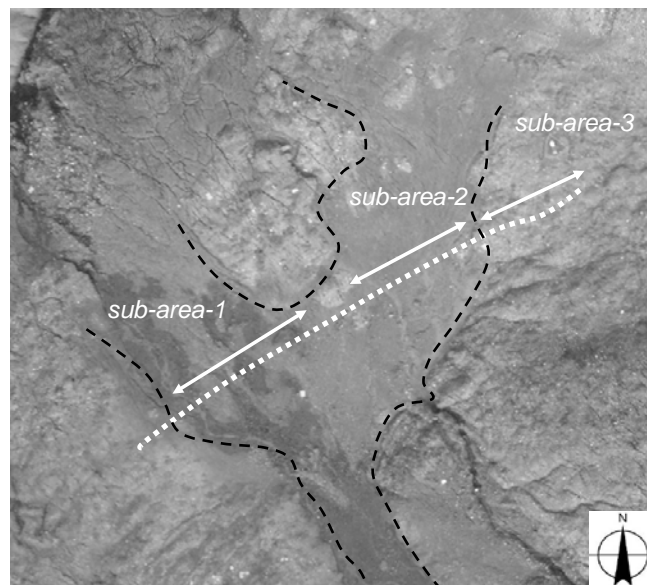


Figure 3-4. Aerial photography of the Super-Sauze landslide from October 2008 (Niethammer et al., 2009); the punctuate line shows the location of the fibre optic cable; the arrows indicate morphological sub-areas.

In this case, with a double cable set-up, the soil surface temperature measured with the upper cable provides the transient and distributed upper boundary condition. The lower boundary condition, which is not measured, is set deep enough to allow us to assume a constant temperature during the analysed time period (see §3.4.3).

3.3.5 Laboratory experiment

The TCS was used to measure the thermal conductivity of disturbed soil samples from the Super-Sauze landslide. Bulk material was collected from the landslide, rock fragments were sieved (sieve mesh of 6.4 mm) and the saturated matrix material was consolidated in the laboratory. The bulk density of the samples after consolidation was 1.63 g.cm^{-3} , which corresponds to the field measured values reported by Maquaire et al. (2003).

3.4 Analysis and interpretation of the temperature time series

3.4.1 Temperature data

Figure 3-5 shows an example of the temperature measurements of profile T1 (1st experimental set-up) between 16 and 30/07/2008. The amplitude of the diurnal variation of soil temperature decreases with depth and a phase shift can be observed. Anomalies in the temperature profile occur during and after three rain events on 20, 25 and 26/07/2008. The daily temperature amplitude is reduced as well as the temperature differences in the soil profile. This could result from lower solar radiation (more clouds during the rainy days) or increased soil moisture content (higher thermal capacity).

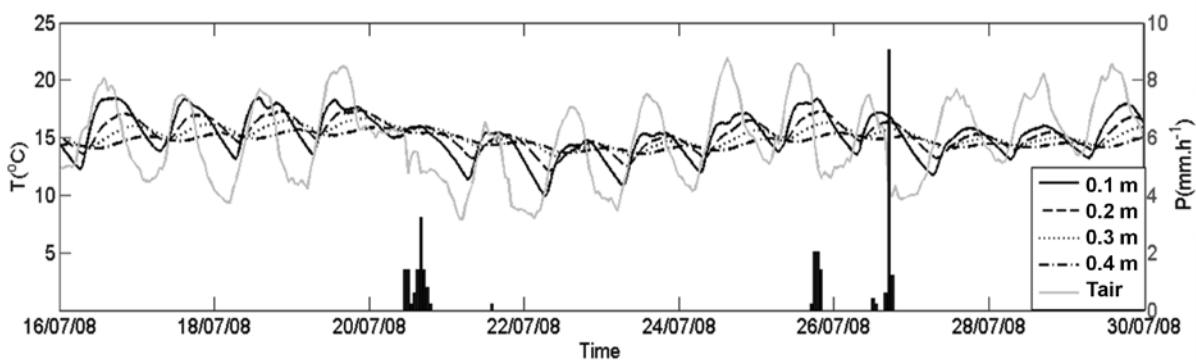


Figure 3-5. Example of the temperature measurements from profile T1. Air temperature and rain data come from meteorological station located around 800 m distance from the experiment area on the landslide.

Figure 3-6 shows the complete set of temperature measurements from the 2nd experiment (sprinkling experiment of 2007). The locations where the cable is at the surface and thus measuring air temperature (Figure 3-6a) are clearly visible. Moreover, the soil temperature measurements in the fibre optic cable show distinct differences in the observed temperature range between the two sprinkling periods. This corresponds to the difference in the sprinkling

water temperature and the air temperature increase. The average water temperature during the first sprinkling period was approximately 14°C, while during the second sprinkling period, average water temperature reached 20°C. The average air temperature during the second sprinkling period was approximately 8°C higher than during the first sprinkling period.

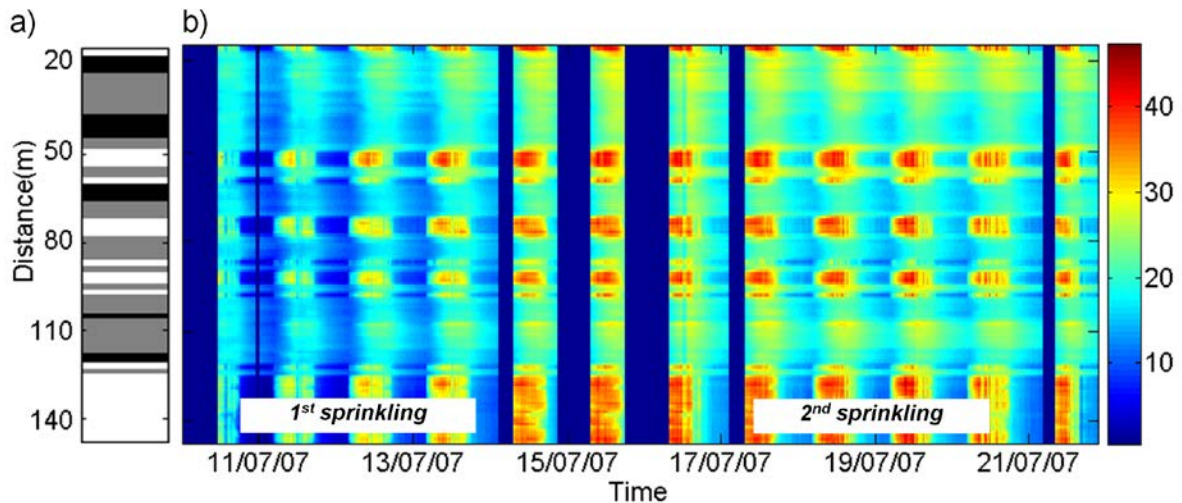


Figure 3-6. Distributed Temperature Sensing measurement from 1st experiment. (a) Soil wetness state observed during installation of the cable: white – surfacing cable, grey – ‘dry’ area, black – ‘wet’ area. (b) Temperature at ~0.25 m depth. Dark blue areas means periods with no measurements due to technical problems.

Moreover, spatial differences in temperature amplitude attenuation and time delay can be observed along the cable. Those differences coincide with the ‘wet’ and ‘dry’ areas identified during the cable installation. Additionally, during the sprinkling periods, the soil surface remains nearly saturated. Lower daily temperature amplitude was observed in areas where applied water accumulated due to local small-scale terrain heterogeneity. In those areas, the temperature of infiltrating water determines the soil temperature at 0.25 m depth. The water temperature during the first sprinkling period varies between 4-9°C (daily minimum) and 13-16°C (daily maximum), while the range of soil surface temperature is between 3-9°C (daily minimum) and 24-33°C (daily maximum). During the drying periods, the locations with low daily temperature amplitudes indicate areas with a higher soil evaporation rate (the soil temperature remains colder during the day) and greater heat capacity (the decrease in soil temperature during the night is limited).

The temperature measurements collected during the 3rd experiment (July 2009) are presented in Figure 3-7. The measurements show a clear difference between the soil temperatures

registered with the upper and lower cables (both a decrease of amplitude and a phase shift). Moreover, changes in soil temperature patterns can be observed during and after the rain event of 17/07/2009. After the rain, the daily temperature amplitude measured by both cables decreased and the temperature difference between the two was reduced. Additionally, differences in temperature patterns between the ‘wet’ and ‘dry’ areas observed during cable installation (Figure 3-7b) are visible. In the ‘wet’ areas the surface and soil temperatures during the day are lower compared to the ‘dry’ areas.

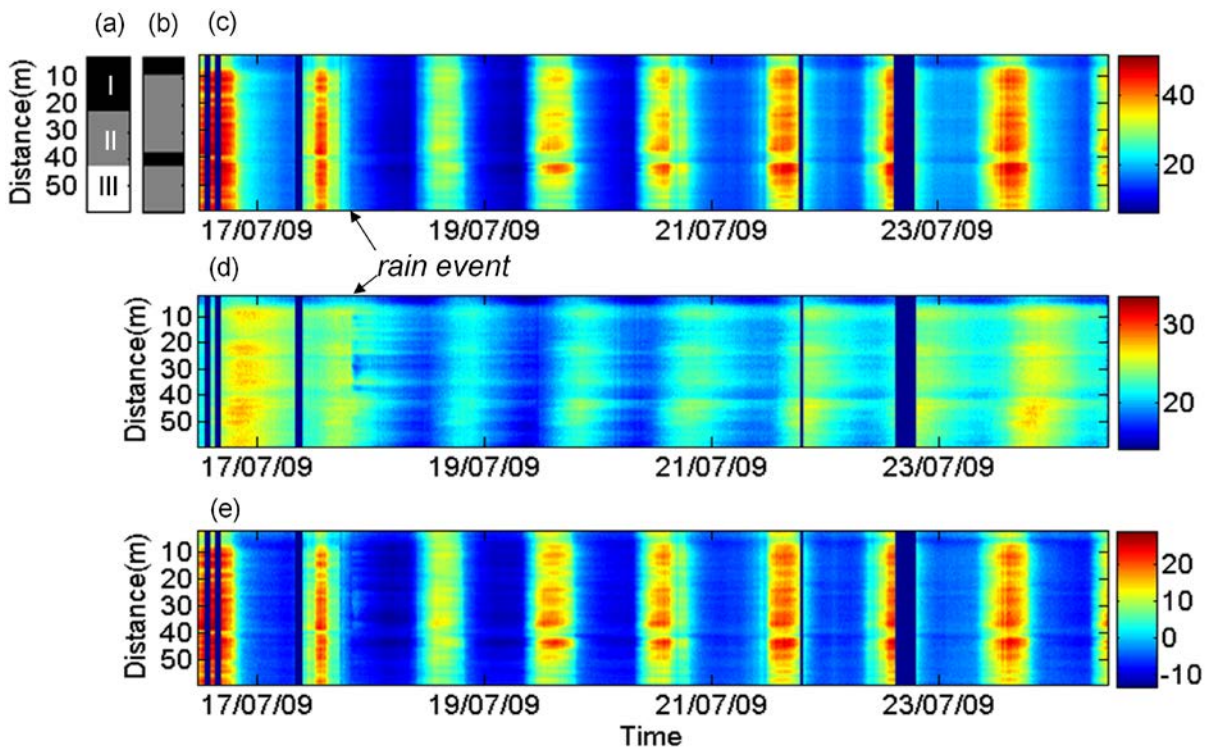


Figure 3-7. Distributed Temperature Sensing measurement from 3rd experiment; (a) Morphological sub-surface areas; (b) Soil wetness state observed during installation (grey – ‘dry’ areas, black – ‘wet’ areas); (c) Soil surface temperature measured at 0.01 m depth; (d) Soil temperature at 0.20 m depth; (e) Difference between soil surface temperature and soil temperature at 0.20 m depth. Dark blue areas means periods with no measurements due to technical problems.

3.4.2 Qualitative and quantitative analysis of temperature data

Analysis of 1st experimental set-up

As a first approach, the amplitude method was applied to the temperature profiles data (T1, T2 and T3) from a two week period in July 2008, in which three rainy days were recorded. Temperature time series of all possible depth combinations were analysed: 0.1–0.2 m, 0.1–0.3 m, 0.1–0.4 m, 0.2–0.3 m, 0.2–0.4 m and 0.3–0.4 m. Figure 3-8c shows the estimated apparent thermal diffusivity from 0.1 to 0.4 m depth for each soil profile.

The inversion method was applied to the temperature profiles data from 15/05/2008 to 1/09/2008. The observed temperatures at 0.1 m and 0.4 m below the surface provide the upper and lower boundary conditions. The apparent thermal diffusivity of each temperature profile was estimated by minimizing the difference between the simulated and the observed temperature at 0.2 m and 0.3 m depth over the subsequent 24-hour time window (Figure 3-8d).

Generally, all three profiles show an increase in apparent thermal diffusivity in response to the rain events using both amplitude and inversion method. However, the amplitude method gives higher results and a larger increase in apparent thermal diffusivity values after rain events. One explanation could be that the amplitude method assumes that the observed temperature signal is an ideal sinusoidal function which leads to an underestimation of the temperature differences within the soil profile. Consequently, the apparent thermal diffusivity is overestimated.

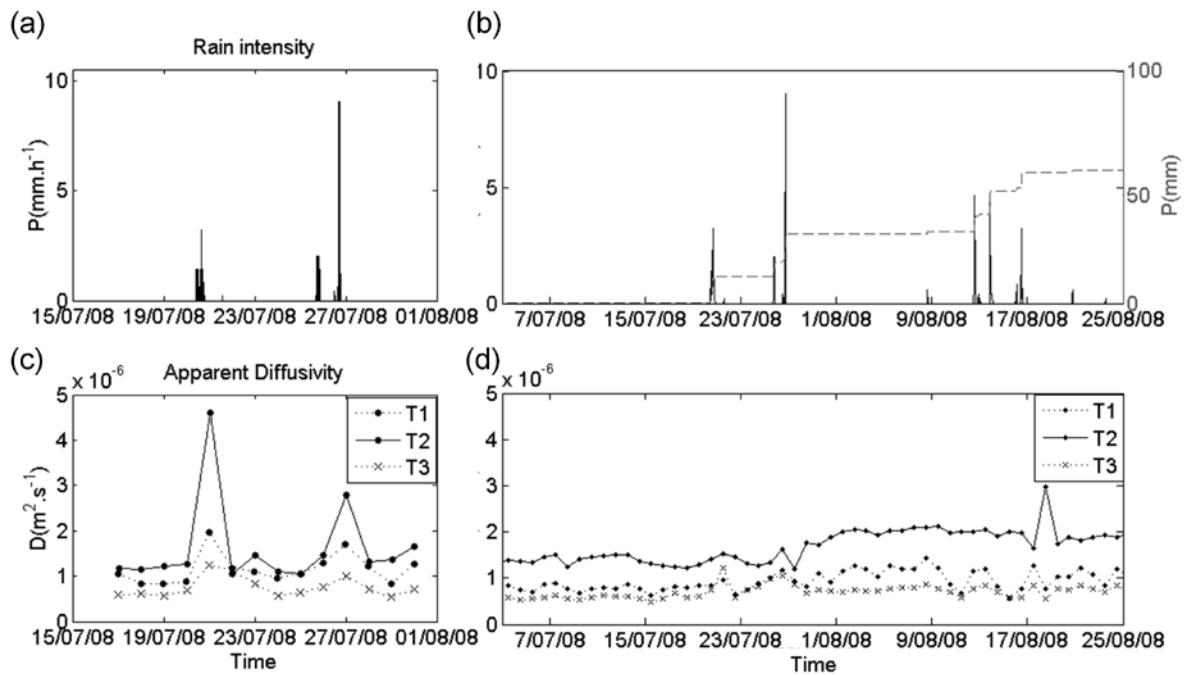


Figure 3-8. Apparent thermal diffusivity values estimated based on temperature data from 1st experiment set-up. Upper panels (a) and (b) show the rain events and rain intensity during analysed time period and lower panels show apparent thermal diffusivity values from (c) the amplitude method and (d) inversion method.

Figure 3-8a and 3-8c show an increase of apparent thermal diffusivity values during and after a rain event due to increases soil wetness. However, the absolute values could not be related to the intensity and amount of rainfall. Since the soil moisture content is not measured over

the observation period it is impossible to relate apparent diffusivity values with soil moisture content. Nevertheless, the ‘wet’ profile T2 gives larger apparent thermal diffusivity estimates than the two ‘dry’ profiles (T1 and T3). Furthermore, the apparent thermal diffusivity values in Figure 3-8d of T2 show a gradual increase. This behaviour can not be explained with the last rain event but results from prolonged soil saturation due to ponding water observed in that area.

Analysis of 2nd experimental set-up

The amplitude method was also applied to the temperature data of the 2nd experiment (2007 sprinkling experiment) by collating the soil temperature measurements ($z \approx 0.25$ m) with soil surface temperature ($z = 0$ m) coming from the coiled up fibre optic cable at the surface. Figure 3-9b shows a significant rise in the apparent thermal diffusivity over the sprinkling periods. During the drying periods, a significant amount of temperature data is missing which hinders the analysis for this period. Nevertheless, based on estimates from the end of the first sprinkling period, and from the beginning of second sprinkling period, it is clear that apparent thermal diffusivity decreased when no water was applied. Moreover, apparent thermal diffusivity values are the same at the beginning of both sprinkling periods. This also agrees with the WCR soil moisture observations (secondary y-axis in Figure 3-9a). The ‘dry’ intervals remain relatively dry during the first sprinkling period, but become progressively wetter during the second sprinkling period.

Subsequently, the inversion method was applied to each measurement interval along the cable separately. The apparent thermal diffusivity behaviour estimated with the inversion method shows no clear relationship with the precipitation patterns or the soil moisture content (Figure 3-9c and 3-9d), although the absence of a continuous temperature time series, and thus apparent thermal diffusivity estimates, is hampering the interpretation. However, the estimates of the apparent thermal diffusivities calculated for the 2nd experiment are in the same range as those for the 1st experiment. The absolute values calculated using the amplitude method are higher and exhibit a stronger response to variations in soil moisture content.

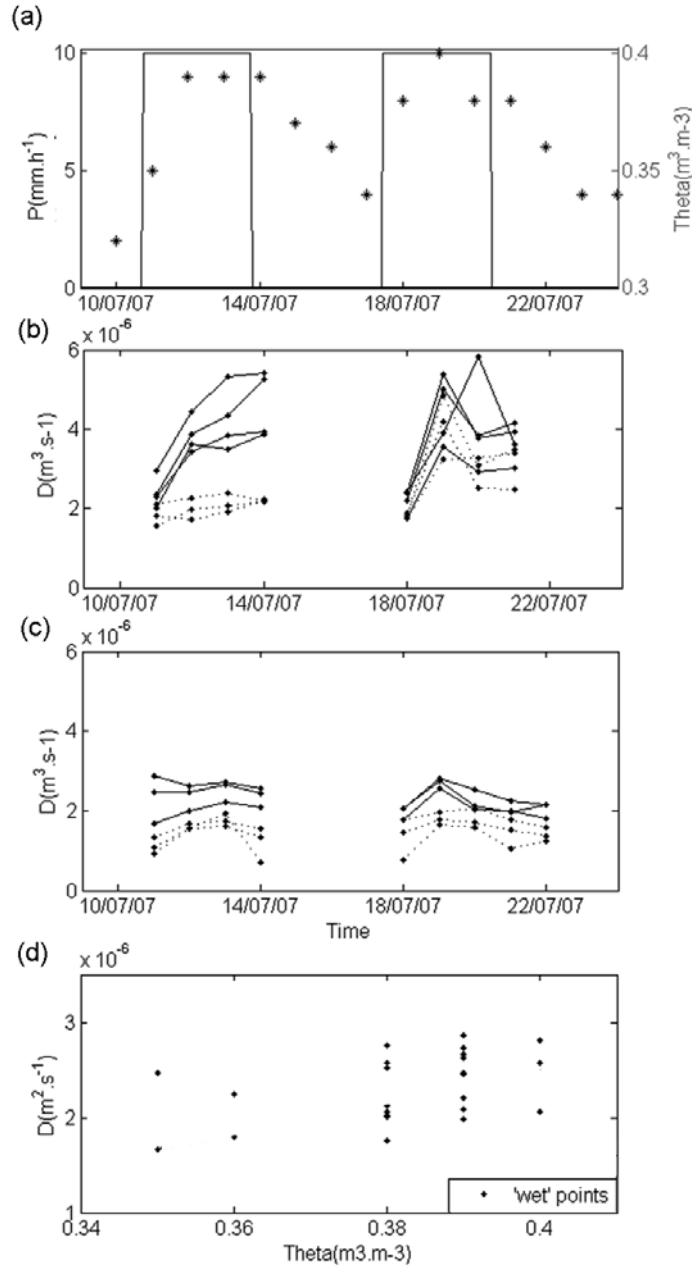


Figure 3-9. Analysis of 2nd experimental set-up. (a) Sprinkling intensity and daily averaged soil moisture observation (measured with WRC); Apparent thermal diffusivity values estimated with amplitude method (b) and with inversion method (c): dashed line represents the 'dry' points and solid lines the 'wet' point; (d) relation apparent thermal diffusivity for 'wet' areas, estimated with the inversion method, and measured soil moisture values (average of 24h).

When analysing the 2nd experiment, it is important to stress the assumption that the point soil surface temperature measurements are representative for the entire experimental site. This assumption may introduce large errors in the calculations, especially in areas with near saturation conditions in the surface soil layer. As a wet soil surface temperature is less variable than a dry soil surface, a sensitivity analysis was performed by smoothing the

observed soil surface temperature to mimic the temperature of a wet soil surface. When the daily amplitude of soil surface temperature is set to be 30% lower than the measured one (by applying a 12h moving average) the estimated apparent thermal diffusivity values shows 70 to 100% increase.

Analysis of 3rd experimental set-up

The 3rd experimental set-up was analysed with both the amplitude and the inversion method. Here the soil surface temperature, measured at 0.01 m depth and the temperature at 0.20 m depth were measured simultaneously with the fibre optic cable. The lower boundary condition was set at 0.8 m with a temperature equalling the monthly average temperature for July 2009 (14°C). Each measuring interval along the cable was analysed separately and the soil column around each measuring interval length of the cable is assumed to be homogenous.

Figure 3-10a gives an example of the measured temperature distribution from this experiment for 19/07/2009. It shows the temperature data of the upper and lower cable, the measured soil moisture content and the calculated apparent thermal diffusivity. The results of the amplitude method are in close agreement with those from the inversion method in terms of the spatial and temporal trend in apparent thermal diffusivity of the soil. The absolute values of the apparent thermal diffusivity estimated with the amplitude method are higher than those from the inversion method. However the maximum difference is not more than 30%. Generally, the apparent thermal diffusivity follows the soil moisture content along the cable (Figure 3-10b and Figure 3-10c). Two wet areas (from the beginning of the cable to 8 m distance and from 38 m to 44 m), mapped during the installation of the cables, can be identified in the temperature and soil moisture observations. These are also clearly visible in the apparent thermal diffusivity results. Moreover, at the end of the cables, starting from 45 m, soil moisture content increase coincides with higher values of apparent thermal diffusivity.

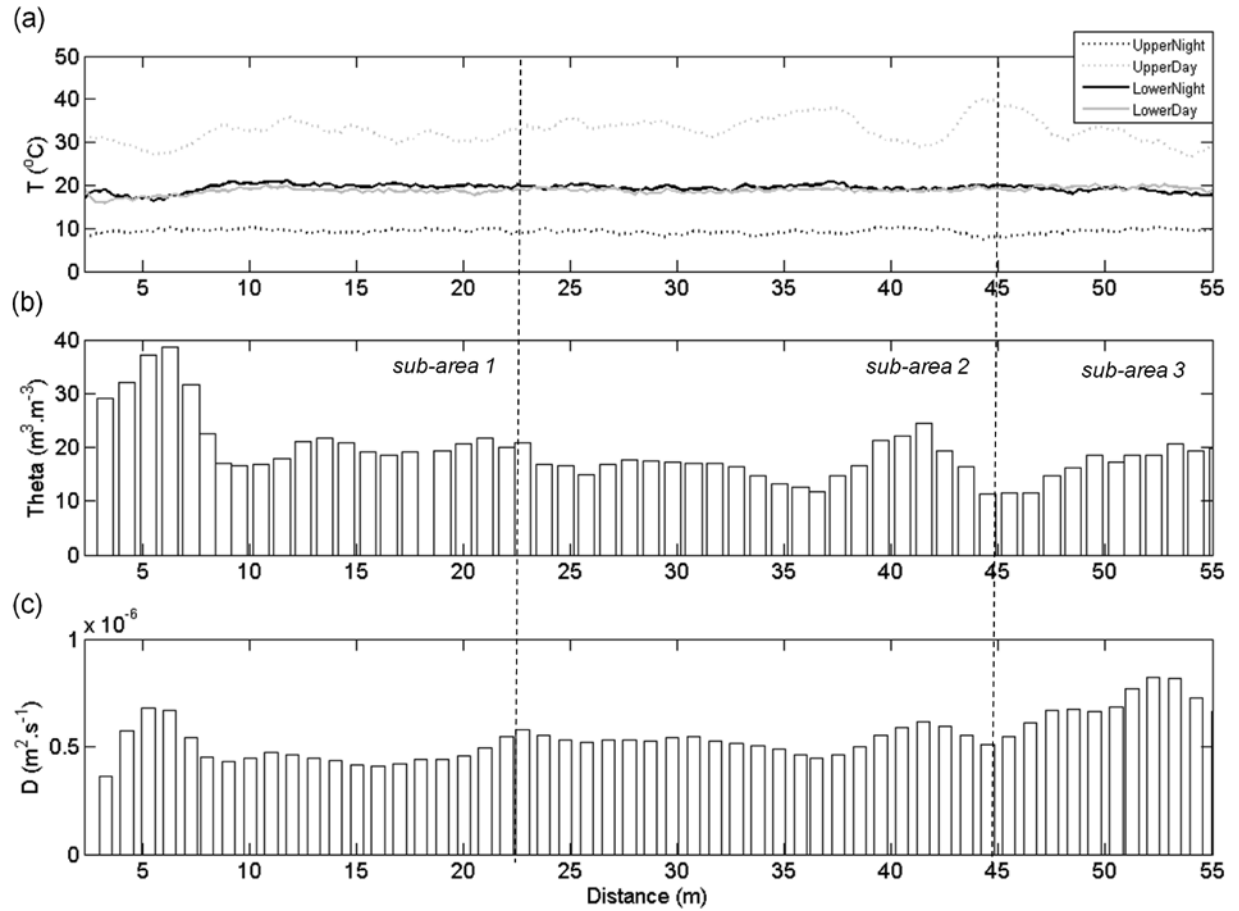


Figure 3-10. Analysis of 3rd experimental set-up: (a) example of temperature data (DTS) from 19/07/2009: soil surface temperature (upper cable) and soil temperature at 0.20 m depth (lower cable), (b) soil moisture measurement (FOM TDR) from 19/07/2009, (c) apparent thermal diffusivity values estimated with inversion method. The area of the experiment is divided into three sub-areas (vertical dashed lines) with different material characteristics

For a more detailed analysis of the results of this experiment, the spatial differences in soil characteristics along the fibre optic cable will need to be taken into account. Figure 3-11 shows that using the morphological partitioning of the data, the apparent thermal diffusivity correlates quite well with the measured soil moisture data (R^2 is 0.91, 0.89 and 0.63 for sub-areas 1, 2 and 3 respectively). The much worst correlation for the sub-area -3 can be explained by the highest soil heterogeneity of the accumulation lobe of the mudslide and, consequently, the highest uncertainty of both FOM TDR soil moisture measurements and the estimates of soil thermal parameters.

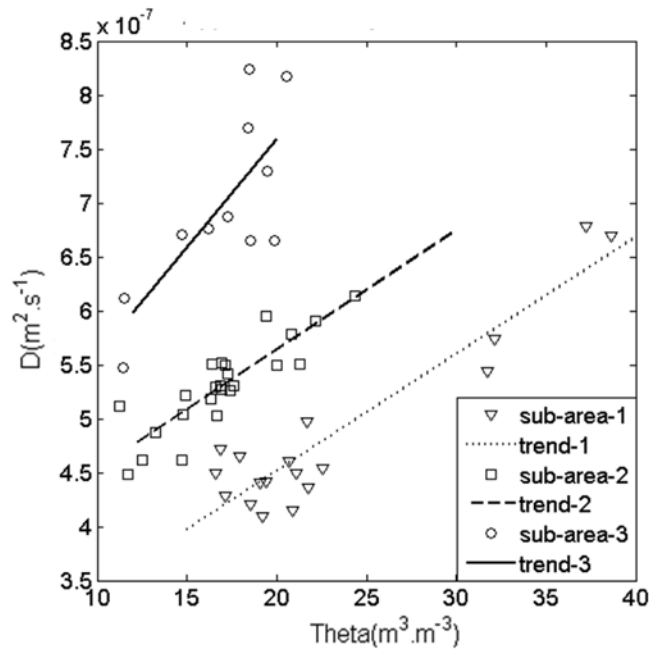


Figure 3-11. Relationship between estimated apparent thermal diffusivity values and measured soil moisture content (FOM TDR) per sub-area.

Laboratory measurements of thermal conductivity

Eight disturbed soil samples from the Super – Sauze landslide were scanned with the use of TCS (see §3.3.3 and §3.3.5). The measured values of thermal conductivity vary between 0.60 and 0.80 $\text{W.m}^{-1}.\text{K}^{-1}$ when samples are dry (relative saturation around 10–20 %), and 1.60 – 1.98 $\text{W.m}^{-1}.\text{K}^{-1}$ when relative saturation of the samples is higher than 50%. Generally, these ranges of thermal conductivity values are consistent with those from the Johansen (1975) model (Figure 3-12). However, in some samples, thermal conductivity becomes constant or even decreases when soil samples approach saturation (especially when the saturation degree is above 70%). This could be caused by the fact that the TCS is performed on disturbed and re-consolidated soil samples. There are no rock fragments in the soil samples (sieved soil samples) and some small air inclusions could not be avoided. Additionally, a water film at the outside of the sample was observed, at near saturated conditions, that could have negatively influenced the optical scanning thermometer.

Based on the measured thermal conductivity values and on the relation $D = \lambda / C_v$, apparent thermal diffusivity of the soil samples was estimated. The volumetric heat capacity changes from around 1.4–1.6 $\text{MJ.m}^{-3}.\text{K}^{-1}$ (for dry soil) to 2.4 – 2.7 $\text{MJ.m}^{-3}.\text{K}^{-1}$ (for wet soil). The maximal apparent thermal diffusivity values are 0.7– 0.8 $\cdot 10^{-6} \text{ m}^2.\text{s}^{-1}$.

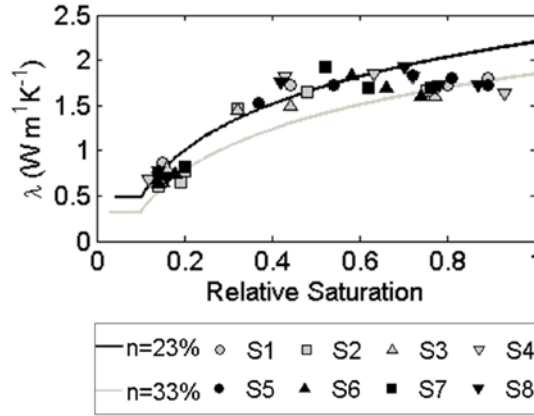


Figure 3-12. The results of TCS; 8 samples, 4-6 measurements per sample. The full lines (black and gray) are the representation of thermal conductivity (λ) calculated with Johansen model with quartz content of 10 % and porosity of 23 % and 33 % respectively (left panel of Figure 3-1).

3.4.3 The influence of the lower boundary condition and the soil moisture distribution on the apparent thermal diffusivity

In this section we analyse the influence of the lower boundary condition on the estimated apparent thermal diffusivity, the representative soil volume associated with this value and the influence of vertical distribution of soil moisture on the apparent thermal diffusivity.

For the 1st experiment, the apparent thermal diffusivity, derived from both amplitude and inversion method, is an average value for the soil column between the depths at which the temperature observations were measured: 0.10 to 0.40 m. Likewise, for the 2nd and 3rd experiments, the apparent thermal diffusivity values estimated with amplitude method are an average value between the soil surface and the installation depth of the cable at ~0.25 m and 0.20 m respectively.

While applying the inversion method to the 2nd and 3rd experiment, the value and the depth of the lower boundary condition (LBC) is less well-defined. In the absence of temperature measurements at depth, a (near-)constant temperature at the lower boundary condition is needed. We used a threshold of the daily temperature amplitude of 0.5°C. Figure 3-13a shows that at 0.8 m depth the assumption of a constant temperature value is valid. A 15°C daily surface temperature amplitude is attenuated almost completely at 0.8 m depth, both for a dry soil ($D=2 \cdot 10^{-7} \text{ m}^2 \cdot \text{s}^{-1}$) and a wet soil ($D=9 \cdot 10^{-7} \text{ m}^2 \cdot \text{s}^{-1}$). A sensitivity analysis of the influence of the LBC shows that changing the depth of the LBC by ± 0.1 m results in a change in

apparent thermal diffusivity values with -1 % and 3 %. Moreover, a 3 % variation in apparent thermal diffusivity values results when changing the temperature at the depth of the LBC by 1°C. This analysis shows that changing the depth or the temperature at the LBC has a limited influence on the absolute values of estimated apparent thermal diffusivity and therefore has a limited influence on the apparent thermal diffusivity trends.

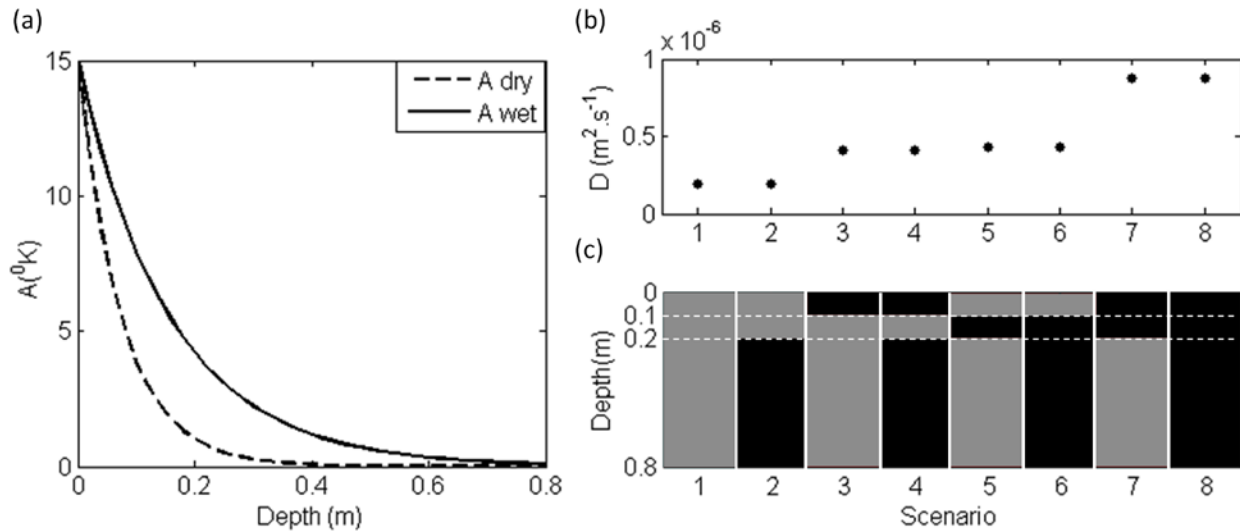


Figure 3-13. Analysing the influence of the lower boundary condition and vertical distribution of soil moisture content on estimation of apparent thermal diffusivity with the inversion method: (a) Attenuation of the temperature signal with the depth; (b) Example of apparent thermal diffusivity values estimated with inversion method for different scenarios of soil moisture distributions with depth; (c) Schematic representation of scenarios of soil moisture distribution with depth: grey colour - dry condition with $D=2 \cdot 10^{-7} \text{ m}^2 \cdot \text{s}^{-1}$, black colour - wet condition with $D=9 \cdot 10^{-7} \text{ m}^2 \cdot \text{s}^{-1}$.

To investigate furthermore the influence of heterogeneous soil moisture conditions in a soil profile, 8 scenarios were designed with different soil moisture distributions (Figure 3-13c). Figure 3-13b shows the resulting apparent thermal diffusivity. Note that we assumed daily temperature amplitude of 15°C, a measured temperature signal at 0.20 m depth and a constant soil temperature at 0.80 m depth. The algorithm optimises the temperature profile based on temperature variations at 0.20 m depth. The results show that the soil moisture state of the lower part of the soil column (below 0.20 m) does not influence the estimation of the apparent thermal diffusivity. This is due to the fact that we analyse a period with a strong downward temperature gradient and thus energy flux. When different soil moisture conditions are assumed for the upper part of the soil column (0-0.10 m dry and 0.10-0.20 m wet or reverse) the estimated apparent thermal diffusivity values are independent of the soil moisture distribution within the first 0.20 m. This shows that the apparent thermal diffusivity estimated with the inversion method represents the average value for the soil column between the upper

boundary and the depth of the cable installation (0.25 m during 2nd experiment and 0.20 m during 3rd experiment). Information about the soil moisture profile within the layer can not be found with this method, only an average value.

3.5 Discussion

This analysis of temperature data shows that temporal and spatial variations in soil thermal parameters can be monitored in weathered clay shales by using high resolution observation of soil temperature. Overall, the observed trends of apparent thermal diffusivity correlate with observed changes in soil moisture content and with rain events.

Nevertheless, absolute values for thermal diffusivity are often overestimated. For the 1st and 2nd experiment, the derived apparent thermal diffusivity values are in the order of $0.5 - 5.8 \cdot 10^{-6} \text{ m}^2 \cdot \text{s}^{-1}$ (amplitude method) or $0.5 - 3.0 \cdot 10^{-6} \text{ m}^2 \cdot \text{s}^{-1}$ (inversion method). These ranges deviate from the values predicted by Johansen (1975) for this type of soil which are in the order of $0.2 - 0.9 \cdot 10^{-6} \text{ m}^2 \cdot \text{s}^{-1}$ (Figure 3-1). Moreover, the maximum values of apparent thermal diffusivity obtained in the laboratory for the disturbed soil samples from the Super-Sauze vary between 0.7 and $0.8 \cdot 10^{-6} \text{ m}^2 \cdot \text{s}^{-1}$ which are consistent with the values from the Johansen model.

It is important to note that the calculated values are actually apparent thermal diffusivities (Horton, 2002) as heat conduction is assumed to be the only mechanism of heat transfer but heat advection can not be totally excluded. Therefore, part of the overestimation could be due to neglecting the heat advection. However, it is the upper boundary condition (soil surface temperature) and the control of the cable installation depth that appear to be the main limitations. The assumption that soil surface temperature is equal over the area is debatable due to spatial differences in moisture conditions on the surface (as shown in §3.4.2 *Analysis of 2nd experimental set-up*). In addition, accurate estimation of the depth of the cable is also crucial for the analysis of the thermal properties. Steele-Dunne et al. (2010) argue that incorrect specification of the cable depth gives rise to errors in estimated apparent thermal diffusivity values. When a smaller distance between the sensors is assumed, a significant decrease in apparent thermal diffusivity value is observed. For the temperature profiles (1st experiment), a 25 % distance reduction causes up to a 40 % decrease in apparent thermal diffusivity (Figure 3-14). On the contrary, the extreme thermal diffusivity values observed

after the rain event are reduced when wider spacing is considered. However, this does not change the temporal trends of the apparent thermal diffusivity values, only the absolute values.

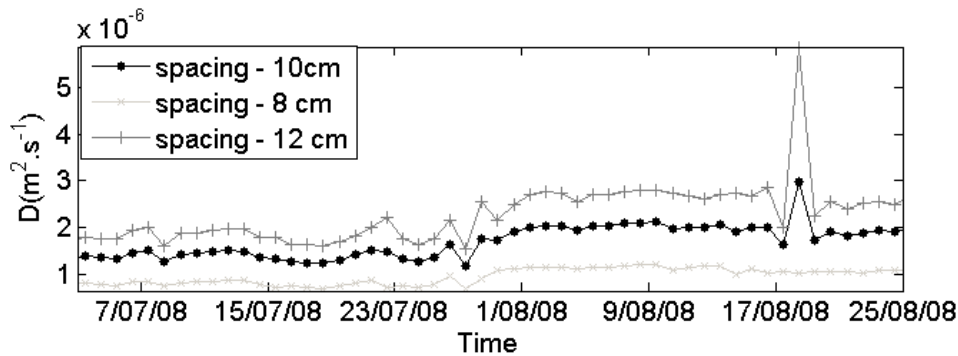


Figure 3-14. Dependence of apparent thermal diffusivity estimation from the distance between temperature sensors. Example for profile T2.

As shown in Figure 3-10 and Figure 3-11 (3rd experiment), a better control of the depth of the temperature observation (lower cable) and additional measurements of the soil surface temperature (upper cable) result in a significant improvement of the calculated apparent thermal diffusivity (the inversion is less uncertain).

The methodology presented here has two main limitations. The first limitation comes from the nature of the relationship between thermal diffusivity and soil moisture content (Johansen, 1975). There is little variation in thermal conductivity when the soil is dry and the contribution of the air fraction dominates soil thermal properties. When the soil becomes wetter, a water film increases the connectivity between the soil particles and a sharp increase in thermal conductivity is observed. When the soil approaches saturation, particles are already well-connected and soil fraction controls the heat transfer. Consequently, when the relative saturation is higher than 50%, changes in apparent thermal diffusivity are very limited. Therefore, it is hard to connect thermal diffusivities with soil moisture content. However, our empirical relationships (Figure 3-11), which are taking into account clearly identifiable sub-areas, are quite promising. The differences between modelled and empirical relationships may come from the fact that Johansen's model does not count for the internal structure of the soil (e.g. clay-particle size, different layering, aggregation, etc.) that might be very important for clay-rich shale (Horn et al., 1994).

A second limitation, directly related to the inversion method, comes from the length of estimation/optimization window. Behaegel et al. (2007) used a 15-day optimization window

to simulate heat diffusion in the thermally active soil layer. Therefore, the apparent thermal diffusivity values are effectively averaged over the 15-day interval. As the goal of this research is to come up with a higher resolution monitoring technique to observe changes in soil moisture conditions, the shortest possible optimization window was applied. This is a 24-hour window as the temperature varies in response to the diurnal variability in net radiation. However, it is obvious that the dynamics of water content changes can be faster than this interval, especially during the short intense rain events. In order to resolve changes in soil thermal properties at finer than daily resolution a ‘moving window’ can be used (the 24-hour optimization window shifted in 3 hourly increments; Steele-Dunne et al, 2010). However, this can only be applied when the distance between temperature observations within the soil profile is limited to centimetres. Nevertheless, apparent thermal diffusivity values obtained with a ‘moving window’ will still represent the daily averaged condition, but shifted every 3 hours.

Another solution might be to combine passive DTS (for long time scale monitoring of the soil thermal properties) and active DTS (to monitor soil thermal properties during and after intense rain events). Active DTS (comparable to the heat-pulse method) involves applying external energy to the fibre optic cable and measuring the temperature responses. This can give a high precision measurement of soil moisture content and allows for high temporal resolution (Steele-Dunne et al., 2010). The use of coupled passive and active DTS might limit the energy demands (passive DTS) and provide better constraint to estimates from passive DTS and inversion method (active DTS).

3.6 Summary and conclusions

This research shows the use of high resolution temperature measurements, specifically Distributed Temperature Sensing, as a geophysical tracer to monitor the spatial and temporal distribution of soil moisture content in a clay shale environment. Three field campaigns were done at the Super-Sauze mudslide in 2007, 2008 and 2009, where two fibre optic cables and several temperature sensors were installed.

Qualitative and quantitative analysis of soil temperature data were presented. The qualitative analysis of soil temperature variation made it possible to observe the soil moisture patterns during the sprinkling experiment of 2007. Moreover, with the soil temperature profiles, it was

possible to monitor spatial and temporal difference in soil moisture patterns. The results of the quantitative analysis of the soil temperature measurement show that, with the use of amplitude analysis as well as the inversion method, it is possible to illustrate the variability of apparent soil thermal diffusivity, although no clear relationship with soil moisture condition could be observed. However, the results of the 2009 experiment show that increased precision of the estimated apparent thermal diffusivity values can be achieved if the sensor installation depth is well known and spatially distributed surface temperature observations can be used as upper boundary condition. Moreover, the relationship between estimated apparent diffusivity and measured soil moisture content shows interesting and promising results when accounting for spatial heterogeneity of soil characteristics.

The methodology presented here was tested on a clay shale material that is especially prone to landslide. Knowledge about the hydrological behaviour of the top soil layer gives information about the available storage capacity and possible occurrence of preferential infiltration of rain water or snowmelt. This information is important to estimate the intensity and time delay of local groundwater recharges, and thus the distribution of pore pressure within the landslide.

The next step in this research is to improve the knowledge of the soil specific relationship between soil moisture and thermal conductivity for the clay shales of the Super-Sauze mudslide as shown empirically in Figure 3-11. When this relationship is known for the full dynamic range, the degree of saturation can be inferred from calculating the apparent thermal diffusivity. The improved knowledge of spatial differences in hydrological behaviour within an unstable slope can be further incorporated into a slope instability assessment or a mass movement analysis. In this way, the analysis of spatial temperature patterns could become a valuable tool to augment the understanding of slope deformations.

Chapter 4

FIELD INVESTIGATION OF FISSURE FLOWS WITH SMALL-SCALE SPRINKLING EXPERIMENTS ON A HYDROLOGICALLY TRIGGERED LANDSLIDE

The unsaturated zone largely controls groundwater recharge by buffering precipitation but at the same time providing preferential flow paths for infiltration. The importance of preferential flow on landslide hydrology is recognized in literature, but its monitoring and quantification remains difficult.

This chapter presents a combined hydrological and hydrochemical analysis of small-scale sprinkling experiments with the aim to show the potential of such experiments for studying the spatial differences in dominant hydrological processes within a landslide. This methodology was tested in the highly heterogeneous black marls of the Super-Sauze landslide. The tests were performed in three areas characterised by different displacement rates, surface morphology and local hydrological conditions. Special attention was given to identify and characterise the preferential flow patterns. Based on the analysis of all available field data, conceptual models of the hydrological response were proposed and confronted with existing knowledge about the Super-Sauze landslide.

Based on: Krzeminska D.M., Bogaard T.A., Debieche T.-H., Cervi F., Marc V. and Malet J.-P., (in review). Field investigation of fissure flows with small-scale sprinkling experiments on a hydrologically-controlled landslide. (submitted to) *Earth System Processes and Landforms*.

Krzeminska D.M., Bogaard, T.A., Debieche T.-H., Marc V. and Malet J.-P. 2012a (in press). Sprinkling tests to understand hydrological behaviour of mudslide. In: *Proc. Int. Conf 'The second World Landslide Forum'*, Rome, Italy.

4.1 Introduction

The texture and structure of the unsaturated zone control the groundwater recharge by attenuating percolation and providing preferential flow paths for infiltrating water. However, monitoring and quantification of percolation processes, subsurface flow paths, and residence time of water in the soil remains a challenge even in seemingly homogeneous soils. The main difficulties in landslides stem from strong heterogeneity of landslide lithology and spatio-temporal variation of hydrological properties and dominant hydrological processes. This is particularly true when dealing with highly heterogeneous unconsolidated, partly weathered, silty-clay sediments, such as black marls (Chapter 2). Additionally, in slow-moving clayey landslides, (constant) movement of sliding material results in the formation of fissures due to compression or extension, and successive opening and closing of fissure apertures depending on material characteristics, differential displacement and deformation rate.

Presence of fissures may influence the rate of groundwater recharge and change the time and intensity of drainage (see Ch.1§1.3.4). They create so called ‘dual permeability’ or ‘multiple permeability’ systems (see Ch.1§1.4): the porous medium consists of two (or more) interacting and overlapping but distinct continua. The water flow occurs in both continua but it is fracture continuum (macropore or fissure) that is the main transport medium, accommodating preferential flow (Gwo et al., 1995; Greco, 2002; Šimůnek et al., 2003; Gerke, 2006; Jarvis, 2007). Due to the complexity of preferential fissure flow processes (see Chapter 1,§1.3) it is very difficult to measure the processes in the field and to quantify them.

There are various experimental techniques that are used to gain insight into processes controlling preferential flow (see Ch.1§1.3.5) however, a consistent measurement method is not yet achieved. In the field the most convenient investigation method is the combination of the environmental or/and artificial tracing with hydrological surveying. However, plot scale artificial tracing of subsurface water flow is seldom studied owing to investigation difficulties in the field (Hirota et al., 2004; Binet et al., 2006). Debieche et al. (2012) used a large scale (14x7 m²) infiltration test to investigate the hydrodynamical and hydrochemical responses of a highly active area of the Super-Sauze landslide. This experiment gave valuable information to identify and understand preferential flow processes, and the development of local perched water tables. However, due to the size and long duration, this kind of experiments are logistically and financially very demanding, and cannot be undertaken on a regular basis

across the study area. Nevertheless, to improve our understanding of landslide dynamics, knowledge is needed on spatial heterogeneity of hydrological behavior and its relationship to differential movement occurring across a landslide.

The main objective of the research presented in this chapter is to test the potential of small-scale ($1 \times 1 \text{ m}^2$) sprinkling experiment to identify, study and quantify the dominant hydrological processes within an active, highly heterogeneous landslide. This chapter presents the results obtained from three sprinkling tests performed on morphologically different areas of the persistently active Super-Sauze landslide (French Alps). The hydrological and hydrochemical observations are generalised into hydrological concepts and collated with current knowledge about the landslide.

4.2 Methodology

4.2.1 Experimental design

The sprinkling experiments were performed with the use of sprinkling apparatus with one nozzle fixed above the sprinkling area. The apparatus has been calibrated in order to provide relatively homogenous distribution of the sprinkling water over the $1 \times 1 \text{ m}^2$ experimental plot: various nozzles in combination with various installation height and different pumping pressure. As a result the 1/4HH-10SQ nozzle was installed at the top centre at around 2 m high. Water supply was pumped in with regulated constant pressure (1.1 bars). The sprinkling was carried out in blocks of 15 min sprinkling and 15 min break with sprinkling intensity of approximately $20\text{--}30 \text{ mm.15min}^{-1}$ (Figure 4-2). This intensity is a trade off between the feasibility of the sprinkling equipment (pump and nozzle) and a realistic sprinkling rate: the applied intensity is comparable to the observed intensity of summer and autumn storms (up to $50 \text{ mm.15 min}^{-1}$; Malet, 2003) and is high enough to ensure infiltration to both matrix and fissure compartments. To monitor actual sprinkling volume, and determine its distribution within the sprinkling plots, the rain gauges (5 per plot) were installed. The actual sprinkling rate has been calculated based on Thiessen polygon method. In order to protect the experiment from wind disturbances and to minimize evaporation the experimental areas were covered with a tent. It is important to stress that the setup of the sprinkling experiment was designed to identify different patterns of the hydrological responses rather than being used for e.g. infiltration capacity measurement.

The 1x1 m² sprinkling tests were carried out in two periods of 7-8 hours sprinkling, composed of 14-17 sprinkling blocks (SB = 15 minutes rain + 15 minutes break), during two consecutive days. In this way, the first day of each sprinkling test started with dry initial conditions while the second one represented wet initial condition. The water used for the sprinkling tests was first collected in water tanks and blended with chemical tracers. The tracing was realised with two tracers: Br⁻ during the first day of experiment and Cl⁻ during the second day of experiment. The aim of introducing this artificial tracing is to reveal event – pre-event water mixing proportions and subsurface flow paths.

Within each sprinkling plot 4-5 piezometers were installed: one in the middle of the plot, two in the direction of expected (sub-)surface water movement (in the direction of fissures, if they were visible at the surface), and one upslope of a plot as the reference (Figure 4-1b). The piezometers were made of PVC tubes with 0.50 m filters, covered with standard filter protection, surrounded by filter sand and closed with granular bentonite. All three experimental setups were built up two days before the sprinkling experiment started.

Groundwater responses were monitored manually every 15 minutes and with the use of automatic recording water pressure devices (Divers and Kellers) with a 3 minute time resolution. The water for hydrochemical analyses was sampled every 1 hour from all piezometers during the sprinkling experiment and one time per day for two consecutive days after the experiment. Additionally, the sprinkling plots A and B were equipped with 1m long access tubes for Theta Probes (PR1/6w-02, Delta-T Devices with reported accuracy of $\pm 0.06 \text{ m}^3 \text{ m}^{-3}$; Van Bavel & Nichols, 2002) in order to monitor changes in soil moisture profile at 6 depths (0.1, 0.2, 0.3, 0.4, 0.6 and 1.0m). The device was not installed in plot C due to technical problems. The initial surface soil moisture (0-0.10 m depth) in the plot B was measured with a manual field operated Time-Domain Reflectometry probe (TDR). The reported accuracy of the FOM TDR is $\pm 0.02 \text{ m}^3 \text{ m}^{-3}$ (IA PAS, 2006).

4.2.2 Analysis methodology

The soil column for water balance and for tracer mass balance calculation was bounded laterally by the 1x1 m² sprinkling surface area and vertically by the maximum depth of the piezometer installed in the center of each plot. The water balance of the sprinkling experiment for 7 or 8 hours duration is:

$$V_P + V_{GW,in} = V_{GW,out} + V_{OF} + V_E + \Delta S \quad (4.1)$$

where V_P is the volume of precipitation (sprinkling), which here represents the amount of sprinkling water, $V_{GW,in}$ and $V_{GW,out}$ are the volumes of groundwater inflow and outflow, V_{OF} is the volume of overland flow, V_E is evaporation volume and ΔS is the change in storage over the duration of the sprinkling experiment.

Moreover, a depletion curve analysis was applied in analogy of hydrograph recession analysis by applying linear reservoir concept (Hornberger et al., 1991; Mikovari & Leibundgut, 1995; Sivapalan et al., 2002). Additionally, assuming that groundwater level is a direct function of change in drained volumes (therefore, a change in storage) it was possible to identify differences in types of storages based on occurrence of inflexion points in the drawdown curves. The time for depletion of the storages is indicated by a depletion factor. Depletion factor (K) is calculated for all segments of the drawdown curve defined by inflexion points using the empirical method explained by Linsley et al. (1982):

$$h_{t+\Delta t} = h_t \cdot e^{\frac{-\Delta t}{K}} \quad (4.2)$$

where h_t is the groundwater level at time t , and Δt the temporal resolution of groundwater level observations [min]. The steeper part of the curve represents fast drainage and is usually assumed to be preferential flow, whereas the gentle part representing slower drainage is comparable to represent matrix flow.

Besides qualitative description of the infiltration process the concentration of the conservative tracers (Br^- and Cl^-) was used to calculate the proportion of different water sources (event – pre-event water) using a two-component end-member mixing (EMMA) model. The EMMA model has been widely used for hydrological studies to separate the different contributions of streamflow (Christophersen & Hooper, 1992; Mulholland and Hill, 1997; Soulsby et al., 2003; James & Roulet, 2006; Cras et al., 2007). The end members are usually defined from the reservoir characteristics so mixing diagrams inform about the variable source areas of runoff. At the same time, they could be used to understand the flow processes which take place during infiltration. The mixing proportions can be calculated using the following equations:

$$\begin{aligned}
\alpha_1(t) \cdot C_{Br^-, EW1} + \beta_1(t) \cdot C_{Br^-, PE} &= C_{Br^-}(t) \\
\alpha_2(t) \cdot C_{Cl^-, EW2} + \beta_2(t) \cdot C_{Cl^-, PE} &= C_{Cl^-}(t) \\
\alpha_{1,2}(t) + \beta_{1,2}(t) &= 1
\end{aligned} \tag{4.3}$$

where $C(t)$ are tracer concentrations [mg.l^{-1}] measured during the sprinkling experiment at different time (sampled from piezometers) and α and β are mixing proportions during the sprinkling tests. PE and EW indicate the pre-event and event water, and the numbers indexes are related to first and second day of experiment respectively. As $C_{Br^-, PE}$ and $C_{Cl^-, PE}$ are assumed negligible in regards with EW concentrations, the equations reduce to:

$$\begin{aligned}
\alpha_1(t) \cdot C_{Br^-, EW1} &= C_{Br^-}(t) \\
\alpha_2(t) \cdot C_{Cl^-, EW2} &= C_{Cl^-}(t)
\end{aligned} \tag{4.4}$$

Besides the added conservative tracers Br^- and Cl^- , also the sulphate concentration in groundwater prior the experiment could be used as an independent variable to define a ‘pre-event’ end member ($C_{SO_4^-, PE}$). Sulphate is the major component of the groundwater chemistry and it can be used as tracer as long as the impact of the difference between groundwater and rainwater concentrations remains far larger than that of the water-rock interaction. When sprinkling is applied (EW), its sulphate content ($C_{SO_4^-, EW}$) can be considered as the second end-member:

$$\begin{aligned}
\alpha_1(t) \cdot C_{SO_4^-, EW1} + \beta_1(t) \cdot C_{SO_4^-, PE} &= C_{SO_4^-}(t) \\
\alpha_2(t) \cdot C_{SO_4^-, EW2} + \beta_2(t) \cdot C_{SO_4^-, PE} &= C_{SO_4^-}(t)
\end{aligned} \tag{4.5}$$

The two estimated mixing proportions (for artificial and environmental tracers) for both experiments are plotted to analyse and validate the mixing assumption.

Furthermore, simple mass balance equations were used (for Br^- and Cl^-) to estimate the most probable water (and tracer) flow paths and to restrain mixing processes:

$$\begin{aligned}
V(t_{end}) &= V_{PE} + V_{INF} - V_{SSF} \\
C_{Br^-/Cl^-}(t_{end}) \cdot V(t_{end}) &= C_{Br^-/Cl^-, PE} \cdot V_{PE} + C_{Br^-/Cl^-, EW} \cdot V_{INF} - C_{Br^-/Cl^-}(t) \cdot V_{SSF}
\end{aligned} \tag{4.6}$$

where $V(t_{end})$, V_{PE} , V_{INF} and V_{SSF} are the estimated total water volume in the soil column at the end of sprinkling tests, the estimated volume of pre-event water, the estimated volume of infiltrated water (fraction of EW) and the estimated volume of subsurface flow (including exfiltration). The volume of pre-event (V_{PE}) is calculated based on initial groundwater level and initial soil moisture content:

$$V_{PE} = A \cdot (h_{t_0} \cdot n + (z - h_{t_0}) \cdot \theta_{ini}) \quad (4.7)$$

where A is the plot area [m^2], h_{t_0} is the groundwater level [m] observed before the experiment, n is average porosity [-], z is the depth of analysed soil column [m] and θ_{ini} is the initial soil moisture [-].

4.2.3 Characteristics of experimental plots

The small-scale sprinkling experiments A and B are located in the upper part of the Super-Sauze landslide (see Chapter 2) which is the most active in terms of displacement rates, abrupt changes in groundwater levels throughout the season and changes in fissure density and openings (Figure 4-1). The experiment C is located in a relatively stable part of the landslide, but still at the direct contact with the most active area, and is representative of small displacement rates, small changes in groundwater levels throughout the season and no changes in fissure characteristics (Figure 4-1b). As such, the three experimental plots are chosen to present different dominant hydrological responses (Malet, 2003; deMontety et al. 2007). All sprinkling experiments were localised in relatively flat areas with slope of 5-7°. The geomorphology of each plot is detailed below:

- Plot A is located in the active area near the crown (ablation zone) consisting of relative fresh but heavily broken marl blocks and deposits (marly fragments of approximately 2 cm). There are wide (aperture of 0.07 - 0.15 m) undulating fissures observed on the surface (see Figure 4-1b for the sketch), partly or totally filled with reworked marl fragments. The open depth of these fissures varies from 0.09 to 0.12 m.
- Plot B is located also in the very active area, at a secondary mudslide deposition area (transit zone). It is gravel crust, characterized by coarse fragments (bigger than 2 mm) overlaying a finer matrix. There are wide open (apertures around 0.10 m) fissures present within plot area with the open depth reaching 0.50 m (see Figure 4-1b for the sketch).

- Plot C is situated in the compacted, relatively stable western part of the landslide consists of fine grained with different rock fragments. No fissures are observed at the surface.

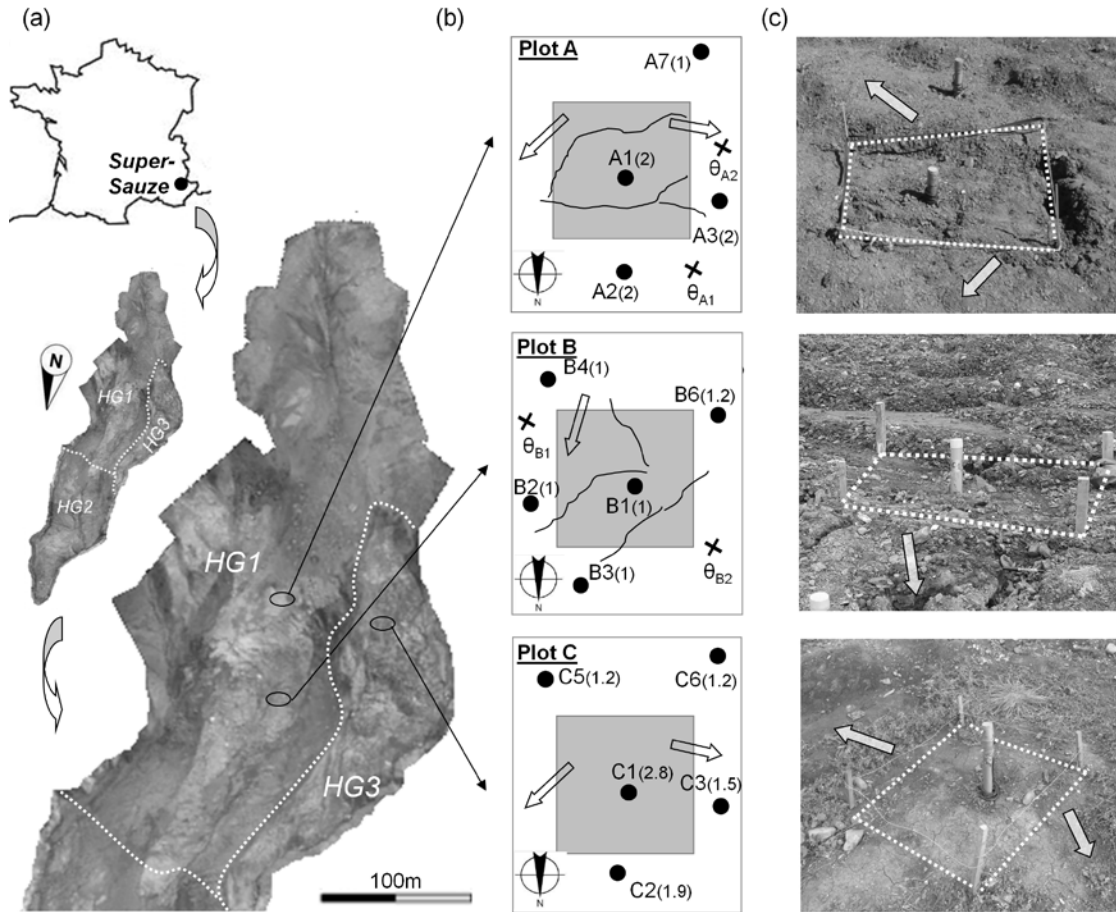


Figure 4-1. (a) The upper part of the Super-Sauze landslide with indicated location of three sprinkling tests (plot A, B and C); the white dashed lines indicate the hydro-geomorphological units (after Malet et al. 2005). (b) Schematic representation of the experimental setup of each area (not scaled); grey squares represents $1 \times 1 \text{ m}^2$ sprinkling plots; dots represent the location of the piezometers; numbers in brackets indicate the depth of the piezometers in metres; crosses indicate the location of the theta probes; undulating lines indicate fissure distribution within the sprinkling plots and arrows show the local slope direction in the area. (c) Photographs of the soil surface of each sprinkling area with arrows showing the local slope direction in the area.

The depth of the surficial unit is significantly different in each plot and is equal: around 10 m in plot A, 3 m in plot B and 5 m in plot B (Travelletti & Malet, 2012). The annual average depth of the saturated zone is 1.9, 1.1 and 2.5m respectively. The porosity values for the experimental plots were assumed to be 0.35, 0.38 and 0.30 in average for plot A, B and C respectively, based on the gravimetric measurement (Malet, 2003).

The depth of the piezometers is different at each area. Within plot A all piezometers were installed at approximately 2 m depth. Within plot B the piezometers depths are around 1 m due to the shallow groundwater level (see also Figure 4-1b-c.). Within plot C the depths of the piezometers were influenced by the presence of rock fragments in the soil and vary from 1.2 to 3.0 m.

The sprinkling water was taken from the Goutta spring above the landslide originating from moraine deposits, and which is not influenced by any mineralization during its transport in the landslide (Debieche et al., 2012).

4.3 Results of sprinkling experiments - hydrological and hydrochemical responses

Within each sprinkling plot different hydrological behaviours were observed. Figure 4-2 summarises the observed groundwater variation and tracer concentration patterns. Figure 4-3 shows the drawdown curves after the second day of sprinkling. For plot A and B the drawdown of the centrally-located piezometers was analysed (A1 and B1), while for plot C the analysis is carried out for piezometer C2 since the groundwater level observed in piezometer C1 was strongly influenced by water sampling.

4.3.1 Plot A

Plot A was a dry area with no groundwater observed within the first 2 m depth (depth A1) before the experiment started. The mean initial volumetric water content of the top soil layer (up to 0.30 m depth), was 0.12 with standard deviation of 0.03. In response to the applied sprinkling neither overland flow nor subsurface runoff was observed. The groundwater fluctuation in A1 showed a very fast vertical movement of water: the significant rise of groundwater level during 15 minutes sprinkling and fast drop of water level in the 15 minutes break (approximately ± 0.25 -0.30 m). Moreover, the drawdown after each day of sprinkling lasted four hours only (Figure 4-2a and Figure 4-3).

The total increase of groundwater level in A1 was more than 0.9m above the soil column depth. In A2 the increase of the groundwater level was limited to maximum 0.21 m and in A3 to 0.27 m above the depth of the piezometer (2.0 m and 1.8 m respectively). Moreover, in A3, located in the direction of the surface fissures, the groundwater level started to react during

the first day after fourth sprinkling block (SB-04). In A2 the groundwater reaction started only during the second day after SB-05. In A7 no change was observed.

The soil moisture variation observed in the soil profile in θ_{A2} (approximately 1 m distance from the sprinkling area) is negligible. In θ_{A1} no changes were observed in the first 0.60 m of soil profile, however, at 1 m depth soil moisture increased till saturation over the two days of the sprinkling experiment.

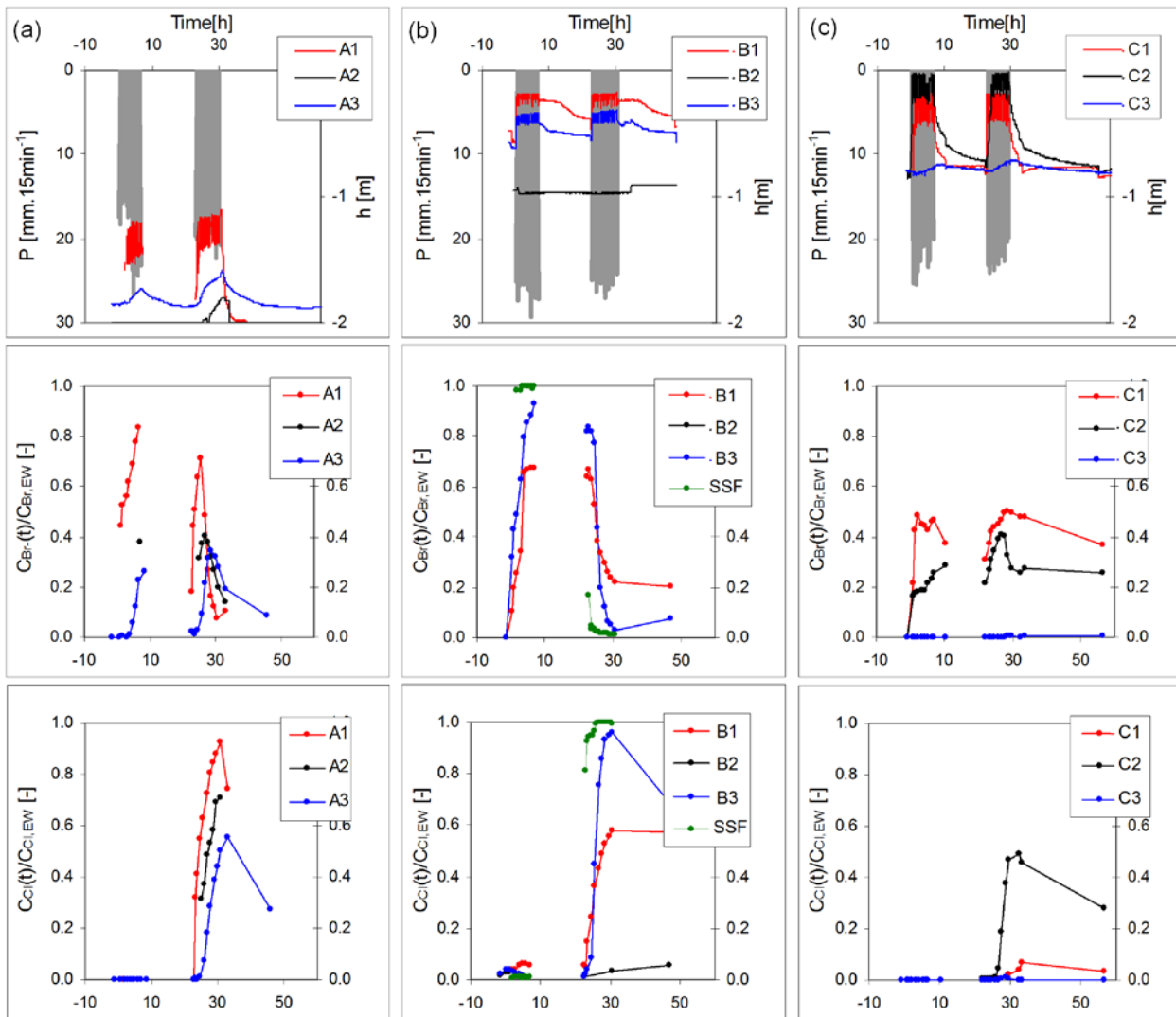


Figure 4-2. Monitoring results of three sprinkling experiments: (a) plot A, (b) plot B and (c) plot C. Upper panels show the intensity of the sprinkling (primary Y-axis) and groundwater responses in piezometers (secondary y-axis). Middle and bottom panels show the ratio between tracer concentration measured in the piezometers or subsurface runoff (SSF) and the applied tracer concentration.

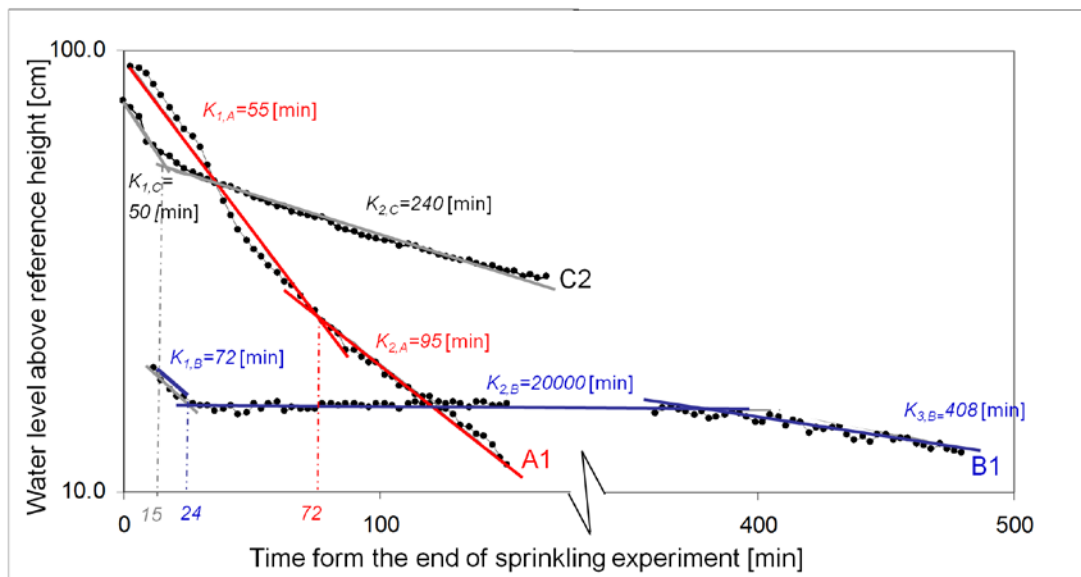


Figure 4-3. Drawdown curves observed in piezometers A1, B1 and C2 after the end of sprinkling experiments and corresponding depletion factors K [min],

The tracer concentration in the piezometers gradually increased with cumulated amount of applied sprinkled water. Similar to the hydrological responses, the most intense changes were observed in A1, reaching 84% (first day) and 93% (second day) of applied tracer concentration at the end of each 7-8 hours sprinkling. Moreover, tracer concentration decreased during the recession phase. At the start of the second day, Br^- concentration had nearly dropped back to the initial value. The same trend was observed for Cl^- during the second day. The tracer concentration in A2 and A3 followed the trend observed in A1. However, the maximal measured tracer concentration in A2 reached 38% (first day) and 71% (second day) of applied concentration. In A3 the maximal tracer concentrations are 26 and 55% respectively. It is important to note that in plot A, on the second day of experiment Br^- was applied during first four sprinkling blocks (SB-01 to SB-04) with very high concentration (461 mg.l^{-1}). This incident determined the behaviour of Br^- concentration at the beginning of the second day of sprinkling: maximum concentration of Br^- was observed after SB-06 in A1, after SB-08 in A2, and after SB-12.

4.3.2 Plot B

Plot B was located at an area with shallow groundwater level (0.35-0.55 m below the surface). The average initial volumetric water content in the first 0.30 m of the soil was 0.25 with standard deviation of 0.07. During the sprinkling experiment an increase of groundwater level

was observed only in B1 and B3 and they amounted 0.25 and 0.20 m respectively. The groundwater level fluctuated on average ± 0.07 m in response to a single sprinkling block. No groundwater level changes in B2 and B6 were registered and no changes were observed in soil moisture content in θ_{B1} or θ_{B2} (located within approximately 1m distance from 1x1 m² sprinkling plot).

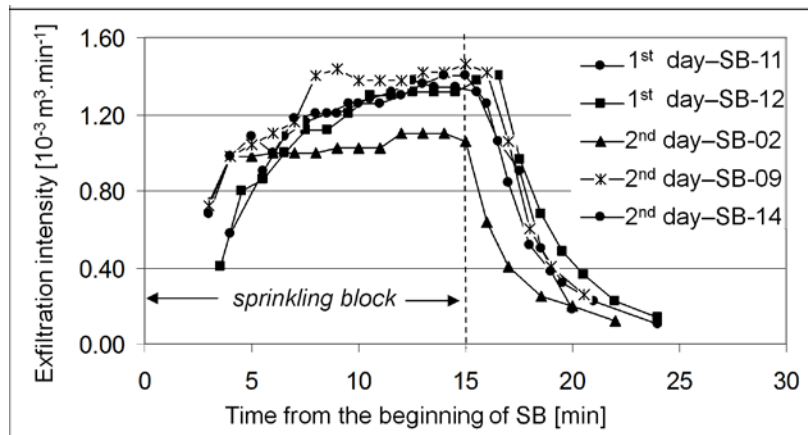


Figure 4-4. Example of the dynamics of the subsurface runoff (i.e. fissure flow) observed in plot B during and after sprinkling blocks (SB).

The exfiltrating subsurface runoff was measured around 1-1.5 m downslope of the experimental plot. The volume of subsurface runoff per sprinkling block increased with time. For the first day, it started with $15.9 \cdot 10^{-3} \text{ m}^3$ during SB-05 and reached $18.3 \cdot 10^{-3} \text{ m}^3$ during SB-14. For the second day, it ranged from $11.4 \cdot 10^{-3} \text{ m}^3$ (during SB-01) to $19.5 \cdot 10^{-3} \text{ m}^3$ (during SB-14). The total volume of measured exfiltrating subsurface runoff was more than 45% of applied water volume during first day and 70% during the second day. Figure 4-4 shows the dynamics of the subsurface runoff: the subsurface runoff starts 3 (first day) or 2 (second day) minutes after the sprinkling starts and it reaches its maximum intensity shortly before the end of 15 minute sprinkling. The subsurface runoff ends 8 - 9 (first day) or 5 - 7 (second day) minutes after the sprinkling ceases.

In B1 and B3 the relative Br^- concentration rose quickly and reached 67% and 93% maximum respectively at the end of the first day. Moreover, it remained at a high level in-between two days of sprinkling (Figure 4-2b). Similar tracer concentration behaviour was observed during the second day of the experiment, when chloride was applied. The observed Br^- concentration gradually decreased while the Cl^- concentration increased reaching 58% (B1) and 99% (B3) of applied concentration. The Cl^- concentration remained high (in B1 58% and in B3 68% of

applied concentration) even 20h after the end of the experiment. It is noteworthy that the concentration of Br^- and Cl^- is most of the time higher in B3 than in B1 and that the tracer concentration in the subsurface runoff equals (first day) or almost equals (second day; 81-99%) that of the sprinkling water.

4.3.3 Plot C

Plot C had wetter initial conditions: the initial groundwater level was around 0.75-1.00 m below surface and the initial volumetric water content varied between 0.20 and 0.25 (0.23 in average) in the first 0.10 m of the soil. In contrast to the dynamics observed in plot A, around 75% of the sprinkling water left the soil column as overland flow. Moreover, during the entire experiment ponding was observed within the 1x1 m² plot.

The groundwater level observed in C1 and C2 respond similarly: an increase of groundwater level up to 0.20 m (for C1) and 0.05 m (for C2) below surface and fluctuations of about 0.20 m after each 15 minutes sprinkling. The drawdown observed in C1 stopped after 4 hours whereas in C2 it took around 12 hours after the sprinkling ceased. C3 showed 0.03-0.07 m groundwater level fluctuation and in C5 and C6 no response was registered.

In C1 the relative concentration of Br^- reached approximately 43-49% of the applied tracer concentration and was around constant during the first day of sprinkling. At the start of the second day Br^- relative concentration was 31% and it rose again up to 50% as soon as new sprinkling water (without Br^-) was applied (Figure 4-2c). Similar trends were observed for C2, with the maximal tracer concentration reaching 28% and 40% of applied concentration for the first and second day respectively. There was no tracer found in C3.

During the second day of the sprinkling experiment, the Cl^- concentration showed very limited increase in C1 but a gradual increase up to around 50% of the applied concentration in C2. The Cl^- concentration decreased after the second day. However, in C2 it remained relatively high even 20 h after the experiment (300 mg.l⁻¹). Again, no tracer was found in C3.

4.4 Discussion of experimental results and model conceptualisation

4.4.1 Water balance and tracer mass balance analysis

The water budget was calculated for each day of the sprinkling experiment from the first sprinkling block (SB-01) till the end of the observed drawdown in the centrally located piezometer. As a first approximation the water balance components were estimated based on the assumption that the whole experimental area ($1 \times 1 \text{ m}^2$) was hydrologically active, meaning all water stored in the soil column was mobile and full mixing of pre-event water and event water occurs. The groundwater flow variations were assumed to be only due to infiltrating sprinkling water over the experimental plot (Figure 4-5). This means we assume no change in overall groundwater flow and no change in deep percolation (plot B and C) due to the sprinkling activity. In case of plot A, where no groundwater level was observed before and short after the experiment, the direction of the estimated subsurface flow cannot be determined so the subsurface flow comprises both vertical deep percolation (P_e) and lateral flows (SSF). The volume of pre-event (V_{PE}) water was estimated based on Eq.4.7, and the volume of infiltrated water (V_{INF}) was calculated as: $V_{EW} - V_{OF}$. The volume of subsurface fluxes (V_{SSF}), which comprises all subsurface fluxes, was estimated using the measured groundwater level responses to the consecutive sprinkling blocks and the change in storage ΔS was calculated as: $V_{INF} - V_{SSF}$. Evaporation (E) is assumed to be negligible as the sprinkling plots were covered with a tent. Table 4-1 shows the measured (^m) and estimated (^e) water balance components.

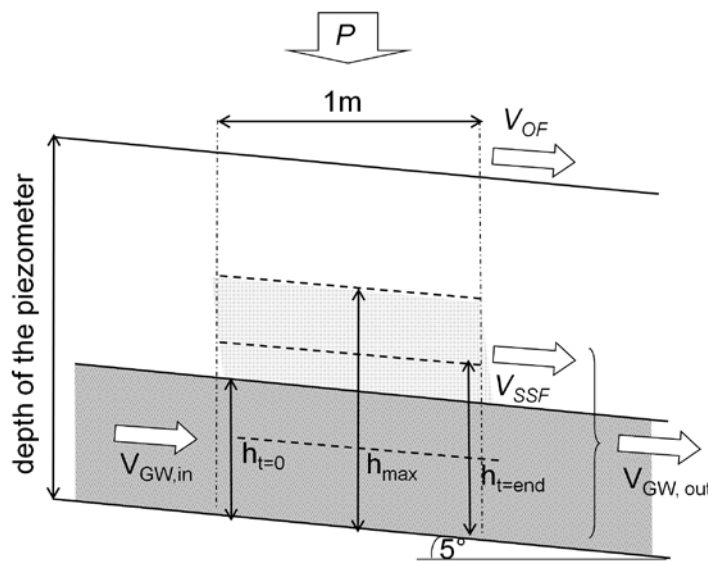


Figure 4-5. Schematic representation of water balance components of experimental plots.

Table 4-1. Measured ^(m) and estimated ^(e) components of water balance for each plot, with the assumption that whole experience area is hydrologically active

	Plot A		Plot B		Plot C	
Day of experiment (duration)	1 st (7h)	2 nd (8h)	1 st (7h)	2 nd (8h)	1 st (7h)	2 nd (7h)
Assumed average porosity, n [-]	0.35	0.35	0.38	0.38	0.30	0.30
^(m) Initial average volumetric soil moisture, θ_{ini} [-]	0.12	0.12	0.25	0.27	0.23	0.25
^(e) Water in soil column, V_{PE} [m ³]	0.23	0.24	0.32	0.34	0.78	0.79
^(m) Sprinkling volume, V_P [m ³]	0.27	0.33	0.36	0.42	0.29	0.30
^(m) Overland flow, V_{OF} [m ³]	Not observed		Not observed		0.22	0.23
^(e) Infiltrated water, V_{INF} [m ³]	0.27	0.33	0.36	0.42	0.09	0.08
^(e) Subsurface flow, V_{SSF} [m ³]	-*	0.23	0.34	0.41	0.09	0.08
- ^(m) exfiltration [m ³]	Not observed		>0.17**	0.30	Not observed	
^(e) Water in soil column, $V(t_{end})$ [m ³]	-*	0.34	0.35	0.35	0.79	0.79
^(e) Change in storage, ΔS [m ³]	-*	0.10	0.02	0.01	0.01	0.01
^(e) Final average volumetric soil moisture, $\theta(t_{end})$ [-]	-*	0.17	0.27	0.28	0.25	0.26

* Estimation not possible because of missing groundwater level observation

**Exfiltration started after 2 hours of sprinkling but was measured only since 3rd hour of sprinkling experiment

The tracer mass balance was used to evaluate the assumption of water mobility and full mixing within the soil column. The bromide and chloride masses were calculated from measured chemical concentration times corresponding water volumes. The tracer mass remaining in the soil column was calculated in two ways: (1) based on the tracer mass balance and (2) based on the measured tracer concentration in the groundwater at the end of the sprinkling experiments. When we consider the entire soil column as hydrologically active, the second calculation method gives higher tracer mass. However, the difference between the two can be minimized by reducing the hydrologically active area. The percent of the experimental area that is hydrological active (x) can be estimated based on Eq. 4.8.

$$\begin{aligned}
 C_{Br^-/Cl^-}(t_{end}) \cdot V(t_{end}) &= x \cdot C_{Br^-/Cl^-, PE} \cdot V_{PE} + C_{Br^-/Cl^-, EW} \cdot V_{INF} - x \cdot C_{Br^-/Cl^-}(t) \cdot V_{SSF} \\
 V(t_{end}) &= x \cdot V_{PE} + V_{INF} - x \cdot V_{SSF}
 \end{aligned}
 \tag{4.8}$$

It is important to note that V_{PE} and V_{SSF} are estimated based on groundwater level observation multiplied by the (hydrologically active) area of the experiment.

Table 4-2 shows tracer mass balance component and it is subdivided in two parts: first, the results based on the assumption that the whole soil column is hydrologically active (i.e. full mixing), second the results taking into account a percentage of the soil column that is hydrologically active.

Furthermore, the influence of porosity values was evaluated. Increasing or decreasing the average porosity with 0.01 and 0.02 results in changes in the water balance components. There is limited influence of porosity on the estimated volume of pre-event water: no changes in plot A (since there was no groundwater before the experiment), $\pm 5\%$ in plot B and $\pm 3\%$ in plot C. The volume of subsurface flow is more sensitive for changes in soil porosity. It varies between $\pm 35\%$ in plot A and $\pm 24\%$ in plot C. Within plot B the change in subsurface flow volume expressed in percentage terms is also significant (between $+11\%$ and -55%) but it corresponds to relatively low absolute values ($0.05\text{--}0.1\text{ m}^3$). Consequently, the changes in volume of water stored in the soil column at the end of experiment are the highest for plot A (between -23% and $+44\%$) and relatively limited for plot B ($\pm 7\%$) and plot C ($\pm 14\%$). The influence of porosity changes on calculated percentage of hydrologically active area (Eq. 4-8) is limited to maximum $\pm 2\%$.

4.4.2 Hydrological and hydrochemical observation

Clearly, a diverse spectrum of results emerges from the experiments. However, the results also show interesting similarities. The sprinkling water infiltrates into the top soil through both matrix and preferential (fissure) flow paths. Once water entered into the soil the plots show basically two types of drainage. First groundwater level depletes fast and slows down after 15-90 minutes. Interestingly, fast infiltration and fast drainage do not coincide. Plot A has both fast infiltration and fast drainage (both in first and second stage), whereas plot B shows high infiltration capacity but the second reservoir shows the slowest depletion of the stored subsurface water. Plot C has low infiltration rate but seems to drain the infiltrated water relatively quickly.

Table 4-2. Measured ^(m) and estimated ^(e) tracer mass balance components and the evaluation of the hydrologically active area assumptions

	Plot A		Plot B		Plot C	
Day of experiment (applied tracer)	1 st (Br ⁻)	2 nd (Cl ⁻)	1 st (Br ⁻)	2 nd (Cl ⁻)	1 st (Br ⁻)	2 nd (Cl ⁻)
Tracer in applied water						
- ^(m) concentration, [] _{EW} [g .m ⁻³]	118	1035	122	128	123	1047
- ^(e) mass [g]	32.3	343.7	44.1	53.5	35.6	322.5
^(e) infiltrated tracer [g]	32.3	343.7	44.1	53.5	10.1	85.2
<i>assuming that whole area is hydrological active</i>						
^(e) Tracer out of soil column via:						
- overland flow, [g]	Not observed		Not observed		22.3	237.3
- subsurface flow, [g]	-*	162.8	>33**	36.2	4.2	2
^(e) Mass of tracer remained in soil column based on mass budget [g] (mass _{in} – mass _{out})	-*	180.9	<11.1	17.3	5.9	83.2
^(m) Tracer concentration in the groundwater, [] (t _{end}) [g.m ⁻³]	91,4	768.5	81.4	73.6	45.8	50.34
^(e) Mass of tracer remained in soil column based on measured concentration, [g] (V(t _{end}) [](t _{end}))	-*	261.3	27.7	25.8	35.7	39.7
<i>assuming that x percentage of the area is hydrological active</i>						
^(e) Percent of the plot area that is hydrologically active, x[%]	-*	53	24	60	17	210
^(e) Tracer out of the soil column via subsurface flow [g]	-*	86.3	>25.7**	34.2	0.7**	4.3
^(e) Mass of tracer remained in soil column based on mass budget [g]	-*	257.4	<18.4**	19.3	9.4**	82.7
^(e) Mass of tracer remained in soil column based on measured concentration, [g]	-*	257.7	18.4	18.9	9.5	80.8

* Estimation/measurements not possible because of the missing groundwater level observation

**Exfiltration started after 2 hours of sprinkling but was measured only since 3rd hour of sprinkling experiment

The tracer information shows similarities with the groundwater patterns. Both bromide and chloride concentrations rise reaching almost the initial concentration of the sprinkling in the centre of plot A and around 60% of the initial concentration of the sprinkling in the centre of plot B within the duration of the experiment. In plot C both tracers reach maximum 0.5 relative concentration indicating more mixing with pre-event water. The location of highest relative concentration is in the centre for plot A and downslope of plot B (in B3). Plot C results are again a bit more diverse, both piezometers C1 and C2 show mixing of sprinkling water with pre-event water for the first day but only the downslope located C2 shows a significant increase of chloride concentration during the second day experiment.

The results of the EMMA model underline the differences in mixing processes and their dynamics observed per plot (Figure 4-6). For all plots the relation between mixing proportion estimated based on both applied tracer and sulphate concentrations do not follow the 1:1 line exactly. This can be an effect of soil – water interaction (dissolution of pyrite). This can be partly due to the uncertainty on the PE sulphate concentrations estimates which may vary quite a lot over short distances. Within plot A and B the mixing processes are clear: the mixing proportions change progressively during the sprinkling experiment from 0% to more than 90% (plot A) or around 70% (plot B) for both tracers and sulphate. In plot C the mixing proportions increase during the first day but they are limited to 64%. Moreover, in plot A and B, the artificial and environmental tracers behave similar over the two days sprinkling experiment showing that mixing processes can be explained with two end-member only: mixing of event water with pre-event water. This is also the case for the first day in plot C. During the second day of the experiment a sharp dilution of SO_4^{2-} was observed in C1 while Cl^- concentration remained low and Br^- concentration increased. This indicates that in plot C, both event waters (EW1 during first day and EW2 during second day of sprinkling) contributed independently in mixing with pre-event water. However, it is important to stress that EMMA results are based only on tracer concentrations and give relative mixing proportion and do not give the absolute mass of mixed tracers.

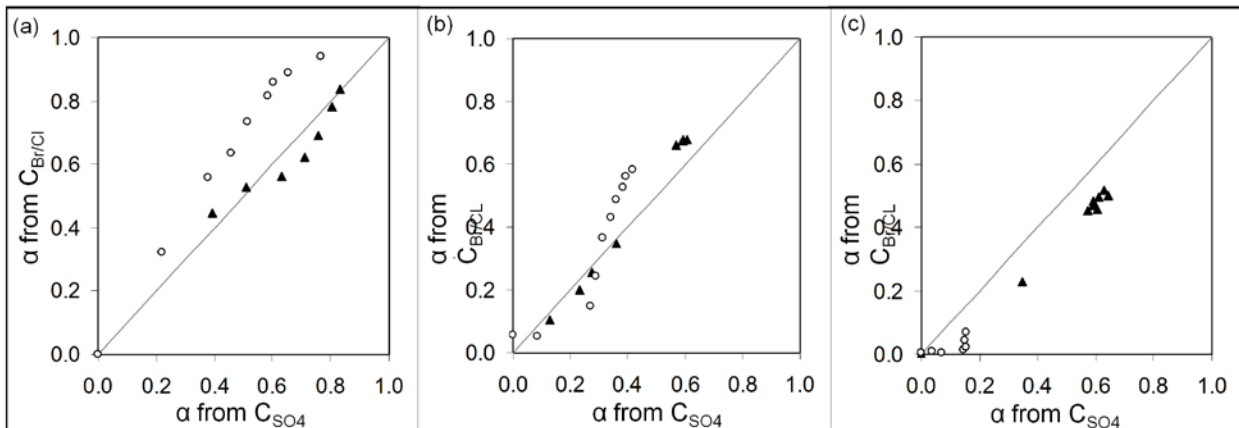


Figure 4-6. EMMA model results for the centrally located piezometers A1 (a), B1 (b) and C1 (c). The full triangles are estimates for the first day of the experiment and the open dots represents second day of the experiment. The grey line is 1:1 line.

The three plots show different spatial responses. In case of plot A three piezometers show a response in water level and in tracer concentration. In plot B and C only two piezometers react to the sprinkling in groundwater level and water quality. This suggests the plot B and C

have structured flow paths whereas plot A is more permeable in all directions. Subsurface flow often follows the slope gradient, however, the presence of fissures and macroporosity (plot A and B) strongly influences flow direction.

Based on the interpretation of the sprinkling experiment, three conceptual models of the observed hydrological behaviour are proposed (Figure 4-7):

- Fast input – fast output (plot A) – very fast infiltration as well as fast drainage;
- Fast input – slow output (plot B) – fast infiltration but very slow drainage;
- Fast but limited input – moderate output (plot C) – limited infiltration and relatively slow drainage (when compared with plot A).

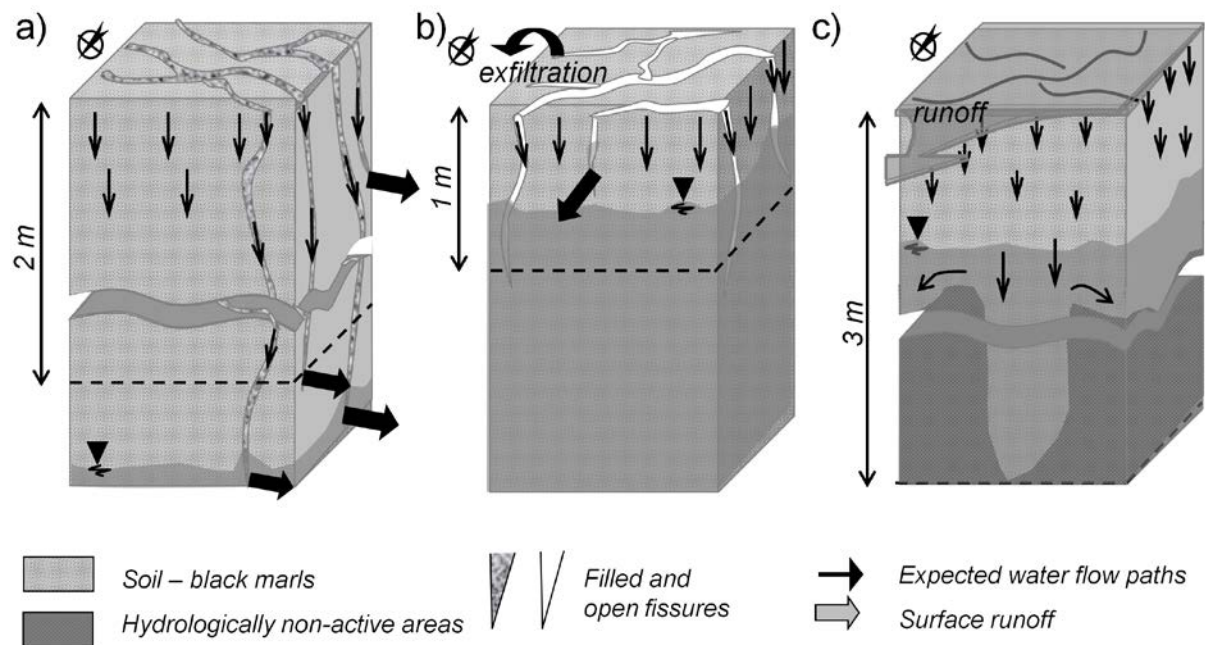


Figure 4-7. Conceptual models for preferential flow within three experimental areas: (a) fast vertical preferential fissure flow and fast matrix flow; (b) combination of matrix flow and preferential flow (isolated fissure flow system), (c) matrix-like infiltration with limited influence of preferential flow. The black dashed lines indicate the depth of centrally-located piezometer.

Concept 1: Fast input- fast output

Plot A represents a fast input-output type of hydrological response: the very fast response to the onset of sprinkling as well as sudden groundwater level drop after sprinkling is finished. The sharp groundwater level decrease in A1 (see Figure 4-3) after the end of the sprinkling

test is an indication of drainage from a highly permeable fraction of the subsurface, e.g.: the fissure fraction. Moreover, the second part of the depletion curve is quite rapid as well, indicating that also the matrix fraction is highly permeable. The very high permeability is confirmed by the fact that groundwater responses are observed not only in the centre of the experimental plot (A1) but also in two directions downslope: relatively quick response in A3 (direction of fissures observed on the surface) and delayed in A2.

A rough quantification of matrix flow and preferential flow can be done by estimating Darcian flow between A1 and A2 (Figure 4-8). The subsurface outflow is estimated from the depletion curve after the final sprinkling block. The total volume of subsurface outflow (through matrix and fissures) from the experimental plot can be estimated from the depletion curve A1. Extrapolating the depletion curve (A1) corresponding to the slow drainage (Figure 4-3) towards the beginning of the drawdown gives an estimate for the groundwater level drop due to matrix flow. The flow cross section is the product of the groundwater level observed in A1 (h_{A1}) and the diagonal width of the experimental plot ($\sqrt{2}$). The hydraulic saturated conductivity of the area (upper part of HG1 unit) is set to be 10^{-5} m.s^{-1} (Malet, 2003). The estimated lateral matrix flow during depletion is approximately 40% of the total subsurface flow while remaining 60% of total subsurface flow is preferential flow through the fissures and deep percolation.

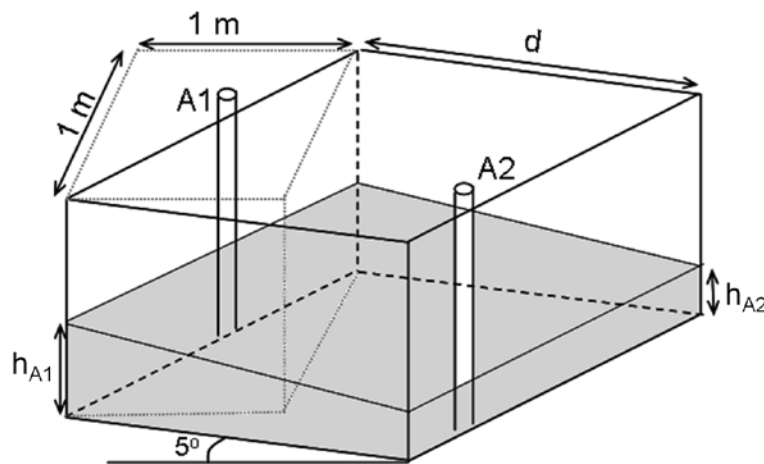


Figure 4-8 The scheme that is used to calculate the Darcy flow between A1 and A2; the soil column contours are marked in grey, h_{A1} and h_{A2} are groundwater levels observed in A1 and A2 respectively, d is the distance between A1 and A2.

There is 0.7m³ of pre-event water (approximately 33-36% of maximal storage capacity) storage in the soil column. Of this pre-event water, 50-54% could mix and readily move with the infiltrating sprinkling water (Table 4-1 and 4-2). Moreover, the incident with the accidentally application of high concentration Br⁻ at the beginning of the second day of sprinkling proves the dominance of fast preferential flow through the plot and short residence times of water within the subsurface.

Concept 2: Fast input – slow output

The hydrological responses in plot B can be described as fast input – delayed output. The presence of a largely open (up to 14 cm) fissure system influences the distribution of infiltrating water and groundwater level recharges. Well connected subsurface structures provide subsurface drainage when the water level surpasses a certain threshold level. The observed hydrological response is a combination of fast vertical infiltration, fast subsurface flow and much slower matrix flow. The shape of the drawdown curve (Figure 4-3) also indicates the combination of mainly preferential flow and some matrix flow.

The behaviour of the tracer concentration indicates complex mixing processes in plot B. The significant amount of pre-event water (approximately 80-84% of maximum storage) is stored in the matrix and 24-61% of this water is involved in mixing process (Table 4-1 and 4-2). The spatial distribution of tracer concentration (lower concentration in B1, higher in B3 and in subsurface flow) indicates a well structured subsurface (including fissure system) that can provide direct drainage for infiltrated water. This fast flow domain is isolated from the matrix (no or poor connection). When the groundwater level is high a well connected preferential flow system becomes active and the applied water drains directly ($K_{1,B}$; Figure 4-3). However, once the water level has dropped several centimetres the drainage stopped (e.g.: dead – end fissure) and the system maintains high groundwater levels for several hours ($K_{2,B}$; Figure 4-3). The last drainage phase ($K_{3,B}$; Figure 4-3) can be interpreted as matrix flow after saturation connecting the wet fissure areas.

The dynamic changes in the Br⁻ and Cl⁻ concentration also show that infiltrating water of the first day replaced the pre-event water and is temporarily stored till the new source of water (sprinkling of second day) appears.

Concept 3: Fast but limited input – moderate output

The general observation of the water balance component (Table 4-1) and drawdown curves (Figure 4-3) indicates that plot C represents an area with limited infiltration capacity where surface runoff is easily generated. However, in this area with matrix-like infiltration preferential flow cannot be neglected. The presence of preferential flow paths (fissures, macropores) that influences the hydrological behaviour at studied scale, stems from the observed drainage at the end of each 15 minutes of sprinkling and depletion constant for the steep part of depletion curve (K_{1C}) which is almost three times higher than the one for gentle second part of the curve (K_{2C}).

The relatively low concentration of tracer in the groundwater (less than 50%) can be related to the low infiltration capacity of the area and significant amount of pre-event water (approximately 92-94% of maximum storage) stored in the soil column. The tracer mass balance for the first day of the experiment (Table 4-2) indicates that around 16-18% of the pre-event water stored in the subsurface is actively mixed with the infiltrated sprinkling water. The opposite conclusion can be drawn when analysing the mass balance for the second day of the sprinkling experiment. Under the assumption that all infiltrated sprinkling water is stored in the $1 \times 1 \text{ m}^2$ plot, a double amount of pre-event water should be involved in mixing processes in order to match the measured Cl^- concentration in C1. However, the concentration of Cl^- in C2 (located outside the sprinkling plot) indicates that there is significant amount of tracer stored outside the experimental plot due to surface ponding and subsurface water flow. Moreover, assuming that the hydrologically active area during the second day of the experiment is the same as during the first day of experiment (around 20%), only 1-2% of infiltrated tracer mass is enough to reach the measured tracer concentration in the groundwater at the end of experiment. This indicates the presence of preferential drainage. Nevertheless, the presence of Br^- in C1 (middle of the sprinkling plot) during the second day, when only Cl^- was applied, confirms that matrix flow dominates in the area and piston flow processes occurred. The rise of the Br^- concentration, in both C1 and C2, observed at the beginning of the second day of sprinkling might be explained by the tracer settled over soil surface during water ponding during first day of sprinkling mobilised by 'new' sprinkled water.

4.5 Discussion of conceptual models for the Super-Sauze landslide

The Super-Sauze landslide is a hydrologically triggered landslide and has received extensive research attention focussed on the hydrological dynamics of the landslide (Chapter 2). How do the current results fit into the existing knowledge of the hydrological behaviour of the Super-Sauze landslides? And how do the small-scale experiments add to this knowledge?

The small number of sprinkling experiments and their small scale in relation to the landslide area (0.17 ha) is not sufficient to cover the whole landslide and the findings can not yet be up-scaled into a complete distributed hydrological concept of the landslide. However, the components of the hydrological system, identified based on small scale sprinkling tests are in line with the conceptual models of subsurface water flow within the Super-Sauze landslide proposed by deMontety et al. (2007) and Debieche et al. (2012). The hydrological interpretation of the Super-Sauze landslide presented by deMontety et al. (2007) and based on the long term observation of spatial distribution of major cations and anions defines dominant hydrological processes along the landslide profile: the upper part of the HG1 unit (ablation zone, directly below the main scarp) is the “transition” zone, the lower part of the HG1 unit (transit zone) is dominated by preferential flow and the lower part of the landslide (accumulation zone) by matrix flow (see §2.4.2, Figure 2.14). This is in agreement with our observed fast input – fast output behaviors in plot A and fast input – slow output behavior in plot B. The stable part of the landslide, where the plot C was located, was not considered in the work of deMontety et al. (2007).

While deMontety et al. (2007) stressed the limitation of their investigation having only qualitative assessment of the water fluxes and the need for more detailed investigations, our experiments show the potential for more quantitative analyses of the components of the hydrological processes acting on the landslide and extension of the conceptual model with the identification of surface hydrological processes such as exfiltration and runoff (Figure 4-9).

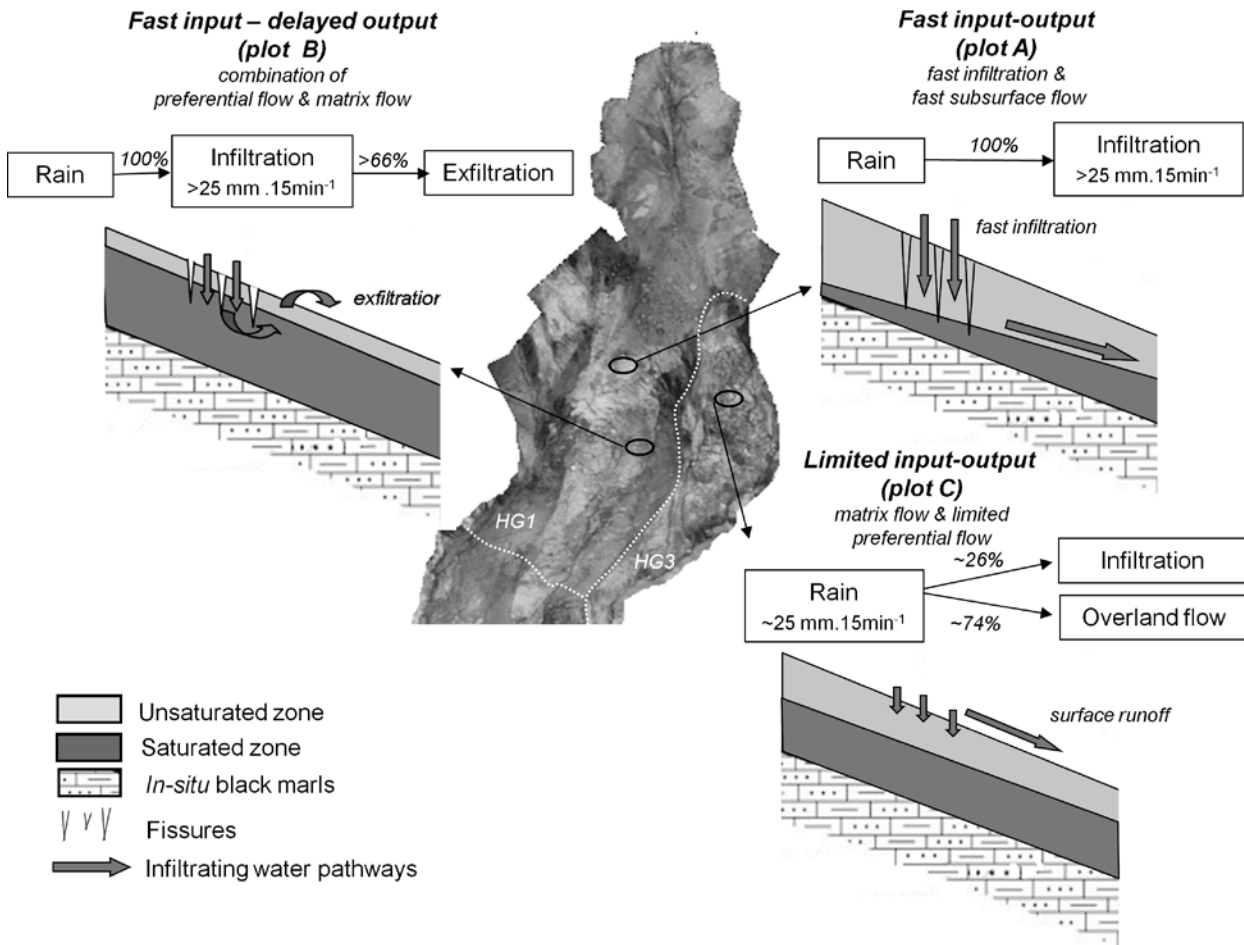


Figure 4-9. Hydrological concept derived from hydrological and hydrochemical analysis of small scale sprinkling experiment and their distribution across the upper part of the Super-Sauze landslide. The white dashed lines indicate the hydro-geomorphological (HG) units defined by Malet et al. (2005).

Furthermore, our results are comparable with the large scale sprinkling experiment performed for more than one week at one location (in the area where plot B was located) at the Super-Sauze landslide (Debieche et al., 2012). Our results confirm that hydrodynamic and hydrochemical responses can not be fully inferred from surface area characteristics (plot C; §4.4.2). The sprinkling water infiltrates into the soil both through the matrix and preferential flow paths. The groundwater flow follows the overall slope direction but presence of fissures and subsurface structures strongly influence the exact direction of the subsurface water flow. Moreover, unweathered marly blocks, characterised by relatively low permeability, decrease the percolation rate and create an area of limited hydrological activity. Furthermore, our results obtained for plot B support the findings of, for example, Trojan and Linden (1992), Zehe and Fluhler (2001), Weiler and Naef (2003), that antecedent water storage influences the initiation of preferential flow: the measured exfiltration volume increases with time.

Lastly, our results fit into the bigger picture of hydro-geomorphological characteristics of the Super-Sauze landslide as proposed by Malet et al. (2005) (see also Ch.2§2.4.2). According to Malet et al. (2005) the upper unit of the Super-Sauze landslide (where plot A and B are located) exhibits very rapid piezometric responses to rainfall ($<1\text{h}$), significant groundwater fluctuations (0.2- 0.5 m in average) and rapid drainage (3-5h) at the event time scale. These behaviours are clearly observed in plot A: highly permeable matrix and fissures compartments. When looking at plot B we also observe rapid piezometric responses ($<1\text{h}$) and relatively high groundwater level increase (0.20-0.25m). However, the water drainage is delayed due to presence of dead-end fissures (see §4.4.2). This behaviour, not distinguished by Malet et al. (2005), may result in prolonged high pore water pressure which can be an important factor for initiation and re-activation of mass movement in the area (Uchida et al., 2001). As a consequence, even small rain amounts can lead to saturation of the subsurface and reduce the soil shear strength. This would support the other finding of Malet et al. (2002) that the area where plot B is located is the most active area of the landslide with surficial displacement rates reaching 0.05 m.day^{-1} . The hydrological responses observed within plot C does not follow the characteristics of HG3 unit presented by Malet et al. (2005): slow piezometric responses ($>5\text{h}$, low groundwater level fluctuations (centimetres) and slow drainage ($>24\text{h}$) whereas in our experiment also higher hydrological dynamics were evident. This higher dynamics is due to presence of a limited number but well connected macropore system that allows for fast drainage in the shallow soil layer (0-0.4 m) and controls short-time scale groundwater level fluctuations. However, the groundwater depletion analyses of our experiment indicate that matrix flow is the dominant process within this area as also identified by Malet et al. (2005).

4.6 Conclusions

This research shows the potential of combined hydrological and hydrochemical analysis of small scale $1\times 1\text{ m}^2$ sprinkling experiments for effectively study the spatial differences in hydrological response to precipitation input. The approach was applied at the specific environment of highly heterogeneous Super-Sauze landslide (French Alps). Thereafter, the conceptual models derived from the experimental results were confronted with existing knowledge of the Super-Sauze hydrological knowledge.

Dual or multiple permeability systems can be found in many hillslopes and they steer the hydrological dynamics of the hillslope. In such cases, laboratory tests for hydraulic soil parameters are insufficient and in-situ measurements or experiments are necessary. Small-scale sprinkling experiments performed with the use of artificial tracer and in-situ observations of hydrological and hydrochemical response showed to be very effective in unravelling complex hydrological systems. They confirm that presence of fissures increases the vertical infiltration rate and controls the direction of subsurface water flow (e.g. McDonnell, 1990; Uchida et al., 2001).

Although we performed only six experiments on three locations, which is spatially limited, we showed that our small-scale sprinkling experiments were capable of capturing the hydrological processes of the Super-Sauze landslide as described in previous studies, outlining the spatial heterogeneity commonly existing in slow moving landslides. The advantage of two days sprinkling with the use of two different tracers is also evident. It allows monitoring threshold behaviour of hydrological systems, to identify preferential flow paths and to perform more in-depth analysis of mixing processes (pre-event – infiltrated water). The quantitative analysis presented in this paper shows the potential of combined small-scale sprinkling experiment for quantification of different types of preferential flow. However, it also shows the importance of careful control of boundary conditions and detailed measurements of soil characteristics and their heterogeneity in the soil profile.

The experiments are relatively inexpensive, can be deployed throughout the landslide area and do not need long-term monitoring programs. This paves the road for more widespread application in order to better understand the spatial differences and similarities of hydrological processes across a landslide area.

Chapter 5

A CONCEPTUAL MODEL OF THE HYDROLOGICAL INFLUENCE OF FISSURES ON LANDSLIDE ACTIVITY

Hydrological processes control the behaviour of many unstable slopes and their importance for landslide activity is generally accepted. The presence of fissures influences the storage capacity of a soil and affects the infiltration processes of rainfall. The effectiveness of the fissure network depends upon fissure size, their spatial distribution, and the connectivity between fissures. Moreover, fissure connectivity is a dynamic characteristic, depending on the degree of saturation of the medium that separates the fissures.

The research presented in this chapter aims to investigate the influence of a fissure network on hydrological response of a landslide. Special attention is given to spatial and temporal variations in fissure connectivity, which makes fissures act both as preferential flow paths for deep infiltration (disconnected fissures), and as lateral groundwater drains (connected fissures). To this end, the hydrological processes that control the exchange of water between the fissure network and the matrix have been included in a spatially distributed hydrological and slope stability model. The ensuing feedbacks in landslide hydrology were explored by running the model with one year of meteorological forcing. The effect of dynamic fissure connectivity was evaluated by comparing simulations with static fissure patterns, to simulations in which these patterns change as a function of soil saturation. The results highlight that fissure connectivity and fissure permeability play an important role in water distribution within a landslide. Making the fissure connectivity a function of soil moisture content results in stronger seasonality of the hydrological responses.

Based on: Krzeminska, D.M., Bogaard, T.A., Van Asch Th. W.J. and Van Beek L.P.H. 2012b. A conceptual model of the hydrological influence of fissures on landslide activity. *Hydrology and Earth System Science* 16:1-16, DOI:10.5194/hess-16-1-2012

5.1 Introduction

In slow-moving landslides, continuous movement of the sliding material results in fissure formation due to compression and extension. These fissures can act as preferential flow paths for infiltration (providing direct access to the lower groundwater and increasing the rate of groundwater recharge) and for lateral groundwater drains (limiting the build up of water pressure). On the other hand, once their storage capacity is exceeded and drainage is impossible, they contribute to maintaining high pore water pressures in the surrounding soils. As such, they have strong influence on groundwater level fluctuation, and thus, on slope stability.

The complexity of the preferential flow processes, and their high spatial and temporal variability, makes it very difficult to measure the processes in the field, to upscale the information to the catchment scale and to incorporate preferential flow into hillslope scale hydrological modelling (see Ch.1§1.3 - 1.4, Ch.3 and Ch.4). The majority of macropore flow models include preferential flow as a modification of hydraulic conductivity function without accounting for the distributed nature of the soil macropores system and dynamically changing characteristics of macropore (i.e. fissure) network.

The main aim of this research is to study the importance of preferential fissure flow for landslide hydrological behaviour and slope stability at the field scale. The conceptual model was based on the Storage and Redistribution of Water on Agricultural and Re-vegetated Slopes model (STARWARS), which is a distributed model coupling hydrological and stability dynamics (Van Beek, 2002). The use of meta-language of PCRaster GIS package provides an expedient way to include and change spatially distributed hydrological and geotechnical parameters of both fissure and matrix fractions.

5.2 Adaptation of STARWARS

5.2.1 General model description

Here, we build on the original version of STARWARS model (Van Beek, 2002) by including a more detailed representation of fissure flow and expanding the original conceptualization of Van Beek and Van Asch (1999). The STARWARS model consists of a core model resolving dynamic equations of saturated and unsaturated flow and of sub-models that describe specific

hydrological processes such as interception, transpiration, snow cover or snow melt (Figure 5-1).

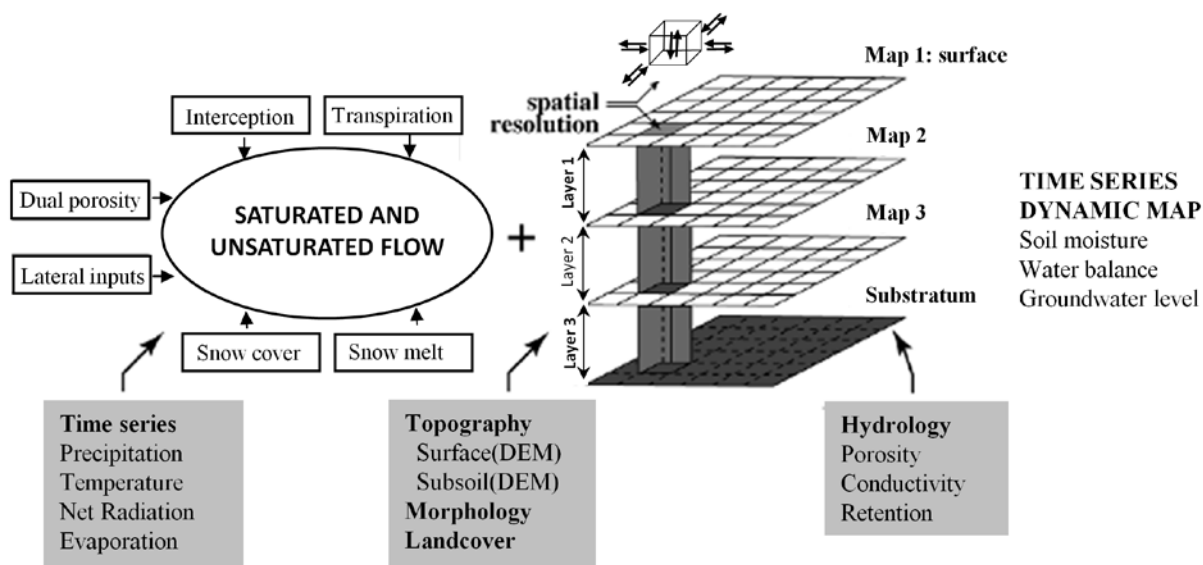


Figure 5-1. Architecture of STARWARS model (core model and sub-models) and schematic representation of the model implementation (adapted from Malet et al., 2005, based on Van Beek, 2002)

The model represents the soil mantle (as a column of three layers) overlying a semi-impermeable bedrock. The layers have variable depth, centred on the mid-point or node of each cell of an equidistant grid in the x- and y-direction. The hydrological model describes the saturated (Q_{sat}) and the unsaturated (P_e) transient flow as a function of gravitational potential only, assuming freely drainable water (unconfined groundwater levels). Precipitation (P) and evaporation (E) constitute the boundary condition at the top of the soil column. The percolation loss across the lithic contact into the underlying bedrock reservoir constitutes the lower boundary condition (LBC). For a complete description of the model the reader is referred to Van Beek (2002).

Within each model time step, all the calculations of particular processes within each soil column are ordered as follows: reading the initial conditions (water level and soil moisture content in the matrix and in the fissures), evaluating upper and lower boundary conditions, the calculation of vertical fluxes, updating the storages, the evaluation of lateral fluxes and updating the storages which set new initial conditions for the next step. Although each soil column has a certain storage volume to accommodate the unsaturated and saturated fluxes, all fluxes are calculated between nodes.

At the end of each model run the factor of safety (f_s) is calculated as the ratio between maximum shearing resistance to failure and shear stress (see Ch.1§12.1). The infinite slope model is used to calculate slope stability (Skempton, 1964):

$$f_s = \frac{c + (\sigma - u) \cdot \tan \varphi}{\frac{(W_{fis} + W_{mat})}{\Delta x^2} \cdot \sin \beta \cdot \cos \beta} \quad (5.1)$$

where c is cohesion, σ is total normal stress, u is pore pressure and φ is the angle of internal friction. W_{fis} and W_{mat} are the weight of the fissure and matrix fraction of the cell, Δx is the length of the cell and β is the slope angle. The normal stress is given by:

$$\sigma = \frac{(W_{fis} + W_{mat})}{\Delta x^2} \cdot \cos^2 \beta \quad (5.2)$$

and the pore pressure is given by:

$$u = F_{fis} \cdot h_{fis} \cdot \gamma_w \cos^2 \beta + (1 - F_{fis}) \cdot h_{mat} \cdot \gamma_w \cos^2 \beta \quad (5.3)$$

where $h_{mat/fis}$ represents the groundwater height above the shear surface within fissure and matrix fraction respectively, γ_w is the density of the water [kN.m⁻³] and F_{fis} is the fraction of the surface area covered by fissures [m².m⁻²].

The interaction between cells is neglected and the calculated stability is dependent on the local cell attributes only. The model uses the soil mantle schematisation shown in Figure 5-2b and the lithic contact is assumed to be the potential shear surface. In this way, f_s serves here as a proxy for the excess shear stress that cannot be accommodated by a particular soil column.

5.2.2 Representation of fissures

Our concept of fissure flow is based on the dual-permeability approach (Šimůnek et al., 2003; Gerke, 2006; Jarvis, 2007). The appearance of fissures creates a system consisting of two overlapping and interacting domains; the fractures and the matrix blocks, which have their own characteristic and properties (i.e. porosity, hydraulic conductivity). Moreover, water flow is allowed in both domains (matrix and fissures).

The explicit inclusion of fissures in STARWARS required an adaptation of the existing model concept (Figure 5-2b). The new concept assumes that fissures are distinct from the matrix and are represented within each cell as a continuous network of highly pervious zones surrounded

by matrix blocks (after Van Beek & Van Asch, 1999). For each layer of the soil column the fissure distribution is prescribed by the fraction of the surface area covered by fissures (F_{fis} , [m².m⁻²]), and mean fissure aperture (a_{fis} [m]). They are distributed evenly throughout the cell (in both x- and y- direction) and they extend vertically over the full depth of a particular layer (Figure 5-2c). The model allows for defining the fissure fraction and its aperture per cell, and per layer. Fissure contents can vary from cell to cell and from layer to layer. The only limitation is that fissures are fully connected vertically, across layers. Additionally, it is possible that fissures will terminate in the first (top) or second layer, and not extend entirely to the bottom.

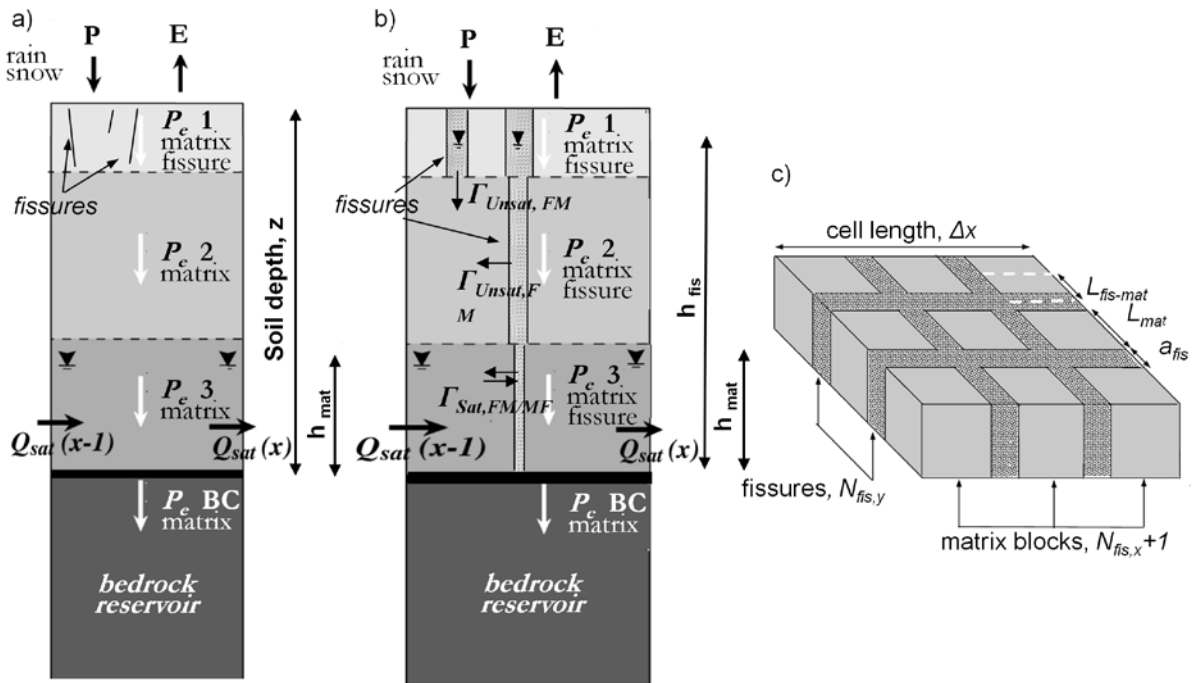


Figure 5-2. Schematisation of (a) the original hydrological model (Malet et al., 2005, after Van Beek, 2002), (b) the hydrological model implemented within this research and (c) fissure representation in the single layer of the soil column. An explanation of the symbols are given in the text.

Moreover, field survey showed that the majority of fissures are partly (re-)filled with landslide material, and thus no continuous open fissures are observed. Therefore, in the model we consider that fissures are filled with reworked material and that they retain their own water level and soil moisture content. It is important to keep in mind, that the fissure characteristics (i.e. porosity, saturated hydraulic conductivity), as all such input parameters in the model, can be spatially distributed.

The number of fissures per cell is calculated as:

$$N_{fis,x} = N_{fis,y} = (1 - \sqrt{1 - F_{fis}}) \cdot \frac{\Delta x}{a_{fis}} \quad (5.4)$$

where Δx is the cell length [m] and the fissures are assumed to extend over the full length of the cell. $N_{fis,x}$ ($=N_{fis,y}$) is the number of fissure in x ($=y$) direction, rounded down to the nearest whole number with a minimum value of 1 if $a_{fis} > 0$. In that case, the fractional area covered by fissures is reset to the area of $(2a_{fis} \cdot \Delta x - a_{fis}^2) / \Delta x^2$. The distance between the fissures equals the width of the matrix blocks. It is assumed that in a cell all fissures are contained by matrix and thus there are $N_{fis,x} + 1$ matrix blocks (looking at the x-direction) of width L_{mat} [m]:

$$L_{mat} = \left(\sqrt{1 - F_{fis}} \right) \cdot \frac{\Delta x}{N_{fis,x} + 1} \quad (5.5)$$

The distance from the centre of a fissure to the centre of each matrix block that defines the different gradients is consequently given by:

$$L_{mat-fis} = \frac{1}{2} (L_{mat} + a_{fis}) \quad (5.6)$$

5.2.3 Adaptation of fluxes calculations

Fluxes within single soil column

Following the original process description of the STARWARS model (Van Beek, 2002), the transient saturated and unsaturated flow is a function of elevation potential only, neglecting the matrix potential for the flow in the unsaturated zone. Therefore, percolation in both matrix and fissures domain, is gravitational and vertical only. The unsaturated flow is controlled by the unsaturated hydraulic conductivity of matrix and fissure domain respectively. The relative unsaturated hydraulic conductivity (k_r [-]) is given by Millington and Quirk (1959):

$$k_r(\theta_E) = \theta_E^\tau \cdot \frac{[\exp(2 \cdot \alpha \cdot \theta_E) - 2 \cdot \alpha \cdot \theta_E - 1]}{[\exp(2 \cdot \alpha) - 2 \cdot \alpha - 1]} \quad (5.7)$$

where θ_E is effective degree of saturation [-], α is the shape factor [-] and τ is the tortuosity parameter set to 4/3 [-]. This equation is applied to calculate unsaturated hydraulic conductivity of both matrix ($k_{r,mat}$) and fissures ($k_{r,fis}$).

The soil water retention curve (Farrel and Larson. 1972) defines the relationship between soil matrix tension and the degree of saturation, for matrix (*mat*) and fissure (*fis*) domain respectively:

$$\theta_{E,mat/fis} = 1 - \frac{1}{\alpha_{mat/fis}} \cdot \ln \left(\frac{|h_{mat/fis}|}{h_{A,mat/fis}} \right) \quad (5.8)$$

where $|h|$ is the absolute matrix suction [m], h_A is the air entry value [m]. If $|h|$ is less or equal to h_A the soil remains saturated throughout.

This relationship is used in the model to determine the relative degree of saturation upon the first-time drainage of a fully saturated layer and to determine the storage at which the potential evaporation is reduced.

When the percolation flux in the lowest layer exceeds the basal loss, a groundwater table is formed and it rises upward with the assumption that it is vertically contiguous (for both, matrix and fissures fraction).

Surface fluxes (infiltration and evaporation) are partitioned on the basis of the respective surface area $A[m^2]$, calculated as $A_{fis} = F_{fis} \cdot \Delta x^2$ for fissure fraction, and $A_{mat} = (1 - F_{fis}) \cdot \Delta x^2$ for matrix fraction. Fissures can be recharged directly by rain or snow melt, or indirectly by overland flow.

The storage capacity of a single cell is the combination of matrix and fissure fraction capacity. The infiltration capacity of the fissure fraction network is not limited *a priori*, meaning that any water which cannot infiltrate into the matrix is passed on to the fissure network. When, after calculating all the fluxes (percolation and lateral exchange) the water storage in the fissures exceeds their capacity, it is returned to the surface as overland flow. Any water remaining as surface detention is redistributed instantaneously as overland flow over the slope.

Lateral exchange $\Gamma [m^3 h^{-1}]$ within the cell is possible only between the saturated zones of matrix and fissure fractions ($\Gamma_{Sat, FM/MF}$), and the unsaturated zones of the matrix fraction and the saturated zone of the fissure fraction ($\Gamma_{Unsat, FM,}$) when water level in the fissure fraction exceeds that found in the matrix fraction. No lateral fluxes occur between the unsaturated zone of the fissure network and unsaturated matrix. However, fissures can drain vertically into the soil when they terminate above the lithic contact.

Fluxes between soil columns

Lateral flow (Q_{sat}) between the cells occurs across the saturated zone only as result of differences in total piezometric head between the adjacent nodes in the x- and y-direction (based on Darcy's law). The total head in each column comprises of the gravitational potential, the elevation of the bottom of the soil column, and the average of the water level in both the fissure network and matrix, weighed by the respective surface area. The specific discharge across the cell boundaries in the x- and y- direction depends on the transmissivity in those directions. Transmissivity per domain is the product of saturated permeability (matrix or fissure), water height (in matrix or fissure) and width (matrix width or fissure width in cell). The fissure connectivity (C_{fis}) represents the chance for fissure network to be connected laterally between the adjacent soil columns and modifies the transmissivity towards that of the fissure network rather than that of the –less permeable- matrix. As such, there is no explicit ‘fissure to fissure in adjacent cell’ exchange of groundwater. Rather, the total saturated lateral flux is subsequently distributed over the matrix and fissure domains on basis of the ratio of the transmissivity values within a column and the connectivity between fissures.

Although field studies have shown that the macropore continuity is dynamic, and positively related to the increase in soil water content (e.g. Tsuboyama et al., 1994; Sidle et al., 2000, Van Schaik et al., 2008), quantification of this relationship remains difficult. Moreover, there is no research on macropore continuity dedicated particularly to fissures.

In order to elaborate on the dynamic nature of fissure connectivity we have made the fissure connectivity term (C_{fis}) dependent on the soil moisture content of the soil column. In this way we conceptualize that the water exchange between soil columns (lateral flow, Q_{sat}) will increase with a rising degree of saturation in the soil column. This shifts the conceptual notion of fissure connectivity from the geometric property of fissure network towards a dynamic aspect of the combined hydrology of heavily fissured soil. In analogy to macropore flow (e.g.: Zehe and Blöschl, 2004), we have established the following threshold relationship of the soil moisture content in the soil column (θ_E) and fissure connectivity (C_{fis}):

$$C_{fis,i} = \begin{cases} C_{fis,min} + \frac{\theta_{E,i} - \theta_{E,fc}}{\theta_{E,Sat} - \theta_{E,fc}} \cdot (C_{fis,max} - C_{fis,min}) & \text{for } \theta_{E,i} \geq \theta_{E,fc} \\ C_{fis,min} & \text{for } \theta_{E,i} < \theta_{E,fc} \end{cases} \quad (5.9)$$

where $C_{fis,i}$ and $\theta_{E,i}$ are fissure connectivity [-] and effective saturation of the soil column [-] at time step i , $C_{fis,min}$ and $C_{fis,max}$ are the minimal and maximal fissure connectivity, set to 0.1 and 0.9 respectively; $\theta_{E,fc} = \theta_{E,pF=2.0}$ is effective saturation at the field capacity [-] and $\theta_{E,sat} = 1$ (full saturation).

Introducing a direct relationship between fissure connectivity and soil moisture (Eq. (5.9)) in the model, will have an effect on the drainage capacity of the fissure network. With $C_{fis} > 0$, the exchange of water in the fissure network between adjacent cells is enhanced, and the fraction of the water flux between the soil columns is controlled by the hydraulic conductivity of fissure network. In this way the dynamic nature of fissure connectivity, which influences the effectiveness of the drainage capacity of the fissures, is emphasized.

5.3 Methodology

5.3.1 'Simple' landslide representation

Model development and evaluation of the proof-of-concept are carried out using an idealised landslide representation. The clone map consists of 30 rows by 175 columns and the grid size of 5x5 m. This gives a spatial domain of 875x150 m. The idealised digital elevation model (DEM) extends between 1725 m a.s.l. (toe of the landslide) and 2135 m a.s.l. (crown of the landslide) which corresponds to a planar slope of 25.1°.

The landslide body is delineated by an ellipse with a length of 800 m and a breadth of 90m. This allows us to account for the effect of converging and diverging topography. The depth of the slip plane along the major slope-parallel-axis of the ellipse is described by the arc of a circle passing through the crown and toe of the landslide body and its mid-point on the vertical, through the centre of the landslide. The maximum depth of the landslide is set to 8 m and it decreases towards the borders (Figure 5-3a).

The soil parameters of each layer are set arbitrarily based on personal experience and measurements performed in clay shale landslide field observation (Malet, et al 2005; Debieche et al., 2012; Krzeminska et al., 2012a). Figure 5-3b shows the example of the distribution of soil parameters with depth for matrix and fissure fractions. The saturated hydraulic conductivity (k_{sat}) was set to $4.1 \cdot 10^{-6}$, $2.8 \cdot 10^{-6}$ and $2.4 \cdot 10^{-6}$ m.s⁻¹ for the matrix

fraction, for layer 1, 2, and 3 respectively. For each layer, the k_{sat} for fissure fraction was assumed to be 20 times higher than that of the matrix.

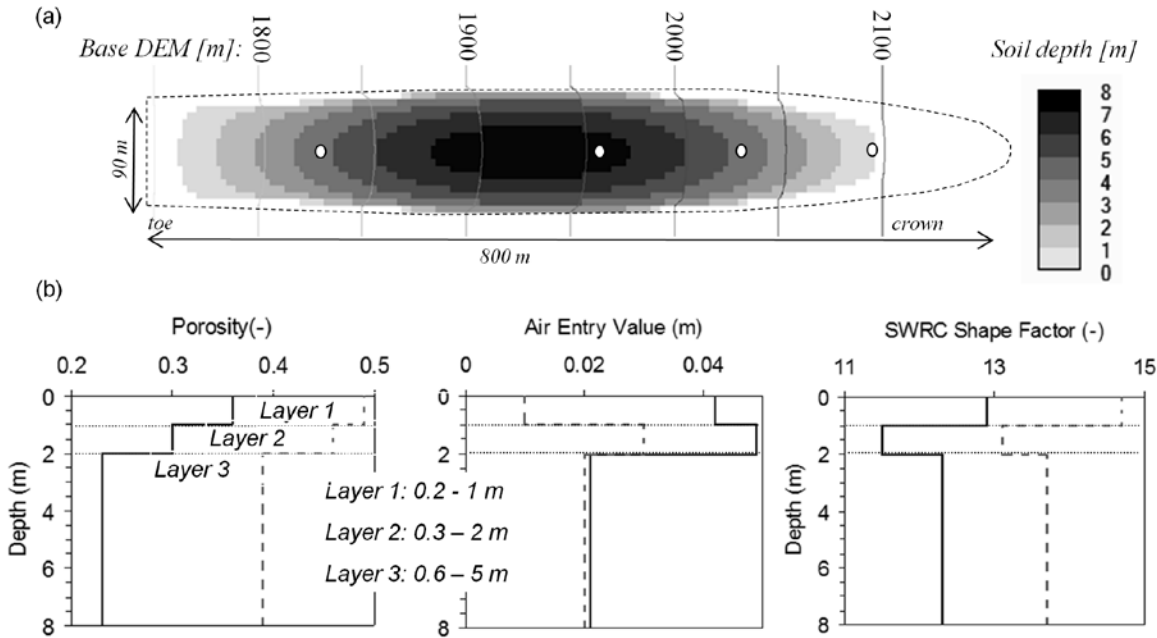


Figure 5-3. (a) Geometry of the idealised, ‘simple’ landslide representation; the contour lines show the DEM of the bedrock and the white dots indicate the points for which the groundwater level fluctuation are reported (see Fig. 5-9); (b) Matrix (solid line) and fissures (broken line) properties.

5.3.2 Modelling strategy

Four scenarios are evaluated:

- scenario 1 – *no fissures* – represents the landslide where no fissures are considered;
- scenarios 2 and 3 – *connected* and *disconnected fissures* - where fissure properties are set to be constant over the simulation period, and fissure connectivity (C_{fis}) is set to be 10% or 90% for disconnected fissures and connected fissures scenario respectively.
- scenario 4 – *dynamic connectivity* – scenario where the dynamic characteristic of fissure connectivity is applied.

Each model run is performed for one calendar year with the use of the same meteorological forcing (rain intensity, air temperature, incoming short wave radiation and relative humidity), generating a dynamic equilibrium of 470 mm of precipitation and around 1200 mm of

potential evaporation. Snow accumulation was inhibited, by keeping the air temperature above freezing point, for the snow cover calculations. Moreover, the vegetation cover is not considered in the model.

The initial conditions (distributed groundwater level and soil moisture) were determined by spinning up the model with the ‘no fissures’ scenario: the total initial storage of the landslide equals 91% of its storage capacity. The same initial conditions (determined for ‘no fissures’ scenario) were applied for all the scenarios. The bedrock is considered to be non-permeable and, thus, no percolation is lost across the lithic contact ($LBC=0$). In this way, the pre-defined bedrock topography (see §5.3.1) constitutes a no-flow boundary condition. The outflow from the landslide area is possible in the form of surface runoff at the toe of the landslide (exfiltration and saturated overlandflow).

For scenarios 2, 3 and 4 (fissures scenarios), an equal distribution of fissures is assumed over the whole landslide. An average fissure fraction was set to 0.30, 0.20 and 0.05, and an average fissures aperture was set to be 0.20, 0.10 and 0.05 m for 1st, 2nd and 3rd layer respectively. It is important to stress that in the model, the geometry of the landslide remains constant during the simulation period and, therefore, no mass displacement is considered. The scenarios have no influence on the mechanical material properties.

The outputs of the simulations were collated and compared with each other, in order to see the effect of the introduction of fissures and their connectivity on the hydrological behaviour of the landslide. To this end, the water balance components were calculated and compared between the different scenarios.

As a last step a sensitivity analysis was performed on the effect of the parameterisation of the matrix on the simulated hydrology. One parameter was perturbed in consecutive model run. A detailed sensitivity analysis of the fissure fraction parameterisation and fissure connectivity was performed to quantify whether the introduction of dynamic fissure behaviour is relevant, or if similar hydrological responses could be obtained with adapted hydraulic parameterisation of the fissure system.

5.4 Simulation results

5.4.1 General water balance components of a landslide

Table 5-1 shows the annual water balance components of four modelled scenarios. The initial conditions of each scenario have the same groundwater levels, soil moisture content and surface detention. Consequently, the total storage at the start of the simulation period is different for the ‘no fissures’ scenario and the other three scenarios (the same groundwater levels but different porosities, because of the introduction of the fissure network).

In general, there are only small differences in the water balance. The majority of the input (rain water) leaves the system as evaporation; between 64.7% of rain volume for the ‘no fissures’ scenario and 65.7% of the rain volume for the ‘connected fissures’ scenario. The relatively high evaporation rate for all of the scenarios is the effect of wet initial conditions (initial water storage in the landslide equals 91% of total available storage capacity) and maintenance of high water level in the lower part of the landslide due to predefined bedrock topography.

Table 5-1. Annual water balance components of four modelled scenarios, calculated for whole spatial domain. Please note that the gaps in annual water balance ($8\text{--}12\text{m}^3$) are the result of numerical accuracy only.

	No fissures	Disconnected fissures	Connected fissures	Dynamic connectivity
Total storage at the start of simulated period [m^3]	57618	62571	62571	62571
Total input (precipitation-evaporation) [$\text{m}^3\text{year}^{-1}$]	21754	21818	21135	21832
Total storage at the end of simulated period [m^3]	57431	62682	61877	62277
Change in total storage over the simulation period [m^3]	-187	111	-694	-294
Total outflow [$\text{m}^3\text{year}^{-1}$]	21933	21696	21816	22114

Over the simulation, the total volume of water stored within the system (including surface detention) decreases for all but the ‘disconnected fissures’ scenario. The highest difference (1.1% of the total volume of rain) is observed for the ‘connected fissures’ scenarios. Figure 5-4a shows the variation in total storage in relation to cumulative inflow (total volume of precipitation). The difference in total storage between the ‘no fissures’ scenario and the other three scenarios, is the consequence of introducing fissures as a fraction of the landslide

material with higher porosity. The same initial groundwater level and soil moisture content but higher porosity results in higher total storage values. However, when looking at the relative changes in total storage, with regard to initial conditions' scenarios, one can see that the dynamics of total storage of 'no fissures' and 'disconnected fissures' are almost equal (Figure 5-4b). The overall behaviour of the system is very similar for all the scenarios with clear consecutive drying and wetting periods. The total storage of 'disconnected fissures' is almost always the highest and that of 'connected fissures', the lowest. The exceptions are the wet periods with total storage of the landslide more than 90% of its storage capacity (MaxStor). During these periods the simulated total storages are the same for all fissures scenarios.

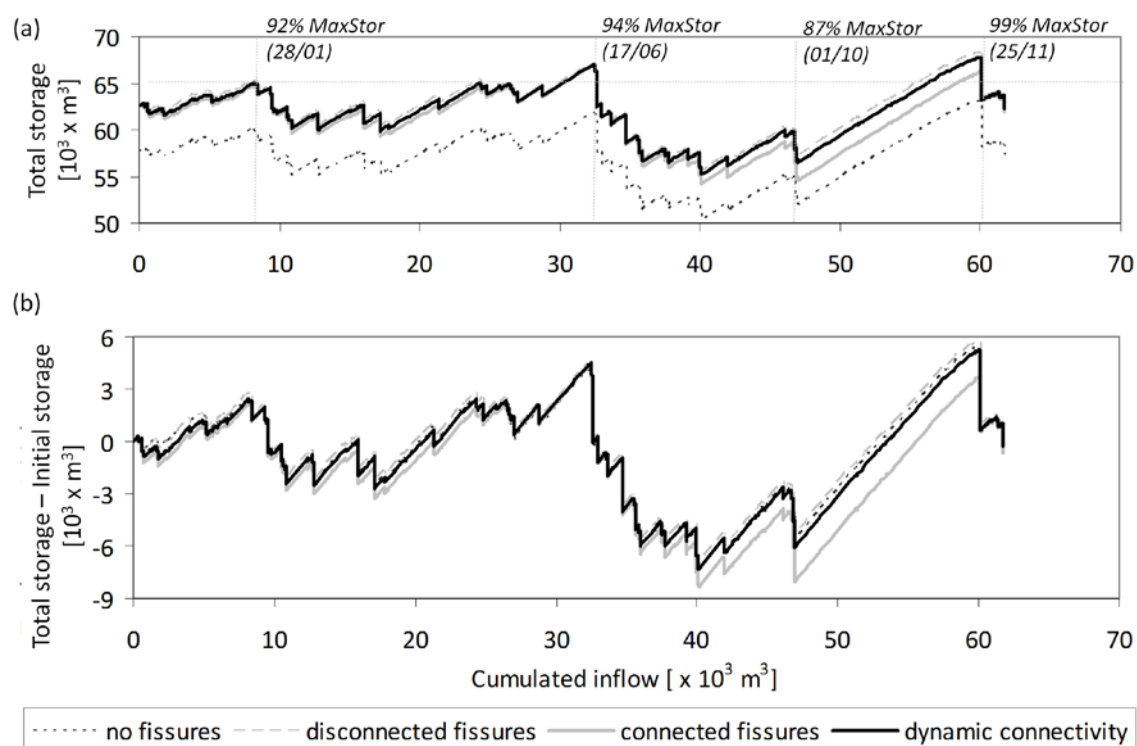


Figure 5-4. Variation in total storage during one-year simulation period expressed as a relationship between cumulative inflow (total rain volume) and changes in storage compared to initial condition.

Figure 5-5 shows cumulative outflow from the modelled area and surface detention over the landslide area in relation to cumulative inflow. There are very small absolute differences in the total cumulative outflow between the scenarios: total cumulative outflow equal to 35.9%, 35.4%, 35.2% of total rain volume for 'dynamic fissures' scenario, 'connected fissures' scenario and 'disconnected fissures' respectively. This is the effect of pre-defined bedrock topography and no-flow boundary conditions that allow water outflow from the landslide in

the form of surface runoff only and limit the variation of the outflow volume scenarios. However, Figure 5-5a shows that during the wetting periods the highest outflow is observed with ‘connected fissures’ and during the drying periods the highest outflow is observed with ‘dynamic fissures’. The outflow observed with ‘disconnected fissure’ scenario is always the lowest. Consequently, the average surface detention, observed within landslide area, is the lowest for the ‘connected fissures’ scenario (58.3 m^3), moderate for ‘dynamic connectivity’ scenario (63.0 m^3) and the highest for ‘disconnected fissures’ and ‘no fissures’ scenarios (72.6 and 75.4 m^3 respectively). During the wet periods observed differences between the scenarios are negligible.

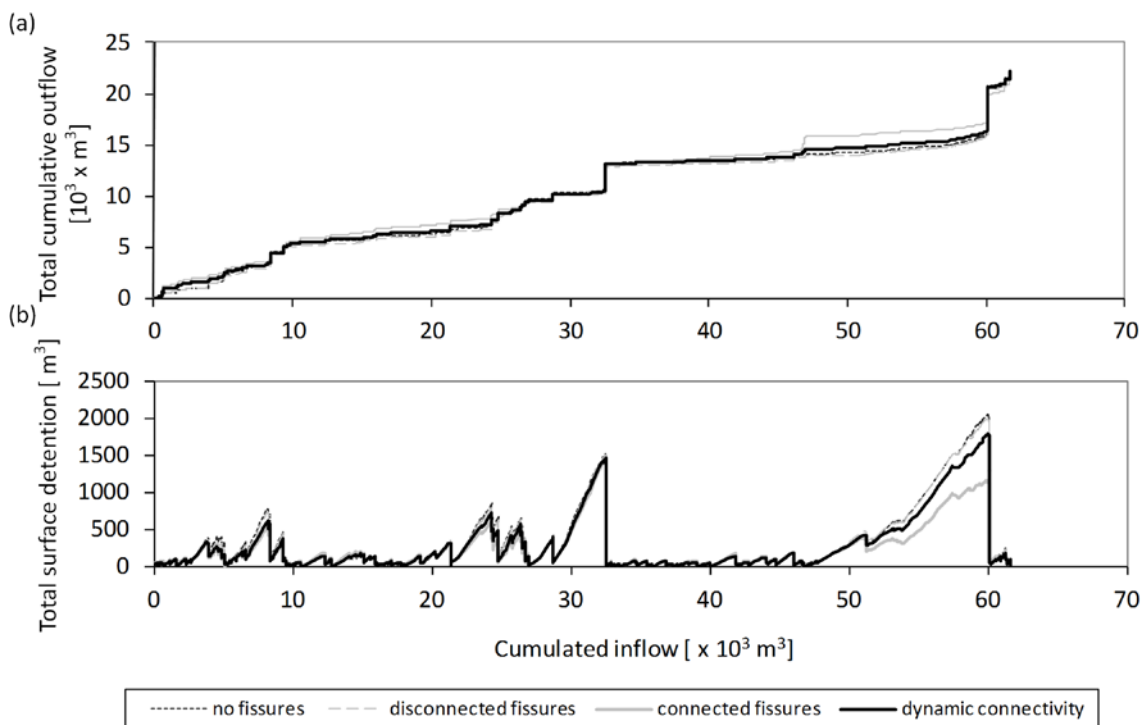


Figure 5-5. Variation in total cumulative outflow and total surface detention during one-year simulation period expressed in relationship to cumulative inflow (total rain volume).

5.4.2 Spatial and temporal differences in groundwater level

The timing and duration of near saturation is an important aspect for landslide (re-)activation. Figure 5-6 shows the total amount of days (during the one-year simulation period) with total saturation (groundwater level reaching the soil surface). Clear differences between the scenarios can be seen. The average number of days with saturation is 121, 134, 152 and 128 days per cell for scenarios 1 to 4 respectively. While the average number of days with

saturation for ‘no fissures’ and ‘dynamic connectivity’ is similar, the spatial distribution of the storage (saturation) is different: much less saturation is observed in the upper part of the landslide when accounting for dynamic connectivity of fissures. The results of the ‘connected fissures’ scenario is strongly affected by pre-defined bedrock topography and converging water flow paths. Faster drainage propagates water downslope and vertically converging flow paths result in accumulation of the water in the lower part of the landslide.

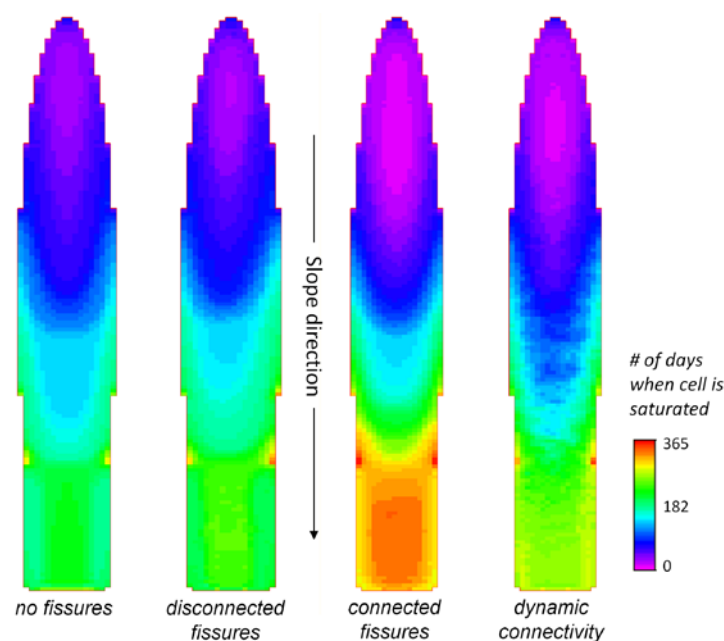


Figure 5-6. The total number of days during one year simulation period that full saturation was found.

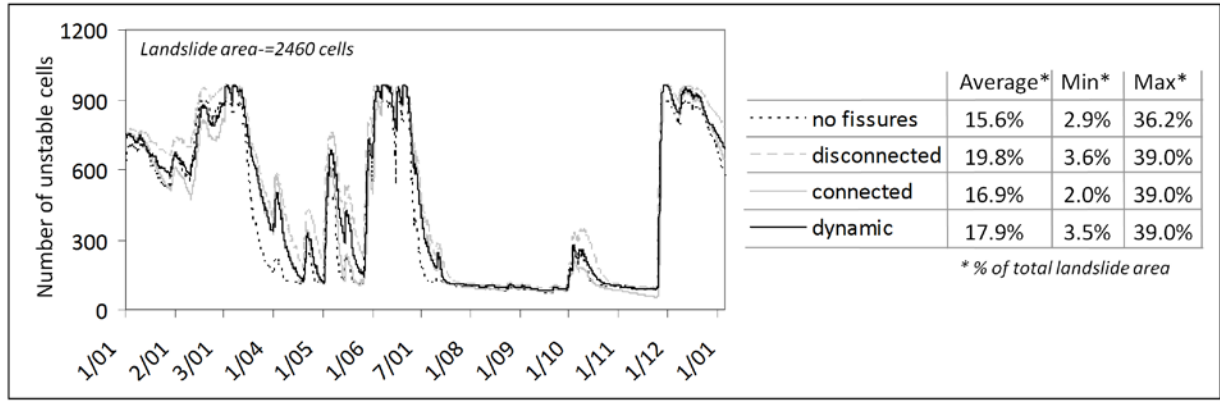


Figure 5-7. The number of unstable cells ($f_s < I$) per time step, simulated with different scenarios.

It is interesting to compare the results presented in Figure 5-6 with Figure 5-7 showing the number of unstable cells ($f_s < I$) observed per time step. The average numbers of unstable cells observed with the scenarios where fissures are implemented are always higher than the one for ‘no fissures’ scenario. The ‘disconnected fissures’ and ‘connected fissures’ scenarios present two extreme behaviours. This is the effect of an increase (‘disconnected fissures’) or

decrease ('connected fissures') of the soil column weight (W_{fis} , W_{mat}) and pore pressure due to different water distribution within the landslide.

Figure 5-8a shows an example of modelled groundwater levels from toe to crown along the landslide for six days during the one year simulation periods. Figure 5-9 presents an example of the modelled groundwater level fluctuations for four points located along the landslide profile (see Figure 5-3a). In the case of 'connected fissures' water entering the fissures network, is drained out of the landslide by fissures that provide continuous areas of high transmissivity. The total lateral saturated water flow (Q_{sat}), which represents lateral drainage within the landslide system (flow between cells), is approximately 1.6 times higher than in the case of the 'no fissures' scenario and 56% of this water is flowing through the fissure network. As a consequence, a general decrease of the groundwater level is found (Figure 5-8a and Figure 5-9b-d). Conversely, the model configuration with 'disconnected fissures' creates areas with very high storage capacities, but with slower lateral exchange between cells. In this way, the groundwater table remains at a higher level compared to the 'no fissures' and 'connected fissures' scenarios. The total lateral saturated flow (Q_{sat}), in the case of 'disconnected fissures', is 1.3 times higher compared to the 'no fissures' scenario, and approximately 30% of this flow occurs between the fissure fraction of one cell and matrix fraction of another cell, or between fissure fractions of the cells.

The groundwater level simulated with the 'dynamic connectivity' scenario is a combination of the modest fluctuations observed for the 'disconnected fissures' scenario, and the larger groundwater level fluctuation observed for that of 'connected fissures'. Fissure connectivity changes in time and space (Figure 5-8b) according to the relationship defined with Eq.(5.9). However, the higher the total storage of the landslide the smaller the observed differences in groundwater level are between the scenarios (Figure 5-8a).

At the lower part of the landslide (Figure 5-9e) the groundwater behaviour depends on parallel flow paths (planar) but also converging flow paths (vertical). The simulation results show that this is especially important if a large volume of water can be transported from upslope via fast flow through a well connected fissures system (the 'connected fissures' scenario). Therefore, in the lower part of the landslide, the highest mean groundwater level is observed when the 'connected fissures' scenario is implemented.

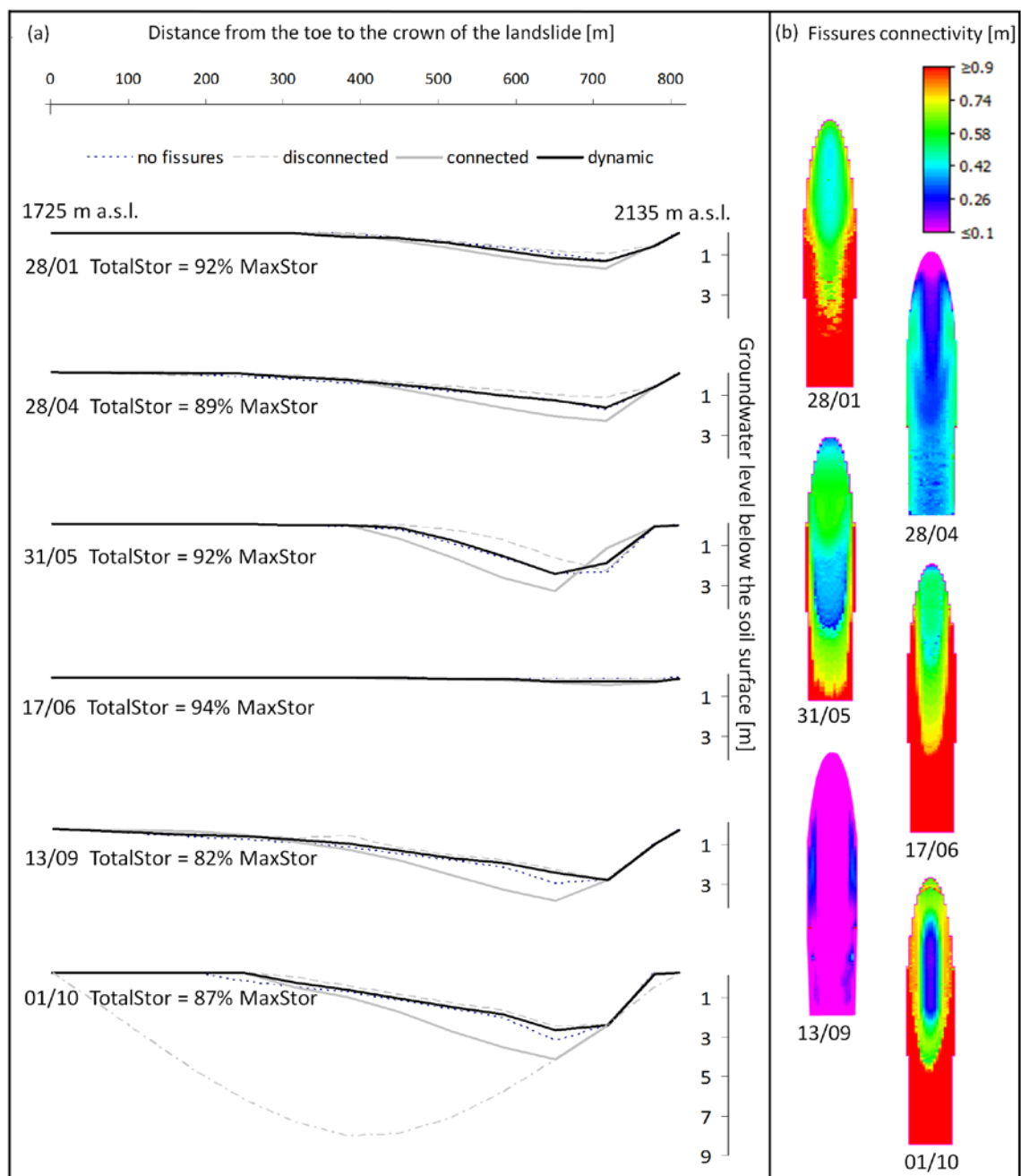


Figure 5-8. (a) Modelled groundwater levels along the landslide profile (major axes of the ellipse); x-axis represents the distance from the toe of the landslide (0 m, elevation of 1725 m a.s.l.) to the crown (800 m, elevation 2135 m a.s.l.). (b) The distribution of fissures connectivity over the landslide area, corresponding to these groundwater levels and observed total storages. The light grey line, present in the last profile of sub-figure (a), represents the bedrock depth. Please note the exaggeration of the vertical scale.

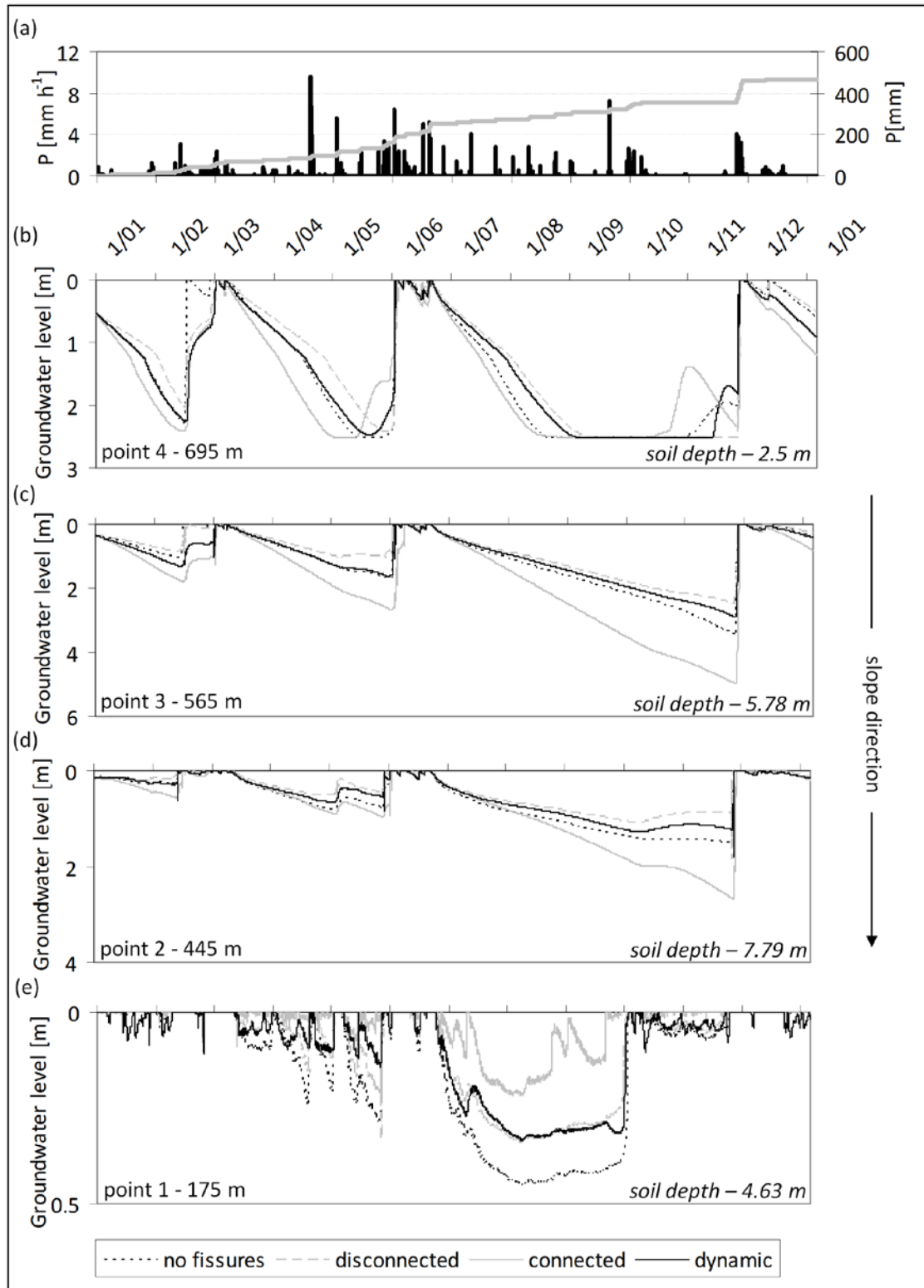


Figure 5-9. Time series results of the one year simulation period. (a) Precipitation, (b-e) examples of groundwater level fluctuations observed in four points located along the landslide profile (major axes of the ellipse) from the toe (0 m) to the scarp (800 m) of the landslide. See Figure 5-8a for the landslide profile and Figure 5-3a for specific location of four points.

There are significant differences between the scenarios in the timing of when saturation is reached (Figure 5-9). The highest groundwater level (saturation) is observed first for ‘disconnected fissures’ or ‘no fissures’, then ‘dynamic connectivity’ and lastly the ‘connected fissures’ scenario. The exception is the lowest part of the landslide (Figure 5-9e) where, in case of the ‘connected fissures’ scenario, most of the water is cumulated and thus groundwater level is the highest.

When looking at the exchange fluxes between the fissure and matrix fraction, clear differences between scenarios are visible. The absolute total exchange fluxes (I) between fissure and matrix fractions ($I_{Sat, FM} + I_{Sat, MF} + I_{Unsat, FM}$) for ‘dynamic connectivity’ equal 79% of the total observed for ‘connected fissures’, and 130% of the one observed for ‘disconnected fissures’. The same relation is observed when comparing unsaturated ($I_{Unsat, FM}$) and saturated ($I_{Sat, FM} + I_{Sat, MF}$) exchange fluxes separately. For all scenarios the saturated exchange fluxes ($I_{Sat, FM} + I_{Sat, MF}$) are around 50-55% of total exchange fluxes. However, there are significant differences in flux directions. The ratio between the total amount of water flowing from the fissure fraction into the matrix fraction ($I_{Sat, FM}$) and the total amount of water flowing from the matrix fraction into the fissure fraction ($I_{Sat, MF}$) are 1.23, 1.12 and 0.95 for ‘disconnected fissures’, ‘dynamic connectivity’ and ‘connected fissures’ respectively. The results of exchange fluxes’ analysis show that there are limited differences in piezometric head in matrix and fissure network for ‘disconnected fissures’. They also show that in the case of ‘connected fissures’ these differences are getting bigger, and that that groundwater level in the matrix is in general higher than the one in the fissure. The ‘dynamic connectivity’ scenario is a combination of two extreme scenarios.

5.5 Sensitivity analysis

In general, the sensitivity analysis of the model is in line with the one presented by Van Beek (2002) and Malet et al. (2005). The porosity (n_{mat} , n_{fis}) and saturated hydraulic conductivity ($k_{sat, mat}$, $k_{sat, fis}$) are the parameters with the largest influence on the hydrological model (modelled storage). This is not surprising, since those two parameters control the soil moisture percolation with depth, groundwater recharge and saturated lateral flow. Changing these two parameters by adding or subtracting 25% and 50% of absolute values for porosity and 50% and 100% of the absolute value for saturated hydraulic conductivity (for both matrix and fissures fractions at one time) results in maximal 10% (for n) or 12% (for k_{sat}) variation in

modelled storage. There is an obvious strong positive relationship between changes in soil porosity, for both matrix and fissures fractions, and both saturated and unsaturated storages. In the case of changes in k_{sat} , the average total storage is almost constant but an increase in k_{sat} , results in an increase in unsaturated storage in both fissures and matrix fraction, and a decrease in corresponding saturated storages.

A more detailed sensitivity analysis of the fissure fraction parameterisation and fissure connectivity was performed to quantify whether the introduction of dynamic fissure behaviour is relevant, or if similar hydrological responses could be obtained with adapted hydraulic parameterisation of the fissure system. Figure 5-10 shows the results of the sensitivity analyses by plotting the number of days a cell was saturated as a function of the hydraulic parameterisation of the fissures ($k_{sat,fis}$, n_{fis}). The reference plot (the ‘dynamic connectivity’ scenario) is located in the upper right corner of the sensitivity matrix. Moving left from the reference plot, along the x-axis $k_{sat,fis}$ decreases, while moving down, along y-axis the porosity of fissure fraction (n_{fis}) decreases. The lower left plot represents the situation of matrix flow only, as the saturated hydraulic connectivity and porosity of matrix and fissure fractions are the same.

Note, however, that this is not similar to the ‘no fissures’ scenario, as the air entry value and shape factor of soil water retention curve are also defined separately for the fissure fraction. Figure 5-10 shows that when decreasing $k_{sat,fis}$ the upper part of the landslide exhibits more saturation, meaning that the groundwater levels remain higher in the upper part of the landslide area. This is due to the reduced drainage capacity of the fissure network. On the other hand, when n_{fis} decreases (getting closer to n_{mat}) there are limited differences in water distribution within the landslide, however, the average total storage of the landslide and the percentage of the unstable area decreases. This is the result of decreased infiltration capacity of the fissures: less water flows to the deeper layers and therefore less water moves from the fissures to the matrix. Consequently it results in a slower groundwater table rise.

Figure 5-11a shows the results coming from the four reference scenarios: ‘no fissures’, ‘disconnected fissures’, ‘connected fissures’ and ‘dynamic connectivity’. Figure 5-11b shows the effect of the influence of a fissure network with different fissure connectivities (from 10 to 90%) that are set constant over the simulation period. The last panel (Figure 5-11c) presents the simulation results for the ‘connected fissures’ scenario but with different lower saturated

hydraulic permeability for the fissure fraction ($k_{sat,fis}$). Figure 5-11 shows that the results of the simulation using constant fissure connectivity differ clearly from the one performed with dynamic fissure connectivity, despite changes in the fissure fraction characteristics; fissure connectivity (Figure 5-11b) and fissure hydraulic permeability (Figure 5-11c). Comparing the results of Figure 5-11b with the ‘dynamic connectivity’ scenario of Figure 5-11a, it can be seen that constant fissure connectivity results in more water in the lower part of the landslide, and gives a larger average unstable area for similar average total storage. The saturated permeability of the fissures (Figure 5-11c) basically affects the drainage capacity, independent of the connectivity fraction.

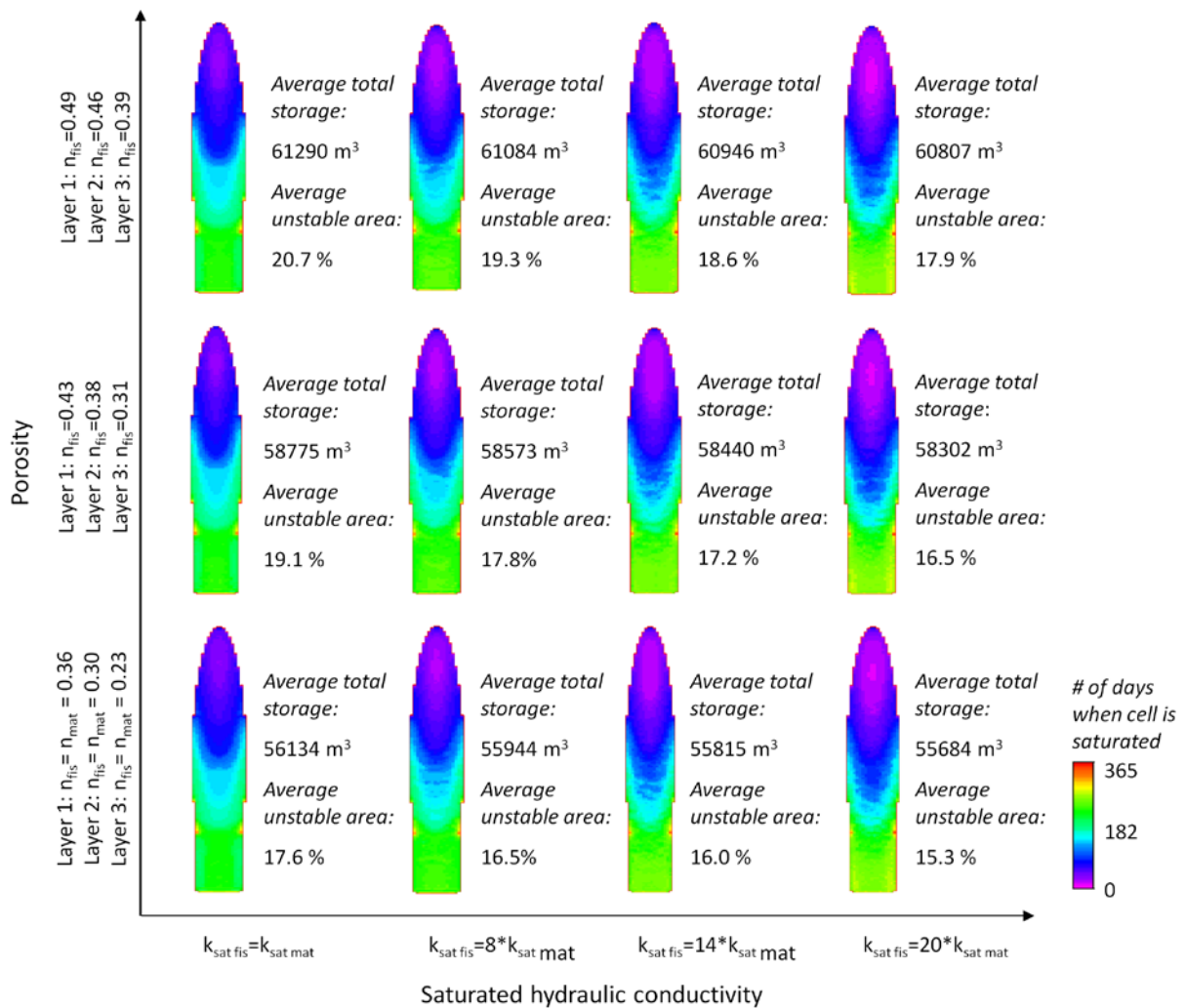


Figure 5-10. Sensitivity analysis of the model for changes in the fissure parameterisation. The unstable area is the area of all cells where $f_s < 1$. The plot located in upper right corner is the reference plot – the ‘dynamic connectivity’ scenario. Moving left along the x-axis $k_{sat,fis}$ decreases while moving down along y-axis the n_{fis} decreases while matrix characteristics remain constant.

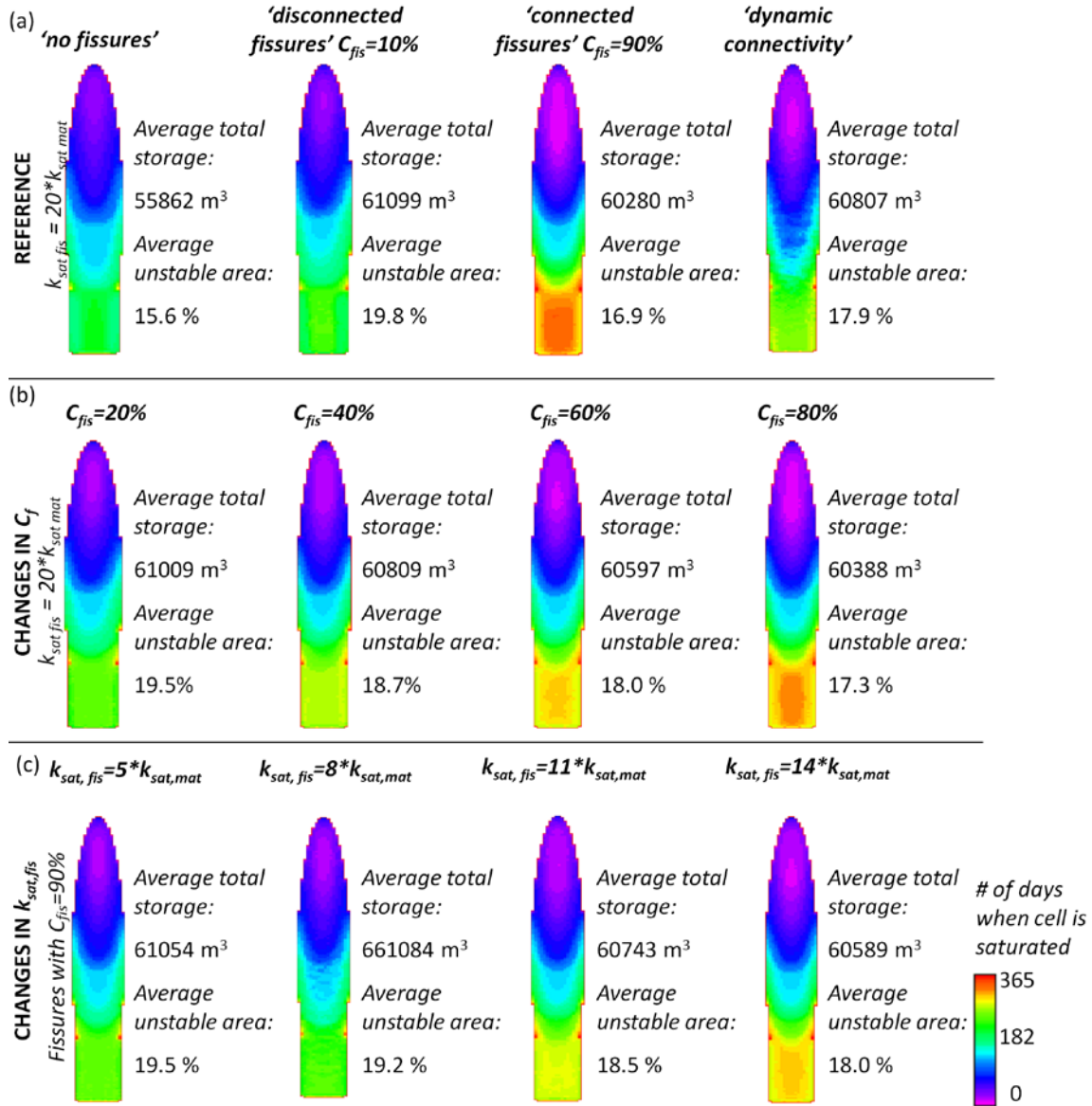


Figure 5-11. Sensitivity analysis of the model for changes in conceptualisation of fissure connectivity: (a) is the reference panel – the ‘no fissures’, ‘disconnected fissures’, ‘connected fissures’ and ‘dynamic connectivity’ scenarios; (b) changing fissure connectivity (C_{fis}) for the simulation with fissures included (C_{fis} is constant over the simulation period); (c) changing saturated hydraulic conductivity for the ‘connected fissures’ scenario.

The general conclusion that can be drawn from the sensitivity analysis is that the results obtained with ‘dynamic connectivity’ scenario cannot be reached using effective hydraulic parameterisation of the fissure fraction with constant connectivity. The ‘dynamic connectivity’ scenario seems to be able to accommodate more water in the system, causing less instability.

6 Discussion and Conclusions

This research aimed to study the importance of preferential fissure flow for landslide hydrological behaviour at the field scale, with a conceptual modelling approach using the Storage and Redistribution of Water on Agricultural and Re-vegetated Slopes model (STARWARS), which is a distributed model coupling hydrological and stability dynamics (Van Beek, 2002). The results highlight that fissure connectivity and fissure permeability are important parameters of the fissure network. Both of these parameters can change the water distribution within the landslide, and influence the timing and the duration of the periods of elevated pore pressure conditions.

The presented conceptual model of fissure flow is based on dual-permeability approach. The use of dual-permeability approach for preferential fissure flow modelling allows incorporating knowledge about commonly observed features of a fissure network as retaining their own porosity and soil moisture content (Malet et al., 2005), matrix – fissure interaction (Van Beek & Van Asch, 1999) as well as providing dynamically changing natural preferential flow paths (Weiler & McDonnell, 2007). This way of simulating preferential fissure flow seems more realistic when compared to the simplistic preferential flow representation in a form of by passing flow (Malet et al., 2005) or modified hydraulic conductivity function only (Mulungu et al., 2005; Zhang et al., 2006). Moreover, the use of GIS based PCRaster programming language gives the opportunity to account for spatial heterogeneity of soil hydrological properties and distributed nature of the fissures systems.

The results presented in this paper are in agreement with previous studies: presence of fissures increases the vertical infiltration rate and influences storage capacity of the soil (McDonnell, 1990; Uchida et al., 2001). When a fissure network consists of disconnected fissures only, the storage capacity increases whereas outflow is impeded. This results in persistently high groundwater levels and less spatial variations across the landslide. A connected fissures network shows fast preferential drainage as the dominant process, and thus results in a lower groundwater level. In this way, fissures and the dynamic variation in their connectivity, control the distribution of soil pore water pressure, which is an important factor for initiation and reactivation of mass movement (Cameira et al., 2000; Uchida et al., 2001; Nobles et al., 2004). The results presented in this paper show that presence of fissures can change the overall stability of the landslide. However, it is important to stress that downslope converging

flow paths, resulting from bedrock topography and no-flow boundary conditions, in combination with extended, well connected fissure network results in accumulation of water from the upper part of the landslide that can lead to very high groundwater level in the lower part of the landslide, and negatively affect the stability of the toe of the landslide. This effect might also be observed in reality, depending on the geomorphology and topography of the valley and the geometry of the toe itself. However, it is necessary to have in mind that the fissure network defined in our study ($F_{fis} = 30\%$ over the whole landslide area) is quite large and it would not often be that extensive in a real case study.

Introducing the dynamic fissure connectivity, dependent upon soil moisture content as earlier proposed for soil pipe networks (e.g.: Nieber and Sidle, 2010), results in composite behaviour spanning the end members mentioned above. This range of hydrological responses under dry and wet conditions introduces stronger seasonality than static fissure connectivity. This is more similar to what is actually observed in nature. Furthermore, the analysis showed that dynamic fissure behaviour could not be mimicked using adjusted hydraulic parameterisation for the fissures. We recognize the difficulties in quantification of the dynamic fissure connectivity, but we believe this research has shown that it is worthwhile to include dynamic fissure characteristics into hydrological modelling of the landslide.

This research indicates the need for further studies in the direction of measurement of fissure characteristics and monitoring of their variation over time. It would be worthwhile to look at orientation of fissures. This would allow us to better define and constrain the relationship between fissure connectivity and saturation degree of the soil. It may also shed light on other relationships, i.e. between fissure volume and differential soil movement within a landslide.

Chapter 6

A MODEL OF HYDROLOGICAL AND MECHANICAL FEEDBACKS OF PREFERENTIAL FISSURE FLOW IN A SLOW MOVING LANDSLIDE

In slow-moving landslides, hydrological regime is complicated due to continuous opening and closing of the fissures. This consecutive opening and closing of fissure aperture controls the formation of critical pore water pressure by creating dynamic preferential flow paths for infiltration and groundwater drainage. This interaction may explain the seasonal nature of the slow-moving landslide activity, including the often observed shifts and delays in hydrological responses when compared to timing and duration of precipitation.

The main objective of this chapter is to model the influence of fissures on the hydrological dynamics of slow-moving landslide and the dynamic feedbacks between fissures, hydrology and slope stability. For this we adapted the spatially distributed hydrological and slope stability model (STARWARS) to account for geotechnical and hydrological feedbacks, linking between hydrological response of the landside and the dynamics of the fissure network and applied the model to the hydrologically Super-Sauze landslide (South French Alps).

Based on: Krzeminska, D.M., Bogaard, T.A., Malet J.-P. and Van Beek L.P.H. 2012 (work in progress). A model of hydrological and mechanical feedbacks of preferential fissure flow in a slow- moving landslide. (to be submitted in) Hydrology and Earth System Science.

6.1 Introduction

The importance of understanding the hydrological system within a landslide is commonly accepted; however, including hydrological processes and their variability in landslide modelling is quite difficult and therefore often limited (Bogaard, 2001; Lindenmaier, 2007). The main difficulties stem from spatial and temporal heterogeneity of bedrock geometry, material layering, hydrological material properties and dominant hydrological processes across the landslide (Malet et al., 2005; Krzeminska et al., 2012a). This is particularly true when dealing with slow-moving clayey landslides, where continuous movement of sliding material results in fissure formation with successive opening and closing of fissure apertures.

Fissures influence the time and intensity of groundwater recharge changing the storage capacity of a soil and affect the infiltration processes of rainfall or snowmelt. Depending on fissure geometry and connectivity between them, they may have adverse or beneficial effect on landslide activity (see Ch.1§1.3 and Ch.5§5.4-5.6). The high spatial and temporal variability of preferential flow processes makes it very difficult to incorporate them in hydrological modelling.

In 1999, Van Beek and Van Asch proposed a spatially distributed physically based model coupling hydrological and stability dynamics, developed in the PCRaster environmental modelling software package. In 2005, Malet et al. applied the STARWARS model to the Super-Sauze landslide using the simple bypass flow scheme representing only shallow bypassing flow without fissure – matrix interaction. Krzeminska et al. (2012b) included more detailed representation of fissure flow in STARWARS model (see Ch.5§5.2.2). Following a dual-permeability approach they assumed the presence of two overlapping and interacting domains, the matrix and fissures blocks, having their own characteristics and properties (i.e. porosity, hydraulic conductivity) and allowing water flow in both domains.

Herein we apply the above model (Krzeminska et al., 2012b; Chapter 5) to the hydrologically controlled slow-moving Super-Sauze landslide and explicitly take into account the mutual dependence of fissures (their geometry and effectiveness for transmitting water downslope), hydrology and landslide activity. The main objective of this study is to model the influence of fissures on the hydrological dynamics of a slow-moving landslide and to formulate a framework to incorporate feedback between fissure flow and stability state into landslide modelling. For a complete description of the STARWARS model the reader is referred to Van

Beek (2002) and a detailed description of fissure flow implementation is presented in Chapter 5.

6.2 Conceptualisation of hydrological and mechanical feedbacks of fissure flow

6.2.1 Hydrological feedback

Hydrological feedback is the mutual dependence of landslide hydrological responses and effectiveness of the fissure network to transport water which increases with soil wetness (Tsuboyama et al., 1994; Noguchi et al., 1999; Sidle et al., 2000). Following the concept presented in Chapter 5, the model accounts for dynamic hydrological feedback between fissure connectivity and the degree of saturation of the soil column (Eq.5.9)

6.2.2 Mechanical feedback

Mechanical feedback is the mutual dependence of fissure geometry and differential displacement observed within a landslide. The density, and thus the volume of the fissures, is an important characteristic determining the influence of fissures on landslide hydrology (see Ch.1§1.3).

Fissures location within the landslide and their morphology correspond to mechanical processes (see Ch.1§1.3.3). The typical surface fissure patterns and their distribution across the Super-Sauze landslide is presented in Chapter 2 §2.5. It is interesting to see that the spatial distribution of fissure patterns is almost not changing despite continuous landslide activity, indicating strong influence of the geometry of the stable bedrock and mechanical properties of the sliding material on fissures occurrence (see Figure 6-3). Consequently, these fissure patterns are good indicators of local deformation level including relatively brittle top soil behaviour (0-1 m) and more ductile behaviour in deeper layers (Stumpf et al., *submitted*)

Moreover, a significant increase of fissure density can be observed in spring or beginning of summer, which correlates with observed landslide acceleration periods (Malet, 2003). Further development of surface fissure patterns depends on the level of landslide activity (e.g. displacement rates) and meteorological conditions (e.g. precipitation). After the acceleration period, fissures may be filled with some surface deposit and/or (partly) closed due to compaction. During the deceleration period, prolonged dry periods may result in increased

brittleness of the upper soil layer and consequently increase in fissure density (Stampf et al., *submitted*).

These observations show that temporal changes in fissure volume and density are the result of complex and interacting processes. Here, we present a first attempt to account for dynamically changing fissure volume by correlating fissure density, and thus fissure volume, with local factor of safety, which is a deterministic measure of mass stability. The factor of safety (f_s) is the ratio between maximum shearing resistance to failure and shear stress (see Ch.1§1.2.1) and is calculated here with the assumptions of the infinite slope model (Skempton, 1964). The interaction between cells is neglected and the shear surface is assumed to be equal to the depth of the particular soil column (see Figure 6-2). These assumptions are very efficient for use in a GIS because calculated stability depends on the attributes of each individual soil column only (Van Asch et al., 1993; Van Beek and Van Asch, 2004). As such, f_s serves here as a proxy for the excess shear stress that can not be accommodated by a particular soil column and, thus, can lead to soil extension (e.g. appearance and/or extension of shear and tension fissures) or compression (e.g. closing of existing fissures and/or appearance of compression fissures and bulges).

We conceptualised the general relationship between factor of safety and fissure volume. When the soil column is relatively stable ($f_s \gg 1$) there are no, or very limited, fissures present within this soil column. When the stability of the soil column approaches the equilibrium limit ($f_s = 1$), more fissures appear and the volume of fissures increase with decreasing f_s . In practice, this means that f_s calculated for particular cell (soil column) controls the volumes of the domains within this cell (matrix/fissures). Equation 6.1 gives the conceptual relationship between fissure density (F_{fis}) and factor of safety (f_s):

$$F_{fis,i} = \begin{cases} F_{fis,max} & \text{for } f_{s,i} < f_{s,min} \\ \frac{(f_{s,max} - f_{s,i})}{(f_{s,max} - f_{s,min})} \cdot (F_{fis,max} - F_{fis,min}) + F_{fis,min} & \text{for } f_{s,min} \leq f_{s,i} \leq f_{s,max} \\ F_{fis,min} & \text{for } f_{s,i} > f_{s,max} \end{cases} \quad (6.1)$$

The $F_{fis,min}$ and $F_{fis,max}$ are the upper and lower limit of fissure density. The $f_{s,min}$ and $f_{s,max}$ define the range of factor of safety that corresponds to the range of changes in fissure density.

6.3 Modelling of the Super-Sauze landslide

6.3.1 Model representation of the Super-Sauze landslide

The geometry, parametrisation and hydrological concepts of the Super-Sauze landslide is a further extension of the work presented by Malet et al. (2005). Figure 6-1 presents the summary of the information used to create the Super-Sauze landslide representation, calibration and validation of the model. Detailed description of the Super-Sauze landslide is presented in Chapter 2.

Landslide geometry

The overall geometry of the Super-Sauze landslide has been defined based on 3D geometrical model of the landslide (Travelletti and Malet, 2012) with the spatial resolution at the pixel of 5x5 m (see Ch.2§2.3.2).

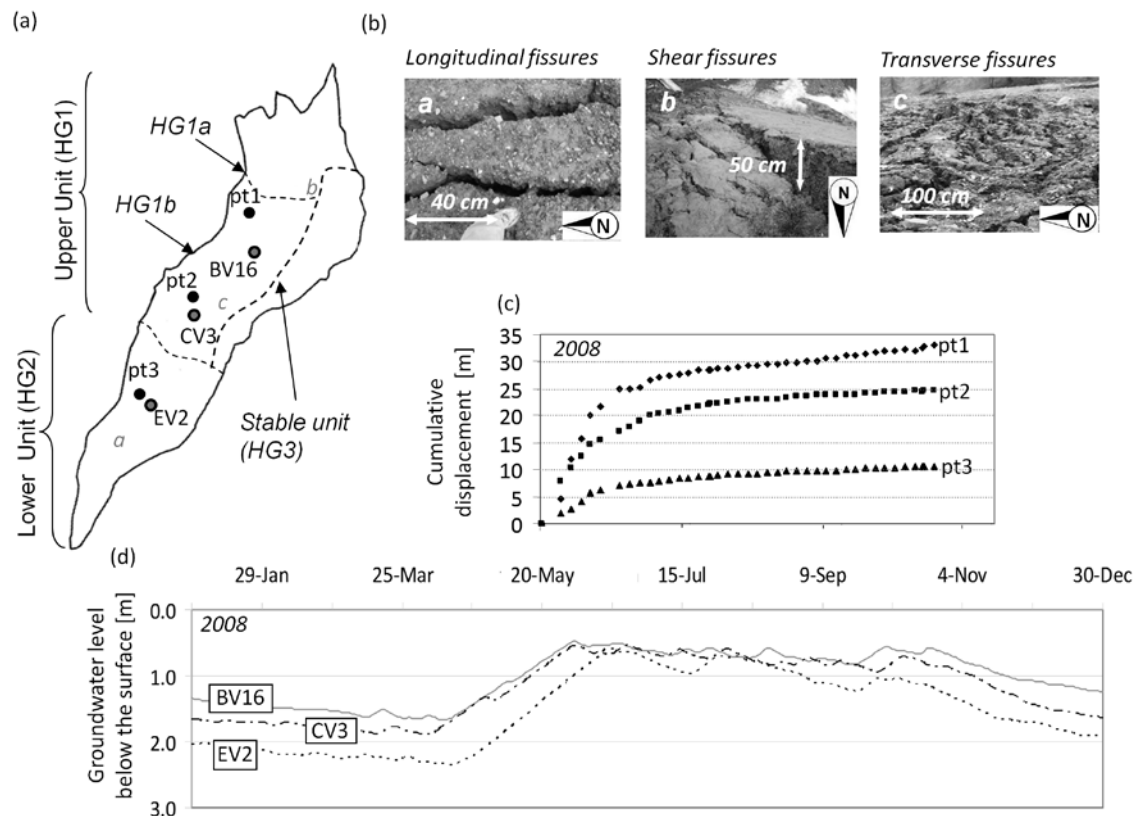


Figure 6-1. (a) The hydro-geomorphological units, localisation of the piezometers, measurement points of displacement and indication of the areas where the pictures of fissures were taken; (b) Examples of fissures observed on the Super-Sauze landslide; (c) Cumulative displacement measured at three points: pt1, pt2 and pt3 (Travelletti et al., 2012a); (d) Groundwater level fluctuation observed at three piezometers: BV16, CV3, EV2. Please note one time scale for panel (c) and (d).

Spatial representation of the Super-Sauze landslide composes of three units corresponding to the hydro-geomorphological units proposed by Malet (2003) (see Ch.2 Figure 2-13). Additionally, the upper unit (HG1) was split into two sub-units, HG1a and HG1b, depending on dominant hydrological processes (Figure 6-1a; Chapter 4).

Vertically, the landslide body is represented by three layers (C1a₁, C1a₂ and C1b; see Ch.2 Figure 2-7 and Figure 6-2). The maximum depth of C1a is 3 m and of C1b 9 m. Following the idea of Malet et al. (2005), we distinguished additional near surface layer (C1a₁) with an assumed maximum depth of 1 m. This layer is the most influenced by fissures.

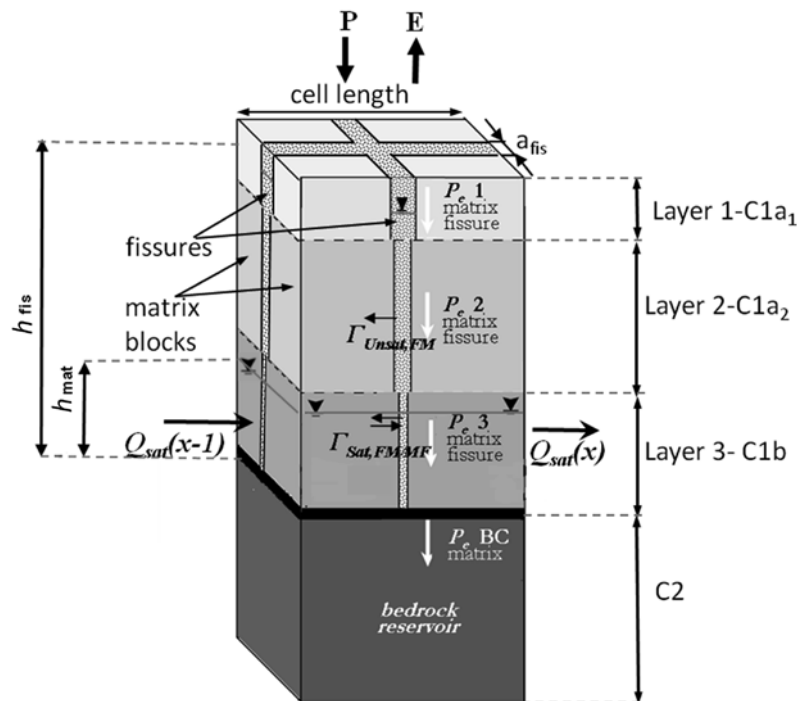


Figure 6-2. Schematisation of the hydrological model of the Super-Sauze landslide.

Fissure fraction characteristics

The maximum fissure fraction ($F_{fis,max}$) of the near surface unit (C1a₁) has been derived from aerial photographs analysis from the period of 2007 – 2008 (Niethammer et al., 2012) and generalised in four zones across the landslide (Figure 6-3c). Zone 1 (F1) represents areas with no, or very limited, fissures observed at the soil surface. However there is field evidence for the presence of preferential flow paths in these areas (Chapter 4). Therefore, $F_{fis,max}$ in F1 is set to be 5% and $F_{fis,min}$ is set to be equal to $F_{fis,max}$ (no mechanical feedback is considered). The $F_{fis,max}$ and $F_{fis,min}$ for deeper layers were set arbitrary taking into account that generally

the volume of fissures decreases with depth (due to compaction and rheology) and that they should be continuous throughout the vertical profile (model requirement; Chapter 5). All $F_{fis,max}$ and $F_{fis,min}$ values are listed in Table 6-1.

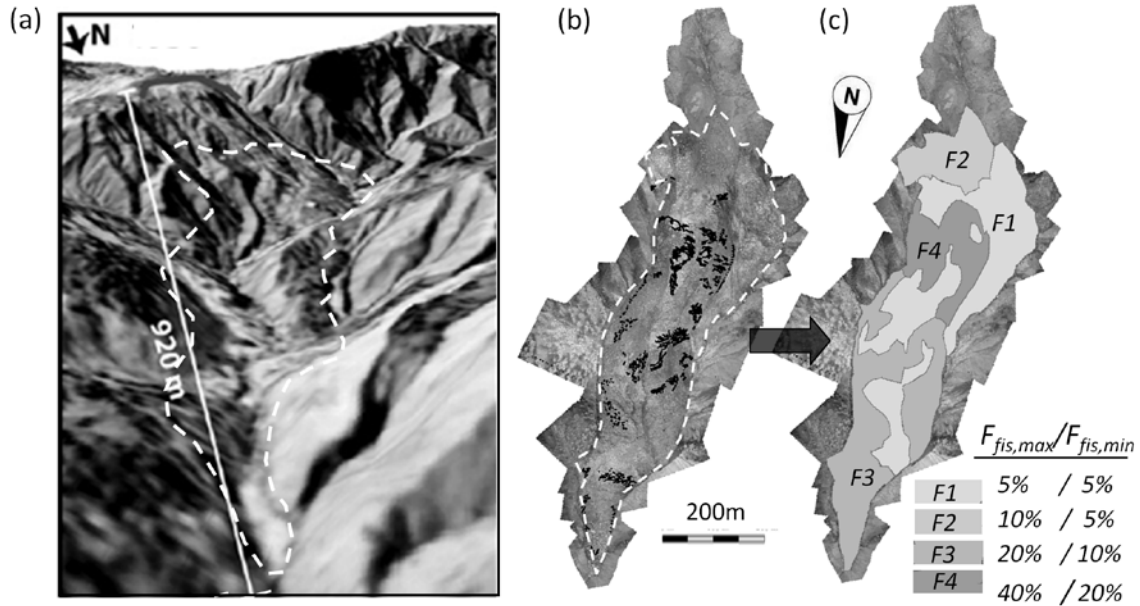


Figure 6-3. (a) The DEM of Super-Sauze landslide area from 1956, before the initial failure of the slope with marked current boundary of the landslide (b) The aerial photography (July 2008) with fissures are marked with black lines; (c) the implemented fissures zones with defined maximal ($F_{fis,max}$) and minimal ($F_{fis,min}$) observed fissure fraction in the surface layer.

Table 6-1: Maximum and minimum fissure fraction as defined per zone and per layer

Vertical layer	Zone 1		Zone 2		Zone 3		Zone 4	
	$F_{fis,max}$	$F_{fis,min}$	$F_{fis,max}$	$F_{fis,min}$	$F_{fis,max}$	$F_{fis,min}$	$F_{fis,max}$	$F_{fis,min}$
Layer 1 (C1a ₁)	5%*		10%	5%	20%	10%	40%	20%
Layer 2 (C1a ₂)	0%*		5%	2%	10%	2%	20%	2%
Layer 3 (C1b)	0%*		2%*		2%*		2%*	

* $F_{fis,max} = F_{fis,min}$ – no mechanical feedback considered

6.3.2 Meteorological data

The meteorological data (rain intensity, air temperature, incoming short wave radiation and relative humidity) was coming from the meteorological station located within 0.8 km distance from the landslide. A snowmelt routine based on the degree-day approach was applied. A temperature threshold (T_s) was used to discriminate rainfall from snow fall and a critical temperature (T_m), above which snowmelt occur, was used to govern the melt equation. A

vegetation cover is not considered in the model as the landslide has no or very limited vegetation.

6.3.3 Model calibration and validation

The model was calibrated against observed snow coverage and groundwater level fluctuation over the period of one calendar year (January – December 2007). The initial distributed water level, soil moisture and snow thickness conditions were produced by running the model for one year (2007), for multiple times until a dynamic steady-state was achieved. The time step resolution of the model is 1h.

Two stage calibration procedure has been applied (Figure 6-4). In the first stage the model including only the hydrological feedback (Chapter 5) was calibrated in order to get estimates of $f_{s,min}$ and $f_{s,max}$ needed for introducing mechanical feedback (see Eq.6.1). As the first step, the ‘snow pack/snow melt’ model was calibrated against binary ‘snow-no snow information’. The effective parameters that produce the snow cover ($S_{C,sim}$) duration comparable to the observed one ($S_{C,obs}$) are: $T_s' = 1^\circ\text{C}$ and $T_m' = 6^\circ\text{C}$. The liquid water holding capacity of snow pack was set to be constant over time and equal 0.10 and a day-degree factor was assumed equal to $2.5 \text{ mm.day}^{-1}.\text{°C}^{-1}$. It is important to note that the relatively high effective values for T_s' and T_m' are the effect of compensating for local variations in meteorological factors (lapse in temperature, shading and radiation) and diurnal changes in temperature when modeling with a 1 h simulation time step. The same duration of snow cover would be obtained using $T_s' = 1^\circ\text{C}$ and $T_m' = 1^\circ\text{C}$ with 24h simulation time step.

Next, the core hydrological model was calibrated. The initial hydrological parameters of matrix and fissure fractions were based on field - measured parameters as reported by Malet et al. (2005) and they were assumed to be equal for the whole landslide. The distinction between parameters for matrix and fissure fraction was made by assuming minimum and maximum measured values being representative for matrix and fissure characteristics respectively (Table 6-3). For example, if the range of measured porosity in the field is 0.36 to 0.49 (Malet et al., 2005) then the minimum (0.36) is assumed to represent matrix porosity and maximum (0.49) fissure porosity. Additionally, the hydraulic conductivity of fissure fraction is assumed to be 10 times higher than the one of matrix fraction.

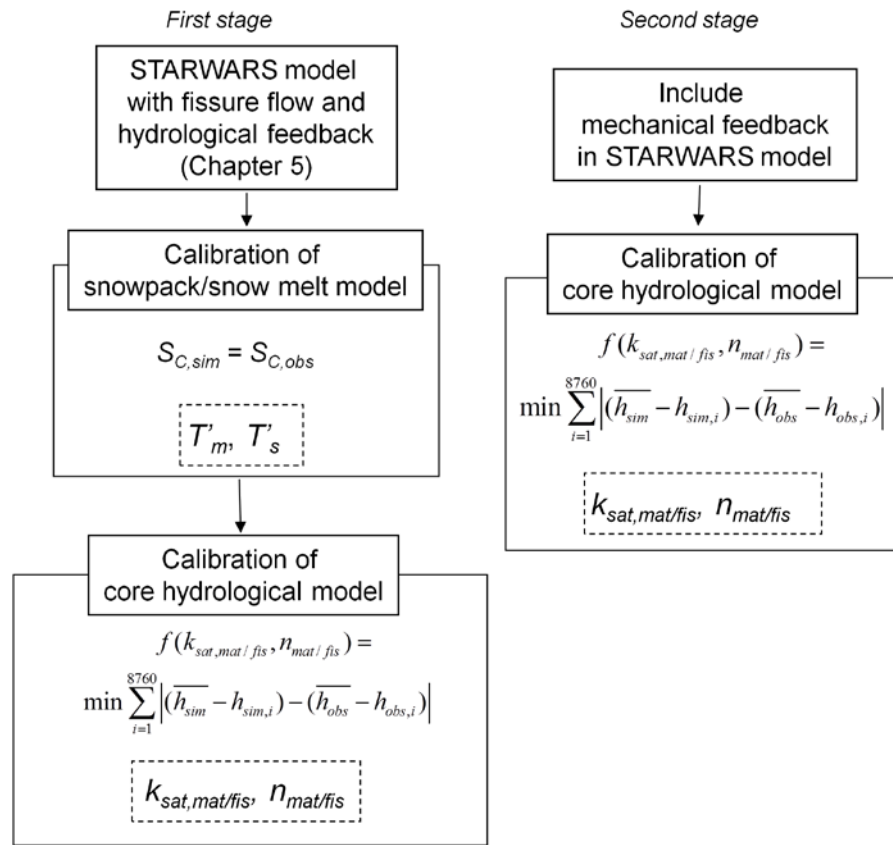


Figure 6-4. The calibration procedure.

The model was calibrated by changing saturated conductivity ($k_{sat, mat / fis}$) and porosity ($n_{mat / fis}$) only. These four parameters were chosen since they show the highest variability when measured in the field and the hydrological model is most sensitive to their variations (see Van Beek, 2002; Malet et al., 2005 and Chapter 5). Observed piezometric water levels were assumed to be representative for particular units within the landslide (Figure 6-1a, Table 6-2). The parameters were differentiated per landslide unit (within the range of $\pm 50\%$ for $n_{mat / fis}$ and $\pm 100\%$ for $k_{sat, mat / fis}$) and adjusted to come to the smallest differences between modelled (h_{sim}) and observed (h_{obs}) groundwater level fluctuations per landslide unit (HG1-HG3).

The stability sub-model was not calibrated but the soil strength parameters, cohesion (c) and the angle of friction (φ), were set for the entire landslide in order for the factor of safety per cell (f_s) to oscillate around unity for the most active areas of the Super-Sauze landslide (see Ch.2 Figure 2-10). Figure 6-5a shows the results from the simulation performed with $c' = 8$ kPa and $\varphi' = 25^\circ$. This parameter's set are in agreement with the values presented by Malet (2003) for C1b sub-layer where, according to our conceptualisation, the slip surface is located. The upper and lower factor of safety, $f_{s, min}$ and $f_{s, max}$ were set to 0.7 and 1.3

respectively as the simulated values of the annual average factor of safety ($f_{s,av}$) falls in this range for more than 75% of landslide area (Figure 6-5a).

Table 6-2. Landslide unit and corresponding measuring points (see also Figure 6-1)

Landslide Unit	Piezometer	Point of displacement measure
HG1a	AV1	-
HG1b	BV16 & CV3	pt1 & pt2
HG2	EV1	pt3
HG3	BV5	-

The second stage of the calibration procedure was based on the simulations performed with both hydrological and mechanical feedbacks. The saturated conductivity ($k_{sat,mat/fis}$) and porosity ($n_{mat/fis}$) were again calibrated. Table 6-3 gives the final calibration results.

The model, including both hydrological and mechanical feedbacks, was validated for the year 2008.

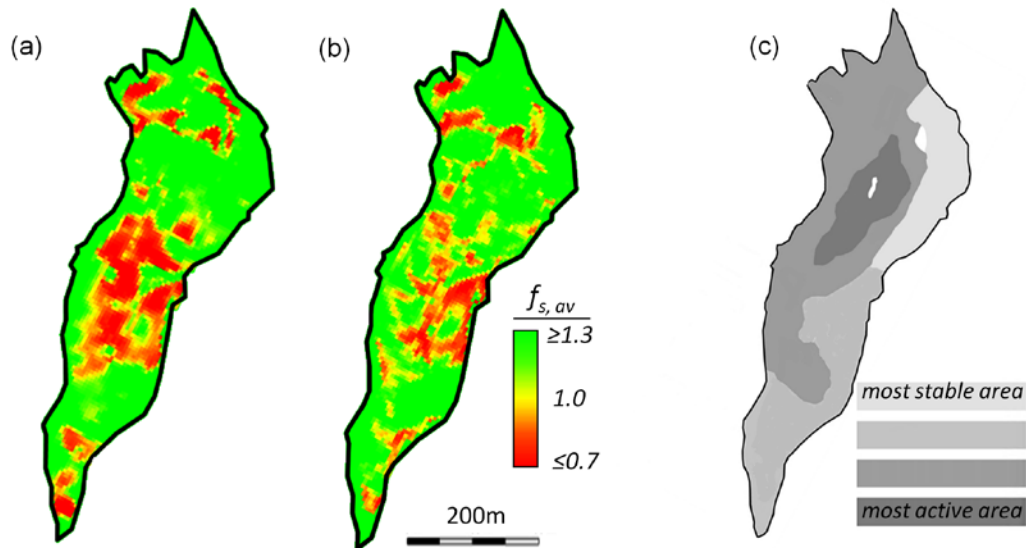


Figure 6-5. The annually averaged factor of safety ($f_{s,av}$) simulated for calibration period (2007) with the model (a) accounting for hydrological feedback only (first stage of calibration) and (b) accounting for both hydrological and mechanical feedback (second stage of calibration); (c) Spatial differences in landslide activity (based on Malet, 2003);

Table 6-3. The range of field measured parameters (Malet et al., 2005) and the set of parameters after model calibration

Parameter	Field measurements	Optimal model parameters	
		Matrix fraction	Fissure fraction
Saturated conductivity – C1a ₁ [m.s ⁻¹]	$6.10 \cdot 10^{-6} \div 1.05 \cdot 10^{-5}$	$6.02 \cdot 10^{-6}$	$6.02 \cdot 10^{-5}$
Saturated conductivity – C1a ₂ [m.s ⁻¹]	$4.86 \cdot 10^{-6} \div 2.08 \cdot 10^{-5}$	$4.05 \cdot 10^{-6}$	$4.05 \cdot 10^{-5}$
Saturated conductivity – C1b [m.s ⁻¹]	$4.05 \div 6.02 \cdot 10^{-6}$	$3.70 \cdot 10^{-6}$	$3.70 \cdot 10^{-5}$
*Porosity - C1a ₁ [-]	0.36÷0.49	0.36/0.25/0.25/0.21	0.49/0.44/0.44/0.34
*Porosity - C1a ₂ [-]	0.30÷0.46	0.33/0.18/0.18/0.18	0.46/0.41/0.41/0.32
*Porosity - C1b [-]	0.23÷0.39	0.27/0.13/0.13/0.13	0.39/0.35/0.35/0.27
**Air entry value (SWRC) - C1a ₁ [m]	0.008÷0.042	0.042	0.008
**Shape factor of the SWRC - C1a ₁ [-]	12.9÷14.7	12.9	14.7
**Air entry value (SWRC) - C1a ₂ [m]	0.035÷0.049	0.049	0.035
**Shape factor of the SWRC - C1a ₂ [-]	11.5÷13.1	11.5	13.1
**Air entry value (SWRC) - C1b [m]	0.016÷0.21	0.021	0.016
**Shape factor of the SWRC - C1b [-]	12.3÷13.7	12.2	13.7

* porosity values vary between units HG1a/HG1b/HG2/HG3

** values taken from Malet et al (2005)

6.4 Simulation results and discussion

Figure 6-6 presents observed and simulated groundwater level fluctuations for 2007 (calibration period) and 2008 (validation period). The simulated groundwater level fluctuations representative for particular hydro-geomorphological units (Table 2) were collated with observed piezometric groundwater levels fluctuation (Figure 6-1d). The general range of the groundwater level fluctuation and the timing of the major peaks are well represented by the model. The root mean square error (RMSE) between observed and simulated groundwater variations representative for four units for the calibration period varies between 0.18 and 0.40 m for the calibration period, and between 0.20 – 0.44 m for the validation period. The differences between observed and modelled groundwater fluctuations mainly stem from collating point measurements with area averaged simulated results. During the winter periods and short after the snow melt the difference are mainly related to inaccuracy of the ‘snow pack/snow melt’ sub-model.

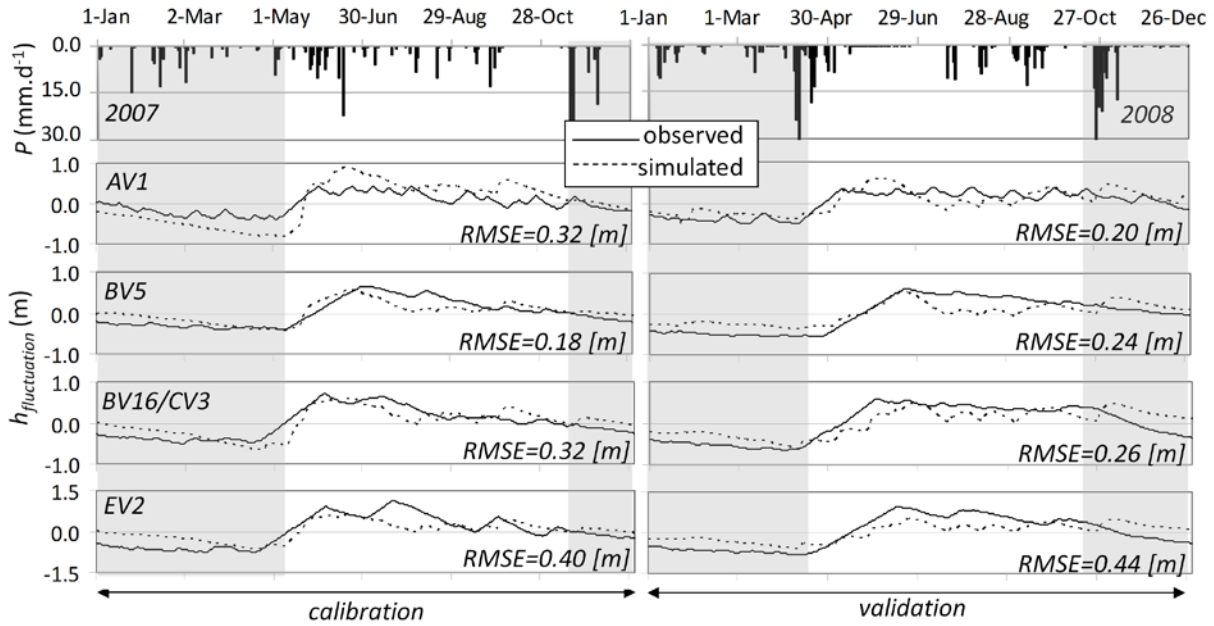


Figure 6-6. Observed and simulated groundwater level fluctuations over years 2007 (calibration period) and 2008 (validation period) with corresponding root mean squares errors (RMSE). The 0 at the y-axis corresponds to average observed or simulated groundwater level. The shadow areas correspond to the period when the snow cover was observed.

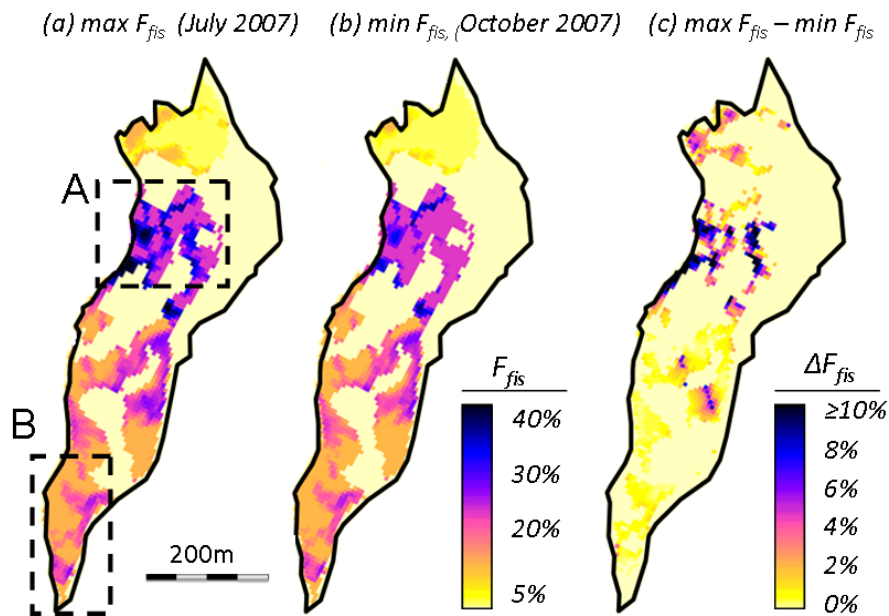


Figure 6-7. The modelled dynamics in fissure fraction during: (a) maximum fissure fraction ($\max F_{fis}$), (b) minimum fissure fraction ($\min F_{fis}$) and (c) the range ($\max F_{fis} - \min F_{fis}$) during one year simulation period (2007). The areas A and B indicated in Figure 6-5a are used for discussion.

The maximum simulated fissure fraction occurs in July 2007 and the minimum simulated fissure fraction occurs in period of October-November 2007 (Figure 6-7). The maximum variation in fissure fraction (ΔF_{fis}) is 13% and it takes place in the area with the highest fissure fraction (F4) and relatively high landslide activity (see Ch.2 Figure 2-10 and Figure 6-1c). This behaviour of the fissure fraction is in agreement with what is expected from field monitoring (Figure 6-1c-d): rising groundwater level is associated increasing displacement rate and results in a more extended fissure network.

The model performance regarding the simulation of spatial differences in potential landslide movement was tested by collating the simulated values of factor of safety with observed displacement rate reported by Travelletti et al. (2012a) for the year 2008 (Figure 6-1c). The modelled distribution of the factor of safety for the year 2007 (Figure 6-5b) represents the observed Super-Sauze landslide activity (Figure 6-5c; Malet, 2003) very well: the middle upper part of the landslide is ‘the most active one’ (f_s is the lowest) while the lower part of the landslide is relatively stable (f_s above 1.0 for most of the time during the simulation period) and the western part is the most stable area. However in the validation period (May-September 2008), there is a 20 days time lag between modelled decrease in f_s and displacement rate reported by Travelletti et al. (2012a) (Figure 6-8a,b). This time lag is also visible between simulated and observed groundwater level variation during the validation period (Figure 6-6) and it results from the ‘snow pack/snow melt’ calibration. The simulated time lag can be significantly reduced by changing the effective critical temperature for snow melt for the validation period ($T_m' = 5^\circ\text{C}$). With this adjustment the simulated spatio-temporal patterns of the factor of safety follow the observed displacement rates very well (Figure 6-8).

In order to study the influence of the implemented dynamic characteristics of the fissure network, $F_{fis}(f_s)$ and $C_{fis}(\theta_E)$, three scenarios were analysed:

- scenario-1 – both hydrological $C_{fis}(\theta_E)$ and mechanical feedbacks are included, $F_{fis}(f_s)$
- scenario-2 – only hydrological feedback ($C_{fis}(\theta_E)$) is included; F_{fis} is assumed to be constant ($F_{fis} = F_{fis,av}$) and $F_{fis,av}$ is estimated based on fissure fraction simulated with scenario-1, averaged over the fissure areas (F1-F4, Figure 6-3c) and over one year simulation period;
- scenario-3 – fissure network is not considered, only matrix fraction is present.

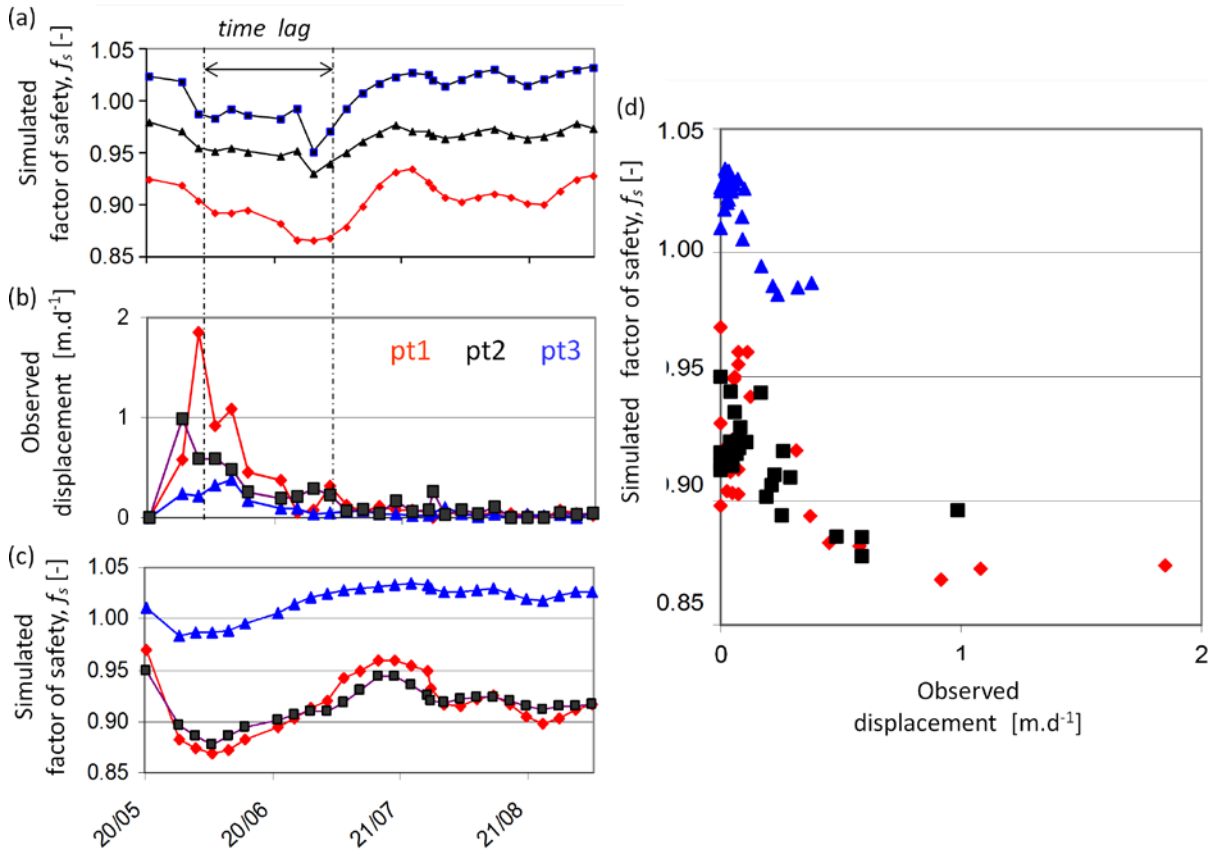


Figure 6-8. (a) Simulated factor of safety without adjustment of “snow pack/snow melt model”; (b) Observed displacement rates for points pt1, pt2 and pt3 (Travelletti et al., 2012a); (c) The factor of safety, f_s , simulated with additional adjustment of ‘snow pack/snow melt’ model; (d) The relationship between the ‘new’ f_s and observed displacement rates (Travelletti et al., 2012a). For the location of the points see Figure 6-1a.

Figure 6-9 shows the difference in groundwater behaviour modelled with three scenarios. The highest differences between the scenarios in simulated groundwater level behaviour can be seen in the middle part of the landslide (HG1b; Figure 6-1a). There are no, or very limited differences observed in groundwater level behaviour within stable unit (HG3; Figure 6-1a).

In general, the minimum simulated groundwater level (h_{min} ; Figure 6-9a) is the lowest for scenario-3 (no fissure network included) and the highest for scenario-2 (fissure network with hydrological feedback only). The analogous trend is observed when comparing the annual range of simulated groundwater level fluctuations ($h_{fluctuation}$; Figure 6-9b): scenario-3 presents the highest variations of simulated groundwater level and in case of scenarios-2 the simulated groundwater level fluctuations are the lowest. The overall modelled groundwater level, averaged over a one year simulation period (h_{av}), is the highest for scenario-2 and the lowest for scenario-3 (Figure 6-9c). The differences between the scenarios are in agreement with the results presented in Chapter 5 for the ‘simple’ landslide representation: introduction of fissure

network and accounting for the dynamically changing fissure connectivity resulted in an increase in total average water stored within the landslide.

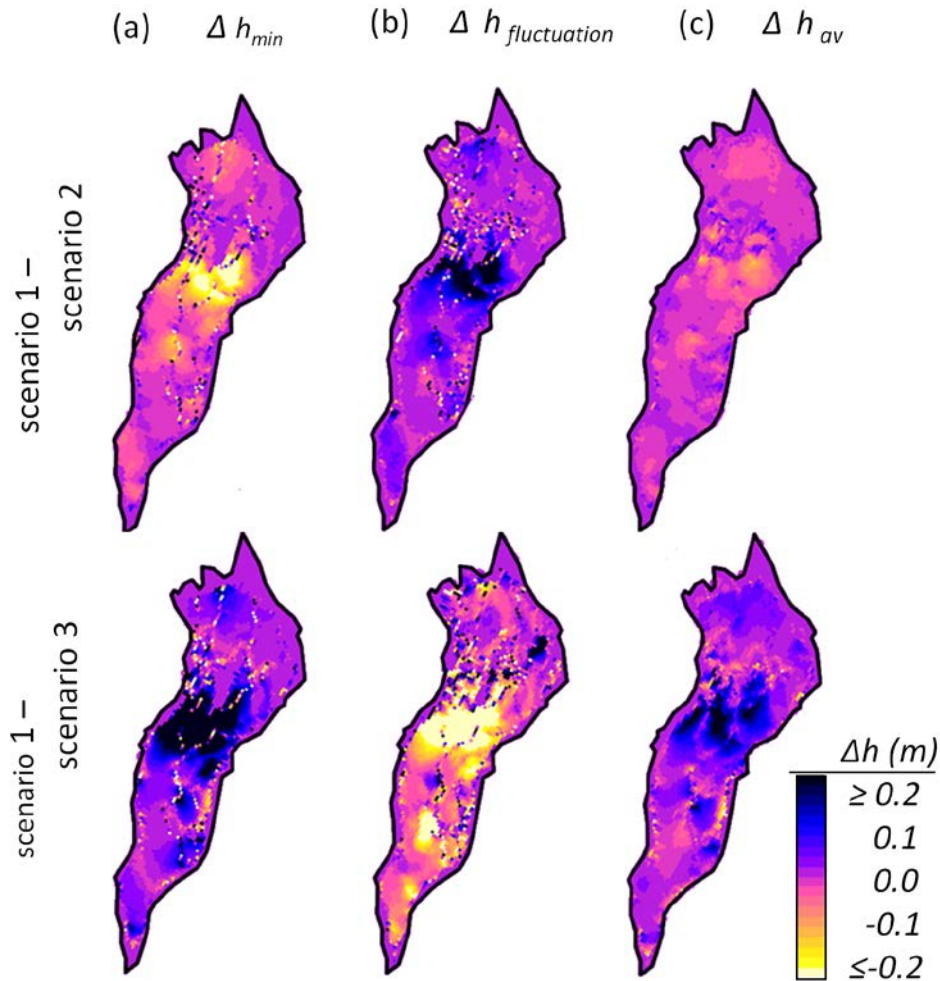


Figure 6-9. Differences in simulated groundwater level behaviour between the three scenarios.

When analysing the differences between the scenarios where fissure network are implemented (scenario-1 - 2) one can see how the model captures the behaviour of the fissure network. Let us analyse two areas within the landslide (Figure6-7a) being representative for:

- fissures network with limited downslope drainage – area A – located in the upper part of the landslide, where the highest fissure fraction ($\max F_{fis} \geq 25\%$) and the highest variability in fissure fraction ($\max F_{fis} - \min F_{fis}$ up to 10%) occurs during the simulation period and
- fissure network with relatively unlimited drainage – area B – lower part of the landslide, where fissure fraction is relatively high (F_{fis} from 10% to 20%)

The area located just below area A is characterised by relatively limited fissure fraction ($F_{fis} = 5\%$). As a consequence of this set up, the fissure network in the area A behave as a dead- end fissures network. The rising saturation of the particular soil column within area A results in rising chance for fissures to be connected (scenario-2). However, with limited drainage possibilities in downstream direction this results in rising of the average groundwater level in the area A (Figure 6-9c). When mechanical feedback is included (scenario-1), the increase in the soil column saturation influences the stability of the soil column and therefore fissure volume. Growing volume of fissures (i.e. increase of available water storage) results in lowering of groundwater level. Nevertheless, the annual average groundwater level in area A simulated with scenario-1 is still higher than the one modelled with scenario-3 (where fissures are not considered). The evidence for dead-end like fissure behaviour at the lower part of area A is: (a) the results of small-sprinkling experiment performed in this area (Chapter 4) showing that infiltration processes are controlled by the extended but poorly connected fissure network and prolonged periods of elevated pore water pressure is observed after the sprinkling; (b) the observation of saturated tension cracks, with the standing water, observed in this part of the landslide (Malet et al., 2005).

The opposite behaviour is observed in the area B. Here, the modelled fissure network extends till the border of the landslide and can provide natural drainage network when the fissures are connected between adjacent cells. Therefore, even if the average groundwater level in the area increases after introducing fissure network, it decreases when accounting for hydrological and mechanical feedbacks (scenario-1) and there are almost no differences when comparing with scenario-3 (where no fissure network is considered). This behaviour is also observed in the field: the average groundwater level observed in the piezometer EV2 is lower than in the middle part of the landslide and it shows moderate piezometric responses.

The results presented herein are in general agreement with previous studies (McDonnell, 1990; Uchida et al., 2001) confirming that presence of fissures influences the percolation processes and storage capacity of the soil. Moreover, they confirm that fissure volume and fissure connectivity control the distribution of soil pore water pressure within the landslide (Cameira et al., 2000; Uchida et al., 2001; Nobles et al., 2004, Krzeminska et al., 2012a,b). The presence of disconnected fissures increases the storage capacity whereas outflow is impeded. This results in persistently high groundwater levels. The presence of connected fissures

network shows fast preferential drainage as the dominant process, and thus results in a lower groundwater level.

Logically, groundwater level behaviour results in analogous differences, between the scenarios, in simulated stability of the particular cells. Implementation of the hydrological and mechanical feedbacks (scenario-1) results in a general increase of stability (f_s) when comparing to the scenarios where only hydrological feedback is considered to be dynamic (scenario-2) (Figure 6-5). The findings are schematically summarised in Figure 6-10.

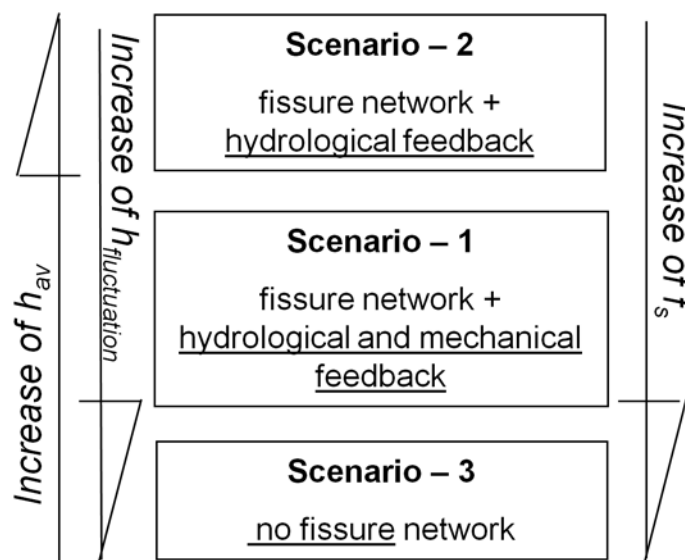


Figure 6-10. General trends in groundwater level (h_{av}) and local factor of safety (f_s) when analysing four scenarios.

Last but not least, it is important to stress the main limitation of the proposed model. The model uses the pre-defined landslide geometry that is not changing during the simulation periods and, and thus, no mass displacement can be considered. Moreover, the implemented feedbacks in fissures characteristics have no influence on the strength properties of the material. The use of the infinite slope model is also an important simplification and calculated f_s represents local conditions only (cell level). However, Milledge et al., 2012 showed that infinite slope model can successfully be applied for landslides with a length/depth ratio of at least 25. The Super-Sauze landslide is a complex slow-moving translational landslide with the length around 900m and the maximal depth of sliding material approximately 9 m (Malet et al., 2005; Travelletti & Malet, 2012).

7 Conclusion

This chapter describes an initial attempt to model the hydrology of the Super-Sauze landslide with accounting for preferential fissure flow and the dynamically changing characteristics of fissure network. The spatially distributed hydrological and slope stability model (STARWARS) has been adapted to account for geotechnical and hydrological feedbacks on changes in fissure volume and fissure connectivity (Van Beek, 2002; Krzeminska et al., 2012b). The hydrological parameters used for model calibration are taken from the work of Maquaire et al (2003) and Malet et al (2005).

The model reproduces the observed hydrological behaviour of the landslide, accounting for spatial differences in hydrological responses and captures all the physical phenomena and their variation in time and space. Our research outlines that fissure volume and fissure connectivity control the distribution of soil pore water pressure within the landslide. Implementation of the dynamic characteristics of fissure network allowed to account for the spatial and temporal variability in the hydrological processes dominating in particular areas of the landslide that are often observed in the field.

It is important to stress that proposed simple linear relationships between saturation of the soil column and fissure connectivity and between the mass movement and fissure volume are theoretical only. However, our research indicates the need for further study in the direction of measurement and monitoring of fissures characteristic and their variation over time. This would allow a better understanding and constrain of the proposed relationship.

Chapter 7

SYNTHESIS

This thesis investigates the influence of fissures on landslide hydrology. Research work included both extended field experiments and hydrological modelling. Based on the analysis of all available field data, a conceptual fissure flow model was proposed and tested in both synthetic and case study modelling.

The main conclusion of this thesis is that preferential fissure flow may change local hydrological regimes depending on fissure network characteristics, especially fissure volume and connectivity between fissures. The field measurements outline the spatial heterogeneity of soil hydraulic properties and dominant hydrological processes existing in slow-moving clay shale landslide. The analysis of field data together with presented modelling results confirms the importance of distributed approaches when modelling differential hydrological response of complex heterogeneous landslides and stresses the need for including spatio-temporal changes in soil hydraulic properties of both fast and slow responding domains.

7.1 Monitoring of soil moisture patterns and dominant processes within a landslide

In case of precipitation triggered landslides, the weather condition, soil moisture content and pore water pressure are the key components to monitor and, furthermore, to be incorporated into modelling of landslide hydrology. The antecedent soil moisture condition and the soil structure control the percolation of the precipitation to the saturated layers. Especially, preferential flow paths and their spatio-temporal variation define the hydrological processes dominating in an area and consequently control the pore water pressure built – up.

This thesis presents the potential of Distributed Temperature Sensing (DTS) measurements (Chapter 3) and combined hydrological and hydrochemical analysis of small scale sprinkling tests (Chapter 4) to monitor and to quantify hydrological state and processes in the unsaturated zone. Both methodologies were tested on a clay shale slow moving landslide – the Super-Sauze landslide.

7.1.1 Potential of DTS for long term monitoring of soil moisture patterns

DTS offers the opportunity to monitor temporal and spatial temperature patterns in a soil which is a big advantage over point temperature measurements. High resolution soil temperature observations can be related to moisture variability via analysis of thermal soil properties (Chapter 3).

The qualitative analysis of measured soil temperature variation allowed observing spatial differences in soil moisture state and estimating the location of surface and subsurface water flow paths. Figure 7-1 shows the example of qualitative interpretation of the soil temperature data. The quantitative analysis of measured soil temperature made it possible to capture the variability of apparent soil thermal conductivity and to correlate this with measured soil moisture content. However, the precision of quantitative analysis strictly depends on careful control of sensor (fibre optic cable) installation depths and accurate control of the upper boundary condition (soil surface temperature).

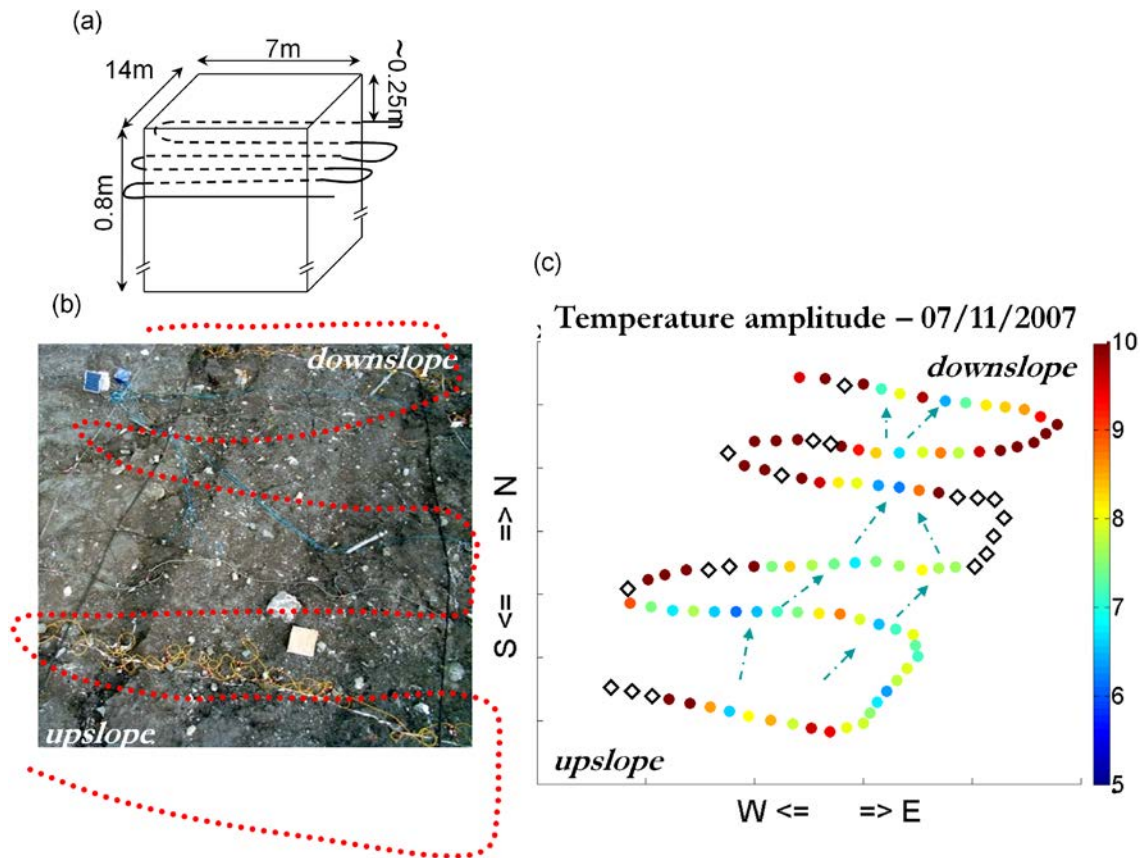


Figure 7-1. (a) Schematisation of single cable experimental set-up (see Figure 3-3); (b) Near Sensing Camera Field Equipment photography of large-scale sprinkling experiment area (Krzeminska et al., 2009); open rhombus indicates the areas where the cable was surfacing and the air temperature was measured; red dot line indicates the location of fibre optic cable; (c) example distribution of measured daily amplitude of soil temperature; blue dash line indicates location of estimated preferential flow paths.

Proper installation and maintaining of fibre optic cables within a heterogeneous and active landslide over a long time period might be problematic and technically constrained. Therefore, when accounting for the limitation of the presented methodology (Chapter 3), DTS should be seen more as support measurements to be applied with other available techniques providing spatial soil moisture information with lower spatial and temporal resolution. DTS can be used to validate microwave remote sensing soil moisture monitoring (Steele-Dunne et al. 2010), which may have limited value on steep topography (Njoku et al., 2000). Combination of satellite data with DTS analysis could determine if satellites can provide useful signal in particular landslide prone areas and, when necessary, provide more detailed (local scale) information about soil moisture spatial variability.

Going into local scale monitoring, DTS can be a complementary measurement for areal photography and thermal photography monitoring of landslide for verification of potential

key areas. Application of DTS measurement in those areas may improve qualitative and quantitative identification of soil surface features, e.g.: differential drainage conditions, wetness patterns, preferential flow pathways (e.g. Krzeminska et al., 2009; Niethammer et al., 2009) as well as subsurface and ground water discharge areas (e.g. Bobba et al., 1992).

Moreover, both microwave remote sensing soil moisture observation and thermal pictures of soil surface can be used to estimate soil moisture content in the top 0-5 cm soil layer (e.g. Jackson et al., 1996; Sugiura et al., 2007). However, surface layer saturation is often not a direct trigger of landslide. It is the combined effect of surface and subsurface saturation that is critical. To estimate the link between surface soil moisture and subsurface saturation for specific case studies DTS measurements can be used locally.

In order to extend the application of DTS the main problems to deal with are:

- installation and calibration – it is necessary to have a few independent temperature and soil moisture sensors in order to define the relation between estimated apparent diffusivity and soil moisture content, account for the spatial and temporal heterogeneity of soil properties and, lastly, to account for instrumental changes over time (e.g.: influence of changes in fibre strain, drift in laser instrument, etc.)
- long-term maintenance – there is a need for (a) constant and stable energy supply, (b) monitoring the continuity of the fibre optic cable (possible break of the fibre due to differential movement of sliding material) and (c) its installation depths changes due to constant movement of reworking material.

Giving further research attention to solve those complications seems worthwhile since, once robust, DTS technique can provide spatial and temporal information about soil moisture state over landslide hotspots with relatively low cost demands. This information could be furthermore incorporated into real time hazard monitoring and risk modelling. As such it could become valuable component of local early warning systems for rainfall induced landslide by providing “timely and effective information that allows individuals exposed to a hazard to take action to avoid or reduce their risk and prepare for effective response”(ISDR, 2004).

7.1.2 Potential of Small Scale Sprinkling Experiments for identification and quantification of dominant hydrological processes

The understanding and quantification of subsurface flow paths requires on-site investigations. Direct measurements of subsurface flow paths need high experimental effort due to spatial variability of surface and subsurface structures and invisibility of the latter. A consistent measurement method is not yet achieved. To our knowledge, there is very limited *on site* experimental research dedicated to fissure flow and not one on landslide terrain. In Chapter 4 the potential of small scale sprinkling experiment for identification and quantification of dominant hydrological processes in the highly heterogeneous environment of a slow moving landslide was discussed. Our motivation was to find a methodology to recover subsurface flow paths in the field, under ‘natural conditions’, in relatively fast and non-destructive manner.

Combining environmental or/and artificial tracing with hydrological surveys analysis for investigating preferential flow in the soils is far from new. The experiments vary from laboratory tests (e.g. Allaire-Leung et al., 2000; Larsbo & Jarvis, 2006) to field experiments of different scales (e.g. Collins et al, 2002; Weiler & Naef, 2003; Mali et al., 2007; Kienzler & Naef, 2008). However, there is no plot scale field measurements dedicated to monitor and quantify preferential fissure flow, being a special case of macropores with apertures up to tens of centimetres.

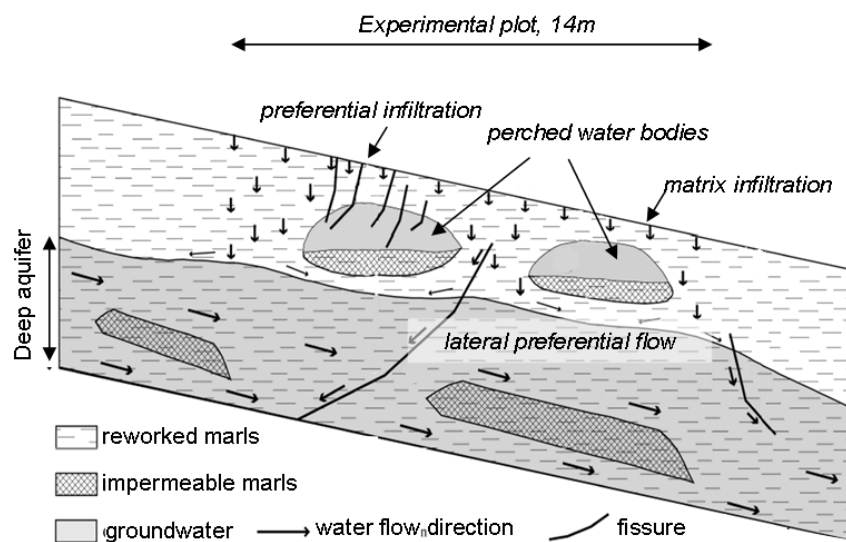


Figure 7-2. Conceptual model of subsurface water flow paths in the most active zone of Super-Sauze landslide (adopted from Debieche et al., 2012).

The idea of using small scale ($1 \times 1 \text{ m}^2$) sprinkling experiments rose after successful performing of large scale (approximately 100 m^2) sprinkling tests in summer 2007 at the Super-Sauze landslide and the Laval landslide (Debieche et al., 2012; Garel et al., 2012). These two experiments gave valuable insight in the preferential infiltration and preferential later drainage processes in those unstable clay-shale hillslopes (Figure 7-2). However, due to the size and long duration, this kind of experiments are logistically and financially very demanding, and cannot be undertaken on a regular basis across the study area.

The small-scale experiments are relatively inexpensive and can be deployed throughout the landslide. Although we performed only six experiments on three locations, which is spatially limited, we show that small-scale sprinkling experiments are sufficient to capture the dominant hydrological processes occurring in the area and have the potential for their quantification. Moreover, combination of the hydrological and hydrochemical analysis of two consecutive days of sprinkling gave a valuable insight about mixing processes (pre-event and event water) and interaction between fissure and matrix domains.

In order to extend the application of small scale sprinkling experiments and overcome present shortcomings the following should be considered:

- detailed measurements of soil characteristics, their heterogeneity in the analyzed soil profile, and their high temporal resolution monitoring during the sprinkling experiment;
- applying non-destructive measure to provide more detailed characteristics of subsurface fissure system, especially in vertical directions. Grandjean et al. (2012) and Travelletti, et al. (2012b) presented promising results based on seismic azimuth tomography or ERT measurements. However, both methodologies need further improvement to provide unique characteristics of subsurface flow paths.

7.2 Modelling the influence of fissure flow on landslide hydrology

The literature review, extensive field campaigns consisting of day-to-day monitoring as well as sprinkling experiments presented in Chapter 3 and Chapter 4 and analysis of all available field observation (see Chapter 2) resulted in the formulation of a conceptual model of the hydrological influence of fissures on landslide activity (Chapter 5). The model expand the original conceptualisation of fissure flow (Van Beek and Van Asch, 1999) by explicit inclusion of fissures and more detailed representation of the fissure flow. Moreover, the

model accounts for dynamic nature of fissures network: (a) fissure connectivity depending on soil moisture content (Chapter 5) and (b) fissure geometry depending on the level of landslide activity (Chapter 6).

In general, the model results show that the presence of fissures may significantly influence water distribution within a landslide by changing the timing and duration of the periods of elevated pore pressure conditions. The significance of the changes in the local hydrological responses depends on size, density and connectivity of the fissure network. Introducing dynamic hydrological feedback of fissure connectivity and soil moisture state of the matrix results in stronger seasonality of landslide hydrological responses and underlines their spatial heterogeneity (Chapter 5), and additional introduction of mechanical feedback of fissure volume and level of landslide activity attenuates the groundwater level fluctuations (Chapter 6). It is also interesting to note the self-regulatory mechanism that is implied by the results presented in Chapter 5 and Chapter 6 (Figure 6-10). The simulated annual average total storage increases when introducing the fissure network and accounting for the hydrological feedback. When both feedbacks (hydrological and mechanical) are included the simulated annual averaged groundwater level decreases.

However, the presented model in its current stage should be considered more as an effective tool helping to understand the possible impact of preferential fissure flow on landslide hydrological responses and to explain spatial and temporal difference in landslide activates than a model providing “better predictions” of possible slope failure. This is because the parameterisation of the model (a large number of input parameters needed and lack of standard field and/or laboratory experiments methodologies to measure them) and limitation in data availability for both model calibration and validation (high spatial and temporal field monitoring data needed). The original core STARWARS hydrological model (Van Beek, 2002), consisting of three vertical layers, is described by 12 parameters: layer-dependent porosity, saturated hydraulic conductivity, air entry value and SWRC shape factor. The explicit inclusion of fissures together with implementation of dual-permeability approach (Chapter 5) doubles this number. In case of the Super-Sauze landslide modelling, additional distinction of hydro-geomorphological units (Chapter 6) further increases the number of needed input information. This raises the question of possibility to measure and classify information about the spatial (vertical and horizontal) distribution of hydrological properties of both matrix and

fissure fraction. Undoubtedly much effort is needed to plan and perform field campaigns and/or lab experiment to get all the necessary input parameters.

On the other hand, the advantage of dual-permeability approach over dual-porosity approach for modelling hydrological responses of clay shale landslide is clear. Dual – porosity approach assumes that the porous media consist of two interacting and overlapping but distinct continuum, where matrix continuum is the main storage medium (no or very limited water flow is allowed) and fracture continuum is the main transport medium (Altman et al., 1996; Šimůnek et al., 2003). This assumption is valid for modelling of water flow in fractured rocks, but not in slow-moving clay-shale landslide such as the Super-Sauze landslide. The definition of ‘matrix continuum’ and ‘fracture continuum’ depends on the scale of the study. In case of fissure flow presented in this thesis fracture continuum is the fissure network consisting of cracks with the aperture up to tens of centimetres filled with reworked material and ‘the rest’ is considered as matrix continuum (matrix with smaller scale macroporosity). In this case subsurface water flow should not be restricted to the fracture continuum only.

Another point to discuss is the calibration of the model. The parameters used in the model are not all independent. Moreover, the calibrated parameters (porosity, hydraulic saturated conductivity) are considered to be constant over time and therefore represent the average soil conditions. In reality this is not a case, especially when analysing slow moving landslide with consecutive acceleration and deceleration periods (extension and compression of the sliding material). Introducing the dynamically changing fissure volume would allow mimicking these seasonal changes in soil properties: more fissures means higher average porosity and higher average saturated conductivity of particular cell or/and layer. On the other hand, together with introducing mechanical feedback we introduce new parameters and new uncertainties into the model.

An important limitation is the use of the factor of safety concept with the infinite slope stability model. This is very efficient for raster-based GIS since the stability on the cell level can be assessed from attributes of each individual cell only (the interaction between cells is neglected) and allows for tight coupling of the slope stability model with PCRaster hydrological model. Coupling the hydrological model with 2D or 3D slope stability model (loose coupling) is possible but it introduces additional errors due to the increased complexity of the recurring calculation and generalisation of attributes over multiple cells.

There is also a question of more accurate definition of proposed hydrological and mechanical feedbacks. As concluded from Chapter 5 and Chapter 6 these feedbacks are likely to be important for landslide hydrological modelling. Therefore there is a need for further studies in the direction of measurement and monitoring techniques to define fissure network characteristics (i.e. fissure depth, volume, density) and their variation in time and space. In this point it is worthwhile to mention: (a) the work of Niethammer et al. (2012) that shows the potential of UAV-based remote sensing for qualitative monitoring of surface feature on regularly basis, and (b) work of Stumpf et al., (*submitted*) that presents the image processing chain to extract quantitative characteristics of surface fissures from heterogeneous sets of VHR aerial images. Combination of the two could provide series of geomorphological surface fissure maps that could be, further on, collated with high resolution displacement measure (Travelletti et al., 2012a) and giving solid basis for better description of proposed mechanical feedback

However, based on the results presented in this thesis it can be concluded that in case of precipitation induced complex slow-moving clay – shale landslide, like the Super-Sauze landslide, the presence of fissures should not be neglected when modelling landslide hydrological responses, landslide initiation and/or its (re-)activation.

REFERENCES

A

- Allaire-Leung S.E., Gupta S.C. and Moncreif J.F., 2000. Water and solute movement in soil as influenced by macropore characteristics: I. Macropore continuity. *Journal of Contaminant Hydrology* 41: 283-301.
- Allaire S.E., Roulier S. and Cessna A.J., 2009. Quantifying preferential flow in soils: a review of different techniques. *Journal of Hydrology* 378: 179–204.
- Altman S.J., Arnold B.W., Bernard R.W., Barr G.E., Iio C.K., McKenna S.A., and Eaton R.R., 1996. Flow Calculations for Yucca Mountain Groundwater Travel Time (GWTT-95). Report SAND96-0819, Albuquerque, N. Mex.: Sandia National Laboratories.
- Anderson L., 2005. Fracture Mechanics: Fundamentals and Applications, 3rd Edition. Taylor & Francis.
- Angulo-Jaramillo R., Gaudet J.-P., Thony J.-L. and Vauclin M., 1996. Measurement of hydraulic properties and mobile water content of a field soil. *Soil Science Society of America Journal* 60(3): 710-715.
- Atkinson T.C., 1991. Techniques for measuring Subsurface flow on Hillslopes. In: Kirkby M.J (Ed): *Hillslope Hydrology, Landscape systems*. A series in Geomorphology, pp 73-117.

B

- Basinger J.M., Kluitenberg G.J., Ham J.M., Frank J.M., Barnes P.L. and Kirkham M.B., 2003. Laboratory evaluation of the dual-probe heat-pulse method for measuring soil water content. *Vadose Zone Journal* 2:389–399.
- Beckers J. and Alila Y., 2004. A model of rapid preferential hillslope runoff contributions to peak flow generation in a temperate rain forest watershed. *Water Resources Research* 40, DOI:10.1029/2003WR002582.
- Behaegel M., Sailhac P. and Marquis G., 2007. On the use of surface and ground temperature data to recover soil water content information. *Journal of Applied Geophysics* 62: 234-243.
- Bell R. and Glade T., 2004. Quantitative risk analysis for landslides – Examples from BÍldudalur, NW-Iceland. *Natural Hazards and Earth System Science* 4:117-131, DOI:10.5194/nhess-4-117-2004.
- Beven K. and Germann P., 1982. Macropores and water flow in soils. *Water Resources Research* 18(5):1311-1325.
- Bievre G., Jongmans D., Winiarski T. and V. V., 2011. Application of geophysical measurements for assessing the role of fissures in water infiltration within a clay landslide (Trieves area, French Alps). *Hydrological Processes*, DOI: 10.1002/hyp.7986.
- Binet S., Jomard H., Lebourg T., Guglielmi y., Tric E., Bertrand C. and Mudry J., 2006. Experimental analysis of groundwater flow through a landslide slip surface using natural and artificial water chemical tracers. *Hydrological Processes* 21(25): 3463-3472.

- Bishop A.W., 1954. The use of the pore pressure coefficient in practice. *Geotechnique* 4: 148-152.
- Bobba A.G., Bukata R.P. and Jerome J.H., 1992. Digitally processed satellite data as a tool in detecting potential groundwater flow systems. *Journal of Hydrology* 131: 25–62.
- Bogaard T.A., 2001. Analysis of hydrological processes in unstable clayey slopes. PhD thesis, University of Utrecht, Netherlands.
- Bogaard T.A., 2002. A state-dependent ground water recharge model for landslide research. Proc. 9th Int. Cong. IAEG, Durban, South Africa, pp 1489-1496.
- Bogaard T.A. and Van Asch T.W.J., 2002. The role of the soil moisture balance in the unsaturated zone on movement and stability of the Beline landslide, France. *Earth Surface Processes and Landforms* 27: 1177-1188.
- Bogaard T.A., Buma J.T. and Klawer C.J.M., 2004. Testing the potential of geochemical techniques for identifying hydrological systems within landslides in partly weathered marls. *Geomorphology* 58: 323-338.
- Boll J., Steenhuis T.S. and Selker J.S., 1992. Fiberglass wicks for sampling of water and solutes in the vadose zone. *Soil Science Society of America Journal* 56: 701-707.
- Bouma J., 1990. Using morphometric expressions for macropores to improve soil physical analyses of field soils. *Geoderma* 46: 3–11.
- Brabb E.E., 1991. *The world landslide problem*. Episodes, 14:52-61.
- Brand E.W., Dale M. J. and Nash J.M., 1986. Soil pipes and slope stability in Hong Kong. *Quarterly Journal of Engineering Geology and Hydrogeology* 19: 301–303.
- Bromhead, E.N., 1992. *The stability of slopes*. 2nd edition, Chapman and Hall, London.
- Brolsma R., 2010. Effect of climate change on temperate forest ecosystems, PhD Thesis, University of Utrecht, Netherlands.
- Brooks S.M., Crozier M.J., Preston N.J. and Anderson M.G., 2002. Regolith stripping and the control of shallow translational hillslope failure: application of a two-dimensional coupled soil hydrology-slope stability model, Hawke's Bay, New Zealand. *Geomorphology* 45:165-179.
- C**
- Cameira M.R., Ahuja L., Fernando R.M. and Pereira L. S., 2000. Evaluating field-measured soil hydraulic properties in water transport simulations using the RZWQM. *Journal of Hydrology* 236(1-2): 78-90.
- Campbell G.S., Calissendorff C. and Williams J.H., 1991. Probe for measuring soil specific heat using a heat-pulse method. *Soil Science Society of America Journal* 55: 291-293.
- Campbell D.I., Laybourn C.E. and Blair I.J., 2002. Measuring peat moisture content using the dual-probe heat pulse technique. *Australian Journal of Soil Research* 40: 177-190.

- Cappa F., Guglielmi Y., Merrien-Soukatchoff V., Mudry J., Bertrand C. and Charmoille A., 2004. Hydromechanical modeling of a large moving rock slope inferred from slope levelling coupled to spring long term hydrochemical monitoring: example of the La Clapière landslide (Southern Alps, France). *Journal of Hydrology* 291:67-90.
- Christophersen N. and Hooper R.P., 1992. Multivariate analysis of stream water chemical data – the use of principal component analysis for the end-member mixing problem. *Water Resources Research* 28(1): 99-107. DOI: 10.1029/91WR02518.
- Coe J.A., Michael J.A., Crovelli R.A., Savage W.Z., Laprade W.T., Nashem W.D., 2004. Probabilistic assessment of precipitation-triggered landslides using historical records of landslide occurrence, Seattle, Washington. *Environmental and Engineering Geoscience* 10: 103-122.
- Collins R., Jenkins A. and Harrow M., 2000. The contribution of old and new water to a storm hydrograph determined by tracer addition to a whole catchment. *Hydrological Processes* 14: 701-711.
- Constantz J., Tyler S.W. and Kwicklis E., 2003. Temperature-Profile Methods for Estimating Percolation Rates in Arid Environments. *Vadose Zone Journal* 2: 12-24.
- Cras A., Marc V. and Travi Y., 2007. Hydrological behaviour of sub-Mediterranean alpine headwater streams in a badlands environment. *Journal of Hydrology* 339(3-4): 130-144, DOI: 10.1016/j.jhydrol.2007.03.004.
- Crozier M.J., 1986. *Landslides – Causes, consequences and environment*, Croom Helm, London.
- Cruden D.M. and Varnes D.J., 1996. Landslide types and processes. In: Schuster R.L. and Krizek R.J. (Eds): *Special Report 247: Landslides: Analysis and Control* Transportation and Road Research Board, National Academy of Science, Washington D. C.
- D**
- Dakin J.P., Pratt D.J., Bibby G.W. and Ross J.N., 1985. Distributed optical fibre Raman temperature sensors using a semiconductor light source and detector. *Electronics Letters* 21(13): 569-570.
- Debieche T.-H., Bogaard T.A., Marc V., Emblanch C., Krzeminska D.M. and Malet J.-P., 2012. Hydrological and hydrochemical processes observed during a large-scale infiltration experiment at the Super-Sauze mudslide (France). *Hydrological Processes*, 26: 2157-2170, DOI: 10.1002/hyp.7843.
- De Montety V., Marc V., Emblanch C., Malet J.-P., Bertrand C., Maquaire O. and Bogaard T.A., 2007. Identifying the origin of groundwater and flow processes in complex landslides affecting black marls: insights from a hydrochemical survey. *Earth Surface Processes Landforms* 32: 32-48.
- De Rooij G.H., 2000. Modeling fingered flow of water in soils owing to wetting front instability: A review. *Journal of Hydrology* 231-232:277-294.
- E**
- EM-DAT, 2006. The OFDA/CRED International Disaster database, <http://www.emdat.be>, 1/06/2012.

F

- Fannin R.J., Jaakkola J., Wilkinson J.M.T. and Hetherington E.D., 2000. Hydrologic response of soils to precipitation at Carnation Creek, British Columbia, Canada. *Water Resources Research* 36(6), pp.1481–1494.
- Farrel D. and Larson W., 1972. Modeling of the pore structure of porous media. *Water Resources Research* 8:699-705.
- Flageollet J.C., Maquaire, O. and Weber D., 1996. Geotechnical investigations into the Super-Sauze landslide. Geomorphological and hydrogeological results. In: *Workshop: 'Landslides-Flash floods', Barcelonnette-Vaison la Romaine*, CERG, Council of Europe, Major Hazards Agreement, Strasbourg, pp. 30-38.
- Flageollet J.-C., Maquaire O. Martin B. and Weber D., 1999. Landslides and climatic conditions in the Barcelonnette and Vars basins (Southern French Alps, France). *Geomorphology* 30: 65-78.
- Flageollet J.-C., Malet J.-P. and Maquaire O., 2000. The 3-D structure of the Super-Sauze earthflow (Alpes-de-Haute-Provence, France): a first stage towards modelling its behaviour. *Physics and Chemistry of the Earth, Part B* 25(9): 785-791.
- Flageollet J.-C., Malet J.-P., Maquaire O. and Schmutz M., 2004. Chapter 14. Integrated investigations on landslides: example of the Super-Sauze earthflow. In: Casale, R., Margottini, C. (Eds): *Natural Disasters and Sustainable Development*, Springer-Verlag, Berlin, pp. 213-238
- Fleming R.W. and Johnson A.M., 1989. Structures associated with strike-slip faults that bound landslide elements. *Engineering Geology* 27: 39-114.
- Flury M., Fluhler H., Jury W.A. and Leuenberger J., 1994. Susceptibility of soils to preferential flow of water: a field study. *Water Resources Research* 30(7): 1945-1954.

G

- Garel E., Marc V., Ruy S., Cognard-Plancq A.-L., Klotz S., Emblanch C. and Simler R., 2012. Large scale rainfall simulation to investigate infiltration processes in a small landslide under dry initial conditions: the Draix hillslope experiment. *Hydrological Processes*, DOI: 10.1002/hyp.9273
- Geoscape Nanaimo, 2012. *Geoscience for Central Vancouver Island Communities*. URL: <http://web.viu.ca/geoscape/images/landslides.jpg> [14.08.2012]
- Genet J. and Malet J.-P., 1997. Détermination de la structure tridimensionnelle du glissement de terrain de Super-Sauze par une investigation géotechnique. Master Thesis, University Louis Pasteur, Strasbourg, France.
- Gerke H.H. and Van Genuchten M.Th., 1993. A dual-porosity model for simulating the preferential movement of water and solutes in structured porous media. *Water Resources Research* 29(2)305-319, DOI:10.1029/92WR02339.

- Gerke H.H., 2006. Preferential flow descriptions for structured soils. *Journal of Plant Nutrition and Soil Science* 169(3): 382-400.
- Glade T. and Crozier M.J., 2005. Landslide hazard and risk - Concluding comment and perspectives. In: Glade T., Anderson M. & M. Crozier (Eds): *Landslide hazard and risk*, Wiley, pp 767-774.
- Grandjean G., Malet J.-P., Bitri A. and Méric O., 2007. Geophysical data fusion by fuzzy logic for imaging the mechanical behaviour of mudslides. *Bulletin de la Société Géologique de France* 178 (2):127-136.
- Grandjean G., Bitri A. and Krzeminska D. M., 2012. Characterisation of a landslide fissure pattern by integrating seismic azimuth tomography and geotechnical testing. *Hydrological Processes* 26: 2120-2127, DOI: 10.1002/hyp.7993
- Greco R., 2002. Preferential flow in macroporous swelling soil with internal catchment: model development and applications. *Journal of Hydrology* 269 (3-4): 150-168.
- Groffman P.M., Hardy J.P., Nolan S., Fitzhugh R.D., Driscoll C.T. and Fahey T.J., 1999. Snow depth, soil frost and nutrient loss in a northern hardwood forest. *Hydrological Processes* 13: 2275 – 2286.
- Gwo J.P., Jardine P.M., Wilson G.V. and Yeh G.T., 1995. A multiple-pore-region concept to modeling mass transfer in subsurface media. *Journal of Hydrology* 164:217-237.
- H**
- Hambrey M. and Alean J., 1994. *Glaciers*. Cambridge University Press, pp 208.
- Haneberg W.C., 1991. Observation and analysis of short-term pore pressure fluctuations in a thin colluvium landslide complex near Cincinnati, Ohio. *Engineering Geology* 31: 159-184.
- Harris C., Haeberli W., Vonder Mühl D. and King L., 2001. Permafrost monitoring in the high mountains of Europe: The PACE Project in its global context. *Permafrost and Periglacial Processes* 12(1): 3-12.
- Heitman J.L., Basinger J.M., Kluitenberg G.J., Ham J.M., Frank J.M. and Barnes P.L., 2003. Field evaluation of the dual-probe heat-pulse method for measuring soil water content. *Vadose Zone Journal* 2:552-560.
- Hencher S.R., 2010. Preferential flow paths through soil and rock and their association with landslides. *Hydrological processes* 24, 1610-1630 DOI: 10.1002/hyp.7721.
- Hendrickx J.M.H. and Flury M., 2001. Uniform and preferential flow mechanisms in the vadose zone. In: National Committee for Rock Mechanics (Eds.): *Conceptual Models of Flow and Transport in the Fractured Vadose Zone*. National Academic Press, Washington DC, USA, pp 149-187.
- Hillel D., 2004. *Introduction to Environmental Soil Physics*. Elsevier Academic Press, pp 494.
- Hirota O., Yasuhiko O., Gen F., Yoichi O. Takuro M. Toshiaki S., Tomomi T. and Kyoji., 2004. A fluidized landslide on natural slope by artificial rainfall. *Landslides* 1: 211-219.
- Horn R., Taubner H., Wuttke M. and Baumgartl T. 1994. Soil physical properties related to soil structure. *Soil and Tillage Research* 30 (2-4):187-216.

- Hornberger G.M., German P.F. and Beven K.J., 1991. Throughflow and solute transport in an isolated sloping soil block in a forested catchment. *Journal of Hydrology* 124: 81-99.
- Horton R., Wierenga P.J. and Nielsen D.R., 1983. Evaluation of Methods for Determining the Apparent Thermal Diffusivity of Soil Near the Surface. *Soil Science Society of American Journal* 47: 25-32.
- Horton R., 2002. Chapter 5.4 – Soil Thermal Diffusivity. In: *Methods of Soil Analysis, Part 4: Physical Methods*. Soil Science Society of America Inc., Madison, Wisconsin, pp 1227-1232.
- Hutchinson J.N., 1988. Morphological and geotechnical parameters of landslides in relation to geology and hydrogeology. In: Bonnard C. (Ed.): *Proc. 5th Int. Symp. on Landslides* Lausanne, Switzerland, Balkema, Rotterdam, pp 3-31.

I

- IA PAS., 2006. *Manual for Field Operated Meter (FOM)*. Institute of Agrophysics, Polish Academy of Science Lublin, pp 34.
- ISDR, 2004. Terminology: basic terms of disaster risk reduction. International Strategy for Disaster Reduction secretariat, Geneva.
- Iverson R.M., 2000. Landslide triggering by rain infiltration. *Water Resources Research* 36: 1897–1910.

J

- Jackson R.D. and Taylor S.A., 1986. Thermal conductivity and diffusivity. In: *Method of Soil Analysis*, 2nd edition. American Society of Agronomy, Madison, Wisconsin, pp 945–955.
- Jackson T.J., Schmugge J. and Engmsn E.T., 1996. Remote sensing applications to hydrology: soil moisture, *Hydrological Sciences Journal* 41(4): 517 – 530.
- James A.L. and Roulet N.T., 2006. Investigating the applicability of end-member mixing analysis (EMMA) across scale: A study of eight small, nested catchments in a temperate forested watershed. *Water Resources Research* 42(8). DOI: 10.1029/2005WR004419.
- Jarvis N.J., 2007. A review of non-equilibrium water flow and solute transport in soil macropores: principles, controlling factors and consequences for water quality. *European Journal of Soil Science* 58(3), 523-546.
- Johansen O., 1975. Thermal conductivity of soils. Ph.D Thesis, University of Trondheim, Norway.
- Johansson S. and Farhadiroushan M., 1999. Fibre-Optic system for temperature measurements at the Lovon dam. *Elforsk Rapport* 99:36, Stockholm, pp. 25.
- Ju S-H., and Kung K-J.S., 1997. Impact of Funnel Flow on Contaminant Transport in Sandy Soils, Numerical Simulation. *Soil Sci. Soc. Am. J.* 61:416-427.

K

- Keaton J.R. and de Graff J.V., 1996. Surface observation and geologic mapping. In: Turner, A.K., Schuster, R.L. (Eds.): *Landslides Investigation and Mitigation*, TRB Special Report 247, National Academy Press, Washington, DC.

- Kersten MS, 1949. Thermal properties of soils. University of Minnesota, Institute of Technology, *Engineering Experiment Station Bulletin* 28:1-226.
- Kienzler P. and Naef F., 2008. Temporal variability of subsurface stormflow formation. *Hydrology and Earth System Sciences* 12: 257–265.
- Kirchner J.W., 2003. A double paradox in catchment hydrology and geochemistry. *Hydrological Processes* 17: 871 – 874.
- Kosugi K., Uchida T. and Mizuyama T., 2004. Numerical calculation of soil pipe flow and its effect on water dynamics in a slope. *Hydrological Processes* 18: 777–789.
- Krzeminska D.M., Bogaard T.A. and Westhoff M., 2009. Spatial and temporal variability of soil moisture patterns related to preferential flow measured using distributed temperature sensing. *Folia Geographica, Series Geographica- Physica* XL: 71-78
- Krzeminska D.M., Bogaard T.A., Debieche T.-H., Marc V. and Malet J.-P., 2012a (*in press*). Sprinkling tests to understand hydrological behaviour of mudslide. *In: Proc. Int. Conf. 'The Second World Landslide Forum'*, Rome, Italy.
- Krzeminska D.M., Bogaard T.A., Van Asch Th.W.J. and Van Beek, L.P.H., 2012b. A conceptual model of the hydrological influence of fissures on landslide activity. *Hydrology and Earth System Science* 16:1-16.
- Krzeminska D.M., Steele-Dunne S.C., Rutten M.M., Bogaard T.A. and Sailhac P., 2012c. High resolution temperature observations to monitor hydrological features in reworked clay shales slopes. *Hydrological Processes* 26:2143-2156, DOI: 10.1002/hyp.7980.
- Krzeminska D.M., Bogaard T.A., Debieche T.-H., Cervi F., Marc V. and Malet J.-P., 2012 (*in review*). Field investigation of fissure flow with small-scale sprinkling experiments on a hydrologically-controlled landslide. (*submitted to*) *Earth System Processes and Landforms*.
- Krzeminska D.M., Bogaard T.A., Malet J.-P. and van Beek L.P.H. 2012 (*work in progress*). A model of hydrological and mechanical feedbacks of preferential fissure flow in a slow moving landslide. *Hydrology and Earth System Science*
- Kung K.-J.S., Hanke M., Helling C.S., Klavivki E.J., Gish T.J. Steenhuis T.S. and Jaynes D.B., 2005. Quantifying pore-size spectrum of macropore-type preferential pathways. *Soil Science Society of America Journal* 69:1196-1208.
- Kuriakose S.L., Van Beek L.P.H. and Van Westen C.J., 2009. Parameterizing a physically based shallow landslide model in a data poor region. *Earth Surface Processes and Landforms* 34(6): 867-881.
- L**
- Lacasse S. and Farrokh N., 2008. Landslide risk assessment and mitigation. *In: Sassa K. and Canuti P. (Eds): Landslides – Disaster Risk Reduction*. Springer, pp 31-61.

- Larsbo M. and Jarvis N., 2003. Macro 5.0 A model of water flow and solute transport in macroporus soils. Technical description. Studies in the Biogeophysical Environment, Emergo 2003:6.
- Larsbo M. and Jarvis N., 2006. Information content of measurements from tracer microlysimeter experiments designed for parameter identification in dualpermeability models. *Journal of Hydrology* 325:273-287.
- Lindenmaier F., 2007. Hydrology of a large unstable hillslope at Ebnet, Vorarlberg: identifying dominating processes and structures. Ph.D Thesis, Universität Potsdam, Germany.
- Linsley R.K., Kohler M.A. and Paulhus J.L.H., 1982. *Hydrology for Engineers, Third Edition*. New York: McGraw-Hill Book Company.
- Liu H.H., Zhang R. and Bodvarsson G.S., 2005. An active region model for capturing fractal flow patterns in unsaturated soils: Model development. *Journal of Contaminant Hydrology* 80 (1-2):18-30.
- M**
- Malet J.-P., Maquaire O. and Klotz S., 2000. The Super-Sauze flowslide (Alpes-de-Haute-Provence, France). Triggering mechanisms and behaviour. In: Bromhead, E., Dixon, N., Ibsen, M.-L. (Eds.): *Landslides in Research, Theory and Practice. Proceedings of the 8th International Symposium on Landslides*, Cardiff, Wales, T. Telford, London, Vol. 2, pp 999-1006.
- Malet J.-P., Maquaire O. and Calais E., 2002. The use of Global Positioning System for the continuous monitoring of landslides. Application to the Super-Sauze earthflow (Alpes-de-Haute-Provence, France). *Geomorphology* 43: 33-54.
- Malet J.-P., 2003. Les glissements de type écoulement dans les marnes noires des Alpes du Sud. Morphologie, fonctionnement et modélisation hydro-mécanique. Ph.D Thesis, Université Louis Pasteur, Strasbourg, France.
- Malet J.-P., Auzet A.-V., Maquaire O., Ambroise b., Descroix L., Esteves M., Vandervaere J.-P. and Truchet E., 2003. Soil surface characteristics influence on infiltration in black marls: application to the Super-Sauze Earth flow (Southern Alps, France). *Earth Surface Processes and Landforms* 28(5): 547-564.
- Malet J.-P., Van Asch Th.W.J., Van Beek L.P.H. and Maquaire O., 2005. Forecasting the behaviour of complex landslides with a spatially distributed hydrological model. *Natural Hazards and Earth System Sciences* 5:71-85.
- Mali N., Urbanc J. and Leis A., 2007. Tracing of water movement through the unsaturated zone of a coarse gravel aquifer by means of dye and deuterated water. *Environmental Geology* 51(8): 1401-1412.
- Maquaire O., Malet J.-P., Remaître A., Locat J., Klotz S. and Guillon J., 2003. Instability conditions of marly hillslopes: towards landsliding or gullyng? The case of the Barcelonnette basin, South East France. *Engineering Geology* 70(1-2): 109-130.
- McDonnell J.J., 1990. The influence of macropores on debris flow initiation, *Quarterly Journal of Engineering Geology and Hydrogeology* 23: 325-331, DOI:10.1144/GSL.QJEG.1990.023.04.06.

- Méric O., Garambois S., Malet J.-P., Cadet H., Gueguen P. and Jongmans D., 2007. Seismic noise-based methods for soft-rock landslide characterization. *Bulletin de la Société Géologique de France* 178 (2): 137–148.
- Mikovari A., Peter C. and Leibundgut Ch., 1995. Investigation of preferential flow using tracer techniques. In: *Tracer Technologies for Hydrological Systems*, Proceedings of a Boulder Symposium, July 1995.
- Milledge D. G., Griffiths D. V., Lane S. N. and Warburton J., 2012. Limits on the validity of infinite length assumptions for modelling shallow landslides. *Earth Surface Processes and Landforms*, DOI: 10.1002/esp.3235
- Miller D.J. and Sias J., 1998. Deciphering large landslides: linking hydrological groundwater and stability models through GIS. *Hydrological Processes* 12: 923–941.
- Millington R.J. and Quirk J.P., 1959. Permeability of porous media. *Nature* 183:387–388.
- Mori Y., Hopmans J.W., Mortensen A.P. and Kluitenberg G.J., 2003. Multi-functional heat pulse probe for the simultaneous measurement of soil water content, solute concentrations, and heat transport parameters. *Vadose Zone Journal* 2: 561–571.
- Mulholland P.J. and Hill W.R., 1997. Seasonal patterns in streamwater nutrient and dissolved organic carbon concentrations: Separating catchment flow path and in-stream effects. *Water Resources Research* 33(6): 1297–1306, DOI: 10.1029/97WR00490.
- Mulungu D.M.M., Ichikawa Y. and Shiiba M., 2005. A physically based distributed subsurface-surface flow dynamics model for forested mountainous catchments. *Hydrological Processes* 19: 3999–4022.
- N
- Nettleton I.M., Martin S., Hencher S. and Moore R., 2005. Debris flow types and mechanisms. In: Winter M.G., Macgregor F. and Shackman L. (Eds.): *Scottish Road network Landslide Study*. Edinburgh: The Scottish Executive. ISBN 0 7559 4649 9, pp. 45–67.
- Nieber J.L. and Sidle R.C., 2010. How do disconnected macropores in sloping soils facilitate preferential flow. *Hydrological Processes* 24: 1582–1594, DOI:10.1002/hyp.7633.
- Niethammer U., Rothmund S. and Joswig M., 2009. UAV-based remote sensing of the slow-moving landslide Super-Sauze. In: Malet J.-P., Remaître A., Bogaard T.A. (Eds.): *Proceedings of the International Conference on Landslide Processes: from geomorphologic mapping to dynamic modelling*, Strasbourg, CERIG Editions, pp. 69–74.
- Niethammer U., James M.R., Rothmund S., Travelletti J. and Joswig M., 2012. UAV-based remote sensing of the Super-Sauze landslide: Evaluation and results. *Engineering Geology* 128 (1): 2–11, DOI:10.1016/j.enggeo.2011.03.012
- Njoku E.G., Jackson T.J. and Koike T., 2000. *AMSRE Science Data Validation Plan*, version 2, 7/00.

Nobles M.M., Wilding L.P. and McInnes K.J. 2004. Pathways of dye tracer movement through structured soils on a macroscopic scale. *Soil Science* 169:229–242.

Noguchi S., Tsuboyama Y., Sidle R.C. and Hosoda I., 1999. Morphological characteristics of macropores and the distribution of preferential flow pathways in a forested slope segment. *Soil Science Society of American Journal* 63: 1413–1423.

P

PCRaster Team, 2011. PCRaster Documentation, release 3.0.1. Faculty of Geographical Sciences, Utrecht University, Netherlands.

Pierson T.C., 1983. Soil pipes and slope stability. *Quarterly Journal of Engineering Geology and Hydrogeology* 16:1-15.

Popov Y.A., Pribnow D.F.C., Sass J.H., Williams C.F. and Burkhardt H., 1999. Characterization of rock thermal conductivity by high-resolution optical scanning. *Geothermics* 28, 253-276.

Popov Y.A., 2005. In: A.Rauen and E. Lippmann (Eds.): *Thermal Conductivity Scanner (TCS). User's Manual*. TCS - Lippmann and Rauen GbR, Germany.

Pollack H. and Huang S., 2000. Climate reconstruction from subsurface temperature. *Annual Review of Earth and Planetary Sciences* 28: 339-365.

R

Remaître A., 2006. Morphologie et dynamique des laves torrentielles : application aux torrents des Terres Noires du bassin de Barcelonnette (Alpes du Sud). Ph.D Thesis, Université de Caen-Basse-Normandie, Caen, France.

Ritsema C. J. and L. Dekker L.W., 1994. How water moves in a water repellent sandy soil: 2. Dynamics of fingered flow. *Water Resources Research* 30(9): 2519–2531, DOI:10.1029/94WR00750.

Ritsema C.J. and Dekker L.W., 2000. Special issue: Water repellency in soils - Preface Preface. *Journal of Hydrology* 231:1-3.

Roth, K., 1995. Steady state flow in an unsaturated, two-dimensional, macroscopically homogeneous, Miller-similar medium. *Water Resources Research* 31: 2127-2140.

Roulier S. and Schulin R., 2008. Guest Editor's preface to special issue on preferential flow. *European Journal of Soil Science* 59.

S

Savage W.Z., Godt J.W. and Baum R.L., 2003. A model for spatially and temporally distributed shallow landslide initiation by rainfall infiltration. In: Rickenmann, D., Chen, C-L. (Eds) *Proceedings of the third international conference on debris flow hazards mitigation: mechanics, prediction, and assessment*. Davos, Millpress, Rotterdam.

- Schmutz M., Albouy Y., Guérin R., Maquaire O., Vassal J., Schott J.-J. and Descloîtres M., 2001. Joint electrical and time domain electromagnetism (TDEM) data inversion applied to the Super Sauze earthflow (France). *Surveys in Geophysics*, 21(4): 371-390.
- Schulson E.M. and Duval P., 2009. Creep and Fracture of Ice. Cambridge University Press, New York.
- Selker J.S., Thevenaz L., Huwald H., Mallet A., Luxemburg W., Van de Giesen N., Stejskal M., Zeman J., Westhoff M. and Parlange M.B., 2006, Distributed fiber - optic temperature sensing for hydrologic systems. *Water Resources Research* 42, W12202, DOI: 10.1029/2006WR005326
- Sidle R.C., Tsuboyama Y., Noguchi S., Hosada I., Fujieda M. and Shimizu T., 2000. Stormflow generation in steep forested headwaters: a linked hydrogeomorphic paradigm. *Hydrological Processes* 14: 369–385.
- Sidle R.C., Noguchi S., Tsuboyama Y. and Laursen K., 2001. A conceptual model of preferential flow systems in forested hillslopes: evidence of self-organization. *Hydrological Processes* 15: 1675–1692, DOI: 10.1002/hyp.233
- Šimůnek J., Šejna M. and Van Genuchten M. Th., 1999. The HYDRUS-2D software package for simulating two-dimensional movement of water, heat, and multiple solutes in variably saturated media. Version 2.0, IGWMC - TPS - 53, International Ground Water Modeling Center, Colorado School of Mines, Golden, Colorado.
- Šimůnek J., Jarvis N.J, Van Genuchten M.T. and Gardenas A., 2003. Review and comparison of models for describing non-equilibrium and preferential flow and transport in the vadose zone. *Journal of Hydrology* 272(1-4):14-35.
- Sivapalan M., Jothityangkoon C. and Menabde M., 2002. Linearity and nonlinearity of basin response as a function of scale: discussion of the alternative definitions. *Water Resources Research* 38(2). DOI: 10.1029/2001 WR000482
- Skempton A.W. and DeLory F.A., 1957. Stability of natural slopes in London clay. In: *Proceedings 4th International Conference on Soil Mechanics and Foundation Engineering*, vol. 2, pp. 378– 381.
- Skempton A.W., 1964. The long-term stability of clay slope. *Geotechnique* 14:95-102.
- Soulsby C., Rodgers P., Smart R., Dawson J. and Dunn S., 2003. A tracer-based assessment of hydrological pathways at different spatial scales in a mesoscale Scottish catchment. *Hydrological Processes* 17(4): 759-777. DOI: 10.1002/hyp.1163.
- Stumpf A., Malet J.-P., Kerle N., Niethammer U. and Rothmund S., 2012 (*in review*) Image-based mapping of surface fissures for the investigation of landslide dynamics. (*submitted to*) *Geomorphology*.
- Steele-Dunne S.C., Rutten M.M., Krzeminska D.M., Hausner M., Tyler S.W., Selker J., Bogaard T.A. and Van de Giesen N.C., 2010. Feasibility of soil moisture estimation using passive distributed temperature sensing. *Water Resources Research* 46, W03534, DOI:10.1029/2009WR008272
- Steenhuis T.S., Ritsema C.J. and Dekker L.W., 1996. Introduction. *Geoderma* 70:2-4.

Sugiura R., Noguchi N. and Ishii K., 2007. Correction of low-altitude thermal images applied to estimating soil water status, *Biosystems Engineering* 96 (3): 301–313.

T

Tabbagh A., Bendjouidi H. and Benderitter Y., 1999. Determination of Recharge in Unsaturated Soils Using Temperature Monitoring. *Water Resources Research* 35(8): 2439–2446.

Tarara J.M. and Ham J.M., 1997. Measuring soil water content in the laboratory and field with dual-probe heat-capacity sensors. *Agronomy Journal* 89:535-542.

Travelletti J. and Malet J.-P., 2012. Characterisation of the 3D geometry of flow-like landslides: A methodology based on the integration of heterogeneous multi-source data. *Engineering Geology* 128: 30-48.

Travelletti J., Delacourt C., Allemand P., Malet J.-P., Schmittbuhl J., Toussaint R. and Bastard M., 2012a. Correlation of multi-temporal ground-based optical images for landslide monitoring: application, potential and limitations. *Journal of Photogrammetry and Remote Sensing* 70:39-55.

Travelletti J., Sailhac P., Malet J.-P., Grandjean G. and Ponton, J., 2012b. Hydrological response of weathered clay-shale slopes: water infiltration monitoring with time-lapse electrical resistivity tomography. *Hydrological Processes*, 26:2106-2119, DOI: 10.1002/hyp.7983

Trojan M. and Linden D., 1992. Micro relief and rainfall effects on water and solute movement in earthworm burrows. *Soil Science Society of American Journal* 56:727-733.

Tromp-van Meerveld H.J. and McDonnell J.J., 2006. Threshold relations in subsurface stormflow: 2. the fill and spill hypothesis. *Water Resources Research* 42. DOI: 10.1029/2004WR003778.

Tsuboyama Y., Sidle R.C., Noguchi S. and Hosada I., 1994. Flow and transport through the soil matrix and macropores of hillslope segment. *Water Resources Research* 30(4): 879-890.

U

Uchida T., Kosugi K. and Mizuyama T., 2001. Effects of pipeflow on hydrological process and its relation to landslide: a review of pipeflow studies in forested headwater catchments. *Hydrological Processes* 15: 2151–2174.

V

Van Asch Th.W.J., Hendriks M.R., Hassel R. and Rappange, F.E., 1996. Hydrological triggering conditions of landslide in varved clays in the French Alps. *Engineering Geology* 42: 239-251.

Van Asch Th.W.J., Van Dijk S.J.E. and Hendriks M.R., 2001. The role of overland flow and subsurface flow on spatial distribution of soil moisture in the topsoil. *Hydrological Process* 15: 2325–2340.

Van Asch Th. W. J., Malet, J. -P., Van Beek L. P. H. and Amitrano D., 2007. Techniques, issues and advances in numerical modelling of landslide hazard. *Bulletin de la Société Géologique de France* 178 (2): 65-88.

Van Bavel M. and Nichols C., 2002. Theta and Profiler Soil Moisture Probes - Accurate Impedance Measurement Devices - New Applications. Technical Report.

- Van Beek L.P.H. and Van Asch T.W.J., 1999. A combined conceptual model for the effects of fissure-induced infiltration on slope stability. *In: Process Modelling and Landform Evolution*. Lecture Notes in Earth Sciences 78: 147-167, DOI: 10.1007/BFb0009716
- Van Beek L.P.H., 2002. Assessment of the influence of changes in land use and climate on landslide activity in a Mediterranean environment. Ph.D Thesis, University of Utrecht, Netherlands.
- Van Beek L.P.H. and Van Asch Th.W.J., 2004. Regional assessment of the effects of land-use change on landslide hazard by means of physically based modelling. *Natural Hazards* 31:289–304.
- Van Genuchten M. Th., Schaap M.G., Mohanty B.P., Šimůnek J. and Leij F.J., 1999. Modeling flow and transport processes at the local scale in space and time. *In: J. Feyen and K. Wiyo (Eds.): Proc. Int. Workshop of EurAgEng's Field of Interest on Soil and Water*. November 24-26, 1999, Leuven, Belgium, Wageningen Pers, the Netherlands, pp. 23-45.
- Van Genuchten M. Th., 2011. Dual-porosity approximations of the hydraulic properties of unsaturated structured media. Keynote Lecture, *Brazilian Meeting of Soil Physics BMSPM2011*, 12-16 September, Piracicaba, Brasil.
- Van Schaik N.L.M.B., Schnabel S. and Jetten V.G., 2008. The influence of preferential flow on hillslope hydrology in a semi-arid watershed (in the Spanish Dehesas). *Hydrological Processes* 22:3844-3855.
- Van Schaik N.L.M.B., 2009. Spatial variability of infiltration patterns related to site characteristics in a semi-arid watershed. *Catena* 78: 36-47.
- Van Schaik N.L.M.B., 2010. The role of macropore flow from PLOT to catchment scale. Ph.D Thesis, University of Utrecht, Netherlands.
- Van Westen C.J., Van Asch T.W.J. and Soeters R., 2005. Landslide hazard and risk zonation: why it is so difficult?, *Bulletin of Engineering Geology and the Environment* 65(2):167-184.
- Varnes D.J., 1978. Slope movement types and processes. *In: Schuster R.L. and Krizek, R.J. (Eds.): Special Report 176: Landslides: Analysis and Control* Transportation and Road Research Board, National Academy of Science, Washington D. C.
- W**
- Walter M., Niethammer U., Rothmund S. and Joswig M., 2009. Joint analysis of the Super-Sauze (French Alps) mudslide by nanoseismic monitoring and UVA-based remote sensing. *First Break* 27(8): 53-60.
- Walter, M., Arnhardt, C. and Joswig, M., 2012. Seismic monitoring of rockfalls, slide quakes, and fissure development at the Super-Sauze mudslide, French Alps. *Engineering Geology* 128(1):12-22.
- Weber D., 1994. Research into earth movements in the Barcelonnette basin. *In: Casale, R., Fantechi, R., Flageollet, J.C. (Eds.): Temporal occurrence and forecasting of landslides in the European Community, Final report, Volume I, Contract EPOCH*, European Commission, Brussels, pp 321-336.

- Weber D. and Herrmann A., 2000. Contribution de la photogrammetrie numerique a l'etude spatio-temporelle de versants instables: l'exemple du glissement de terrain de Super-Sauze (Alpes-de-Haute-provence, France). *Bulletin de la Societe Geologique de France* 171 (6): 637-648.
- Weber, D. 2001. Contribution Contribution de la geomorphologie a la connaissance des mouvements de terrain dans les 'Terres Noires ' alpines : le glissement-coulee de Super-Sauze (Alpes de Haute Provence, France), Ph.D thesis, Universite Louis Pasteur, Strasbourg, France.
- Weiler M. and Naef F., 2003. An experimental tracer study of the role of macropores in infiltration in grassland soils. *Hydrological Processes* 17: 477-493.
- Weiler M. and McDonnell J.J., 2007. Conceptualizing lateral preferential flow and flow networks and simulating the effects on gauged and ungauged hillslopes. *Water Resources Research* 43, W03403, DOI: 10.1029/2006WR004867
- Wieczorek G.F., 1996. Landslide triggering mechanisms. In: Turner A.K. and Schuster S.L. (Eds):. *Special Report 247: Landslide investigation and mitigation*. Transportation and Road Research Board, National Academy of Science, Washington D. C.
- Wienhöfer J., Lindenmaier F. and Zehe E., 2011. Challenges in Understanding the Hydrologic Controls on the Mobility of Slow-Moving Landslides. *Vadose Zone Journal* 10(2): 496-511, DOI:10.2136/vzj2009.0182.
- Wilhelm F., 1975. *Schnee- und Gletscherkunde*. Walter de Gruyter Press, pp. 434.
- Wu W. and Sidle R.C., 1995. A distributed slope stability model for steep forested basins. *Water Resources Research* 31: 2097–2110.
- Z**
- Zehe E. and Fluhler H., 2001. Preferential transport of isoproturon at a plot scale and a field scale tile-drained site. *Journal of Hydrology* 247 (1-2): 100-115.
- Zehe E. and Blöschl, G.: 2004. Predictability of hydrologic response at the plot and catchment scales – the role of initial conditions. *Water Resources Research* 40(10): W10202, DOI:10.1029/2003WR002869
- Zhang G.P., Savenije H.H.G., Fenicia F. and Pfister L. 2006. Modelling subsurface storm flow with Representative Elementary Watershed (REW) approach: application to the Alzette River Basin. *Hydrology and Earth System Science* 10: 937–955.
- Zurmühl T., Durner W., 1996. Modeling transient water and solute transport in biporous soil. *Water Resources Research* 32(4):819–829.

ACKNOWLEDGEMENTS

The PhD thesis is never a work of one author: many people contributed to this dissertation in innumerable ways, and I am grateful to all of them.

First of all I would like to thank Professor Huub Savenije, for giving me the opportunity to conduct PhD research and to share his enthusiasm for the “art of hydrology”. Then my compliments go to my daily supervisor and first-help-line Thom Bogaard. Thank you for guiding me through the scientific world, for your patience in answering thousands of my “small questions” and endless correcting of my “Polish English”. Also fieldwork, the foundation of this research, would have been impossible without your invaluable help and enthusiasm no matter what - I know, I know it is only mental!!

Speaking of fieldwork, I would like to thank Jean-Philippe Malet for introducing me to “his landslide”, providing gigabytes of field monitoring data and hosting me during several stays at the EOST in Strasbourg - I cannot imagine this research without your help and enthusiasm. I also would like to say a big “thank you” to everyone who ever joined me for the fieldwork for helping with carrying the equipment, installing it and listening to all the complaints of stressed PhD researcher.

I would like to acknowledge all the co-authors of my publications from TU Delft, Université de Strasbourg, Université d’Avignon and Utrecht University. This research would not have been possible without cooperation and inspiring discussion with such great colleagues. Special thanks go to Rens van Beek, master of STARWARS model, for providing the code, guiding me through the script and helping to interpret the results.

Besides acknowledging my co-authors, I would like to say a big “thank you” to my fellow-researchers from the Mountain Risk project. Thank you for being a part of my scientific “Wonderland” - project meetings, conferences, social networking and other great moments we

shared together. I would like to thank to all the ‘staff members’ of the project for being there for us, and for sharing your knowledge and expertise. Many thanks go to Jordi Corominas for his support and hospitality at the Politecnica de Catalunya.

Also many thanks go to my ‘office-hours company’: thanks for sharing the best and worst moments during my stay at TUDelft. Martine and Martijn: thanks to you Matlab coding is no longer a mystery for me. Susan: without you many of my “cable questions” would be a nightmare to answer – thanks for your support.....not just scientific!!; Miriam: thanks for hosting me in your office, for all the positive energy, and for giving me support and motivation at the last stage of writing.

Finally, but most important I wish to thank my husband Pawel for always being there for me. On the personal level I have to thank a great number of people including friends and family, for their friendship, support and constant motivation. It would not be possible to mention everyone here by name. I promise to thank you personally, when we meet each other next time!!

SURNAME(S): Krzeminska (Pradzynska)

FIRST NAME(S): Dominika Malgorzata

DATE OF BIRTH: 8th of February 1979

NATIONALITY: Polish



Dominika Krzeminska completed high school at XIV Stanislaw Staszic High School in Warsaw, Poland, in 1998 and started to study Environmental Engineering at Warsaw University of Technology, Poland. She specialised in the field of hydrology and water management. During her study she spend three months at Free University Brussels, Belgium, at the Department of Hydrology and Hydraulic Engineering within the Erasmus Programme. In 2003 she graduated on the topic “The use of the Geographic Information Systems (GIS) for water balance calculation and water management at the basin scale”. Simultaneously she also completed postgraduate studies in the area of Safety of Human-Technology-Environment Systems at Warsaw University of Technology, Poland.

After her MSc-degree Dominika started to work in the field of Environmental Engineering and Environmental Health and Safety (EHS) in both research institutes and private companies. She was a young researcher at Warsaw University of Technology (Poland), Technical University of Crete (Greece) and at Free University Brussels (Belgium).

In 2007 she started a PhD-study at the Civil Engineering Department of the Delft University of Technology within ‘Mountain Risks’ Marie Curie Research Network on the influence of preferential fissure flow on landslide hydrological responses. She carried out extended field experiments in French Alps, laboratory experiments at the University Louis Pasteur in Strasbourg, France, and proposed a conceptual hydrological model of preferential fissure flow using PCRaster GIS-package. Dominika presented her work on several international conferences: EGU, ERB and ‘Mountain Risks’ conferences. In 2008 she won the Young Scientists Outstanding Poster Prize (YSOPP) at the EGU, Vienna.

The findings of her PhD study resulted in publication in peer-reviewed journals and conference proceedings.

PEER-REVIEWED JOURNALS

Krzeminska D.M., Bogaard T.A., Malet J.-P. and van Beek L.P.H. (*work in progress*). A model of hydrological and mechanical feedbacks of preferential fissure flow in a slow moving landslide. (*to be submitted to*) *Hydrology and Earth System Science*.

Krzeminska D.M., Bogaard T.A., Debieche T.-H., Cervi F., Marc V. and Malet J.-P., (*in review*). Field investigation of fissure flow with small-scale sprinkling experiments on a hydrologically-controlled landslide. (*submitted to*) *Earth System Processes and Landforms*.

Krzeminska D.M., Bogaard T.A., Van Asch Th.W.J. and Van Beek, L.P.H., 2012. A conceptual model of the hydrological influence of fissures on landslide activity. *Hydrology and Earth System Science* 16:1-16.

Krzeminska D.M., Steele-Dunne S.C., Rutten M.M., Bogaard T.A. and Sailhac P., 2012. High resolution temperature observations to monitor hydrological features in reworked clay shales slopes. *Hydrological Processes*, 26: 2143-2156, DOI: 10.1002/hyp.7980.

Debieche, T.-H., Bogaard, T.A., Marc, V., Emblanch, C., Krzeminska, D.M., Malet, J.-P. 2012. Hydrological and hydrochemical processes observed during a large-scale infiltration experiment at the Super-Sauze mudslide (France). *Hydrological Processes*, 26: 2157-2170, DOI: 10.1002/hyp.7843

Grandjean, G, Bitri, A., Krzeminska, D.M. (2011) Characterization of a landslide fissure pattern by integrating seismic azimuth tomography and geotechnical testing. *Hydrological Processes*, 26: 2120-2127, DOI: 10.1002/hyp.7993

Steele-Dunne, S. C., M. M. Rutten, D. M. Krzeminska, M. Hausner, S. W. Tyler, J. S. Selker, T. A. Bogaard, and N. C. van de Giesen (2010), Feasibility of Soil Moisture Estimation using Passive Distributed Temperature Sensing. *Water Resources Research* 46 W03534, DOI:10.1029/2009WR008272.

Krzeminska D.M., Bogaard T.A. and Westhoff M., 2009. Spatial and temporal variability of soil moisture patterns related to preferential flow measured using distributed temperature sensing. *Folia Geographica, Series Geographica- Physica*, XL: 71-78

PEER-REVIEWED CONFERENCE PROCEEDINGS

Krzeminska D.M., Bogaard T.A., Debieche T.-H., Marc V. and Malet J.-P., 2012 (*in press*). Sprinkling tests to understand hydrological behaviour of mudslide. *In*: Proceedings of the Second World Landslide Forum, 3-7 October, Rome.

Cervi F., Debieche T.-H., Krzeminska D.M., Marc V., Bogaard T.A. and Malet J.-P., 2011. Variable contributions of mixing end members during small-scale sprinkling experiments in partially weathered black marls. *In*: Proceedings of the Second Italian Workshop on Landslides (IWL2) – Large slow active slope movements and risk management, 28-20 September, Naples, Italy.

Krzeminska D.M., Bogaard T. A. and Steele-Dunne S. C., 2010. On the potential of high temporal and spatial resolution soil temperature monitoring for hazard analysis of rainfall induced landslide. *In*: Proceedings of the ‘Mountain Risks’ International Conference – Bringing science to society, 24-26 November, Firenze, Italy.

Krzeminska D.M., Bogaard T.A., Debieche T.-H., Marc V., Ponton J. and Malet J.-P. 2009. Quantitative analysis of preferential flow during small scale infiltration tests on an active mudslide, French Alps. *In*: Proceedings of the ‘Landslide Processes’ International Conference, Strasbourg, France, 6-7 February 2009.